

## University of Southampton Research Repository

Copyright © and Moral Rights for this thesis and, where applicable, any accompanying data are retained by the author and/or other copyright owners. A copy can be downloaded for personal non-commercial research or study, without prior permission or charge. This thesis and the accompanying data cannot be reproduced or quoted extensively from without first obtaining permission in writing from the copyright holder/s. The content of the thesis and accompanying research data (where applicable) must not be changed in any way or sold commercially in any format or medium without the formal permission of the copyright holder/s.

When referring to this thesis and any accompanying data, full bibliographic details must be given, e.g.

Thesis: Author (Year of Submission) "Full thesis title", University of Southampton, name of the University Faculty or School or Department, PhD Thesis, pagination.

Data: Author (Year) Title. URI [dataset]



**University of Southampton**

Faculty of Engineering and Physical Sciences

School of Electronics and Computer Science

**Investigation of Encapsulant Materials for  
Packaging Flexible Gas Sensor for E-textile  
Application**

by

Ashwini Valavan

Thesis for the degree of Doctorate

October 2023



# University of Southampton

## Abstract

Faculty of Engineering and Physical Sciences

School of Electronics and Computer Science

Doctor of Philosophy

### **Investigation of encapsulant materials for packaging flexible gas sensor for e-textile application**

By

Ashwini Valavan

Toxic gases and particulate matter (such as CO<sub>2</sub>, NO<sub>2</sub> etc.) account for millions of deaths every year due to respiratory-related issues. Wearable gas sensors offer a good platform for continuously monitoring the quality of air can give information about the degree of air pollution at any location and time. This will allow the wearer to monitor their exposure and to participate in crowd sensing air pollution in which the data can be shared and used for mapping polluted areas and enable safety measures for preventing and mitigating the effect of these gases on humans and their environment. In this regard, e-textiles provide an attractive platform for a wearable gas sensor. This work builds upon previous research conducted at the University of Southampton that developed a flexible circuit fabrication and packaging technology that enables the circuits to be woven into a textile. The packaging process previously demonstrated used a conformal polymer (Kapton) film bonded to the substrate but for an e-textile gas sensor, it is important that this packaging is gas permeable whilst remaining flexible and waterproof. There have not been any reported approaches for the encapsulation of flexible gas sensors with thermoplastic films previously. This work focuses on investigating the various techniques and flexibility of the materials that are waterproof and gas permeable for addressing the above issue. A flexible strip with a MOX gas sensor was built to detect carbon monoxide. A novel way of packaging flexible electronics using vacuum forming was achieved using breathable and waterproof thermoplastic polyurethane film. The sensor was also encapsulated with two different thermoplastic materials - microporous polytetrafluoroethylene Zitex G - 104 and PTFE glass fibre fabric using flexible jigs. Zitex G - 104 and PTFE fibre glass fabric encapsulated flexible sensor have negligible effect on the sensor response to Carbon monoxide whereas TPU acts as a gas barrier film. It was found that the Zitex G - 104 packaged sensor has the highest mechanical robustness to bending and washing cycles.



---

**TABLE OF CONTENTS**

<b>TABLE OF CONTENTS</b> .....	<b>iii</b>
<b>List of Tables</b> .....	<b>vii</b>
<b>List of Figures</b> .....	<b>viii</b>
<b>Research Thesis: Declaration of Authorship</b> .....	<b>xvii</b>
<b>Acknowledgements</b> .....	<b>xviii</b>
<b>Definitions and Abbreviations</b> .....	<b>xix</b>
<b>Glossary of Terms</b> .....	<b>xxiv</b>
<b>Chapter 1 Introduction</b> .....	<b>1</b>
1.1 Introduction to Electronic Textiles (e-textiles) .....	2
1.1.1 Platform technology in Functional Electronics Textiles (FETT) project .....	2
1.1.2 Application of Functional Electronics Textiles (FETT) project to gas sensors .....	3
1.2 Aim.....	3
1.3 Objectives.....	4
1.4 Statement of Novelty.....	4
1.5 Thesis structure.....	4
1.6 List of publications.....	8
<b>Chapter 2 Gas Sensing Technologies and Encapsulation Techniques – A Review</b> .....	<b>9</b>
2.1 Solid state gas sensors .....	9
2.1.1 Catalytic Combustion .....	9
2.1.2 Electrochemical .....	10
2.1.3 Chemiresistor.....	11
2.2 Mass Sensitive gas sensors.....	23
2.2.1 Surface Acoustic Wave (SAW).....	23
2.2.2 Quartz Crystal Microbalance (QCM).....	24
2.2.3 Film Bulk Acoustic Resonator (FBAR) .....	24
2.2.4 Micro-cantilever .....	24
2.2.5 Capacitive micromachined ultrasonic transducer.....	25
2.3 Optical absorption .....	25
2.4 Discussion .....	27
2.5 Review of encapsulation techniques .....	33
2.6 Types of encapsulation techniques.....	33
2.6.1 Glob top and dam and fill .....	33

2.6.2	Casting, potting and encapsulation.....	34
2.6.3	Conformal coating.....	34
2.7	Packaging technology used in gas sensor .....	35
2.8	Conclusion .....	35
<b>Chapter 3</b>	<b>Flexible Carbon Monoxide Sensor – Design and Characterisation .....</b>	<b>37</b>
3.1	Gas sensing operation of MiCS 5524 sensor .....	37
3.2	Fabrication of flexible circuit strips .....	38
3.2.1	Substrate preparation.....	39
3.2.2	Photolithography .....	39
3.2.3	Mounting of Surface mount devices (SMD).....	41
3.2.4	Sensor connection checking.....	41
3.3	Experimental setup of gas sensor testing chamber .....	43
3.3.1	Characterization of gas testing chamber and reference sensor.....	45
3.3.2	Warm-up time evaluation of MiCS-5524 gas sensor chip .....	48
3.3.3	Testing of MiCS-5524 with Carbon monoxide.....	52
<b>Chapter 4</b>	<b>Encapsulation Materials and Process Evaluation.....</b>	<b>57</b>
4.1	Gas and water permeability of polymers .....	57
4.2	Selection of materials for packaging flexible gas sensor.....	58
4.3	Adhesive used for bonding materials.....	58
4.3.1	Liquid Adhesives for high surface tension.....	58
4.3.2	Pressure sensitive adhesive .....	59
4.4	Contact angle experiment for hydrophobicity of materials.....	59
4.4.1	Theory .....	59
4.4.2	Experiments and results.....	60
4.5	Peel test .....	62
4.5.1	Sample preparation.....	63
4.5.2	Peel test experiment.....	64
4.6	Peel test results.....	65
4.7	Peel strength for adhesives bonded between Zitex G - 104 and Kapton N, and on Kapton E .....	66
4.8	Process for packaging gas permeable and waterproof materials on flexible gas sensing system.....	72
4.8.1	Vacuum forming.....	72



4.8.2	Platilon U 4201 AU processing for moulding using the vacuum former – heat power setting and window size reduction.....	75
4.8.3	Platilon U 4201 AU Vacuum forming – optimization of substrate size optimization	80
4.8.4	Platilon U 4201 AU Vacuum forming – optimization of positioning the samples for the moulding process .....	82
4.8.5	Platilon U 4201 AU processing for moulding on flexible CO sensor strip packaging	84
4.8.6	Moulds for non-melt processible thermoplastic material .....	87
4.8.7	Process of applying Pressure Sensitive Adhesive for bonding.....	88
4.8.8	Packaging assembly with additional substrate of optimized width.....	91
4.9	Conclusion.....	96
<b>Chapter 5 Gas Sensing of Textile Integrated Flexible CO Sensor .....</b>		<b>97</b>
5.1	Gas sensing experiments - Response of, and PTFE Fibre glass fabric, Zitex G - 104 and Platilon U 4201 AU coated filaments.....	97
<b>Chapter 6 Evaluation of E-textile Gas Sensor Under Mechanical Stresses - Bending and Washing Environments.....</b>		<b>105</b>
6.1	Stress analysis.....	105
6.2	Bending test.....	108
6.2.1	Experimental setup .....	108
6.2.2	Result .....	108
6.2.3	Analysis .....	114
6.3	Washing test .....	114
6.3.1	Experimental setup .....	115
6.3.2	Results .....	116
6.3.3	Analysis .....	123
<b>Chapter 7 Flexible Nitrogen Dioxide Gas Sensor .....</b>		<b>125</b>
7.1	Interface circuit for VOCsens NO <sub>2</sub> microsensor .....	125
7.2	Flexible Circuit Design and fabrication .....	126
7.3	Characterisation of NO <sub>2</sub> reference sensor .....	128
7.4	Characterisation of flexible NO <sub>2</sub> Filament .....	130
<b>Chapter 8 Conclusion and Future Recommendations .....</b>		<b>133</b>
8.1	Conclusions .....	133
8.2	Research Limitations.....	134
8.3	Future Recommendations.....	135

<b>Bibliography .....</b>	<b>137</b>
<b>APPENDIX A .....</b>	<b>146</b>
Characterization of reference sensor - response time.....	146
Characterization of reference sensor - recovery time.....	147
Characterization of flexible CO sensor .....	148
<b>APPENDIX B .....</b>	<b>153</b>
MAKING OF PDMS.....	153
PACKAGING ASSEMBLY .....	154
<b>APPENDIX C .....</b>	<b>155</b>
SENSITIVE MATERIAL IN NO2 BARE DIE.....	155

## List of Tables

Table 2.1 Working of MOX gas sensor based on the nature of target gas [22].....	11
Table 2.2 Showing the electrical changes in CP due to the interaction with gas molecules [29] 13	13
Table 2.3 Showing the minimum detection limit for different gas sensors .....	28
Table 2.4 Summary of flexible and e-textile gas sensor .....	29
Table 3.1 Resistances across the power supply contact pads in the flexible sensor strip for all 9 sensors.....	42
Table 3.2 Components inside the chamber .....	45
Table 3.3 Theoretical and experimental values of diluted CO gas concentration inside the chamber for each constant flow regulator valve opening time.....	47
Table 3.4 Response time, Recovery time and average response for all the sensors .....	55
Table 4.1 Materials to be used for encapsulation and bonding.....	58
Table 4.2 Summary of encapsulation method for different encapsulants with best adhesives for bonding the flexible CO gas sensor circuit strip.....	95
Table 4.3 Peel Test – Modes of Failure .....	96
Table 5.1 Time Taken for PTFE Fibre glass fabric encapsulated filaments.....	99
Table 5.2 Time Taken for Zitex G - 104 Encapsulated filaments.....	101
Table 6.1 Material properties .....	106
Table 6.2 Neutral axis calculated.....	106
Table 6.3 Bending test for unencapsulated CO flexible circuits.....	109
Table 6.4 Bending test for PTFE Fibre glass fabric with acrylic adhesive.....	110
Table 6.5 Bending test for Zitex G - 104 with NLP 11051.....	111
Table 6.6 Bending test for Platilon U 4201 AU with heat bonding.....	112
Table 6.7 Washing test for unencapsulated flexible circuit.....	116
Table 6.8 Washing test for PTFE Fibre glass fabric with acrylic adhesive .....	118
Table 6.9 Washing test for Zitex G - 104 with NLP 11051 .....	119
Table 6.10 Washing test for Platilon U 4201 AU .....	121
Table 7.1 Selection of resistors for achieving high sensitivity by output voltage less than 1V. 126	126
Table 7.2 Calculated and experimental gas concentration inside the chamber for NO <sub>2</sub> .....	128
Table 8.1 Comparison of packaged e-textile based gas sensor .....	134

---

## List of Figures

Figure 1.1 Different types of gas sensing mechanisms.....	1
Figure 1.2 Schematic diagram of electronic filament inside a yarn [15].....	3
Figure 1.3 Electronic filament placed in the pocket by weaving process.....	3
Figure 1.4 Schematic diagram of the methodological framework for the research.....	5
Figure 2.1 (a) Topology of an electrochemical sensor (b) screen printed electrochemical as a sensor on PET foil [20].....	10
Figure 2.2 Schematic diagram of Metal-oxide semiconductor gas sensor .....	12
Figure 2.3 Basic structure of conducting polymer-based gas sensor.....	13
Figure 2.4 a) gold electrodes on non-woven polypropylene b) ink-jet printed PANI on top of the electrodes c) wires glued to the contact pads for measurement [31].....	14
Figure 2.5 a) Sewing PANI coated polyester yarn on cloth b) Conductive yarn attached to pocket of lab coat with comparator circuit connected to LEDs to indicate the exposure level c), d) and e) demonstrates turning on of LED for 3 different concentrations 5ppm, 25ppm and 50ppm .....	15
Figure 2.6 Different types of carbon nanomaterials-based gas sensing technologies .....	16
Figure 2.7 (a) Basic structure of carbon black composite inside an inorganic polymer film (b) Shows the working mechanism of carbon black. These materials form a conductive path between electrodes and in the presence of gas, the polymer swells due to adsorption of gas molecules thus make the carbon composites to move apart from each other breaking the conductive path and increasing the resistance [22].....	16
Figure 2.8 Fabricated CP gas sensor with different polymers embroidery onto cotton strained fabric [42] .....	18
Figure 2.9 Preparation of nanotube micro-yarn by electrospinning (a) Schematic diagram of the process (b) actual image of preparing micro-yarn [45] .....	19
Figure 2.10 (a) the electro spun PAN micro-yarn (b) the helix structure of the micro yarn [45] .....	19
Figure 2.11 Showing the SEM images (a) cotton substrate (b) bare cotton fibres (c) ZnO nanorod coated cotton fibres (d) high magnification image of ZnO nanorods on a cotton fibre, (e) Normal photograph of bare and ZnO nanorods coated fabric (f) multifunctional smart fabric sewn on toy dress [47] .....	20
Figure 2.12 (a) RGOY prepared from micro fibre bundle and on the right the red, blue, black, and white spheres represent O <sub>2</sub> , N <sub>2</sub> , C and H <sub>2</sub> atoms respectively. (b) RGOCY and RGOPY wound on plastic bobbin (c) RGOCY integrated into a fabric (d) wearable gas sensor with an alarm system [54] .....	21
Figure 2.13 Fabrication of MOF textile sensors for NO and H <sub>2</sub> S detection: (a) the materials required for the sensors, cotton swatch, , the triphenylene based ligands and the nickel metallic nodes; (b) the conductive SOFT devices on cotton swatch obtained by solvothermal condensation of reagents in water, with micrographs showing the MOF coating on the cotton fibres and the nanorod texture of the MOF; (c) the sheet resistance measurements of the swatches [58].....	22

Figure 2.14 Gas sensing demonstration – Optical Images. Optical images of BTB, MR, and MnTPP devices for different concentrations of (a) ammonia or (b) HCl and the corresponding RGB colour information extracted from the optical images for (c) ammonia and (d) HCl [7] .....	26
Figure 2.15 (a) Glob top encapsulation and (b) dam and fill type encapsulation [90].....	33
Figure 2.16 (a) Casting (b) Potting and (c) encapsulation [92].....	34
Figure 2.17 (a) non-conformal coating and (b) conformal coating.....	35
Figure 3.1 Showing the mechanism of CO sensing in MOX sensor (a) the oxygen molecules get adsorbed on the surface of the sensing layer on the chip when connected to the battery in presence of air; this attracts electrons from the metal oxide layer (b) in the presence of CO, the oxygen reacts with CO thus releasing allowing the electrons to flow inside the chip which increases the conductivity .....	38
Figure 3.2 (a) Supply and (b) Measurement circuit design recommended in the datasheet (redrawn) of MICS 5524 with equivalent electrical circuit diagram (F,C,G and D are pin details on datasheet) .....	38
Figure 3.3 Schematic illustration of the Mask Layout for modified circuit design using CorelDRAW .....	39
Figure 3.4 a) pouring resist on wafer with copper plated Kapton, b) monitor to set the values of speed and time (c) photoresist coated wafer d) Wafer placed inside oven e) wafer placed in LV202E for UV exposure f) Wafer in the developing solution and then g) etched in the etching tank to get h) circuits by standard photolithography .....	40
Figure 3.5 Flexible circuit strip with gas sensor chip MiCS-5524 attached on Kapton attached to the alumina tile using Kapton tape after mounting SMD resistors.....	41
Figure 3.6 Resistance across the power supplier contact pads and output contact pads (across $820\Omega$ ) is observed using multimeter to check the connection of the components in the flexible sensor strip .....	42
Figure 3.7 Schematic diagram of gas sensor test rig.....	44
Figure 3.8 Experimental setup for detection carbon monoxide gas in fume hood.....	44
Figure 3.9 Showing increase in concentration with increase duration of CO gas passed inside the chamber.....	46
Figure 3.10 Showing decrease in concentration read on the reference sensor.....	46
Figure 3.11 Showing decrease in concentration of CO <sub>2</sub> inside chamber with lid closed over 7 hours.....	48
Figure 3.12 Warm up – the sensors were left on for one hour and a constant increase in voltage is observed .....	49
Figure 3.13 Gas sensor baseline resistance vary with fan on inside the chamber, fan off and chamber lid open.....	50
Figure 3.14 Temperature and Relative Humidity variation showing the temperature increases with decrease in relative humidity for different environmental conditions .....	50
Figure 3.15 Factors influence the baseline resistance when the chamber lid is open.....	51

Figure 3.16 Three sensors placed on hotplate to demonstrate sensor baseline variation for different temperatures.....	51
Figure 3.17 Influence of temperature on sensor voltage.....	52
Figure 3.18 Influence of temperature on sensor baseline resistance.....	52
Figure 3.19 Sensor response by measuring the output voltage for each sensor.....	53
Figure 3.20 Calculated resistance of the gas sensing response of each sensor.....	54
Figure 3.21 Sensor response decreases with increase in concentration of CO gas.....	54
Figure 3.22 Average response and recovery time for all the unencapsulated sensor filaments ..	56
Figure 4.1 Zitex G - 104 bonded to CO filament using Permabond POP Primer and cyanoacrylate semiflexible liquid adhesive .....	59
Figure 4.2 Contact angle measurement [101] .....	60
Figure 4.3 (a) DSA30 Krüss tensiometer for contact angle measurement (b) Zitex G - 104 sample with a droplet .....	60
Figure 4.4 Contact angle measurement for (a) PTFE Fibre glass fabric, (b) PTFE etched side (c) Zitex G - 104 (d) Platilon U 4201 AU (e) Silicon Pressure adhesive (SPA) (f) Acrylic adhesive .....	61
Figure 4.5 Contact angles for one side etched PTFE Fibre glass fabric (etched side), non-etched part of PTFE Fibre glass fabric, Zitex G - 104 and Platilon U 4201 AU 420162	
Figure 4.6 Contact angles for Pressure sensitive adhesives, NLP11051 and acrylic.....	62
Figure 4.7 (a) T-Peel method for demonstrating bond strength of adhesive between flexible materials [102] (b) the average peel force obtained during the test defines the bond strength of the adhesive [103] .....	63
Figure 4.8 Application of NLP11051 on Kapton N for peel test using 500g weight on the roller (standard ASTM F88).....	64
Figure 4.9 (a) tensiometer tensile tester with 1) load cell, 2) movable grip and 3) fixed grip b) closer look of the sample (Zitex G - 104 attached to Kapton with NLP11051) fixed to the grip and forms T shape.....	64
Figure 4.10 Showing three primary adhesive failure modes (a) adhesive failure (b) cohesive failure and (c) substrate failure [103] .....	65
Figure 4.11 Peel strength for PTFE Fibre glass fabric on Kapton N using NLP 11051 for bonding .....	66
Figure 4.12 Peel Strength for PTFE Fibre glass fabric on Kapton N using acrylic adhesive for bonding .....	66
Figure 4.13 Peel Strength for PTFE Fibre glass fabric on Kapton E using acrylic adhesive for bonding .....	66
Figure 4.14 Peel Strength for Zitex G - 104 on Kapton N using NLP 11051 for bonding.....	67
Figure 4.15 Peel Strength for Zitex G - 104 on Kapton N using acrylic adhesive for bonding ..	67
Figure 4.16 Peel Strength for Zitex G - 104 on Kapton E using NLP11051 for bonding .....	67

---

Figure 4.17 Average Peel Strength for PTFE Fibre glass fabric, Zitex G - 104, Platilon U 4201 AU and Kapton E .....	68
Figure 4.18 Maximum Peel Strength for PTFE Fibre glass fabric, Zitex G - 104, Platilon U 4201 AU and Kapton E.....	68
Figure 4.19 SEM image of (a) Kapton N (b) Kapton E (c) Kapton E with uneven epoxy layer.	69
Figure 4.20 (a) Platilon U 4201 AU placed on top of Kapton with epoxy (b) After using heat gun (240°C) until Platilon U 4201 AU .....	69
Figure 4.21 Peel strength for Platilon U 4201 AU on Kapton N using heat gun for bonding – weak bonding .....	70
Figure 4.22 Peel strength for Platilon HL9007 on Kapton N using heat gun for bonding – substrate failure .....	70
Figure 4.23 Peeling test of Platilon U 4201 AU on Kapton with epoxy adhesive using heat gun – substrate failure.....	71
Figure 4.24 Peel strength for Platilon HL9007 on Kapton E using heat gun for bonding.....	71
Figure 4.25 After peel test – the epoxy layer from the Kapton is removed .....	72
Figure 4.26 The thermoplastic film is initially heated until it softens (b) the vacuum is applied and atmospheric pressure forces the softened material on top of the target mould. Image adapted from [15].....	73
Figure 4.27 Front view of Formech 450DT and reduced processing window is shown with flexible electronic test circuit with series resistors .....	74
Figure 4.28 Showing temperature rise with increase in percentage of heating percentage .....	74
Figure 4.29 (a) the material appears translucent and when heated up to desired heat setting and temperature turns to (b) soften, pliable and more transparent state (c) due to the weight of the material and heating it sags and forms rings on the substrate to be vacuum formed .....	75
Figure 4.30 (a) TPU clamped under reduced Kapton N 75 um window gives (b) even vacuum forming over the substrate without forming rings .....	76
Figure 4.31 Showing polyurethane bonds to 75µm thickness Kapton N window on heating in Formech 450DT .....	77
Figure 4.32 Reduced window size with non-etched (both sides) PTFE Fibre glass fabric for vacuum forming.....	77
Figure 4.33 Showing holes created due to overheating at 50% for 70s and above.....	78
Figure 4.34 Showing the material forming a dome when the stage is moved upward using the lever (left) and leaving uneven bonding on to the Kapton substrate (right) ....	78
Figure 4.35 Platilon U 4201 AU (left side) and Platilon HL9007 (right side) vacuum formed on Kapton E – Backside view (Kapton E on top and Platilon U 4201 AU and Platilon HL9007 on bottom). Top part was bonded using heat gun.....	79
Figure 4.36 Peel strength for Platilon U 4201 AU on Kapton E after vacuum forming and using heat gun for bonding .....	79

Figure 4.37 Peel strength for Platilon HL9007 (with hot melt adhesive) on Kapton E after vacuum forming and using heat gun for bonding .....	80
Figure 4.38 Cross section view of simple CO filament on Kapton E.....	81
Figure 4.39 Showing 3 different substrate (Kapton) width Image shows sensor chips places on bare Kapton.....	81
Figure 4.40 (a) Platilon U 4201 AU vacuum formed on the sample with 1cm width (b) and not sealed well at the sides due to the size of the chip .....	81
Figure 4.41 (a) vacuum formed using PU forms bubble around the chip due to straight sides (not angled) (b) reduced bubble size due to usage of heat gun and applying vacuum again.....	82
Figure 4.42 Samples positioned at extreme right, centre, and extreme left under the window for vacuum forming.....	82
Figure 4.43 (a) vacuum formed with Platilon U 4201 AU (b) bubble around the chip due to the dome formed after pulling the lever forward to bring the samples near the softened material.....	83
Figure 4.44 The vacuum formed Platilon U 4201 AU on the samples. The top and bottom are well moulded (vacuum formed well whereas the sample at the centre is not) than the centre .....	83
Figure 4.45 (a) vacuum formed using PU forms bubble around the chip due to straight sides (not angled) (b) reduced bubble size due to usage of heat gun and applying vacuum again.....	84
Figure 4.47 (a) flexible CO sensor strip attached the Kapton with epoxy (b) attaching the wires by soldering to the contact pads .....	85
Figure 4.48 (a) Sample placed in vacuum former table/stage (b) Platilon U 4201 AU vacuum formed on flexible sensor strip .....	86
Figure 4.49 (a) blisters or tiny bubbles on Platilon U 4201 AU after heating with heat gun at 240°C (b) wire is cut due to the pressure created between the table and the window	86
Figure 4.50 (a) 3D printed male (top) and female (bottom) moulds with material Verclear (b) 3D printed male mould (top) and PDMS female mould (bottom) .....	87
Figure 4.51 (a) Zitex G - 104 is cut into dimensions of actual circuit strip (b) after moulding using both 3D printed, and 3D printed with PDMS moulds (horizontal view) (c) PDMS + 3D printed moulding gives more conformality than both 3D printed moulds (vertical view) (d) tearing of material when 3D moulds are used and is solved by using PDMS mould .....	87
Figure 4.52 CorelDraw design for adhesive film and solid mould for bonding (a) for the PSA and (b) for the Zitex G - 104 and PTFE Fibre glass fabric encapsulants .....	88
Figure 4.53 (a) Graphtec Cutting Plotter CE600-40 (b) cut samples of adhesives – NLP 11051 (top) and acrylic adhesive (bottom) (c) cut samples of Zitex G - 104 (top) and PTFE Fibre glass fabric (bottom) .....	89
Figure 4.54 Heat press used for bonding NLP 11051 and Zitex G - 104 .....	90
Figure 4.55 Packaging assembly for Zitex G - 104 and PTFE Fibre glass fabric on flexible CO circuit strip.....	90



Figure 4.56 Showing Zitex G - 104 after packaging not sealed at the (a) side A and (b) side B.	91
Figure 4.57 Zitex G - 104 on substrate width of 1.5 and 2cm .....	91
Figure 4.58 Peel Strength for Kapton E and Kapton N bonded using NLP11051 – adhesive failure .....	92
Figure 4.59 Peel Strength for Kapton E on Kapton N bonded using acrylic adhesive – cohesive failure .....	92
Figure 4.60 Peel Strength for Kapton E on Kapton N using NLP11051 and acrylic adhesive....	92
Figure 4.61 Peel Strength for Kapton E on Kapton N using two acrylic adhesives .....	93
Figure 4.62 (a) Packaging assembly for flexible CO circuit strip with additional Kapton (b) simple cross section of the packaged flexible sensor .....	94
Figure 4.63 Zitex G - 104 (top) and PTFE Fibre glass fabric (bottom) encapsulated flexible CO sensor .....	94
Figure 4.64 Width of the sample strip of (a) PTFE Fibre glass fabric before moulding (b) PTFE Fibre glass fabric after moulding (c) Zitex G - 104 before moulding and (d) Zitex G - 104 after moulding .....	95
Figure 5.1 Cotton woven fabric with pockets open at both ends .....	97
Figure 5.2 Gas sensing response before and after encapsulating with PTFE Fibre glass fabric a) Sensor 1, b) Sensor 2 and c) Sensor 3.....	98
Figure 5.3 Gas Sensing response before and after encapsulating with Platilon U 4201 AU for sensor 7 .....	99
Figure 5.4 Gas sensing response before and after encapsulating with Zitex G - 104 a) Sensor 4, b) Sensor 5 and c) Sensor 6.....	101
Figure 5.5 Gas Sensing response before and after encapsulating with Zitex G – 104 for sensor 4 5 and 6.....	102
Figure 5.6 Gas Sensing response before and after encapsulating with Platilon U 4201 AU) Sensor 7, b) Sensor 8 and c) Sensor 9 .....	103
Figure 6.1 Neutral axis when flexible materials are subjected to bending [14].....	105
Figure 6.2 Neutral axis analysis for a) unencapsulated filament, b) PTFE Fibre glass fabric, c) Zitex G - 104 and d) Platilon U 4201 AU encapsulated filament.....	107
Figure 6.3 Bending rig for cyclic bending connected to microcontroller for setting number of cycles, position, and speed.....	108
Figure 6.4 Change in resistance due to bending and number of bending cycles survived by unencapsulated filament.....	110
Figure 6.5 Change in resistance due to bending and number of bending cycles survived by PTFE Fibre glass fabric encapsulated filament.....	111
Figure 6.6 Change in resistance due to bending and number of bending cycles survived by Zitex G - 104 filament.....	112
Figure 6.7 Change in resistance due to bending and number of bending cycles survived by Platilon U 4201 AU filament .....	113

Figure 6.8 Average number of cycles survived by all the unencapsulated filament, PTFE Fibre glass fabric, Zitex G - 104 and Platilon U 4201 AU encapsulated filaments	113
Figure 6.9 a) Without encapsulant b) with PTFE Fibre glass fabric c) With Zitex G - 104 d) with TPU	114
Figure 6.10 Cotton woven fabric with pockets open at one end and other end sewed	115
Figure 6.11 Washing machine WME7247 Beko with 58min wash cycle at 40°C, 1000 rpm and 15min spin for all the filaments	115
Figure 6.12 Percentage change in resistance across the filament of Unencapsulated filaments with wash cycles	117
Figure 6.13 Gas sensing response of Unencapsulated CO filaments after every 3 <sup>rd</sup> wash cycles for 45ppm	117
Figure 6.14 Percentage change in resistance across the filament of PTFE glass fibre fabric encapsulated filaments with wash cycles	118
Figure 6.15 Gas sensing response of PTFE glass fibre fabric encapsulated CO filaments after every 3 <sup>rd</sup> wash cycles for 45ppm	119
Figure 6.16 Percentage change in resistance across the filament of Zitex G - 104 fibre fabric encapsulated filaments with wash cycles	120
Figure 6.17 Gas sensing response of Zitex G - 104 encapsulated CO filaments after every 3 <sup>rd</sup> wash cycles for 45ppm	120
Figure 6.18 Percentage change in resistance across the filament of Platilon U 4201 AU encapsulated filaments with wash cycles	121
Figure 6.19 Percentage change in gas sensor response for unencapsulated and Zitex G - 104 and PTFE glass fibre fabric encapsulated filaments	122
Figure 6.20 Average and Maximum number of wash cycles survived by unencapsulated filaments, PTFE Fibre glass fabric, Zitex G - 104 and Platilon U 4201 AU encapsulated filament	122
Figure 6.21 Filament functionality failure due to cracks in the copper tracks after washing (a) PTFE (b) Zitex G - 104 and (c) Platilon U 4201 AU encapsulated filament	123
Figure 7.1 Wheatstone's bridge circuit design and simulation on Multisim	125
Figure 7.3 (a) Pin details of VOC sens NO <sub>2</sub> bare die and (b) the bare die attached to the rigid PCB before wire bonding	126
Figure 7.4 Showing (a) and (b) wires bonded to rigid PCBs from (c) pin 3 and pin 6 of the NO <sub>2</sub> bare die	127
Figure 7.5 Flexible NO <sub>2</sub> sensor design representing Wheatstone's bridge	127
Figure 7.6 Sensor response for Daeger NO <sub>2</sub> sensor for different duration of flow regulator valve opening	129
Figure 7.8 Leak test with NO <sub>2</sub> reference sensor – average 50s for 46.6ppb, 80ppb and 120ppb, 70s for 140ppb and 80s for 180ppb	130
Figure 7.9 Showing SEM image of small remains of the sensitive material on the IDE of the NO <sub>2</sub> bare die	130

Figure 7.10 Baseline voltage measurement for the flexible NO<sub>2</sub> filament ..... 131

Figure 7.11 Output Voltage measurement for the flexible NO<sub>2</sub> filament for 180ppb of NO<sub>2</sub>  
experiment 1 ..... 131

Figure 7.12 Output Voltage measurement for the flexible NO<sub>2</sub> filament for 180ppb of NO<sub>2</sub>  
experiment 2 ..... 132



## Research Thesis: Declaration of Authorship

Print name: Ashwini Valavan

Title of thesis: Investigation of Encapsulant Materials for Packaging Flexible Gas Sensor for E-textile Application

I declare that this thesis and the work presented in it are my own and has been generated by me as the result of my own original research.

I confirm that:

1. This work was done wholly or mainly while in candidature for a research degree at this University;
2. Where any part of this thesis has previously been submitted for a degree or any other qualification at this University or any other institution, this has been clearly stated;
3. Where I have consulted the published work of others, this is always clearly attributed;
4. Where I have quoted from the work of others, the source is always given. With the exception of such quotations, this thesis is entirely my own work;
5. I have acknowledged all main sources of help;
6. Where the thesis is based on work done by myself jointly with others, I have made clear exactly what was done by others and what I have contributed myself;
7. None of this work has been published before submission Parts of this work have been published as:-

Signature: ..... Date: .....

## **Acknowledgements**

This research was funded in the UK by the Engineering and Physical Sciences Research Council (EPSRC) via the project: Wearable and Autonomous Computing for Future Smart Cities Grant number: EP/P010164/1. This Ph.D. would not have been possible without securing the funding of this work. I'd like to thank my supervisor Prof. Steve Beeby for firstly giving me an opportunity to pursue a PhD and for constantly encouraging and motivating me during tough times. I would like to thank Dr. Nick Harris and Dr. Abiodun Komolafe for guiding and supporting me especially. They were very helpful in making time to clear any doubts throughout my PhD. I would also like to thank my colleagues I worked with especially Dr. Zeeshan, Dr. Yang Wei, Dr. Watcherapong, Dr. Russel, Dr. Sasikumar, Dr. Yi Li, Dr. Nick Hillier, Dr. Mahmoud Wagih and Dr. Chiranjeevi and Betul Gokkaya. A very special thanks to Glenn Topley for helping me with mechanical work involved in building gas testing rigs, I would also like to thank Mark Long and Jamie Stone for mechanical work involving 3D moulds. A very special thanks to Antony Woods and Jeff Hooker for helping me with lab equipment during difficult times without which I would have struggled finishing work on time.

Finally, I would like to convey my sincere thanks to my parents Indira and Valavan without whom I wouldn't have come this far in life and would like to thank them for constantly providing encouragement and providing good education throughout my life and for being there during my happy and hard times. I would also like to convey my sincere thanks to my brother Bala Muthiah and my sister-in-law Rachel, and lovely Alice and Lili. Lastly, I am truly grateful for having gained the best set of friends over years who motivated me and have been there throughout my difficult times. I would like to specially mention Sneha who was there every single day to motivate me and to have happy conversation outside of my research. I would like to thank Sandhiya, Palani, Gobiha and Arjun for being there to help me out with technical concepts. A very special thanks to Monika and Patty for all the wonderful advice and help over a coffee break which truly helped me being motivated. A special thanks to Sandeep Surya for proof-reading my thesis.

## **Definitions and Abbreviations**

<b>EPSRC</b>	Engineering and Physical Science Research Council
<b>FETT</b>	Function Electronic Textiles Project
<b>EPSRC</b>	Engineering and Physical Sciences Research Council
<b>EDIP</b>	Electronic Bare Die in Plastic
<b>E-textile</b>	Electronic Textile
<b>MEMS</b>	Micro-Electro Mechanical Systems
<b>SEM</b>	Scanning Electronic Microscope
<b>SMD</b>	Surface Mount Components
<b>1D</b>	One Dimensional
<b>2D</b>	Two Dimensional
<b>3D</b>	Three Dimensional
<b>I2C</b>	Inter-integrated Circuit
<b>LED</b>	Light Emitting Diode
<b>MOX</b>	Metal Oxide Semiconductor
<b>NDIR</b>	Nondispersive Infra-Red
<b>SAW</b>	Surface Acoustic Wave
<b>QCM</b>	Quartz Crystal Microbalance
<b>CMU</b>	Capacitive Micromachined Ultrasonic Transducer
<b>FBAR</b>	Film Bulk Acoustic Resonator
<b>MOF</b>	Metal Organic Frameworks
<b>PCB</b>	Printed Circuit Board
<b>SOI</b>	Silicon on Insulator
<b>SPE</b>	Solid Polymer Electrolyte

<b>PC</b>	Personal Computer
<b>IDE</b>	Interdigitated Electrodes
<b>DC</b>	Direct Current
<b>SA</b>	Self Adhesive
<b>ALD</b>	Atomic Layer Deposition
<b>CDA</b>	Clean Dry Air
<b>RT</b>	Room temperature
<b>OSHA</b>	Occupational Safety and Health Administration
<b>Ppm</b>	Parts per million
<b>Ppb</b>	Parts per billion
<b>NA</b>	Neutral Axis
<b>F(ec)</b>	Failure due to electrical connectivity
<b>F(en)</b>	Failure due to encapsulation layer
<b>F(b)</b>	Failure due to bonding

### **Chemicals and Materials**

<b>CO</b>	Carbon monoxide
<b>CO<sub>2</sub></b>	Carbon dioxide
<b>NO<sub>2</sub></b>	Nitrogen dioxide
<b>SO<sub>2</sub></b>	Sulphur dioxide
<b>PM</b>	Particulate matter
<b>O<sub>3</sub></b>	Ozone
<b>CH<sub>4</sub></b>	Methane
<b>Cl<sub>2</sub></b>	Chlorine
<b>F<sub>2</sub></b>	Fluorine



<b>N<sub>2</sub>O</b>	Nitrous oxide
<b>O<sub>2</sub></b>	Oxygen
<b>NH<sub>3</sub></b>	Ammonia
<b>C<sub>2</sub>H<sub>5</sub>OH</b>	Ethanol
<b>HCL</b>	Hydrochloric acid
<b>PSA</b>	Pressure Sensitive Adhesive
<b>SPA</b>	Silicone Pressure Adhesive
<b>IPA</b>	Isopropyl alcohol
<b>VOC</b>	Volatile Organic compounds
<b>DI</b>	Deionized
<b>DMMP</b>	dimethyl methyl phosphonate
<b>PTFE</b>	Polytetrafluorethylene
<b>PEDOT: PSS</b>	Poly(3,4-ethylenedioxythiophene)-poly (styrene sulfonate)
<b>PPy</b>	Polypyrrole
<b>SWCNT</b>	Single walled carbon nanotube
<b>MWCNT</b>	Multiwalled carbon nanotube
<b>SWNT-COOH</b>	Carbon nanotube, single-walled, carboxylic acid functionalized
<b>PSMA</b>	Polystyrene-co-maleic anhydride
<b>PVP</b>	Polyvinylpyrrolidone
<b>PSE</b>	Poly (styrene-co-maleic acid) partial isobutyl/methyl mixed ester
<b>PAN</b>	Peroxyacetyl nitrate
<b>PVA</b>	Polyvinyl alcohol
<b>MnTPP</b>	5,10,15,20-Tetraphenyl-21H,23H-porphine manganese (III) chloride
<b>MR</b>	Methyl red

<b>BTB</b>	Bromothymol blue
<b>PDMS</b>	Polydimethylsiloxane
<b>PE</b>	Polyethylene
<b>PA</b>	Polyamide
<b>PEN</b>	Polyethylene Naphthalate
<b>PVC</b>	Polyvinylchloride
<b>PI</b>	Polyimide
<b>PET</b>	Polyethylene terephthalate
<b>EVA</b>	Ethylene-vinyl acetate
<b>PET</b>	Polyethylene terephthalate
<b>RGO</b>	Reduced Graphene oxide
<b>RGOCY</b>	Reduced Graphene oxide cotton yarn
<b>RGOPY</b>	Reduced Graphene oxide polyester yarn
<b>Kapton N</b>	Normal Kapton
<b>Kapton E</b>	Kapton with epoxy

### **Metals**

<b>Pt</b>	Platinum
<b>Ti</b>	Titanium
<b>Au</b>	Gold
<b>Ag</b>	Silver
<b>Pd</b>	Palladium

### **Symbols in Equations**

<b>R<sub>0</sub></b>	Resistance of sensor in ambient air
<b>R<sub>s</sub></b>	Resistance of sensor in presence of gas

<b><math>R_L</math></b>	Load Resistance
<b><math>Q</math></b>	Flow rate of gas
<b><math>D</math></b>	Diffusion coefficient
<b><math>A</math></b>	Area
<b><math>dc</math></b>	Change in concentration
<b><math>dx</math></b>	Change in length
<b><math>V_s</math></b>	Supply voltage
<b><math>V_L</math></b>	Voltage across load resistor

## **Glossary of Terms**

<b>Average</b>	Sum of number of samples divided by number of samples
<b>Response</b>	Ratio of resistance in presence of gas to resistance in air
<b>Electrode</b>	Electrical contact on sensing device for measurements
<b>Fabric</b>	Material fabricated by weaving or knitting using yarns
<b>Polymer</b>	Chemical material made of repeating molecules to form a chain
<b>Substrate</b>	Base material on which other components are built on
<b>Washability</b>	Ability of a material to withstand washing
<b>Durability</b>	Ability of a material to withstand mechanical stress
<b>Ground looping</b>	Two or many circuits having the same group which causes potential difference and affects the output of the sensors
<b>Melt Processible</b>	Ability of a material to melt when heat is applied at a certain temperature
<b>Glass transition temperature</b>	Temperature at which material changes from rubber solid state to soft pliable state
<b>Relative humidity</b>	Amount of water vapour in air to the maximum amount of water the air can store
<b>Diffusion coefficient</b>	Proportionality constant between the molar flux to molecular

## Chapter 1 Introduction

Among the types of pollutions such as noise, water, light, soil and thermal, the World Health Organization (WHO) considers air pollution to be the most dangerous, carrying major health risks to humans [1]. The addition of harmful gases (pollutants) into air mainly due to sources like industries (e.g., power plants, factories), vehicles, electric utilities can result in an unhealthy environment depending on pollutant concentration. Pollutants can be classified into two types: primary pollutant and secondary pollutants. Primary pollutants are formed and emitted from a source directly. Examples include carbon dioxide (CO<sub>2</sub>), carbon monoxide (CO), hydrogen sulphide (H<sub>2</sub>S), ammonia (NH<sub>3</sub>), nitrogen dioxide (NO<sub>2</sub>), sulphur dioxide (SO<sub>2</sub>), volatile organic compounds (VOC) and particulate matter (PM). Secondary pollutants are formed by the interaction between two primary pollutants (e.g. Ozone O<sub>3</sub>) [2][3]. Exposure to these air pollutants (depending on the concentration) could lead to devastating health issues endangering vital body organs such as the eye, skin, respiratory and nervous systems.

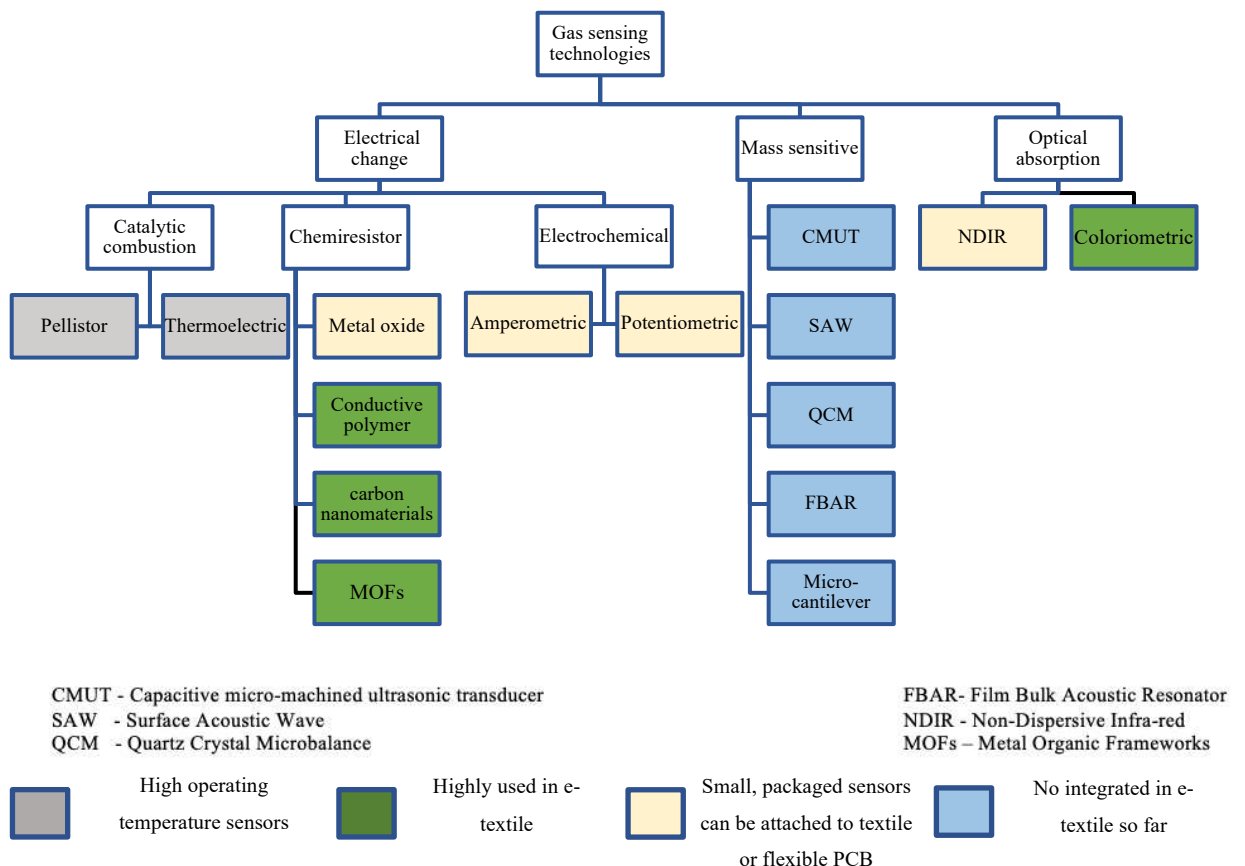


**Figure 1.1 Different types of gas sensing mechanisms**

Recent studies also showed that even at low concentration of PM 2.5 and NO<sub>2</sub> can cause heart problems [4][5]. Hence, it is important for an individual to monitor the quality of the air they inhale

even for very low pollutant concentrations. Gas sensors can provide continuous monitoring of air quality. It detects and monitor the concentration of one or more gas molecules present in the air by converting the gas concentration into an electronic signal. An array of different gas sensors is typically used for sensing different gases at the same time. Gas sensors are classified on their sensing mechanism and these range from the use of metal oxide semiconductor (MOS), conductive polymer, catalytic combustion, electrochemical, to non-dispersive infrared (NDIR) [6]. Hence, the above fig 1.1 briefly depicts the various kinds of gas sensing technologies.

## **1.1 Introduction to Electronic Textiles (e-textiles)**

E-textiles are a class of wearable sensors that disguise sensors inside a piece of fabric making them invisible to the user [7]. This can be achieved by using a variety of technologies such as weaving [8], knitting, embroidery [9], screen printing [10] and ink-jet printing [11]. E-textiles are applicable in a wide range of field such as military and medical applications. One such example is a textile based electrochemical sensor that continuously monitors and detects the glucose level of diabetic patients in real-time by using sweat samples[12]. MIT has built a toxic gas detector in the form of badges that can be attached to the apparel of the soldiers to sense sarin in the battle field [13] but in this case the sensor is simply attached to a fabric rather than integrated within it. As sensors are being integrated in textiles, it is important to retain the properties of textiles such as drape, flexibility, bendability, twistability, washability, and durability without affecting the performance of the sensor. Most of the e-textile gas sensors are claimed to be mechanically robust and ideally waterproof and washable with good repeatability and reproducibility. This requires flexible device that can be coated with a suitable encapsulating material that does not affect the performance of the sensor.

### **1.1.1 Platform technology in Functional Electronics Textiles (FETT) project**

The FETT project integrates electronics into the core of the yarn which can be woven or knitted on to textiles as a part of e-textile. These are 1D electronic strips of width ranging from 0.8 mm to 2.0 mm containing small dimensional components like microcontrollers and LEDs. This strip can be integrated into a yarn as shown in fig 1.2 or incorporated into textiles pockets formed during the weaving process shown in fig 1.3 leaving the circuit invisible to the wearer [14][15]. The project has demonstrated a novel packaging technology that encapsulates die attached to the Kapton substrate using a thermally moulded Kapton. This project concluded this type of packaging ensured the flexible strip survived more than 1500 bending cycles and up to 45 wash cycles [15].

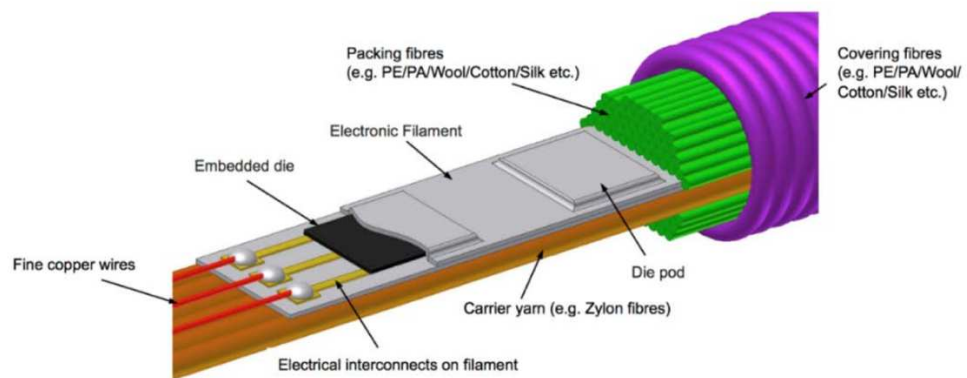


Figure 1.2 Schematic diagram of electronic filament inside a yarn [15]

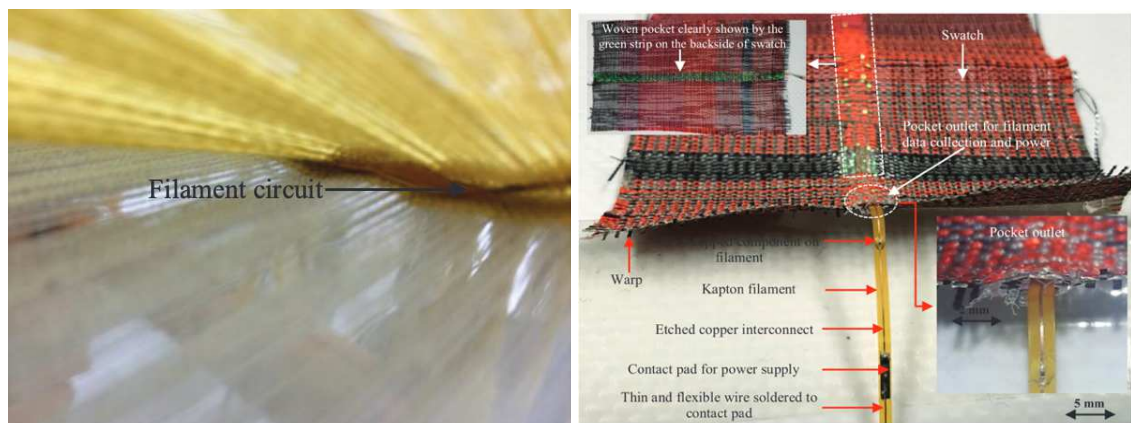


Figure 1.3 Electronic filament placed in the pocket by weaving process

### 1.1.2 Application of Functional Electronics Textiles (FETT) project to gas sensors

The FETT project has integrated microcontrollers and LEDs onto flexible substrate like Kapton, however they have not demonstrated integration and packaging of gas sensors for e-textile application. This thesis describes the application of the FETT packing technology to gas sensors for e-textiles by vacuum forming. This involves the investigation of influence of the packaging process and encapsulating film on the performance of the gas sensor. The reliability of the packaged flexible gas sensor is investigated by mechanical bending and machine-washing tests. The packaged flexible sensor circuit will be integrated into textile by weaving the filament into a piece of fabric.

## 1.2 Aim

To investigate the influence of encapsulated flexible gas sensing system with different thermoplastic material on the performance of the sensor. The encapsulated system should survive from mechanical stress caused by bending and twisting of the e-textile. It should also be waterproof,

washable, and unaffected by detergent used during washing such that it is suitable for a real time e-textile pollution monitoring application.

### 1.3 Objectives

- Build a test rig for gas sensing calibration of the flexible gas sensing system with carbon monoxide
- To demonstrate a flexible gas sensing circuit to detect carbon monoxide
- To investigate the performance of the flexible gas sensing circuit for different concentrations of carbon monoxide
- To demonstrate the performance of encapsulated flexible gas sensing circuit for different concentrations of carbon monoxide
- To establish the degree of waterproofing and ability to survive bending and washing cycles and survive exposure to detergents while washing the encapsulated gas sensing system
- To build an e-textile electronic gas sensing system to measure nitrogen dioxide and evaluate the sensor performance after encapsulating and compare the results with sensor response to carbon monoxide

### 1.4 Statement of Novelty

This work demonstrates the first application of (Functional Electronics Textiles) FETT packaging technology for flexible gas sensors and comprehensive evaluation of encapsulating materials and their effect on performance of the e-textile gas sensor based on discrete Micro electromechanical systems (MEMS) gas sensor. This includes:

- Demonstrating a working flexible gas sensor filament
- Identification of thermoplastic materials that are breathable, waterproof, and suitable for encapsulating the flexible gas sensing filament.
- Demonstrating a practical e-textile gas sensor system using the flexible circuit technology.

### 1.5 Thesis structure

A brief explanation on each topic is discussed below with a schematic representation of the research methodology shown in Fig 1.4.



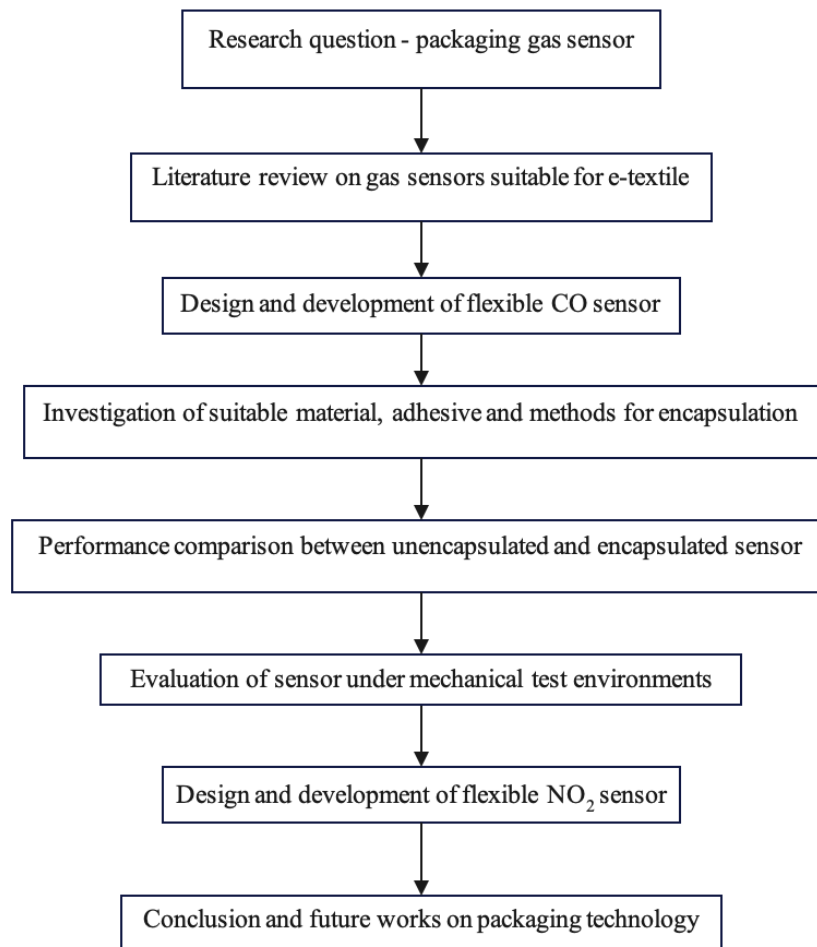


**Figure 1.4 Schematic diagram of the methodological framework for the research**

□ **Chapter 1: Introduction**

This chapter includes an introduction about e-textiles gas sensors and need for encapsulation. It includes the background of encapsulation technology used in FETT project using thermoset Kapton for packaging flexible sensor and its use in packaging an e-textile gas sensor.

□ **Chapter 2: Gas Sensing technologies and Encapsulation Techniques – A Review**

This chapter includes a review on different types of gas sensing technologies based on structure and working principle (thermal, electrical, mass sensitive and absorption of light), review on flexible gas sensor that can be potentially used in e-textile and review on e-textile gas sensors. This chapter also includes a detailed review of various encapsulating techniques and techniques used for e-textile gas sensors. The outline of this chapter is given below,

- o Solid state gas sensors–Working principle of Catalytic Combustion, electrochemical and Chemiresistor – Metal oxide semiconductor, Conductor polymer, Carbon nanomaterials (carbon black, carbon nanotube/nanofibre, Graphene) and metal organic frameworks
- o Mass sensitive gas sensors–Working principle of Surface Acoustic wave, Quartz Crystal microbalance, Film Bulk acoustic resonator, microcantilever and capacitive micromachines ultrasonic transducer
- o Optical absorption–Working principle of non–interactive Infrared and colorimetric gas sensor and their application in e-textile
- o Discussion–A brief discussion on various types of gas sensor and their efficiency in terms of sensing and potential in e-textile application in terms of number of bending and washing cycles flexible gas sensor can withstand. This brings the need for packaging flexible gas sensor for more durability
- o Review of encapsulation techniques – Glob top and dam and fill, Casting, potting and encapsulation, conformal coating and encapsulation technology used in gas sensor and in e-textile gas sensor

□ **Chapter 3: Flexible Carbon Monoxide Sensor – Design and Characterisation**

- o Fabrication of flexible circuit strips - The schematic design of flexible carbon monoxide gas sensor with commercially available chip MICS 5524. A detailed explanation of fabricating flexible sensor by standard lithography technique is explained that includes substrate preparation, pattern transfer by UV exposure using UV box and mounting of SMD components using solder paste and the reflow oven for curing the solder paste.
- o Experimental setup of gas sensor testing chamber - This chapter also includes the experimental setup for gas sensing. The schematic design of the testing rig and an actual image of the experimental setup is given and explained. The experimental rig is a small plastic chamber with a reference carbon monoxide sensor, cables for measuring output of flexible gas sensors and flexible gas sensors fixed to the walls of the plastic chamber, and inlet for gas from a gas cylinder with a constant flow controller, wireless Bluetooth connected temperature and humidity sensor and a fan for uniform distribution of incoming gas.

o Characterization of gas testing chamber - This chapter includes the characterization of the reference sensor and characterization of the flexible gas sensor. This includes warm-up time evaluation of MiCS-5524 gas sensor chip and testing of MiCS-5524 with carbon monoxide.

□ **Chapter 4: Encapsulation Process and Materials Evaluation**

o Selection of materials for packaging flexible gas sensor - This chapter includes the materials that have been used for the investigation of best suited encapsulating material for a flexible CO gas sensor.

o Types of adhesives used for packaging—Theory of flexible adhesives film in the form of heat laminator, acrylic and silicone adhesives are explained in this chapter.

o Contact angle, swelling test and peeling test - The hydrophobicity test for these materials by contact angle measurement and swelling test are reported in this chapter. The bond strength was measured by peeling test for different types of adhesives.

o Process for packaging gas permeable and waterproof materials on flexible gas sensing system - The process for encapsulating the flexible circuit is explained for vacuum forming and mould processing for thermoplastic materials in this chapter.

□ **Chapter 5: Gas sensing of textile integrated flexible CO sensor**

o Gas sensing experiments for encapsulated circuits-the encapsulated circuits are tested with carbon monoxide and the performance of the encapsulated and unencapsulated circuits are reported. The gas sensing performance of the packaged sensors inside textile pocket is also reported.

□ **Chapter 6: Evaluation of e-textile Gas Sensor under Mechanical Stresses - bending and washing environments**

The encapsulated circuits are tested for their mechanical stability by bending tests and washing in the washing machine using detergents. The procedure and results are presented the number of bending and washing cycles the encapsulated circuits can withstand.

This chapter will report the integrating of encapsulated flexible sensors by weaving them into a piece of fabric. The textile integrated sensors are exposed to carbon monoxide and the results will be reported.

□ **Chapter 7: Flexible Nitrogen Dioxide Gas Sensor**

This chapter will include the design of flexible nitrogen dioxide sensor and the fabrication process by standard lithography technique. This chapter will also include the characterization of nitrogen reference sensor and flexible nitrogen dioxide sensors.

□ **Chapter 8: Conclusion and Future Recommendations**

This chapter will conclude by addressing the research gap and comparing the results achieved with the aim and objectives of the thesis

## 1.6 List of publications

- Valavan, A.; Komolafe, A.; Harris, N.; Beeby, S. Encapsulation Process and Materials Evaluation for E-Textile Gas Sensor. *Proceedings* **2019**, *32*, 8 <https://doi.org/10.3390/proceedings2019032008>.
- Komolafe, A.; Wagih, M.; Valavan, A.; Ahmed, Z.; Stuijks, A.; Zaghari, B. A Smart Cycling Platform for Textile-Based Sensing and Wireless Power Transfer in Smart Cities. *Proceedings* **2019**, *32*, 7. <https://doi.org/10.3390/proceedings2019032007>
- A. Valavan, A. Komolafe, N. R. Harris and S. Beeby, "Vacuum Thermoforming for Packaging Flexible Electronics and Sensors in E-Textiles," in *IEEE Transactions on Components, Packaging and Manufacturing Technology*, vol. 13, no. 5, pp. 715-723, May 2023, doi: 10.1109/TCPMT.2023.3283015.

## Chapter 2 Gas Sensing Technologies and Encapsulation Techniques – A Review

There are different types of gas sensing techniques based on the working principle. Gas sensors work on adsorption or absorption of gas molecules on the sensing material present in the sensor. These process cause changes in the sensor which can be divided into (1) an electrical change (change in resistance, conductance, or impedance) or (2) change in the resonant frequency. The optical gas sensors like NDIR (Non-dispersive Infrared - NDIR) are based on the absorption of light by the gas molecules. In this chapter, the principle of operation for different types of gas sensors and their potential in the textile application are discussed.

### 2.1 Solid state gas sensors

Solid state gas sensors have no moving parts making them small and highly suitable for portable applications. They can detect very low gas concentrations such as in the range of parts per billion (ppb). The concentration of a gas by a solid-state sensor is generally given by the change in resistance or conductance of the sensor. Based on this, they are broadly classified as (a) catalytic combustion, (b) electrochemical and (c) chemiresistor.

#### 2.1.1 Catalytic Combustion

The catalytic combustion gas sensor (CCGS) is based on the ignition of combustible gases in the presence of a catalyst that results in a change of the resistance or voltage of the sensor. In some cases, the gases require a certain temperature for combustion to occur which is provided by the heater. An example is a pellistor gas sensor based on Wheatstone's bridge that has two coils as the heater and as a resistance thermometer, along with an active (sensing bead with catalyst) and inactive bead (reference). Due to the combustion process in the presence of combustible gas, the active bead becomes hot causing difference in temperature (affecting the resistances) between active and inactive bead [16]. Another type is the thermoelectric gas sensor. It works on the Seebeck effect that gives change in voltage due to the change in the temperature. The CCGS has an operating temperature that ranges from 80-100° [17]. Thermal conductivity gas sensor works by heating a coil at a certain temperature such that the heat is transferred from the device to the environment and the concentration of gas is measured by detecting the amount of heat transferred depending on the thermal conductivity of the gas. This type of sensor cannot detect gases that have thermal conductivity equal to air (such as nitrogen, oxygen and carbon monoxide) [17] [18].

### 2.1.2 Electrochemical

Electrochemical gas sensors (EGS) as shown in Fig 2.1 (a) consist of a working electrode, reference electrode, an electrolyte (solid in MEMS type sensors) and a porous membrane that allows the gas to diffuse through. When a target gas gets oxidized or reduced at the working electrode terminal, it generates a current due to the movement of electrons produced during the redox reaction in the external wiring and the current is proportional to the gas concentration. This type of EGS is called an amperometric sensor. Another type of EGS is the potentiometric sensor that gives a voltage signal equivalent to the concentration of the gas. It measures the potential due to the concentration difference between the working electrode and the reference electrode. In the Proetex FP6 project, T.Radu et al. designed a potentiometric CO<sub>2</sub> sensing boot by fixing a commercially available sensor with a wireless module [19]. The sensor was fixed to a waterproof pocket of the boots such that it allows only gas to pass through. A Zigbee module was used for transmission of data and the results were viewed using the software HyperTerminal in a remote PC. This wearable sensor was able to detect gas concentration up to 42800ppm.

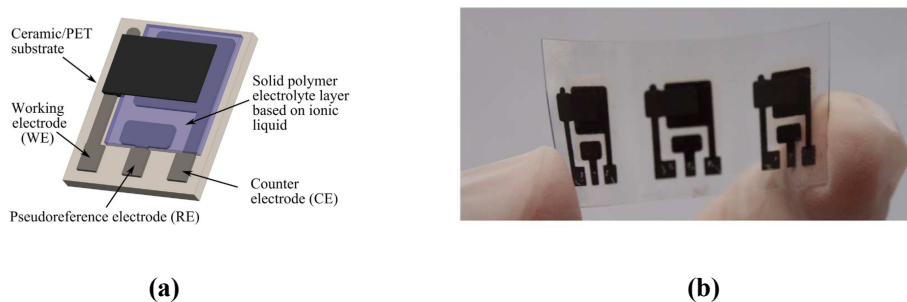


**Figure 2.1 (a) Topology of an electrochemical sensor (b) screen printed electrochemical as a sensor on PET foil [20]**

Although this sensor is highly sensitive to gas and waterproof which is desirable for e-textile applications, it lacks flexibility, consumes more power, and requires heavy batteries and quickly depletes the battery. Electrochemical sensors can be made flexible and compact by using solid polymer electrolyte (SPE). Flexible EGS was fabricated by screen-printing the SPE on polyethylene terephthalate (PET) foil with screen-printed electrodes from graphite ink [20] is shown in Fig 2.1 (b). The SPE layer was formed by ionic liquid [C2mim] [NTf2], poly (vinylidene fluoride) matrix (PVDF) and 1-methyl-2-pyrrolidone. It is an amperometric sensor that gives current in the presence of gas. This sensor detects a minimum concentration of 0.006 ppb of NO<sub>2</sub>. Humidity from 10-90% has no significant effect, however, the effect of wash cycles and bending cycles on the sensor response have not been reported.

### 2.1.3 Chemiresistor

Chemi-resistor sensors (CRS) change their electrical resistance when exposed to target gases. They are classified into three categories (a) metal oxide semiconductors (MOS), (b) conductive polymers, and (c) carbon nanomaterials. The CRS works based on electron-hole interaction in the sensing mechanism which mainly depends on the electron acceptor or donor capabilities of the target gas. Gases that are electron donor (reducing gases) are Methane (CH<sub>4</sub>), Carbon Dioxide (CO<sub>2</sub>), Sulfur Dioxide (SO<sub>2</sub>) and Ammonia (NH<sub>3</sub>), Electron Acceptor gases (oxidizing gases) include are Nitrogen Dioxide (NO<sub>2</sub>), Chlorine (Cl<sub>2</sub>), Fluorine (F<sub>2</sub>), Nitrous Oxide (N<sub>2</sub>O), Oxygen (O<sub>2</sub>) and Ozone (O<sub>3</sub>). It is important that the sensing material in the CRS has high selectivity towards the target gas and avoids cross-sensitivity. The resistance of the system that determines the target gas concentration is measured using two or four probe resistance measurement, or simply by using multimeter such as Keithley. The different types of CRS based gas sensing techniques are discussed in this section.

#### 2.1.3.1 Metal-Oxide semiconductor (MOX or MOS) gas sensor

Metal oxide semiconductors gas sensors are semiconductor type sensors that offer low cost with high sensitivity and low power consumption. In the presence of air, for an n-type MOS sensor, the sensitive layer adsorbs oxygen molecules on its surface which attracts the electrons in the MOS due to the high electron affinity of oxygen. In the presence of reducing gas (loses electrons), an oxidation reaction takes places between the gas molecules and oxygen layer, thus removing the adsorbed oxygen layer from the surface. This reaction will release the electrons that were held on the grain boundary of MOS due to oxygen thus there is a decrease in the potential barrier, and this increases conductivity. When the concentration of the oxygen is very minimal, the metal oxide layer is heated with the help of a heater such that there is a flow of electrons near the grain boundary [21].

**Table 2.1 Working of MOX gas sensor based on the nature of target gas [22]**

Type of Sensing material	Oxidising gas	Reducing gas
N type	Resistance increases	Resistance decreases
P type	Resistance decreases	Resistance Increases

The n-type MOX gas sensor works in the opposite way when an oxidising gas meets the MOX as shown in table 2.1. Metal oxide semiconductor gas sensor can be fabricated by screen printing,

chemical vapours deposition, spray pyrolysis, sol-gel, physical vapours deposition and drop coating [22].

Most of the MOX gas sensors have poor gas selectivity without a heater system. A typical MOX gas sensor is shown in Fig 2.2. The selectivity and sensitivity of gas detection depend on certain temperatures for a specific gas. However, the electric power consumed by the heater can be significant. It is also necessary to properly package the heater to make it suitable for textiles at the operating temperature which typically ranges from 300-800°C. The selectivity can also be improved by fabricating an array of sensors as shown in [23]. Samantha Benedict et al. fabricated an array of ZnO sensors on flexible acetate sheets for detecting CO, SO<sub>2</sub>, H<sub>2</sub> and NO<sub>2</sub> gases. They designed a micro-heater that consumes 2mW and this is lowest among flexible sensors.

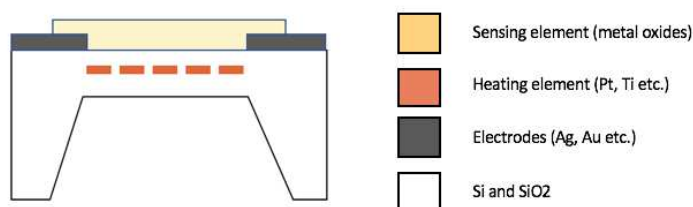


**Figure 2.2 Schematic diagram of Metal-oxide semiconductor gas sensor**

The heater element can be replaced by using UV radiations to operate the sensor work at room temperature. Zheng et al. demonstrated this by fabricating a flexible and transparent wearable MOX sensor by pulse laser deposition [24]. The sensor detects acetylene at room temperature by UV light activation with visible NDIR light or solar energy. The authors also designed a similar sensor using ZnO nanoparticles for detecting ethanol using light radiation of 370nm[25]. The sensor performance depended on the light of radiation and for a variation in the intensity from 3 to 8mW, optimal sensor performance was obtained at 5mW. Metal oxide gas sensors can be combined with conductive polymers can increase the performance of the sensor [26] and can make the sensor flexible that would be easy to integrate on to fabrics. By doing this, the metal oxide can be used for gas detection at room temperature [27] [28].

### 2.1.3.2 Conductive Polymer (CP)

Polymers that act like semiconductors in which when exposed to the gas, the doping concentration of the polymer changes thus changing the resistance of the polymer are called the conductive polymers. The change in resistance depends on the type of polymer doping and the nature of the gas (electron donor or acceptor). CPs are subdivided into an intrinsic conductive polymer and an extrinsic conductive polymer. Intrinsic CP (e.g., polypyrrole [PPy]) are conductive due to the backbone of the polymer that consists of conjugated p-electrons or by doping where the electrons or



holes increases by oxidation or reduction process. Extrinsic CP (e.g., carbon black) are insulators and can be made conductive by adding conductive particles inside them.

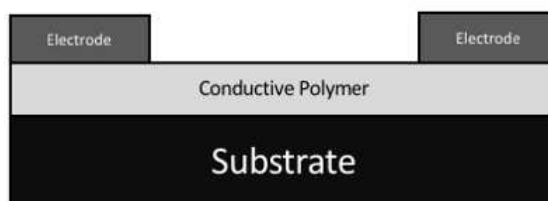


**Figure 2.3 Basic structure of conducting polymer-based gas sensor**

The most used polymers are polyaniline (PANI), polypyrrole (PPy), and Poly(3,4-ethylenedioxythiophene) (PEDOT). The CP has a simple structure as shown in Fig 2.3 with a substrate on which the polymer is synthesised chemically or electrochemically (such as galvanostatic, potentiostatic, cyclic voltammetry or potentiodynamic methods) [29] with electrodes for the detection of a change in resistance. These polymers can be deposited on a flexible substrate by dip-coating, spin coating, electrochemical deposition, thermal evaporation, layer-by-layer self-assembly, vapour deposition and drop-coating [29].

**Table 2.2 Showing the electrical changes in CP due to the interaction with gas molecules [29]**

Polymer type	Nature of the gas	Electrical conductivity	Electrical resistance	Transient doping level
P type (Electron acceptor)	Electron acceptor	Increases	Decreases	Increases
P type	Electron donor	Decreases	Increases	Decreases
N type (Electron donor)	Electron acceptor	Decreases	Increases	Decreases
N type	Electron donor	Increases	Decreases	Increases

Conductive polymers as gas sensors work with temporary doping process due to the interaction of gas molecules with the polymer layer. Upon exposure to a target gas, a transient redox reaction between the polymer and the gas increases or decreases the doping level of CP and alters its conductivity and resistance as shown in table 2.2. This behaviour applies to most of the polymers

except PANI protonation which involves an exchange of hydrogen atom ( $H^+$ ) and the change in the resistance that occurs in gas sensing system depends on the acidic or basic nature of the gas. The CP is made into n-type or p-type by the doping either by oxidation or reduction processes of the polymer using specific oxidising and reducing agents. Redox doping non-redox doping, photo-doping, charge injection doping, electrochemical doping are different methods of doping [30].

Conductive polymers are flexible and are easily integrated into textiles due to its flexible nature and very easy to fabricate onto any substrate. They are light, highly elastic and has high mechanical stability. Stempien et al. also fabricated an ammonia gas sensor that was inkjet printed on a non-woven fabric using PANI and gold electrodes as shown in Fig 2.4. The sensor was able to measure a concentration range from 15 to 100 ppm [31]. Presence of water can influence the sensor performance. Collins et al. reported on conductive polymer gas sensor for fabrics using PPy or PANI coated in poly (ethylene terephthalate) or nylon threads and woven on to the fabric to sense Dimethyl methyl phosphonate (DMMP),  $NH_3$  and  $NO_2$  [32]. It was observed that swelling of the polymer above 15% concentration of relative humidity.

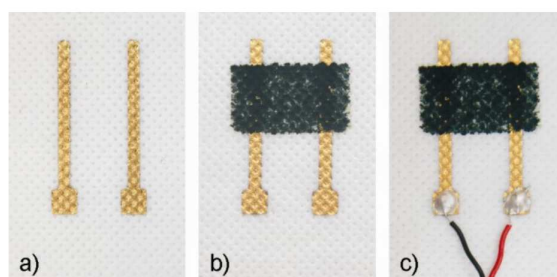


**Figure 2.4 a) gold electrodes on non-woven polypropylene b) ink-jet printed PANI on top of the electrodes c) wires glued to the contact pads for measurement [31]**

Dilek Kincal et al. [33] presented gas sensors for fabrics based on conductivity switching in PPy with different substrates and dopants for sensing  $NH_3$  and  $HCl$  gases and the reactivity of gases can be changed by doping of PPy coating. The sensor PPy as the sensing material on a textile substrate with electrodes separated by 1-inch separation with which resistance was measured by four-point measurement. The gases were given in alternative cycles and  $N_2$  was used for purging for each cycle and to avoid the formation of salt on the textile surface. The surface resistivity was determined by measuring the thickness of the substrate polymer. It was observed as the thickness of the polymer coating (PPy) and the polymer substrate (PET) is more, lower is the surface resistivity of the PPy. A decrease in conductivity contrast was observed due to salt formation on the textile which was removed by  $N_2$  purging as mentioned above.

Having a conductive polymer printed or integrated directly onto a piece of fabric may have performance issues due to the sweat from the user [34][35][36]. This can be avoided by having a sensor fabricated on a flexible waterproof substrate such as Kapton which can later be attached to

the fabric. CO sensor using PANI on Kapton strips with gold electrodes was reported [37]. The mechanical stability of the sensor was tested by applying strain in three different ways, by applying the current in parallel, perpendicular and a 45-degree angle to the strain direction. The strain of 10% was applied and a decrease in resistance was observed up to strain of 3% and an increase of resistance was seen after up to 45% where the strip ruptures. It was also reported that the orientation of the electrodes did not affect the electrical properties.

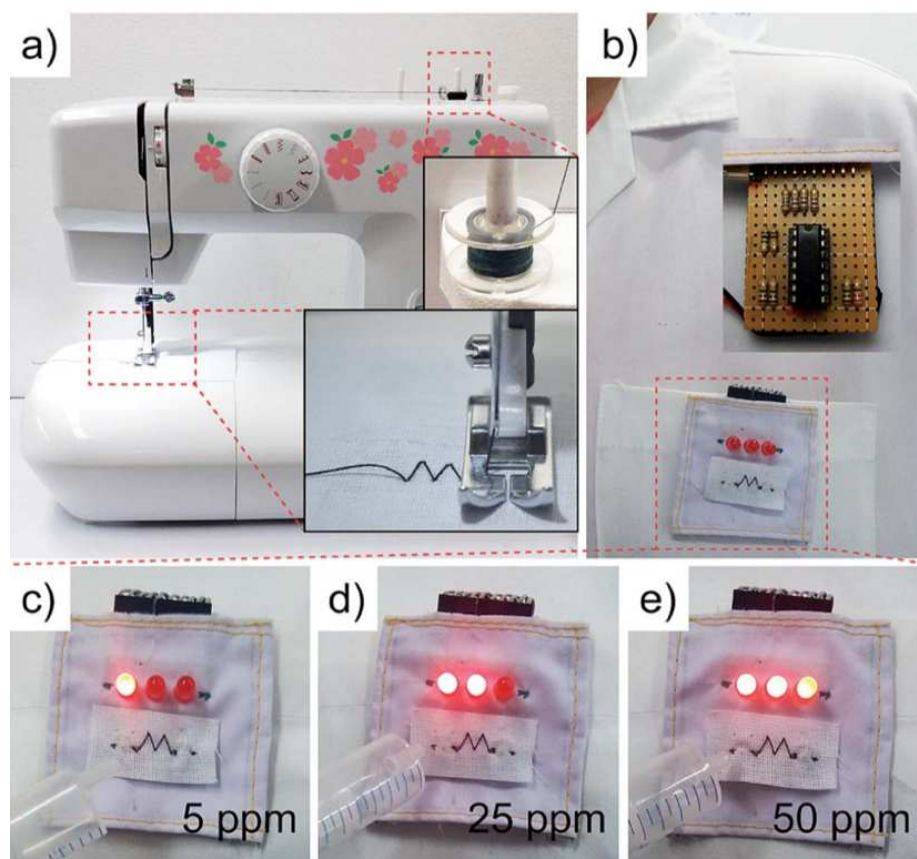


**Figure 2.5 a) Sewing PANI coated polyester yarn on cloth b) Conductive yarn attached to pocket of lab coat with comparator circuit connected to LEDs to indicate the exposure level c), d) and e) demonstrates turning on of LED for 3 different concentrations 5ppm, 25ppm and 50ppm**

Fig 2.5 (a) depicts that the PANI-coated polyester yarn being sewn to fabric, and Fig 2.5 (b) shows that LEDs coupled to a comparator circuit and placed to the lab coat's pocket to serve as an exposure indicator. Conductive polymers can also be incorporated in yarns as demonstrated in [38] to detect ammonia in real time. PANI was used as the sensitive layer and incorporated in three different yarns: polyester (showing high sensitivity to Ammonia and fastest recovery time), cotton and rayon by dip coating process. The yarn was sewn onto a textile for real time monitoring. Three LEDs were used to indicate 3 different concentrations (5ppm - LED on ,25ppm - 2 LEDs on, 50ppm - 3LEDs on) as shown in Fig 2.5 (c), (d), and (e). The sensor is also flexible and showed no significant variation in sensor response for bending angles  $0^\circ$  to  $45^\circ$ ,  $90^\circ$  and  $135^\circ$ .

### 2.1.3.3 Carbon Nanomaterials

Carbon nanomaterials are of various types as shown in Fig 2.6 such as carbon black, nanoparticles, nano porous carbon, nano-fibre, graphite that work on change in electrical property or mass sensitivity [39]. Adsorption of gas molecules on carbon nanomaterials cause mass loading thus changing the electrical resistance. A mixture of conductive polymer with these materials have achieved high performance in sensing gases with shorter response and recovery time.

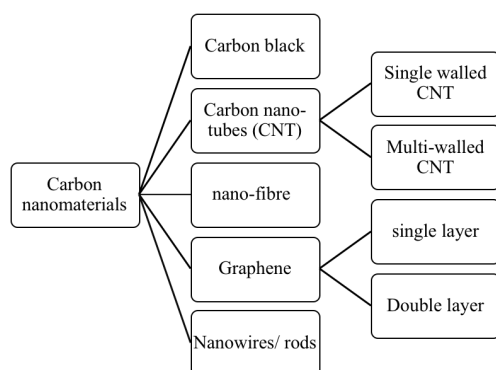


Figure 2.6 Different types of carbon nanomaterials-based gas sensing technologies

#### 2.1.3.3.1 Carbon black

Carbon black exists in the form of powders or finely divided pellet [39] are formed due to incomplete combustion or thermal decompositions of hydrocarbons. This is an example of extrinsically conductive polymer type in which carbon black particles are filled inside an inorganic polymer as shown in Fig 2.7 (a).

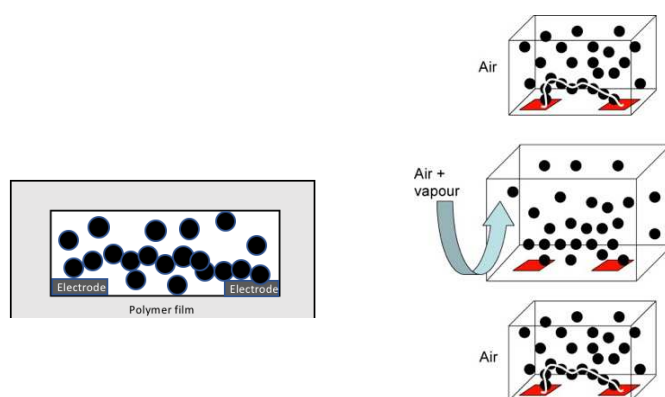


Figure 2.7 (a) Basic structure of carbon black composite inside an inorganic polymer film (b) Shows the working mechanism of carbon black. These materials form a conductive path between electrodes and in the presence of gas, the polymer swells due to adsorption of gas molecules thus make the carbon composites to move apart from each other breaking the conductive path and increasing the resistance [22]

This polymer composites consist minimum concentration of carbon black particles to start electrical conduction in the polymer. The particles are filled densely such that they create a conductive path as shown in Fig 2.7 (b).

When the outer inorganic polymer is exposed to the gas, the gas molecules are adsorbed on the polymer causing it to swell. This makes the carbon black particles dispersive or move apart from each other such that the conductive path is broken, and this increase the resistance. The point at which the resistance starts to increase is called the percolation threshold. The gas concentration can be determined by the change in resistance.

These materials can be easily incorporated into textiles. [34] fabricated a gas sensor with four carbon black composite polymer and integrated into textile for detection of acetone. The polymer composite was fabricated on a flexible polymer and then fitted into textile by weaving. [35] built two types of polymer-based carbon black carbon monoxide sensor. One contained a mixture of conductive and non-conductive (iron porphyrin) whereas the other is a non-conductive polymer in which carbon black was incorporated into the film. The test was done by an alternative supply of CO and clean air in the presence of water in the background and a resistive heating system that maintained the temperature at 28°C. Au-Pd electrodes were used, and the sensor was able to sense CO with a minimum detection limit of 150ppm at room temperature. The main issue with carbon black composites is they lack selectivity to different gases and have a very long response and recovery times.

#### **2.1.3.3.2 Carbon nanotube**

Carbon nanotubes are made of fullerene structure of carbon and are classified into single-walled carbon nanotube (SCNT or SWCNT) and multi-walled carbon nanotube (MWCNT). SWCNT consist of single-walled graphite sheets in a cylindrical shape whereas MWCNT consist of many graphite shells [40]. CNTs can be fabricated by arc-discharge, laser ablation, chemical vapour deposition, plasma torch or by super-growth CVD [41] and can be easily integrated with fabrics. [42] designed an electronic nose with a hybrid conductive polymer made of SWNT-COOH nanocomposites and was tested under the exposure of VOCs that are released from the human body. Four different polymers, polyvinyl chloride (PVC), cumene terminated polystyrene-co-maleic anhydride (cumene-PSMA), poly (styrene-co-maleic acid) partial isobutyl/methyl mixed ester (PSE) and polyvinylpyrrolidone (PVP) were deposited on the IDE and was embroidered to the fabric to sense different odours from the body.

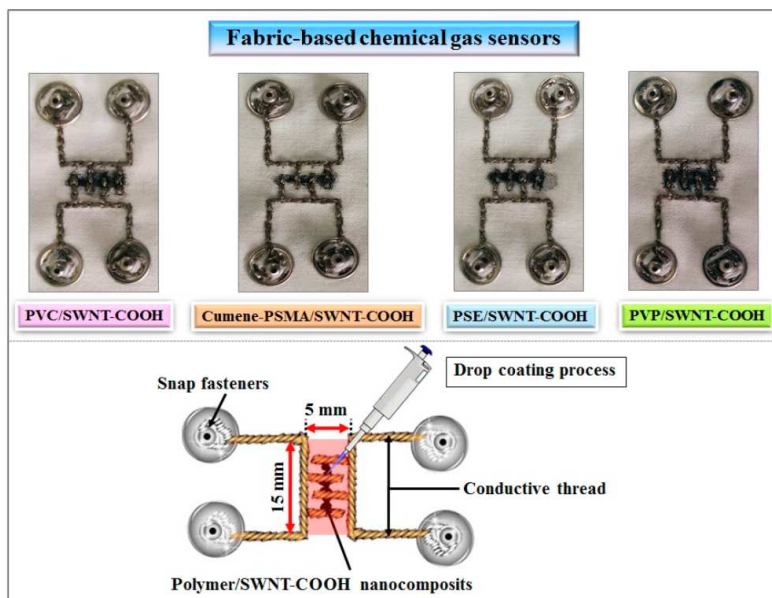


**Figure 2.8 Fabricated CP gas sensor with different polymers embroidery onto cotton strained fabric**  
[42]

In this work, the IDE was fitted into fabric by embroidery and then the sensing material was drop coated onto the electrodes are shown in Fig 2.8. Static and dynamic measurements were taken. The static measurement was done in a chamber with VOC gases. The sensing device was connected to the data acquisition system with the help of conductive threads and snap fasteners. The resistance of the device was measured using a data acquisition card by LabView by acquiring real-time signals. The dynamic measurement was done by switching between the sample gases and nitrogen gas. It was noticed that cumene PSMA based SWNT-COOH and PSE/SWNT-COOH have the highest response for ammonium hydroxide and trimethylamine. However, the sensor response due to bending to show the flexibility of the system was not reported.

The main reason for CNTs capability of being integrated with textiles is due to their hydrophobicity and mechanical strength [43] that could survive bending cycles making it useful for a flexible application. Jin-Woo Han et al reported a SWCNT gas sensor that senses ammonia with a detection limit of 8ppm on a cotton yarn with gold electrode clip where the distance varied from 1.0-4.0. The flexibility of the CNT cotton yarn was done by bending tests. The CNT cotton yarn was knitted on a piece of fabric and bending tests were done by bending the sensor up to 90° with a very small change in the output response. The flexibility of CNT is due to the hydrogen bonding between CNT and cotton leads. This bonding retains the chemical and electrical properties even after bending.

A wearable room temperature gas sensor using Polyvinyl alcohol (PVA) MWCNTs fabricated on a piece of fabric is reported [44]. The flexibility was checked by bending up to 60° both in forward and reverse direction with stable electrical performance. However, the change in resistance of the sensor was noticed due to the swelling of the PVA layer on adsorption of vapours.

Nanotubes can be made into yarns for e-textile and this was demonstrated by Lee et al. [45]. In this, first the PAN nano-fibre was coated with SnO<sub>2</sub> by electrospinning and then this micro-yarn was made to undergo calcination to produce nanotube micro-yarn. It is shown in Fig 2.9 (a) & (b). This nanotube involves a 1000 cycle process of atomic layer deposition (ALD) to get a 70nm thickness of nanotube for a micro-yarn to detect H<sub>2</sub> at 400°C. The influence of humidity or the bending of the yarn on the sensor response has not been reported. The electro spun PAN micro-yarn is shown in Fig 2.10 (a), and the micro yarn's helix structure is shown in Fig 2.10 (b).

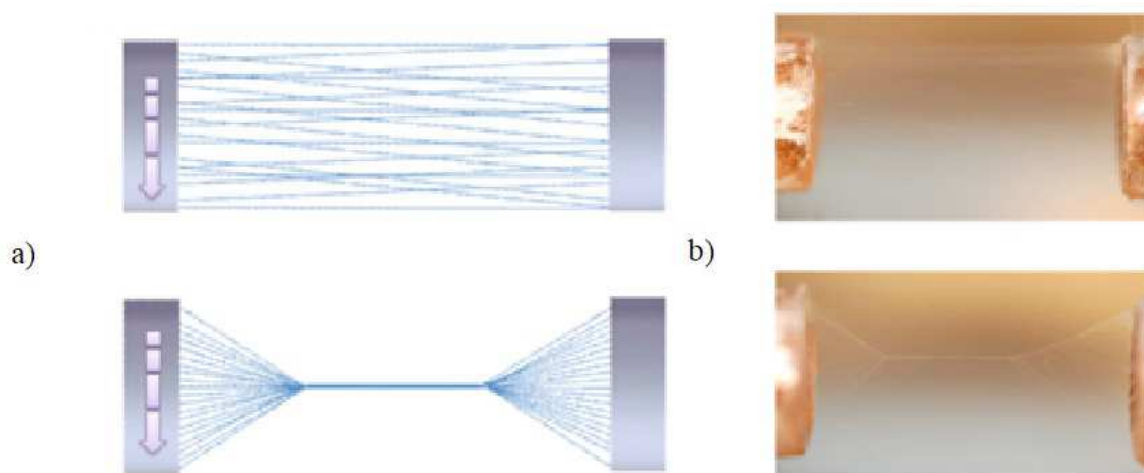


**Figure 2.9** Preparation of nanotube micro-yarn by electrospinning (a) Schematic diagram of the process (b) actual image of preparing micro-yarn [45]

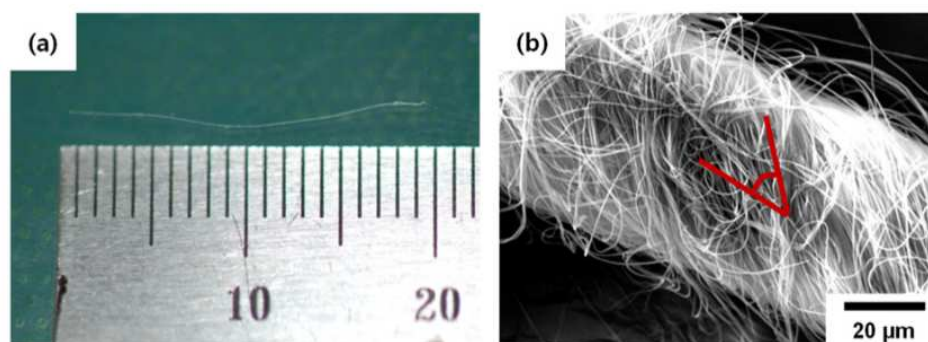


**Figure 2.10** (a) the electro spun PAN micro-yarn (b) the helix structure of the micro yarn [45]

### 2.1.3.3.3 Carbon fibre

Carbon nanofibers are stacked up carbon nanotubes that contain sp<sup>3</sup> hybridised carbons on the surface [39]. Monereo et al. [46] demonstrated a flexible sensor based on carbon nanofibers on Kapton to measure CO, NH<sub>3</sub> and humidity. The sensitive material was printed on the Kapton substrate by ink-jet printing. It was noticed that due to bending, a shift in the baseline resistance was

observed. The sensor response was also affected by the humidity at room temperature leading to a shift in the baseline resistance. There was no significant variation in the response for  $\text{NH}_3$  when the relative humidity was 50%.

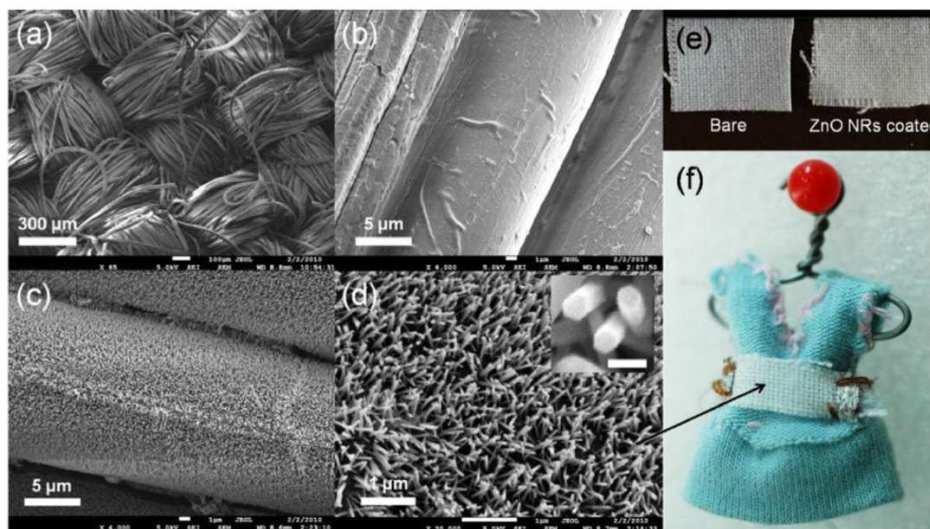


**Figure 2.11** Showing the SEM images (a) cotton substrate (b) bare cotton fibres (c) ZnO nanorod coated cotton fibres (d) high magnification image of ZnO nanorods on a cotton fibre, (e) Normal photograph of bare and ZnO nanorods coated fabric (f) multifunctional smart fabric sewn on toy dress [47]

#### 2.1.3.3.4 Nanorods

Another type of nanomaterial shown is a nanorod. A wearable breath monitoring system that has ZnO nanorods fitted into three different substrates such as polyester, cotton and polyimide for textile integration is reported [48]. The ZnO nanorods were fabricated with Pt or silver IDE by magnetron sputtering to sense acetone and ethanol. ZnO nanostructures have gas sensing capabilities due to the high density of surface reaction and surface to volume ratio and can be fabricated by thermal evaporation deposition, chemical vapour deposition or aqueous chemical growth [49]. Z.H.Lim et al., built a ZnO nanorods for a cotton textile as a multifunction smart textile that senses temperature, optical and  $\text{H}_2$  sensing at room temperature [47]. These nanorods were grown uniformly to form a conductive fabric. The resistance was measured when the sensor was exposed to hydrogen and clean dry air (CDA) was used to produce a dry environment. The sensor was mechanically tested with multiple stress and washing cycles and it was observed that the nanorod shows robustness against stress and wash cycles with good response and no cracks on the nanorod were observed. However, the number of stress and wash cycles have not been reported.



### 2.1.3.3.5 Graphene

Graphene has very good properties of chemical stability and electron mobility that makes it work at room temperature with short response and recovery time. It also can detect a very low concentration of gases in ppb levels [50][51][52]. It is a 2D structure of carbon atoms and can be synthesised by micromechanical method, chemical vapour deposition, epitaxial growth, chemical exfoliation or thermal deposition [53]. The adsorption of gas molecules on the surface of the graphene layer changes the electron concentration of the graphene layer thus causing a change in resistance.

Yong Ju Yun et al. [54] fabricated an ultrasensitive room-temperature graphene-based single yarn with a very high response to  $\text{NO}_2$ . This RGO (reduced graphene oxide) sensor was also able to function after several wash cycles and could withstand 1000 cycles of bending with a bending radius of 1mm which makes it reliable for e-textile applications and it is depicted in Fig 2.12. Two types of yarns were fabricated such as RGOY (cotton yarn) and RGOY (polyester yarn) and both were able to detect  $\text{NO}_2$  with a min detection limit of 250 ppb.

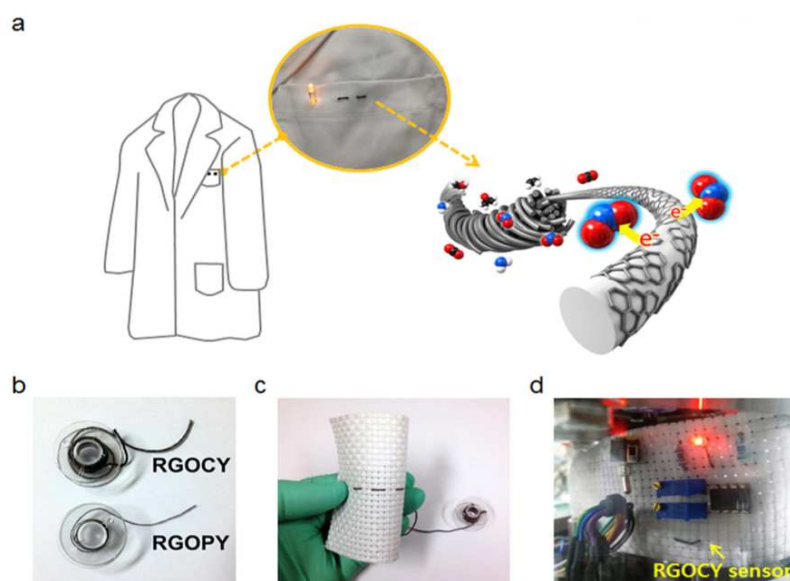


**Figure 2.12 (a) RGOY prepared from micro fibre bundle and on the right the red, blue, black, and white spheres represent  $\text{O}_2$ ,  $\text{N}_2$ , C and  $\text{H}_2$  atoms respectively. (b) RGOY and RGOY wound on plastic bobbin (c) RGOY integrated into a fabric (d) wearable gas sensor with an alarm system [54]**

RGOY was confirmed to sense much diluted  $\text{NO}_2$  without cross-sensitivity. This was then weaved into a cotton fabric and connected to a circuit with LED as an alarm to detect 5.0ppm of  $\text{NO}_2$ . The sensor was able to withstand 10 wash cycles without significant change in the electrical conductivity.

Graphene is very thin and light material and is used in wearable e-textiles. as it can be easily made into yarns and are capable of withstanding a number of bending cycles without a change in the performance such as changes in electrical properties. [55] Yong Ju Yun et al. fabricated elastic wristbands that sense  $\text{NO}_2$  using super elastic reduced graphene oxide (RGO) elastic yarn. These are flexible and highly stretchable for wearable devices applications. This sensor achieved a very high mechanical stability that was able to take 5000 cycles of stretch-release with high sensitivity to  $\text{NO}_2$  with a minimum detection level of 500 ppb. Similarly, Hyung Ju Park et al [56] demonstrated a  $\text{NO}_2$  gas sensor based on RGO nanofibrous mesh (nylon-6 nanofibre) with mechanical reliability for 5000 bending cycles with 1.0 mm bending radius. However, the performance of the sensor was influenced by humidity which caused swelling of the nylon-6 (hydrophilic and porous platform). [57] reported a graphene with metal nanoparticle (palladium) based  $\text{NO}_2$  and  $\text{NH}_3$  flexible sensor which survived  $10^4$  bending cycles with slight degradation in the sensitivity.

### 2.1.3.4 Metal Organic Frameworks (MOFs)

Metal organic frameworks are newly developed devices for chemical sensing. It is a porous material that consists of metallic clusters linked by organic ligands (linkers) that makes them useful for gas sensing, separation and storing.

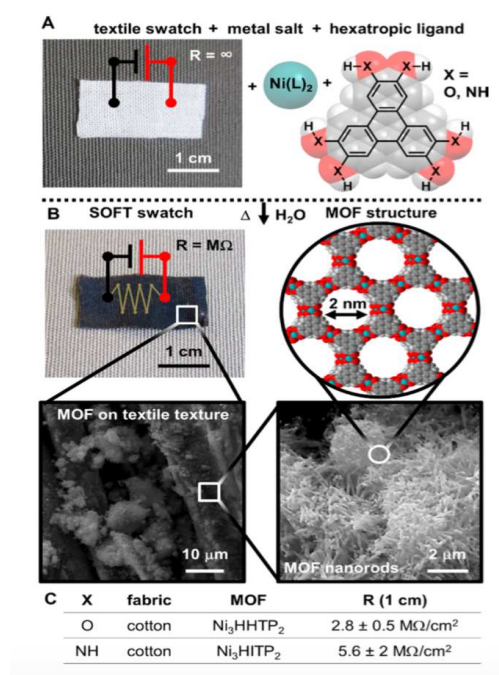


**Figure 2.13** Fabrication of MOF textile sensors for  $\text{NO}$  and  $\text{H}_2\text{S}$  detection: (a) the materials required for the sensors, cotton swatch, the triphenylene based ligands and the nickel metallic nodes; (b) the conductive SOFT devices on cotton swatch obtained by solvothermal condensation of reagents in water, with micrographs showing the MOF coating on the cotton fibres and the nanorod texture of the MOF; (c) the sheet resistance measurements of the swatches [58].

Like conductive polymers, the gas concentration can be found by the change in electrical properties (resistance capacitance). M. Smith et al. demonstrated a flexible MOFs detecting NO, H<sub>2</sub>S and H<sub>2</sub>O [58]. The organic ligands used are 2,3,6,7,10,11-hexahydroxytriphenylene (HHTP) or 2,3,6,7,10,11-hexaaminotriphenylene (HATP) ligands with metallic nickel (II) nodes natural (cotton) and synthetic (polyester) fabrics.

The fabrics swatch was achieved through direct growth of the solution phase's self-assembly process using their molecular precursors along with the organic ligands and metallic nodes. The fabric shown in Fig 2.13 were evaluated inside a Teflon box with gold pins as electrodes. The sensor was able to detect Nitrogen oxide (NO) with a limit of detection (LOD) = 0.16ppm and 1.4ppm and H<sub>2</sub>S LOD = 0.52ppm and 0.23ppm for Ni<sub>3</sub>HITP<sub>2</sub> and Ni<sub>2</sub>HATP<sub>2</sub> respectively. The fabric swatches retained its performance up to 10 bending and folding cycles, also washing but the number of cycles was not reported.

## 2.2 Mass Sensitive gas sensors

Mass-sensitive sensors are similar to piezoelectric substances. These kinds of sensors have a sensitive layer such as organic polymers or carbon nanomaterials. In the presence of the target gas, the gas molecules adsorb on the sensing material, which causes it to swell thus increasing the mass of the sensor. The change in the mass of the device gives an electronic signal such a frequency with which the concentration of gas can be found.

### 2.2.1 Surface Acoustic Wave (SAW)

SAW (Surface Acoustic Wave) works due to the interaction of acoustic signals that converts mechanical energy into electrical and vice versa. The acoustic wave travels along the electrodes. When a sensitive material is present in between the electrodes, due to gas adsorption, a change in phase and amplitude of the sound is observed [59]. There are two modes namely delay line and resonator. The delay line sensor causes a delay in time between the input and output signal in the presence of chemical molecules on the sensitive material placed between the IDTs. A resonator type sensor grating reflectors near to the IDTs and this creates a resonating cavity. Chi-Yung Cheng et al. [60] presented a SAW based gas sensor on three different material of fabric such as wool, cotton and polyester for the detection of nicotine and 3-ethenylpyridine produced by smoke with two methods. The first method was to measure the mass difference due to adsorption of the smoke on to the sensor and the second method is to use a SAW with hollow nanospheres as sensitive material. For the first method, it was noticed that the mass gain and residence period of smoke in wool was higher than cotton and polyester. The SAW sensor was constructed by lithographic technique to have IDT of 50 pairs on each side and has a central frequency of 114.2 MHz. There exists a frequency

shift of 119Hz in the sensor even when dry air with a relative humidity of 20% due to swelling of the sensing material by absorption of water molecules.

### 2.2.2 Quartz Crystal Microbalance (QCM)

QCM based gas sensor converts a mass change in the quartz crystal to the electronic signal due to adsorption of gas molecules. When a voltage is applied to the quartz crystal, oscillation or vibration occurs with certain resonant frequency. The concentration of the gas is measured by taking note of the shift in frequency of quartz crystal resonator due to the adsorption of the sensitive material by the gas causing in a mass loading. [61] reported on a wearable sensor using QCM for detecting odorant diffusion. A drop in resonant frequency was demonstrated due to mass loading. Pavel Kulha et al. [62] reported on ink-jet printed QCM using diamond powder to sense ammonia under room temperature. The impedance of the sensor is measured using Omicron Bode 100 - vector network and impedance analyser for the change in the concentration of ammonia. A shift of 38 Hz in the serial resonant frequency was observed for 50ppm of  $\text{NH}_3$ . The sensor also showed shifts of 63Hz and 147Hz in the frequency due to change in relative humidity for 50% and 75%.

### 2.2.3 Film Bulk Acoustic Resonator (FBAR)

In FBAR, when RF signal is applied to the electrodes, standing waves with a resonant frequency are produced [63]. The shift in this resonant frequency gives the concentration of the gas due to mass loading in the presence of gas. Like QCM, FBAR sensors need an external oscillator circuitry to excite the system. It has better mass sensitivity when compared to QCM due to higher resonant frequency [64]. Mengying Zhang et al. [65] reported an ethanol gas detector based on FBAR driven by Colpitts oscillator. It consists of a piezoelectric film between two electrodes on  $\text{SiN}_x$  substrate with micro resistor heater to control the temperature and humidity generator to control humidity. A frequency shift 3.2 times higher than sensor frequency was observed due to humidity.

### 2.2.4 Micro-cantilever

Micro-cantilever gas sensor works on the principle of bending of the cantilever due to mass loading as a result of gas adsorption by a sensitive material. A microcantilever gas sensor for detecting CO with poly (ethylene oxide) with nickel atoms as the sensing material was presented [66]. The resistance of the cantilever is measured using Kiethley precision multimeter. An increase in resistance due to the decrease in the sensing material thickness in the presence of CO was observed. The recovery of the sensor is achieved only for small exposures of CO and degradation of sensing material was noticed for higher exposures. This sensor was able to fully recover under small exposures of CO. However, for very high exposures, an irreversible change was observed.

### 2.2.5 Capacitive micromachined ultrasonic transducer

The mass-sensitive gas sensor that does not work on piezoelectric principle is the capacitive micro-machined ultrasonic transducer (CMUT) gas sensor which is designed in such a way that the sensitive material absorbs the target gas, and due to the mass loading effect in the system, the resonant frequency changes. The shift in resonant frequency gives the concentration of the gas. They consist of two electrodes where one is fixed and the other is movable and there exists also a membrane in between the electrodes. When DC voltage is applied to the electrodes, the membrane is deflected towards the bottom electrode. The motion of the resonator gets converted into electrical output [67]. Prince Bahoumina et al. [68] fabricated a flexible CMUT gas sensor with silver nanoparticle with PEDOT:PSS-MWCNTs as sensitive material, fabricated on flexible paper by ink-jet printing for detection of volatile organic compounds (VOCs). Two capacitive resonators were used to find differential detection (one with sensitive and another with reference channels). Due to the absorption of the vapour by the sensitive material the mass increases and that results in the change in the resonant frequency of the CMUT. The sensors were operated with three different frequencies with two modes of resonant frequencies and a frequency shift of -100MHz was observed in each resonant mode. The main advantage of CMUT gas sensing is that an array can be fabricated in a very small area that allows detection of various gases at the same time. However, concentration of individual gas components cannot be measured leading to cross sensitivity.

## 2.3 Optical absorption

The most used optical absorption type gas sensor is the non-dispersive infra-red gas sensor. It consists of an infrared light source, a chamber, optical band-pass filter and detector [69]. When NDIR passes through the sample, the gas molecules of the natural frequency matching the frequency of the radiation will absorb the radiations. The wavelength at which the absorption of the radiations is observed will help to identify the concentration of the gas. It works based on Beer-Lambert Law where the light passing through a material attenuates because of change in the properties of material change due to absorbance. The detector gives an electronic signal that gives the concentration of the gas. It consists of fixed narrow band filters and IR detectors. The optical filter is placed before the detector and the wavelength that can be absorbed by the target gas is passed through. The advantage of this sensor is that there will not be in physical contact with the target gas hence poisoning of the sensor can be avoided. A portable solid state NDIR CO<sub>2</sub> was demonstrated [70]. NASA reported on wearable NDIR gas sensor by GSS (gas sensing solutions) called CoZIR sensor for detection CO<sub>2</sub> inside spacecraft to get an accurate measurement of carbon dioxide that the crew members are exposed to [71]. The sensor was covered with 3D-printed housing package such that it can be fixed on to the clothing of the crew member that can measure a concentration about 5000ppm with a power

consumption of 3.5mW. The data can be viewed in an iPad application. A lot of gases get absorbed at the same wavelength of infrared radiations hence this leads to cross-sensitivity of the sensor.

Another type of optical gas sensor is the colorimetric type which works on absorption and changes the colour of the sensing material when the light is illuminated on it in the presence of the target gas. Chenwen Lin et al. presented on miniaturised CO sensor on colorimetric with a minimum detection limit of 1ppm [72]. Potassium disulfitopalladate is used as the sensing element drop-casted on porous silica gel substrate. The issue with this type of sensor is that it requires a light source for the sensor to function and a device to monitor the absorbance change. However, this may make the overall sensing system bulky and may not be applicable for portable applications. The bulkiness was reduced with this type of gas sensor by fabricating in the form of threads as demonstrated by [73] and tested with ammonia and HCL gas. The sensor was dyed with 5,10,15,20-Tetraphenyl-21H,23H-porphine manganese (III) chloride (MnTPP), Methyl red (MR) and Bromothymol blue (BTB) and in the presence of the gases, the colour change of threads dyed with these dyes were tracked for a concentration range of 50-1000ppm as shown in Fig 2.14. The dyed thread was also coated with PDMS which is a gas permeable material to make the thread washable. The PDMS coating protected the dyed threads with 10-20% leaching of dye under aqueous environment during the washing test run at the speed of 6400rpm for 30s. The thickness of the PDMS layer affected the response of the system as thickness increases the rate of colour changing in the dye decreases.

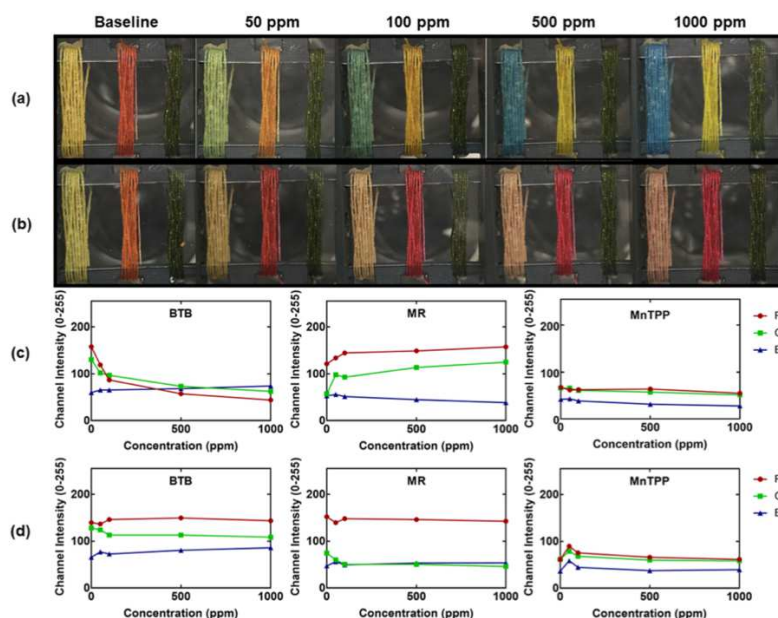


**Figure 2.14 Gas sensing demonstration – Optical Images. Optical images of BTB, MR, and MnTPP devices for different concentrations of (a) ammonia or (b) HCl and the corresponding RGB colour information extracted from the optical images for (c) ammonia and (d) HCl [7]**

## 2.4 Discussion

Different types of gas sensors have been discussed in this review and it has been seen that conductive polymer and carbon nanomaterial-based gas sensors are highly used as wearables by integrating with textiles. Most of the e-textile gas sensors reported are based on chemiresistor except metal oxide semiconductor. From all the MOX based gas sensors discussed, the operating temperature ranges from 80°C to 400°C. To avoid high operating temperature, UV irradiation can be used [25][74]. However, this device needs a source of UV for the activation of the sensor. The MOX sensors have been miniaturised with proper packaging such that the heat does not radiate. The commercial gas sensor chips available in the market are MOX gas sensors such as CO<sub>2</sub> gas sensor chip by Sensirion (World's smallest gas sensing chip) [75] with I2C for data transmission. These chips can be very useful in portable applications. For e-textile, small chips like this can be fixed on a flexible substrate with conductive tracks forming a closed circuit for gas detection and transmission of data for flexible applications. Even though the sensor chip is protected by proper packaging, they are not reliable in the presence of water or may even fail to function over time. The best suited for smart textile is the conductive polymer-based sensor mainly due to its natural flexibility and its ability to operate at room or ambient temperature. Most of the smart textile gas sensors are based on conductive polymers. This polymer can be directly deposited on the textile by printing methods[31][76]. As discussed in the literature, the performance of CP can be affected by humidity where swelling of polymers can be. Among all the sensors, Carbon nanomaterials seem to have the best performance even in the presence of water due to high mechanical stability and hydrophobicity. However, the maximum number of wash cycle reported was 10. The mass sensitive type gas sensors are also temperature and humidity dependent that cause a significant shift in the resonant frequency of the sensor. The primary criterion for an e-textile gas sensor is to retain the basic properties of a textile that can be bent, washed using detergents and has long durability as well as being able to sense the target gases. The encapsulation of these gas sensors has not been discussed. The challenge is to investigate an encapsulation layer that protects the sensor circuit from the harsh environment and allows only the target gas pass through it.

One of the main criteria for a gas sensor is the minimum detection level or limit of detection (LOD) which is the lowest concentration of gas that a sensor can detect. This is very important as some of the harmful gases such as phosgene, chlorine, sarin etc can be very dangerous at very low levels (e.g., the recommended exposure limit for an 8-hour shift for phosgene is 100 ppb according to OSHA standards). The outdoor concentration of various gases is in the order of parts per billion [77]. Carbon nanomaterials seem to have a very low detection limit in combination with metal oxides or conductive polymers as shown in the Table. 2.3. The overview of the flexible and e-textile gas sensor in brief is given in Table 2.4.

Table 2.3 Showing the minimum detection limit for different gas sensors

Gas	Type of sensor	Type/ Polymer combination	Minimum detection limit	References
NH <sub>3</sub>	Nanofiber	SNF/PANI	400ppb	[78]
		PANI/PAN	10ppm	[79]
PEDOT: PSS/PVP		5ppm	[80]	
DMMP		Metal oxide with PAN/PVP	0.1ppb	[27]
CO	Carbon black composites	Polypyrrole with iron porphyrin with polyethylene oxide	150ppm	[35]
DMMP		PPy-COOH	0.5ppb	[81]
NH <sub>3</sub>	Carbon nanotube	SWCNT	8ppm	[43]
C <sub>2</sub> H <sub>5</sub> OH		MWCNT/ PVA	9.17ppb	[44]
NO <sub>2</sub>	Graphene	Reduced graphene oxide yarn (RGOY)	500ppb	[55]
		RGOCY (cotton) and RGOPY (polyester)	250ppb	[54]



Table 2.4 Summary of flexible and e-textile gas sensor

Gas sensor type	Target gas	Substrate	Sensitive material	Electrodes	Fabrication techniques	LOD (ppm)	Highest Sensitivity	Temp °C	Durability -stretch, Bending cycle/angle/time	Durability based on washing cycles	Ref
Conductive polymer	NH <sub>3</sub>	Non-woven polypropylene fabric	PANI	Gold	Inkjet printed	-	-	-	-	-	[31]
		Nylon 6	PANI	-	Diffusion polymerization mixed bath (DPMB)	-	-	RT	-	-	[76]
		Kapton	PANI	Gold	Spin-coating	-	-	22	Upto 45% of strain•	-	[37]
		Cotton, rayon, and polyester	PANI	Stainless-steel thread	Dip-coating	5	57% at 50ppm	RT	0°,45°,90° and 135°•	-	[38]
	Acetone	Polyimide	poly-iso-butylene PIB, poly-styrene PS, poly(N-vinyl-pyrrolidone) PVP, poly-vinyl-butyril PVBU	Ti/Au	Spin coating	50	-	RT	10 mins	-	[34]
	ammonium hydroxide, ethanol, pyridine, triethylamine,	Cotton satin	polyvinyl chloride (PVC), cumene terminated polystyrene-co-	The silver-plated nylon 234/34 4-ply conductive thread	embroidery /Drop-coating	-	-		-	-	[42]

	methanol, and acetone		maleic anhydride (cumene-PSMA), poly (styrene-co-maleic acid) partial isobutyl/methyl mixed ester (PSE) and polyvinylpyrrolidone (PVP)/functionalized-SWCNT								
Carbon nanotube	NH <sub>3</sub>	Neoprene rubber	SWCNTs cotton yarn	copper	Dip coating	-	-	RT	-	-	[36]
		Cotton textile	CNT cotton yarn	Gold	Ink based dip coating	8	-	RT	90°	-	[43]
	Ethanol	Cotton	MWCNT and PVA coated MWCNTs	-	-	9.17	0.56% and 0.04%	RT	60°	-	[44]
	H <sub>2</sub>	Polyacronirile Nanofiber twisted into yarn	SnO <sub>2</sub>	-	Electrospinning and ALD	-	-	400	-	-	[45]
Nanorods	Acetone and ethanol	Polyester, cotton, and polyimide	ZnO	Silver coated Conductive yarn for IDE	Solution process	10	68% for 100ppm of ethanol- (poly-	100-300	-	-	[48]

							imide substrate )				
	H <sub>2</sub>	Cotton	ZnO	-	Solution process	-	83% for 1000ppm	RT	*	*	[47]
Graphene	NO <sub>2</sub>	Cotton yarn and polyester yarn	RGO	-	Dip-coating	0.25	~11% for 1.25ppm	RT	1000 at 1mm radius	10	[54]
	NO <sub>2</sub>	commercial spandex and polyester core-spun elastic yarns	RGO	-	Dip-coating	0.5	55% at 5.0ppm	RT	5000 stretches at 400% strain	-	[55]
	NO <sub>2</sub>	-	RGO nanofibrous nylon 6	-	Electrospinning	-	13.6% at 1ppm	RT	5000 at 1mm	-	[56]
	NH <sub>3</sub> and NO <sub>2</sub>	PI	Palladium nanoparticle graphene	Au/Ti IDEs	Spin-coating	1.2		150	100000	-	[57]
	NO <sub>2</sub>	Commercial silk fabric	RGO	-	Dip-coating	1	-	RT	1000	-	[82]
		Cotton (CT) and elastic (ET) threads	rGO/ZnO-CT and ET	Silver wires connected with conductive silver paste	Dip-coating	0.0435	44% at 15ppm	RT	3000 bending at 1mm and 1000 twisting (360°)	8	[83]

Nano fibre	NH <sub>3</sub>	-	SiO <sub>2</sub> /PANI nanofiber	-	Electrospinning	0.4	3.36% at 5ppm	RT	-	-	[78]
		PAN nanofibre	PANI/PAN Uniaxially aligned coaxial nanofiber yarn (UACNY)	IDE	Electrospinning	-	32.214 % at 1000ppm	RT	-	-	[79]
MOFs	NO and H <sub>2</sub> S	Cotton swatch	Ni <sub>3</sub> HITP <sub>2</sub> and Ni- <sub>2</sub> HATP <sub>2</sub>	Gold	Solution process	NO - 0.16ppm and 1.4ppm and H <sub>2</sub> S LOD = 0.52ppm and 0.23 ppm for Ni <sub>3</sub> HITP <sub>2</sub> and Ni- <sub>2</sub> HATP <sub>2</sub>	-	RT	10	-	[58].
SAW	nicotine and 3-ethenylpyridine	Wool,cotton, polyester	hollow mesoporous carbon nanospheres (O-HMC)	Gold IDE	Lithography	-	~1850Hz shift for wool	RT	-	-	[60]
Colorimetric	NH <sub>3</sub> and HCL	Thread	5,10,15,20-Tetraphenyl-21H,23H-porphine manganese (III) chloride (MnTPP), methyl red (MR), and bromothymol blue (BTB)	-	Dip and dry process	-	-	-	-	10	[73]
	HCL	Polyamide fabric	Rhodamine Dye	-	Dyeing and screen printing	1	-	RT	-	4	[84]

## 2.5 Review of encapsulation techniques

E-textiles have a wide range of applications that include military, biomedical, industries and fitness tracking. As sensors being integrated with textiles, the influence of the environment can degrade the performance of the sensor over time due to moisture, dust and mechanical stress caused by bending and twisting. To make an efficient smart textile, the sensor must meet certain criteria before it can be incorporated into textiles such that it retains the characteristics of textiles. This includes the sensor being mechanically robust, waterproof, and washable using detergents [85]. The reliability of a sensor can be enhanced by packaging encapsulation which is the process of protecting the sensor by covering with a material. The main requirement for a material for encapsulation of e-textile are that (a) they should be hydrophobic, (b) mechanically robust, (c) the encapsulant layer should not affect the performance of sensor, (d) flexible, (e) inert to corrosive and harsh chemicals and (f) easily applicable to the sensor [86]. Encapsulation makes the flexible sensor mechanically robust such that they can survive bending cycles. There are different techniques for encapsulating flexible circuits for e-textile applications like strain sensor (silicone encapsulant) [87], supercapacitors (hydrophobic polyester fabrics) [88], and LEDs (Thermoplastic polyurethane) [89]. However, there haven't been reports on encapsulating a flexible e-textile gas sensor. The challenge with packaging a flexible gas sensor is that the choice of materials should be flexible, waterproof, washable but gas permeable. This section review about different techniques of encapsulation and the materials used.

## 2.6 Types of encapsulation techniques

### 2.6.1 Glob top and dam and fill

Glob topping is a form of liquid type encapsulation where high viscous liquids like thermoset or thermoplastic epoxy or silicone are dispensed on the device using a syringe and cured by heat or light [90].

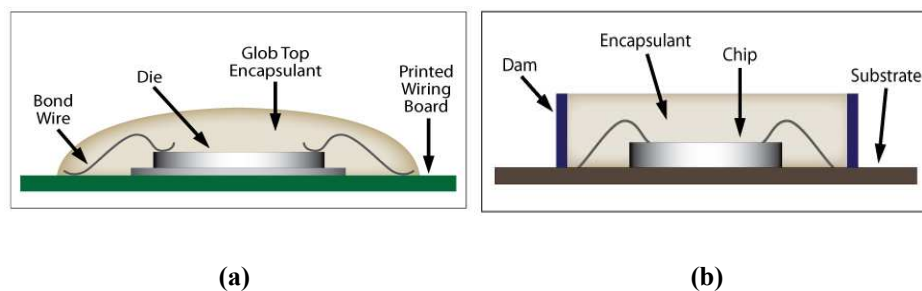


Figure 2.15 (a) Glob top encapsulation and (b) dam and fill type encapsulation [90]

The epoxy-based glob top is rigid whereas silicone and polyurethane are flexible as shown in Fig 2.15 (a). This technique is easy to apply however, the spread of the epoxy over the device depends on the viscosity of the epoxy. There is no control over the area to be covered. Epoxies with high viscosity are used for large coverage and low viscous epoxies are used for small coverage.

Another technique like glob top is the dam and fill method. It is a two-step process where an adhesive or epoxy of high viscosity is dispensed around the chip to create a dam. The fill process includes a glob-top epoxy dispensed on the top of the chip using a syringe and letting the epoxy flow until it reaches the dam [91] as shown in Fig 2.15 (b). The advantage of this technique is that it has precise control over how much area needs to be covered when compared to glob top. This can be achieved by printing techniques such as dispenser printing to create the dam and then fill the epoxy. However, this increases the bulkiness of the filament restricting flexibility.

### 2.6.2 Casting, potting and encapsulation

Casting is a simple and low-cost process as shown in Fig 2.16 (a) in which the material is poured into a mould of the desired shape with the device to be coated placed inside the mould. The material is then cured, and the mould is removed. Moulds can be rigid or flexible and easy to peel off the encapsulated device. The potting method as shown in Fig 2.16 (b) is like casting where the material is poured in a container called the pot in which the device is placed. In potting, the pot or the case becomes a part of the final encapsulated device as shown in Fig 2.16 (b). The issue is to have a flexible case to coat flexible devices and can make the coated device bulky. The materials used for this method are epoxies, silicone, and urethanes. In the encapsulation process, the device is immersed in-between two removable moulds (silicone or Teflon).

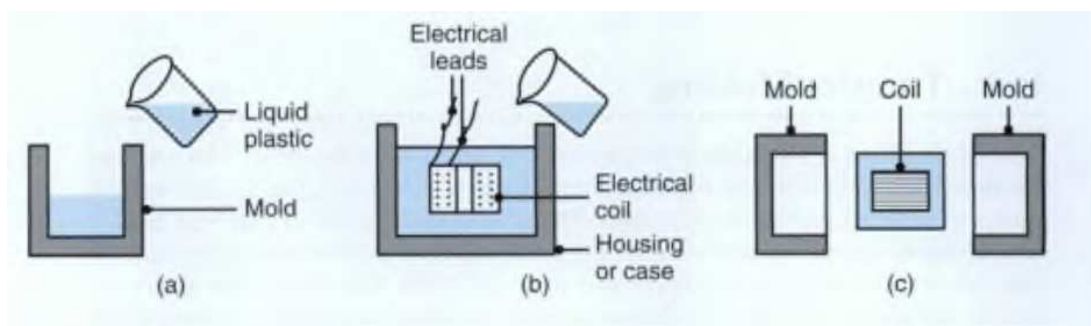
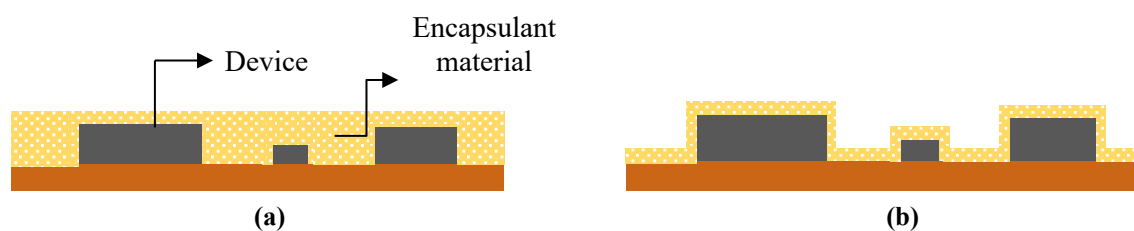


Figure 2.16 (a) Casting (b) Potting and (c) encapsulation [92]

### 2.6.3 Conformal coating

Polymer coating with the techniques discussed above can have a non-uniform thickness and the coating can add stress to the device and can make them less flexible. Conformal coating as shown in Fig 2.17 is a way of applying a polymeric layer that contours that device with uniform thickness.

This method reduces material and can make lightweight packages for flexible devices. The materials generally used for epoxies, silicone, polyurethanes and parylenes [92].



**Figure 2.17 (a) non-conformal coating and (b) conformal coating**

There are different techniques to achieve a conformal coating. Thermoplastic polymer films can be made soft and mouldable at a certain temperature slightly higher than the glass transition temperature ( $T_g$ ) where the polymers converts from solid to rubber form. This material becomes solidified when cooled. The only disadvantage in this method is the thermal stress including deformation and fracturing the material[93]. Another method to get conformal coating is by using moulds; one replicating the device area (male moulding tool ) that needs to be encapsulated and another with a cavity that matches with the device (female moulding tool) [15]. The material is placed in-between the moulds with and heated until the material deforms to the shape of the mould. The deformed (moulded) material is then attached on top of the device for encapsulation using adhesive.

## 2.7 Packaging technology used in gas sensor

The most common way of encapsulating a gas sensor is by have a stainless steel mesh covered around the sensor unit in plastic or resin housing for mostly MOX or electrochemical gas sensors that are commercially available ex Figaro gas sensors [94]. Another material that is been used in gas sensor packaging is PTFE. Thomas Tille reported Metal oxide semiconductor CO and NO<sub>2</sub> sensor with PTFE membrane for dust and moisture protection in a polyimide housing [95].

## 2.8 Conclusion

In this chapter, different types of gas sensors and their potential application in e-textiles is reviewed. The gas sensors can be broadly classified based on electrical changes in the sensor, change in mass of the sensor that leads to change in frequency or amplitude of signals, or absorption of light by the target gases. The chemiresistor type gas sensors are suited for e-textile applications and their performance after being incorporated in fabrics with performance affected by humidity. The mass sensitive type gas sensors are influenced by humidity leading to unreliable response for target gases. The durability of sensors is promising in graphene and CNT based gas sensors that can survive bending cycles and wash cycles. However, MOX sensors are promising due to small size with high

sensitivity and quickest response, recovery time and commercially available. They are also typically available as SMD which would be easy to mount of flexible PCBs as demonstrated previously in FETT with other sensors. They can be attached to flexible platforms that can be incorporated in textiles. Protecting them by an encapsulant layer would increase the reliability and durability of the sensor. Different techniques of encapsulation coating were discussed, and vacuum forming is a novel method for packaging a flexible gas sensor using gas permeable thermoplastic materials that are also waterproof.



## Chapter 3 Flexible Carbon Monoxide Sensor – Design and Characterisation

A chemiresistor is a metal oxide semiconductor-based transducer in which the resistance of the sensor changes with the change in the concentration of the target gas. They have high efficiency when compared to other gas sensing techniques. However, the important issue for metal oxide being directly integrated into textiles for a wearable application may have negative effects on the user due to its high operating temperature. The metal oxide type can be used as e-textile with proper packaging such that its heat resistant to the user. There are many commercially available MEMS gas sensing chip in the market with rigid packaging (e.g., Surface Mount Device [SMD]). In this chapter, the performance of commercially available reducing gas sensor chip integrated with the flexible material is shown. Surface mount components are easy to attach onto a flexible substrate. Metal oxide semiconductor gas sensors are commercially available in the form of SMD and have high sensitivity and short response and recovery time. For this purpose, MiCS 5524 [96] a reducing gas sensor that can detect carbon monoxide (1-1000ppm), ethanol (10-500ppm), hydrogen (1-1000ppm), ammonia (1-500ppm) and methane (>1000ppm) was chosen and tested with CO. This chapter includes the fabrication of flexible CO sensor using Metal Oxide Semiconductor (MOX) sensor and characterization of the testing chamber, reference sensor and the MOX sensor.

### 3.1 Gas sensing operation of MiCS 5524 sensor

When MiCS-5524 is powered with 5V, the heater is turned to have flow of electrons near the grain boundary of the sensitive material. In presence of air, the oxygen molecule is adsorbed on the surface of the sensing layer and attracts the electrons from the metal oxide layer thus reducing the flow of electrons through the circuit. Carbon monoxide is a reducing gas, reacts with the oxygen molecules when it encounters the sensor and removes them from the surface of the sensor. This allows the electrons to flow through the chip and the conductivity of the sensor increases. This also depends on the type of sensitive material used (N or P type) as discussed in section 2.1.3.1 in chapter 2.

The chemical reaction at the boundary of sensitive material in presence of Oxygen (air) gas is given by eqn. (1),



The chemical reaction in presence of Carbon Monoxide gas is given by eqn. (2),



At higher temperatures greater than 200°C, O<sup>-</sup> can be found to be adsorbed on the surface of the sensitive material. The chemical reaction taking place on the sensitive material surface is given in eq (3) and the mechanism of MICS 5524 MOS sensor is explained in Fig 3.1.

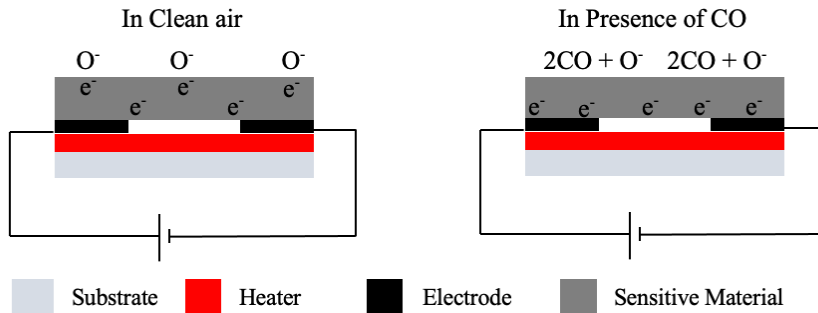


**Figure 3.1** Showing the mechanism of CO sensing in MOX sensor (a) the oxygen molecules get adsorbed on the surface of the sensing layer on the chip when connected to the battery in presence of air; this attracts electrons from the metal oxide layer (b) in the presence of CO, the oxygen reacts with CO thus releasing allowing the electrons to flow inside the chip which increases the conductivity

### 3.2 Fabrication of flexible circuit strips

To design a flexible sensor, a commercially available MOX sensor chip MiCS-5524 was designed with the recommended supply and measurement circuit given in the datasheet as shown in Fig 3.2.

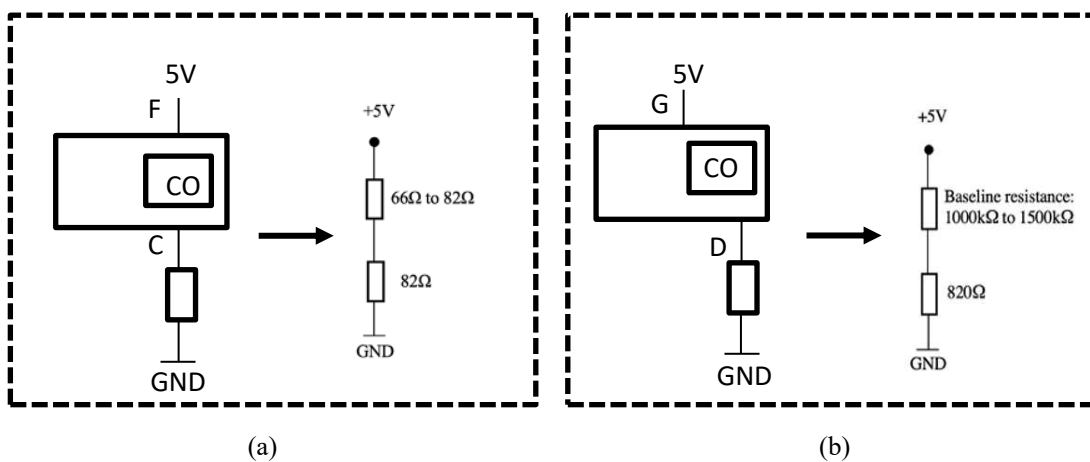


**Figure 3.2** (a) Supply and (b) Measurement circuit design recommended in the datasheet (redrawn) of MICS 5524 with equivalent electrical circuit diagram (F,C,G and D are pin details on datasheet)

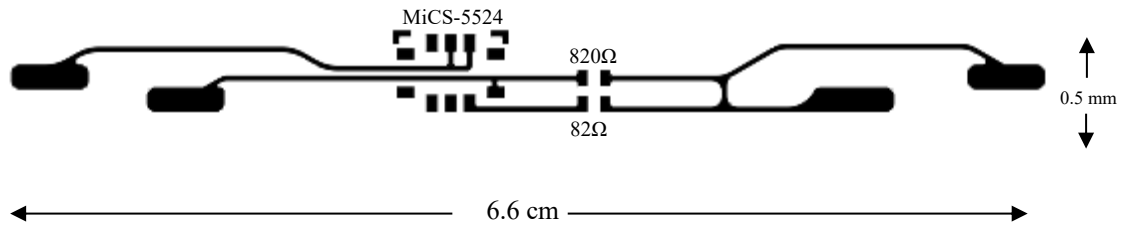


Figure 3.3 Schematic illustration of the Mask Layout for modified circuit design using CorelDRAW

### 3.2.1 Substrate preparation

- The copper-coated Kapton was cut into the shape of 6-inch Si wafer and attached to the 6-inch silicon wafer using photoresist. The chuck or the wafer holder is attached to the spin coater that is held by vacuum suction. Once the vacuum in the monitor is above 15, the spin coater becomes ready. The photoresist S1813 was poured on to the wafer as shown in Fig 3.4 (a), which acts as a glue to stick copper plated Kapton onto the wafer. The setting for the speed and time was adjusted using the monitor Fig 3.4 (b). The spin coater lid is then closed and run for the resist coating.
- After the spin coating of the resist, the copper plated Kapton is attached to the wafer. This substrate was then spin coated with the same S1813 photoresist.
- On top of the copper coated Kapton, the positive resist was spin-coated on the substrate for 30 secs (at 500 rpm for 2 secs and then 1500 rpm for 25 secs and 500rpm for 3 secs) as shown in Fig 3.4 (c)
- The resist coated substrate was cured at 110° C using hot temperature oven Thermo Scientific Heraeus Oven for 3mins shown in Fig 3.4 (d)

### 3.2.2 Photolithography

- Thermally cured wafer with resist was placed under UV lamp (located on the bottom side of the device) operated with a wavelength of 395 nm using LV202E Mega UV unit shown in Fig 3.4 (e). The box was closed and preheated for 5 mins as suggested by the LV202E manual.
- The acetate mask was placed first, and the resist coated wafer on top of it. The box was closed The UV light was exposed for 30 secs

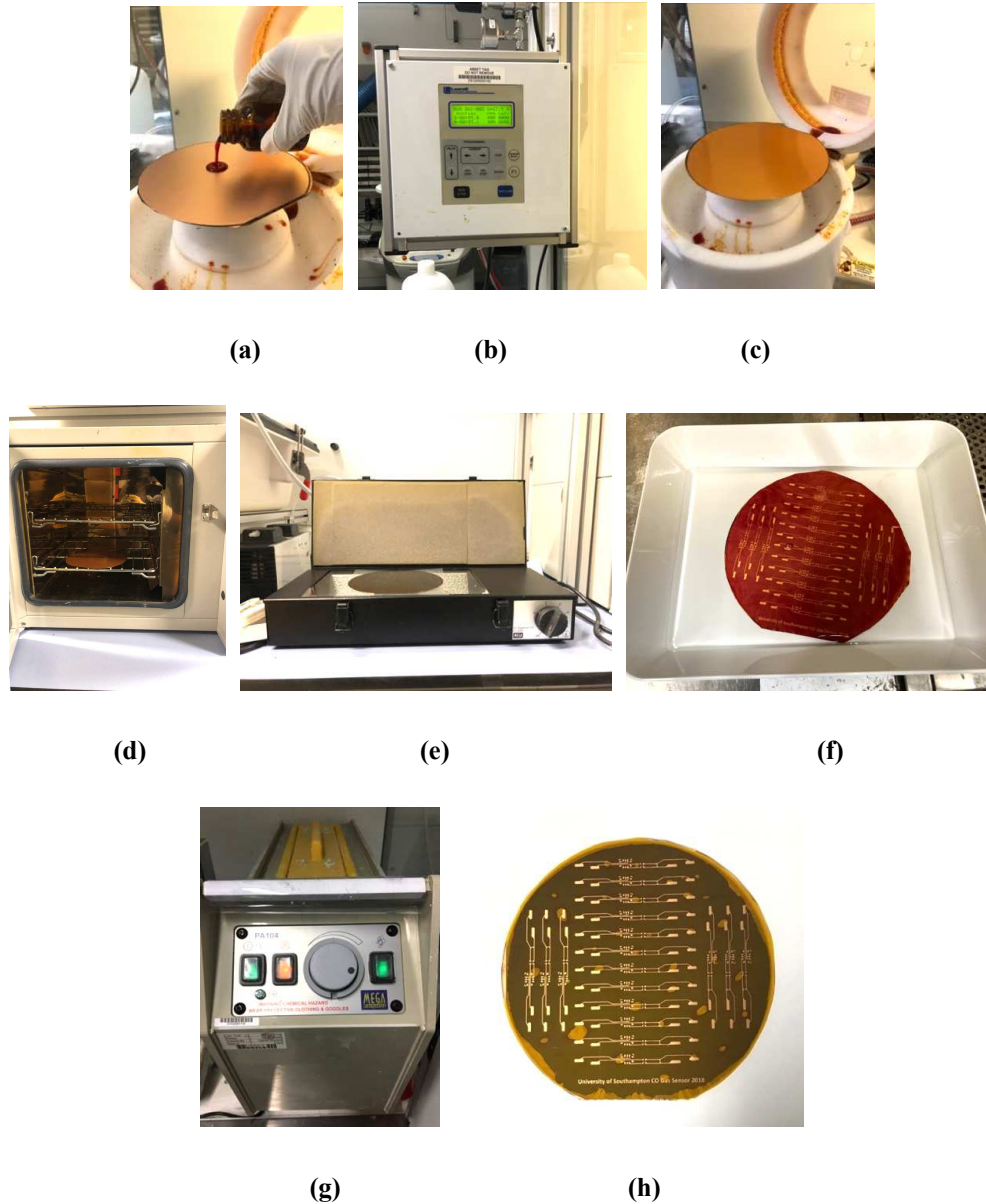


**Figure 3.4 a) pouring resist on wafer with copper plated Kapton, b) monitor to set the values of speed and time (c) photoresist coated wafer d) Wafer placed inside oven e) wafer placed in LV202E for UV exposure f) Wafer in the developing solution and then g) etched in the etching tank to get h) circuits by standard photolithography**

- The UV exposed substrate was then developed using the solution AZ400k and water (1:4) in a dish as shown in Fig 3.4 (f) for 10-15 seconds until photoresist has been visibly removed and rinsed with water and dried.
- The copper was wet etched using fine etch crystal solution for 8 mins in Mega Electronics PA104 PCB Bubble Etch Tank Fig 3.4 (g), rinsed with water and dried
- The Kapton substrate with copper tracks was cleaned with Isopropyl alcohol (IPA) and acetone to remove extra traces of resist. The etched wafer is shown in Fig 3.4 (h)

### 3.2.3 Mounting of Surface mount devices (SMD)

- The substrate was cut into individual strips and was attached to alumina (ceramic) tile for mounting the SMD using Kapton tape along the sides of the circuit strip (both length wise and width wise) as shown in Fig 3.5. This was applied to a flat surface thus providing an even surface for application of solder paste and SMD components. This also avoids curling the circuit strip while heating in the reflow oven and displacing the components as shown in Fig 3.5.
- CW8400 from RS components Flux pen was used before applying the solder paste to the copper pads to remove dirt on the strip providing better adhesion of the solder paste. The lead-free solder paste by BLT was diluted using flux pen to have a better flow and was applied to the copper pads using a needle.
- Once the solder paste was applied, Loctite 401 (20 g) was used as an under fill at the places where the SMD components are to be placed. For circuits used for mechanical testing involving bending and washing tests in chapter 6, EP37-3FLF was used as underfill. This adhesive was chosen as a result of high durability achieved in the FETT project [15].
- Using a tweezer, the SMD for CO sensor (MiCS 5524 by SGX SensorTech) and the resistors (Vishay CRCW Series Thick Film Surface Mount Fixed Resistor 0805 case  $82 \Omega \pm 1\%$  and  $820 \Omega \pm 1\%$ ) were attached to the copper pads.
- The solder paste was cured in the reflow oven. It was preheated until it reached  $100 \text{ }^\circ\text{C}$  and then the circuit strip was placed and heated until the oven reached  $250 \text{ }^\circ\text{C}$ . The curing process was completed and indicated by shiny silver colour of solder paste
- The copper wires were used for the power, ground and output connections and they were attached by using soldering iron

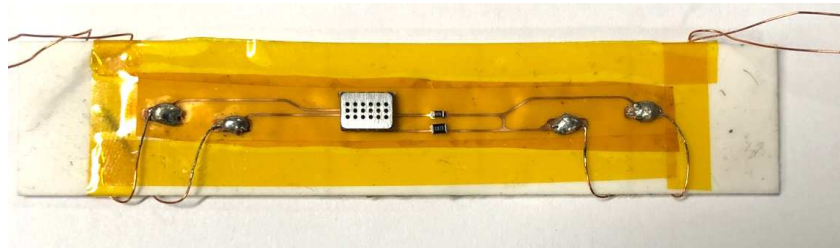


**Figure 3.5 Flexible circuit strip with gas sensor chip MiCS-5524 attached on Kapton attached to the alumina tile using Kapton tape after mounting SMD resistors**

### 3.2.4 Sensor connection checking

The sensor circuit connections are important to get reliable output from the sensor. For this purpose, the resistances were measured across the contact pads for connecting the sensor to the (a) power supply and (b) the output voltage across the  $820 \Omega$  resistor using a multimeter. Any variation in these

measured values directly corresponded to circuitry failure such as any damage in the copper tracks or the SMD components not soldered well, or the wires soldered to the copper pads were not well soldered. These lead to open circuit and the sensor could not function as it was supposed to be or could exhibit normal functionality.

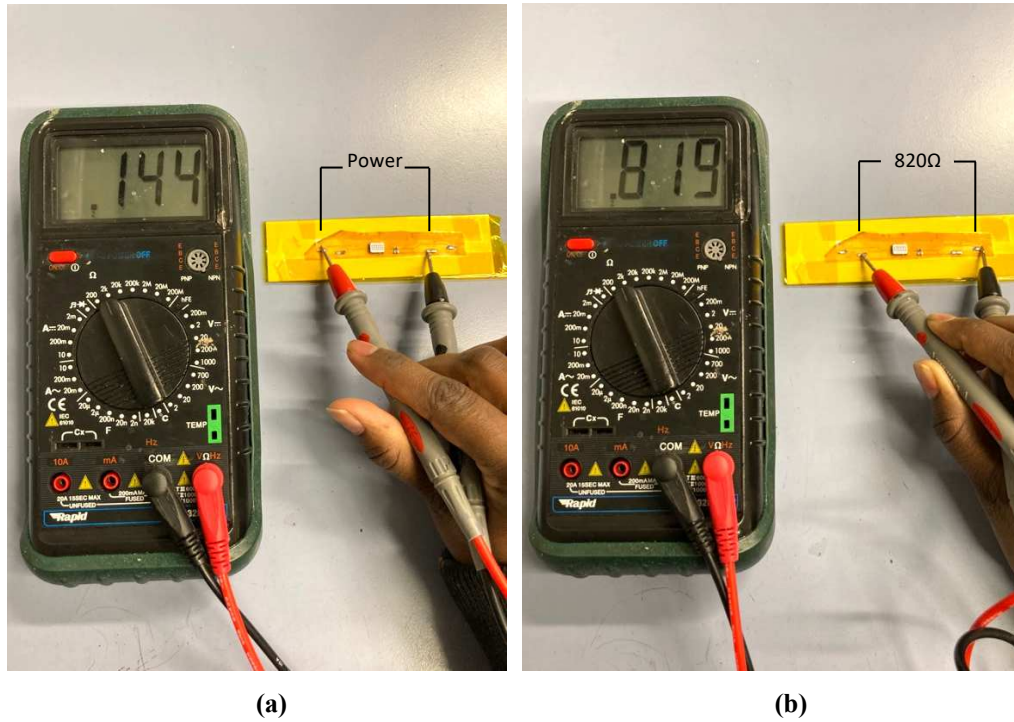


**Figure 3.6 Resistance across the power supply contact pads and output contact pads (across 820Ω) is observed using multimeter to check the connection of the components in the flexible sensor strip**

As shown in Fig 3.6 (a) the resistance of the contact pads to the power supply was about 144 Ω and were like all the 9 sensors measured as shown in Table 3.1. The same was with the load resistor. These values may change mildly due to the ambient temperature.

**Table 3.1 Resistances across the power supply contact pads in the flexible sensor strip for all 9 sensors**

	Resistance (Ω)								
Measurement Taken across	Sensor 1	Sensor 2	Sensor 3	Sensor 4	Sensor 5	Sensor 6	Sensor 7	Sensor 8	Sensor 9
Power	144	144	146	146	144	146	144	146	146
Load resistor	821	819	820	818	821	822	819	817	820

Since the resistance could change with ambient temperature, the resistance was checked before each experiment. The resistances were checked before sensors were powered on for each experiment at these points given below,

- At the contact pads in the flexible circuit
- At both the ends of the wires connected to the contact pads after soldering
- At the ends of the wires connected via chassis wire connector. This was when the sensors were placed inside the chamber
- For the resistance across the load resistor, the resistance was checked on the terminal board of ADC 20/24 after connecting the wires from the chamber

### **3.3 Experimental setup of gas sensor testing chamber**

The gas chamber was made of plexiglass (acrylic) with dimensions of 150mm (L) x 150mm (W) x 160mm (H) and a thickness of 4mm as shown in Fig 3.7. The chamber was made airtight by attaching rubber beading on the top lid. The advantage of having a smaller chamber is it requires a less amount of carbon monoxide to reach higher concentration. The air in the gas chamber is not removed by a vacuum pump and this gives an ambient (indoor) environment to test the samples. However, the air inside the gas chamber would reduce the concentration due to dilution of gases. Hence to find the concentration of gas inside the chamber after the gas cylinder valve is opened, a reference detector was used.

The inlet of the gas is positioned at one side of the chamber and the gas is vented out by opening the top lid of the chamber. A 5 V DC axial fan was attached to the side wall of the chamber to uniformly distribute the carbon monoxide inside the chamber (Sensor response was affected without fan shown in Appendix A). CO is slightly lighter than air hence the fan is fixed on one side of the chamber so that CO is mixed well with the air inside and uniformly distributed.

The carbon monoxide was given using a cylinder of known concentration of carbon monoxide (1000 ppm), balanced with air as shown in Fig 3.8. UEI CO71 carbon monoxide alarm was used as a reference detector to know the concentration of the gas inside the chamber when gas is let into the chamber. The experiment was done under the fume hood to extract the gas from the outlet. A wireless thermometer/hygrometer was placed inside the chamber to monitor the temperature in °C and relative humidity in %.

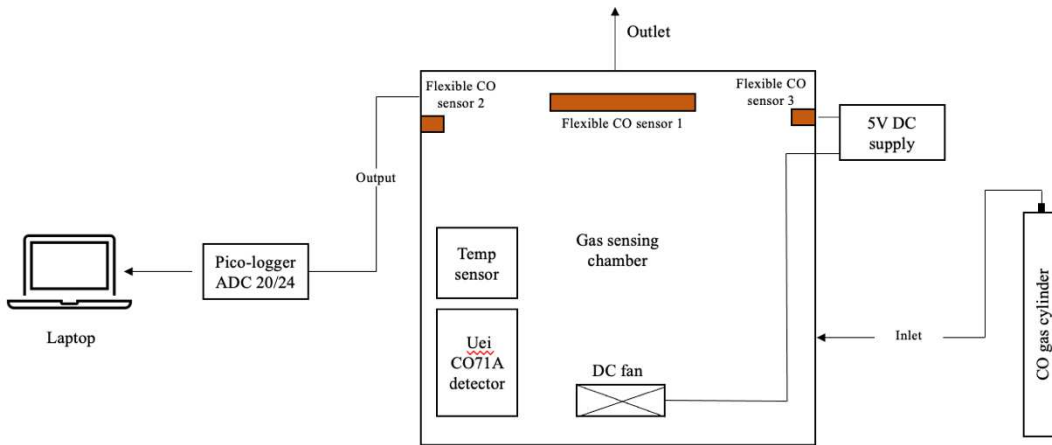


Figure 3.7 Schematic diagram of gas sensor test rig

The flexible sensors mounted in ceramic tile was stuck to the walls of the gas chamber using bluetack. All the sensors were connected to the ACD 20 using 12 pin Phoenix contact cable assembly connected tightly sealed in a hole drilled at one of the walls of the chamber.

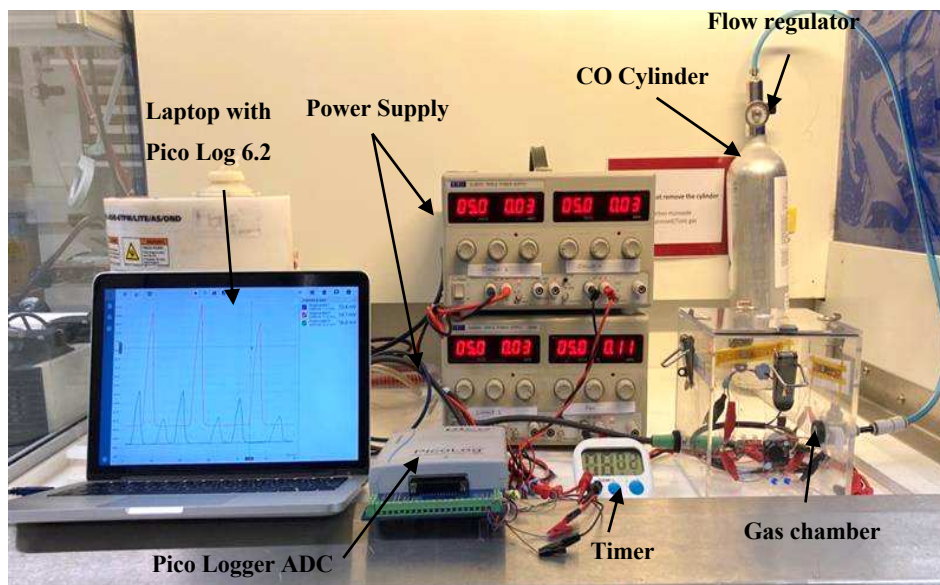


Figure 3.8 Experimental setup for detection carbon monoxide gas in fume hood

Each wire from the cable were connected to the circuits using crocodile pins inside the chamber, and the wires from the cable assembly were directly connected to the terminal board of the ADC 20. The devices were chosen such that they fit inside the chamber. The devices used for the experiments are shown in Table 3.2. Two power supplies were used to power the devices without any ground looping issues.



**Table 3.2 Components inside the chamber**

Device	Company	Range	Accuracy	Dimensions (mm)
Reference sensor	UEi CO71A	1 -999ppm	$\pm(3\%$ of reading +1ppm)	40.1*49.5*378.4 (Height*width*depth)
Temperature sensor/ Hygrometer	Sensor blue wireless	-50 - +300°C	$\pm 0.5^\circ\text{C}$ (-20 to 100°C)	38*62*13 (Height*width*depth)
Timer	Omnia Stores Digital Timer and Stopwatch	1 -99 mins	-	80*75*20cm (Height*width*depth)
CO cylinder	58L Safety monitors	1000ppm	$\pm 2\%$	360*90 (Height*Diameter)
Flow regulator	SGI constant flow regulator	0.5 lpm	-	82.5 (Height)
DC axial fan	Sunon	-	-	25*25*6 (Height*width*depth)

### 3.3.1 Characterization of gas testing chamber and reference sensor

The gas chamber was characterized with the help of the reference detector UEI CO71. The CO gas was sent inside the chamber and the concentration was noted down by observing the value read on the reference sensor. A timer was used to note down the settling time of the concentration observed on the reference sensor. The reference sensor was reading 0ppm until the carbon monoxide was sent inside the chamber which tells that the reference sensor is not affected by any other gas molecules inside the chamber. Once the chamber was characterized, the commercial chip was tested. After each experiment, the gas was vented out from the chamber by opening the top lid to the fume hood extract.

The concentration was plotted for the reference sensor to read a steady state value after the gas is entered inside the chamber. The valve of the cylinder was opened for a known time (in seconds) to send in gas and to observe the concentrations for a different time duration of valve opening. The time taken to reach a constant concentration was noted using a timer. The concentration was observed to be increased as the time of gas entering inside the chamber was increased as shown in Fig 3.9. The average concentration observed for each time duration of valve opening is plotted against time. The permissible exposure according to OSHA PEL standards is 50ppm for 8 hours. The target is to achieve 50ppm to have a CO triggering value. To get different concentrations for testing, the cylinder

valve was opened for 10, 20, 30 and 40 seconds. It is observed that for a higher time duration of the valve being opened (gas in time), the concentration increased.

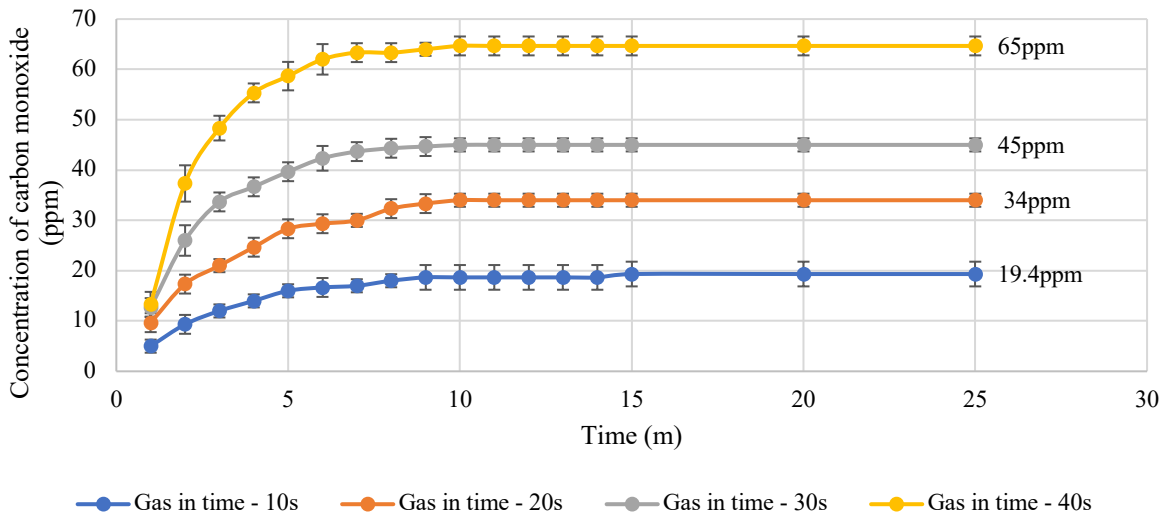


**Figure 3.9 Showing increase in concentration with increase duration of CO gas passed inside the chamber**

It was observed that the reference sensor took about 10 mins to reach a steady state value for different concentrations ranging from 19.4ppm to 65ppm as shown in Fig 3.9. After each experiment, the chamber top lid was opened to vent out the gas inside the chamber to the extract in the fume hood. It was made sure that the fume hood sash was completely pulled lower to avoid exposure of CO from the chamber. The time taken for the reference sensor to read 0ppm was noted to be about 15 mins as shown in Fig 3.10.

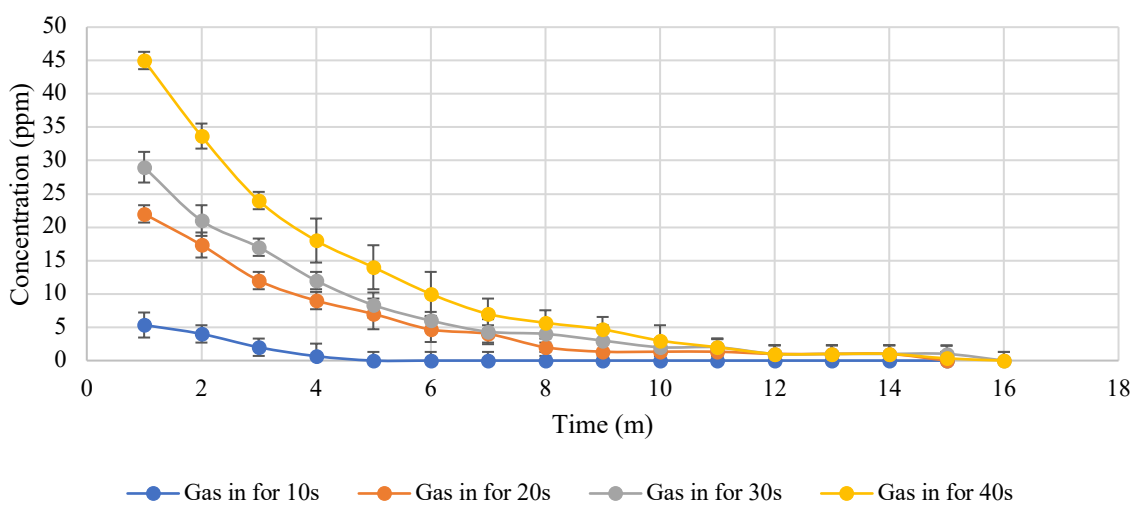


**Figure 3.10 Showing decrease in concentration read on the reference sensor**

The concentrated CO gas is mixed with air instead of the chamber which will reduce the concentration of the gas.

**Table 3.3 Theoretical and experimental values of diluted CO gas concentration inside the chamber for each constant flow regulator valve opening time**

Gas valve open time (s)	Concentration of the gas in the cylinder (ppm)	Volume of gas coming from the cylinder (ml)	Volume of chamber with air and concentration (ml)*	Concentration of the gas in the chamber – theoretical (ppm)	Average Concentration of the gas in the chamber – practical (ppm)
10	1000	83	3683	22.5	19.4
20		166	3766	44	35
30		250	3850	64.9	45
40		333	3933	84	65

1 cm<sup>3</sup> = 1 ml

The dilution concentration could be calculated by  $C_1V_1 = C_2V_2$ , where  $C_1$  was the concentration of the gas inside the cylinder,  $V_1$  was the volume of the gas coming from the cylinder,  $C_2$  was the concentration of the gas diluted inside the chamber (mixed with air),  $V_2$  was the volume of the air/gas inside the chamber with the incoming gas from the cylinder ( $V_1+V_2$ ). Using this formula, the theoretical values were calculated and compared with the practical values as shown in Table 3.3.

For each experiment, the amount of gas used was 7L. The difference in the concentration values from theoretical and experimental could be due to accuracy of the concentration of the gas in the cylinder, which was  $\pm 2\%$ , or timing between opening and closing of the constant flow regulator valve which was performed manually or could be due to the leakage in the chamber itself as the experimental concentration values were lower than the theoretical values.

The leakage in the chamber was checked by letting the gas flow in with the chamber closed and the concentration of the reference sensors were observed. The concentration reading on reference sensor was noted for every 20 mins. It was observed that the concentration read on the reference sensor decreased over time and read 0ppm as shown in Fig 3.11. This showed that there was a leakage in the chamber and the chamber was not completely airtight.

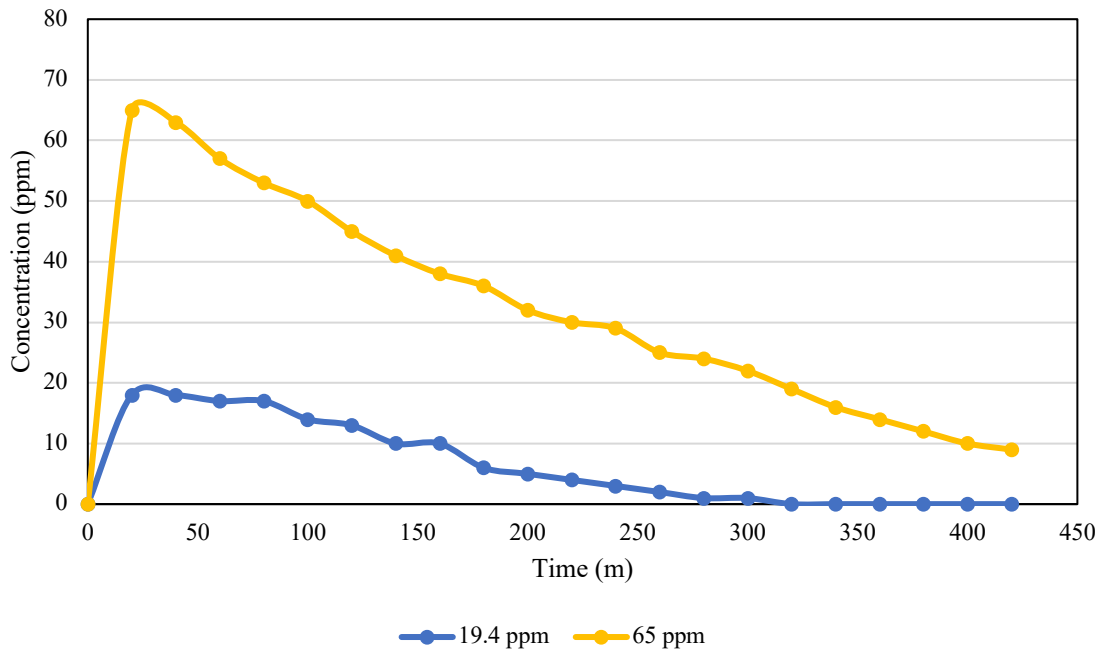


Figure 3.11 Showing decrease in concentration of CO<sub>2</sub> inside chamber with lid closed over 7 hours

### 3.3.2 Warm-up time evaluation of MiCS-5524 gas sensor chip

The heater element was required to bring a chemical equilibrium where the resistance of the sensor stabilised after adsorption and desorption of chemical compounds taking place on the sensing material [97]. The warm-up period was the time taken to achieve a stabilised sensor resistance after the device was powered. The sensor also should be heated to allow oxygen in the air to bond with the metal oxide layer that attracts the electrons thus increasing the resistance of the sensor. 9 flexible CO filament were powered with 5V, and the output voltage was measured in ambient condition.

It was observed that when the sensor was powered, the sensor voltage was noticed to be increasing as shown in Fig 3.12. This could be because the heater takes time to reach a certain temperature that attracts the oxygen molecule on the surface of the sensor that increases the sensor resistance. However, it was also noticed that the settling time varied between different sensors. The sensor resistance in the air was not a constant value for all the sensors as the sensor resistance in air varies over a wide range from 100 to 1500 k $\Omega$  in presence of air as per the datasheet. This also showed that the type of metal oxide layer used in the sensor is an N-type from the response obtained where the resistance increased with increase in the concentration of adsorbed oxygen as per the literature. It was also observed that the resistance of the sensor in ambient air varied over a longer time, which could be because of other gas molecules other than oxygen.

Hence the sensor was turned ON for one hour before testing the sensor with carbon monoxide to get a stabilized value. The resistance drift could also possibly be due to the variation in the ambient

temperature or due to the fan inside the chamber that affected the temperature of the heater element inside the sensor.

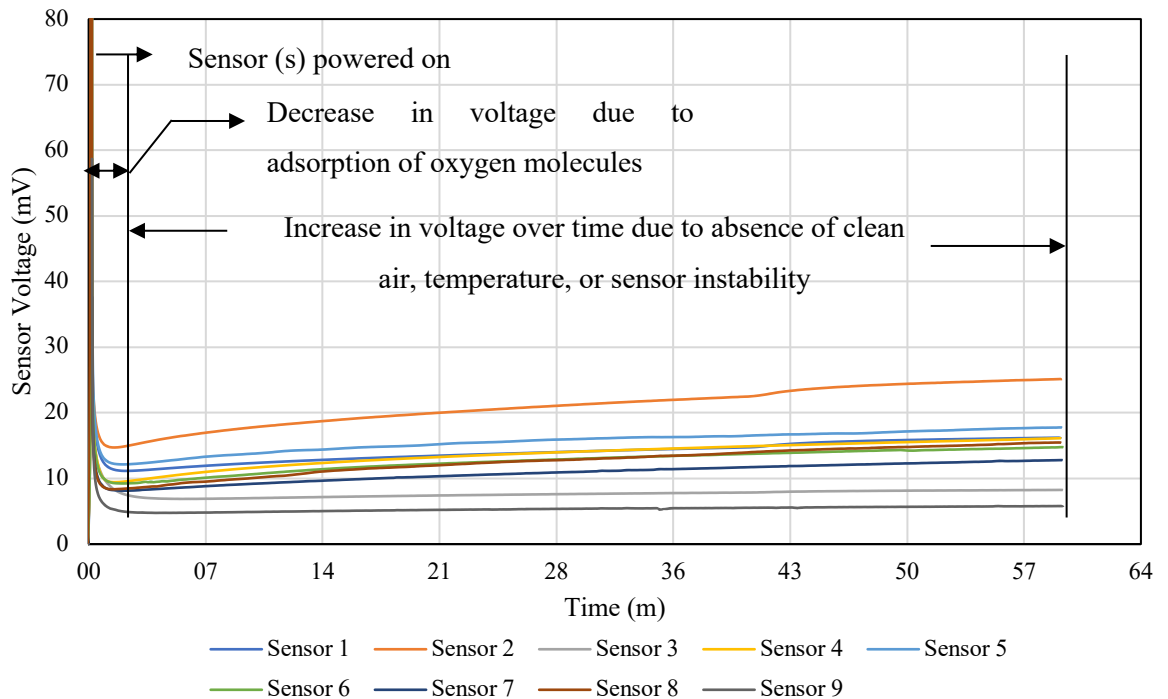


**Figure 3.12 Warm up – the sensors were left on for one hour and a constant increase in voltage is observed**

The temperature effect of the fan on the sensor resistance was observed by turning ON and OFF the fan. Three devices were placed on the sides of the chamber using Blue Tac. The experiment was run for four different conditions; Chamber closed with fan on, Chamber closed with fan off, Chamber open with fan on, Chamber closed with fan off. Each condition was run for 1 hour shown in Fig 3.13. The temperature and the relative humidity were constantly observed and noted for every 5 mins. It was observed that when the chamber was closed with fan on, there was an increase in the baseline resistance of the sensors. When the fan was turned off, the baseline resistance keeps increasing. However, when the chamber lid was open, the baseline resistances rapidly fell.

Another factor was that gas sensors were temperature and relative humidity sensitive as seen in the literature. The variations in the baseline resistance might be because of the temperature and relative humidity variation.

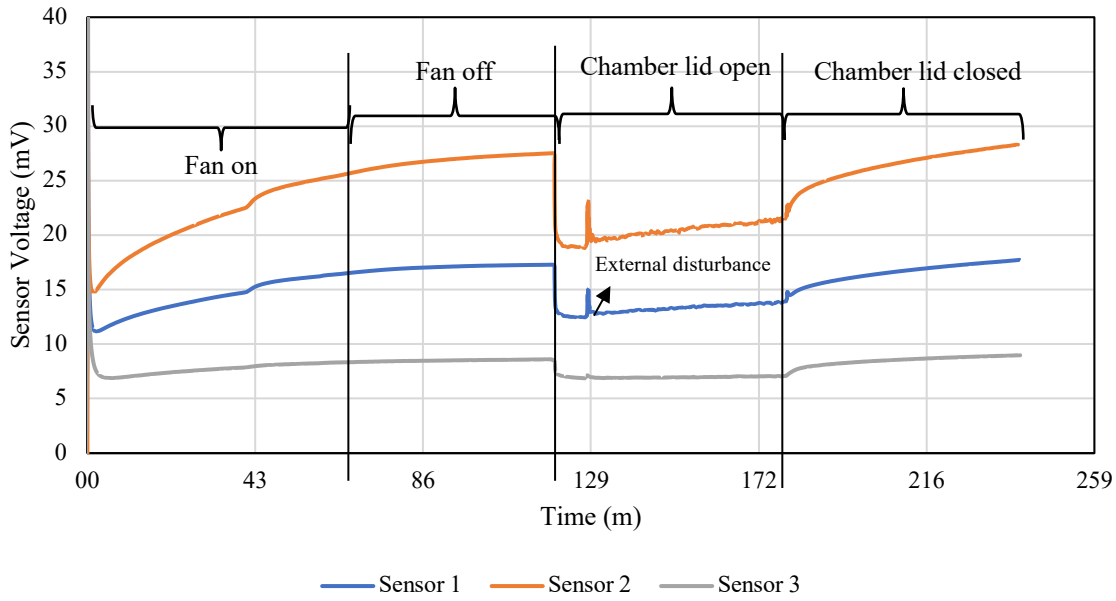


**Figure 3.13 Gas sensor baseline resistance vary with fan on inside the chamber, fan off and chamber lid open**

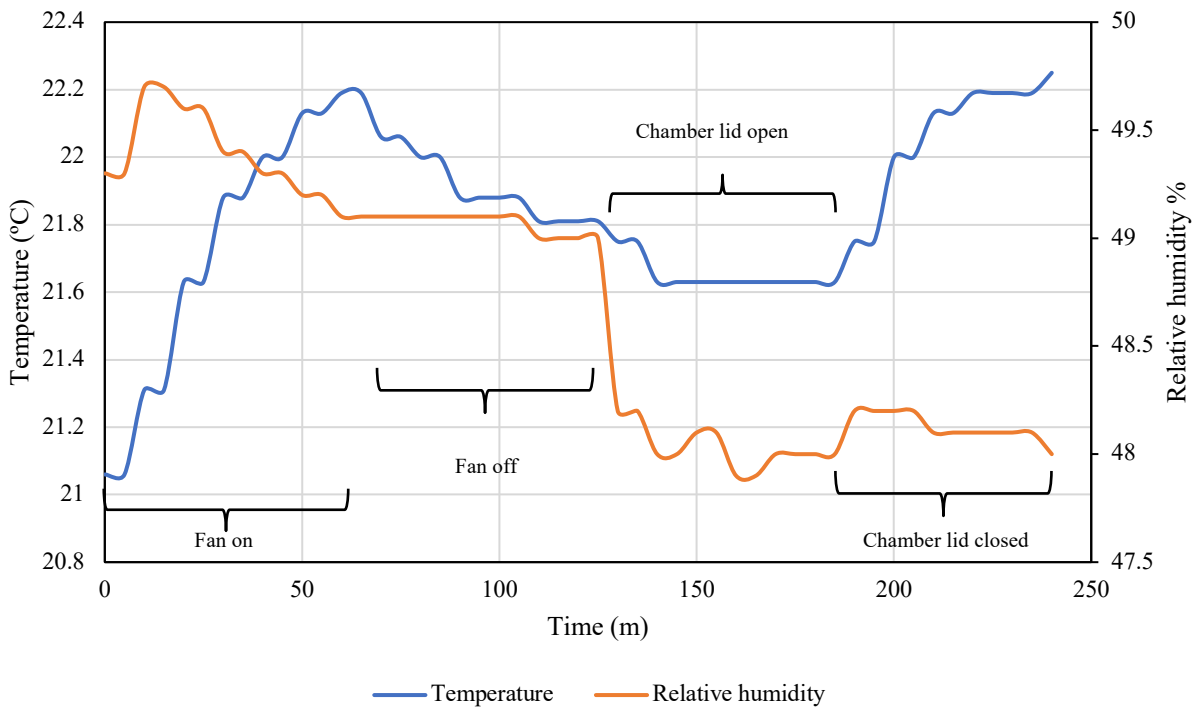


**Figure 3.14 Temperature and Relative Humidity variation showing the temperature increases with decrease in relative humidity for different environmental conditions**

As shown in Fig 3.14, the temperature was higher/ increased when the fan was on and decreased with the fan was off and the chamber lid was open whereas the relative humidity did the opposite as the temperature and relative humidity were inversely proportional.

The MICS gas sensor has also been observed to be sensitive to external vapours present in the lab such as hand sanitizer and acetone as shown in Fig 3.15. The experiment was run by keeping the chamber lid open and bring acetone and hand sanitizer vapours near to the chamber randomly. As seen in Fig 3.15, the sensors were responding to these vapours.

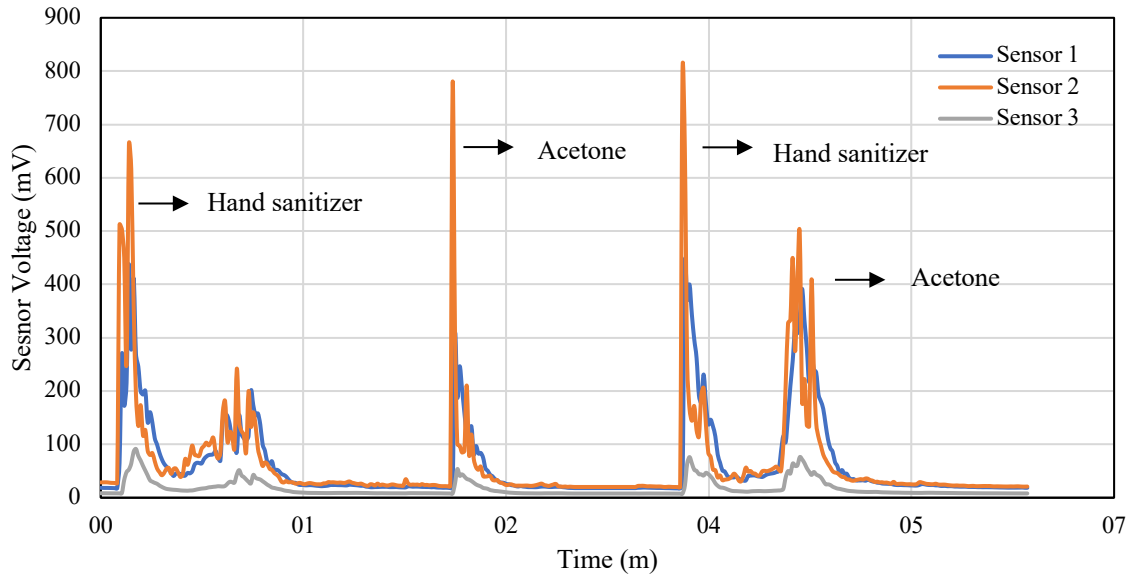


**Figure 3.15 Factors influence the baseline resistance when the chamber lid is open**

To check the baseline resistance variation with temperature, three sensors were placed on a hotplate as shown in Fig 3.16. For MICs 5524 the ambient operating temperature:  $-30\text{ }^{\circ}\text{C}$  to  $+85\text{ }^{\circ}\text{C}$ . Hence the experiment was run from room temperature up to  $70\text{ }^{\circ}\text{C}$ .

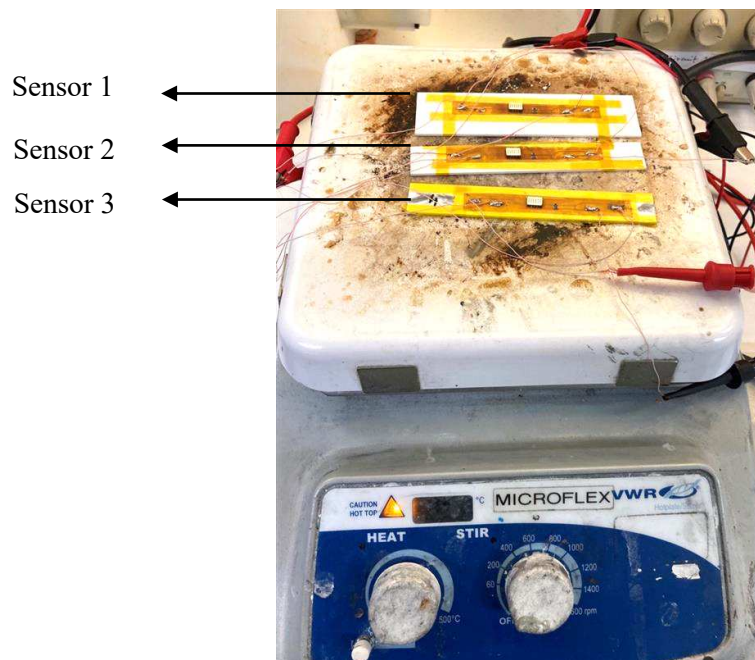


**Figure 3.16 Three sensors placed on hotplate to demonstrate sensor baseline variation for different temperatures**

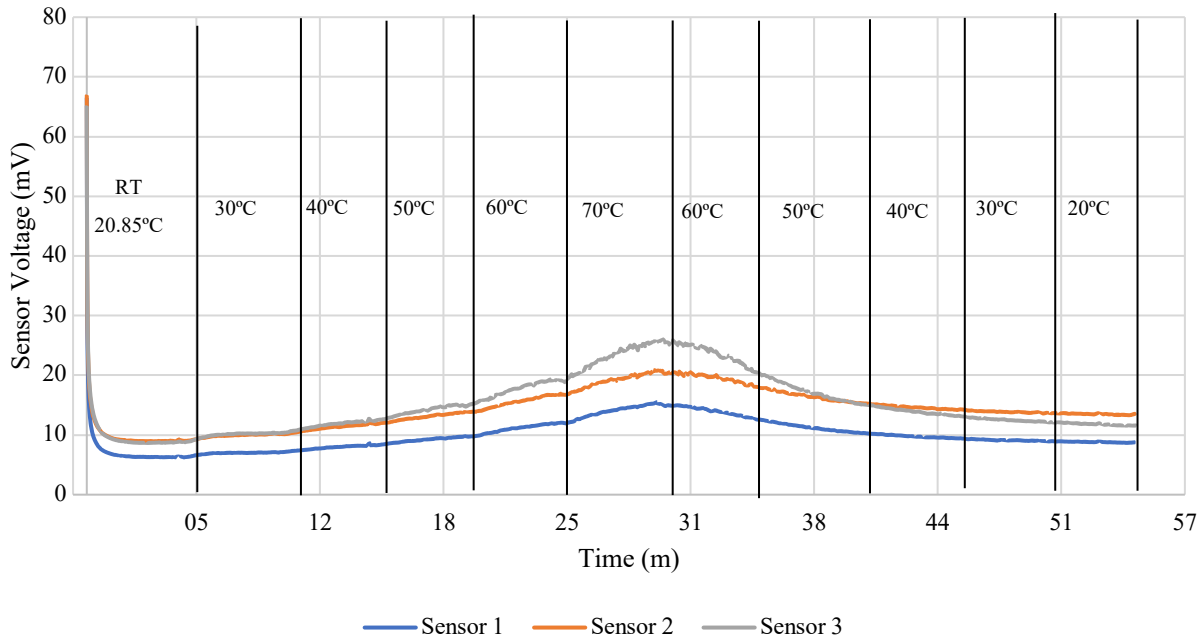


Figure 3.17 Influence of temperature on sensor voltage

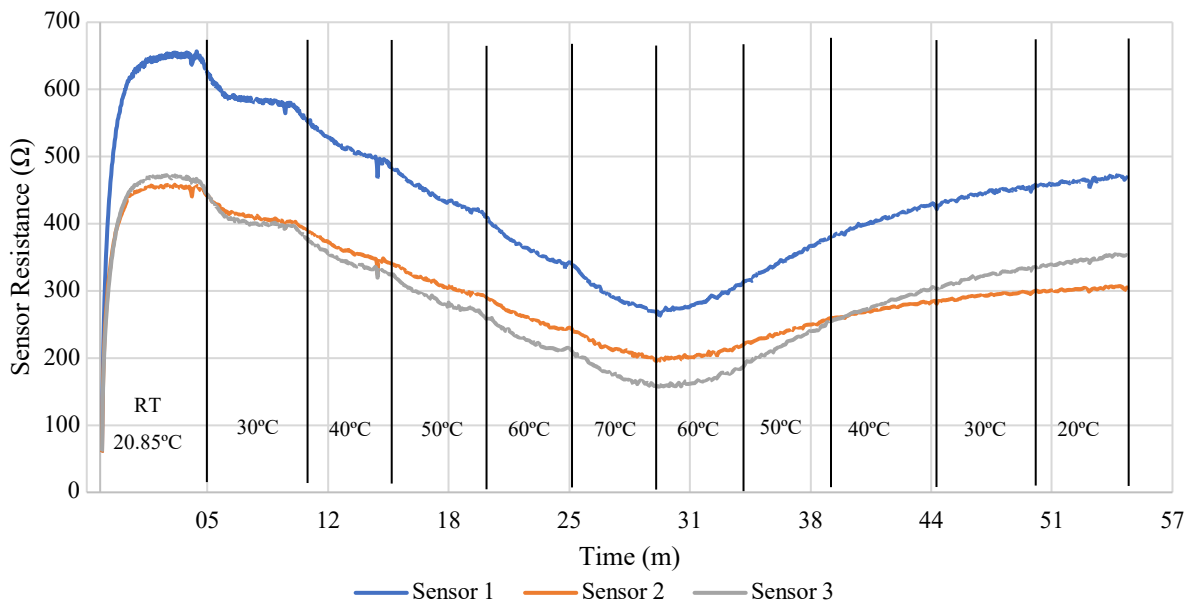


Figure 3.18 Influence of temperature on sensor baseline resistance

The baseline voltage increased with increase in temperature and decreased with decrease in temperature as shown in Fig 3.17. The baseline resistance variation is also shown in Fig 3.18.

### 3.3.3 Testing of MiCS-5524 with Carbon monoxide

The sensor was given 5V using a power supply and the output voltage across the load resistor in the presence of carbon monoxide was observed using a multimeter as shown in Fig 3.19. As mentioned in the datasheet of MiCS 5524, the voltage across  $R_L$  was directly linked to the resistance



of the sensor. When the gas was sent in, the voltage across the load resistor was observed and the concentration was read from the reference sensor at room temperature. It was observed that as the concentration increased, the voltage (in mV) was observed to be increasing. This was due to the reaction of reducing gas like CO with the adsorbed oxygen on the sensor that releases the free electrons held by the oxygen molecules flow back through the sensor that increases the conductivity. The starting voltage (or  $R_0$ ) was varying as seen before due to the temperature or the sensor instability. Each sensor has different baselines resistance.

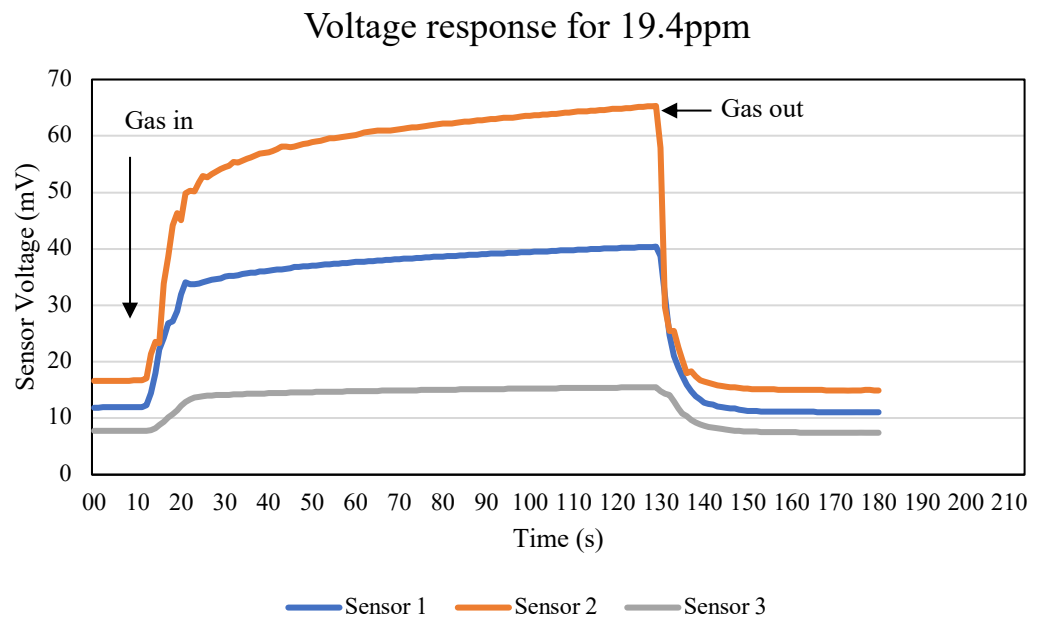


**Figure 3.19** Sensor response by measuring the output voltage for each sensor

The resistance was calculated for obtained voltage values to find the response. Using this voltage, the sensor resistance was calculated by using the voltage divider rule as given below eqn. (3),

$$R_s = \frac{R_L}{V_L} (V_s - V_L) \quad (3)$$

Where,  $V_L$  was the voltage across the load resistor,  $V_s$  was the supply voltage,  $R_L$  was the load resistor ( $820\Omega$ ) and  $R_s$  was the sensor resistance.

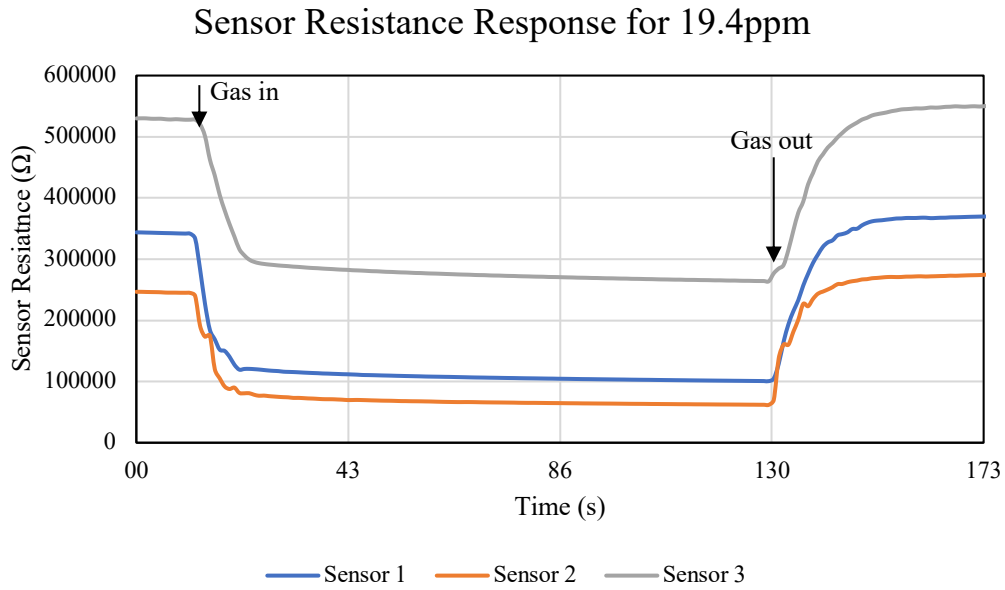


**Figure 3.20** Calculated resistance of the gas sensing response of each sensor

The resistance of the sensor decreased with increase in concentration. The issue encountered in Fig 3.19 and Fig 3.20 was that the starting voltage and resistance ( $R_0$ ) in the presence of ambient air varied for each experiment. However, taking the ratio  $R_s/R_0$ , could show the variation in sensor response at different concentrations. The response was given by  $R_s/R_0$  where  $R_s$  was the sensor resistance and  $R_0$  was the sensor resistance the in air. The response at different concentration are shown in Fig 3.21.

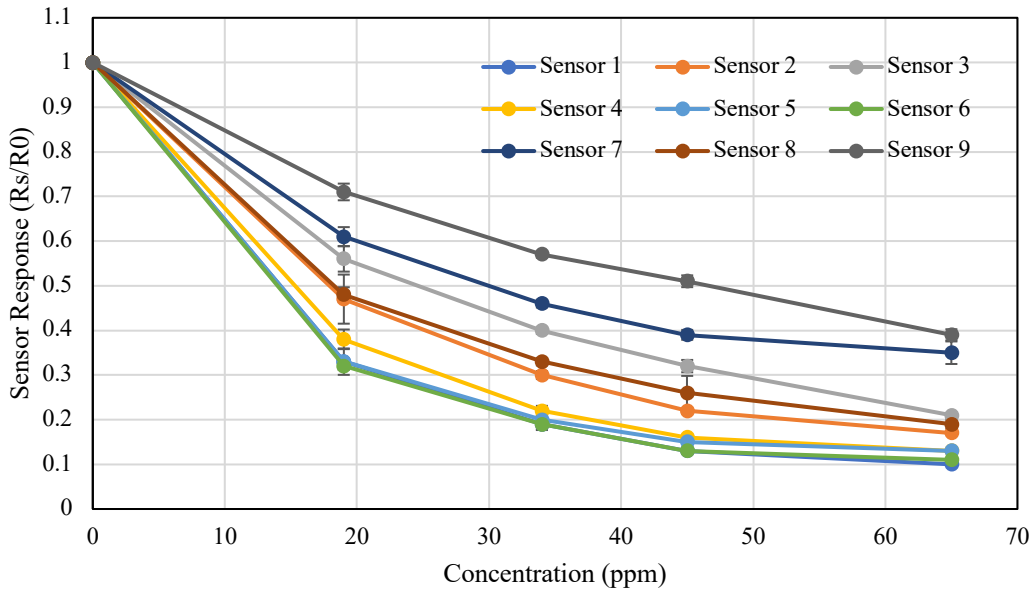


**Figure 3.21** Sensor response decreases with increase in concentration of CO gas

**Table 3.4 Response time, Recovery time and average response for all the sensors**

	Average Response time (s)				Average Recovery time (s)				Average Sensor Response			
	19.4 ppm	34 ppm	45 ppm	65 ppm	19.4 ppm	34 ppm	45 ppm	65 ppm	19.4 ppm	34 ppm	45 ppm	65 ppm
<b>Sensor 1</b>	10.3	27	38	51	4.6	2	2.3	1	0.40	0.27	0.20	0.17
<b>Sensor 2</b>	15	26	37	49	3.3	3.3	1	1	0.47	0.30	0.22	0.17
<b>Sensor 3</b>	9	18	33	40	4.6	6	4	2.3	0.57	0.40	0.33	0.27
<b>Sensor 4</b>	28.6	33	34	39	4	1	1	1.6	0.38	0.23	0.16	0.13
<b>Sensor 5</b>	36	35	29	35	1.6	1.3	1	1	0.34	0.20	0.16	0.14
<b>Sensor 6</b>	37	36	36	36	1.3	1.3	1	1.6	0.32	0.19	0.14	0.11
<b>Sensor 7</b>	8	12	12	5	5	7	6.3	9.3	0.61	0.46	0.39	0.35
<b>Sensor 8</b>	36	55	55	65	4.3	5	3.6	5	0.48	0.33	0.26	0.19
<b>Sensor 9</b>	6	15	24	33	5	7	7	10.3	0.71	0.57	0.61	0.39

The time taken to reach 90% of the final steady state value ( $t_{90}$ ) after gas in is the response time and the time taken to reach 90% of the baseline resistance after the gas is vented out is the recovery time. The recovery time ( $t_{10}$ ) was calculated by taking the time taken to obtain 10% of the maximum value added to the baseline voltage (as baseline varies with time for all the sensors). The average response time and recovery time are given in the Table 3.4. The response of the sensor is also denoting the sensitivity of the sensor. The average response of all the sensors before encapsulating are also provided in Table 3.4.

The recovery time was lower than the response time for all the sensors as shown in Fig 3.22. The recovery time for all the sensors is similar however there was a significant variation in the response time. The reason for faster recovery times may also be an impact of cooling down the sensors when the chamber lid was opened to vent out the gas leading to quicker reduction in output voltage of the sensors.

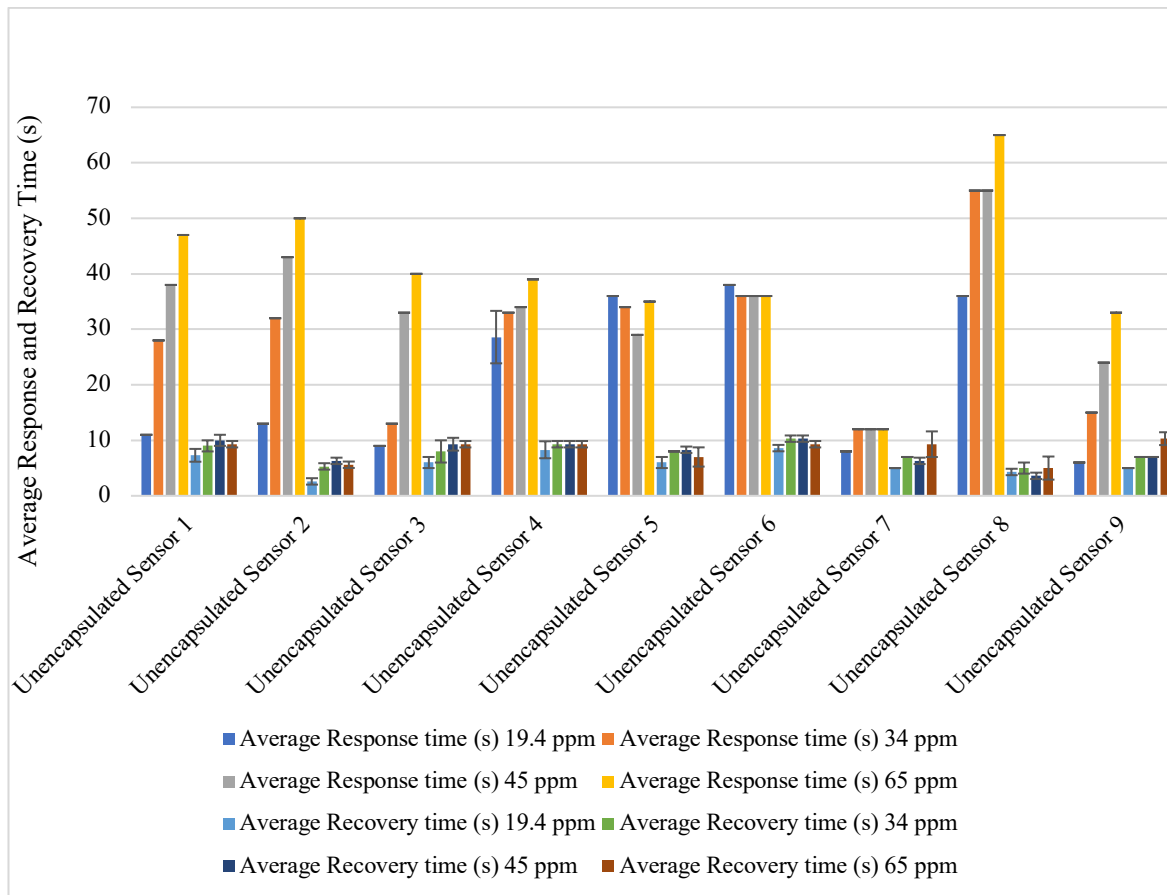


**Figure 3.22 Average response and recovery time for all the unencapsulated sensor filaments**

## Conclusion

- In this chapter, MOX sensor chip was used to build a flexible CO sensor filament. The working of CO MOX type gas sensor was explained, and the fabrication of the flexible filament was discussed in detail.
- Experimental rig for gas testing and characterisation of gas chamber with the help of a reference sensor was discussed. Based on different gas concentration readings of the reference sensor, the flexible filament was characterised with CO gas.
- It was also observed that temperature and humidity affect the baseline resistance of the flexible filament. An algorithm development is required to compensate the effects of temperature and humidity to avoid any false trigger of the gas sensor response
- Cross sensitivity of the sensor in presence of acetone and hand sanitizer can also trigger sensor response in absence of CO. Sensitive material that are highly selective only to CO is the best way to avoid cross sensitivity
- The sensor voltage increased with decrease in gas concentration. The response time increases with increase in concentration and recovery time decreases with increase in concentration.

# Chapter 4 Encapsulation Materials and Process Evaluation

This chapter includes material selection, and peel strength of the adhesives used, processes used for moulding materials and application on the flexible circuit. Further, we discussed characterization based on hydrophobicity, mechanical strength, and suitability to integrate with textile.

## 4.1 Gas and water permeability of polymers

Thermoplastic materials are polymers that have been used in textiles for coating with materials like polyimide, polyvinyl chloride (PVC), acrylics and others like polytetrafluoroethylene (PTFE), and polyurethane [98]. These materials have been used in textiles as waterproof and windproof fabrics. For instance, Gore-Tex is made of expanded PTFE (e-PTFE) that is used in windproof and waterproof jackets [99]. For gas sensor encapsulation, it is important that these materials are waterproof and gas permeable and there are few materials that have these properties.

Polymers are porous structures that allow gas molecules and liquids up to some extent depending on the pore size. The permeation occurs through the polymer is by pressure, temperature, or concentration gradient. The permeability takes place in three processes,

- Absorption – the molecules at a high concentration or pressure
- Diffusion – movement of molecules inside the polymer
- Desorption – release of molecules at low concentration or pressure

The diffusion of molecules through a polymer is given by Fick's law as given in eqn. (4),

$$Q = -D.A.dc/dx \quad (4)$$

Where,  $Q$  is the flux (of gas or liquid molecules) going through the polymer,  $D$  is the diffusion coefficient,  $A$  is the area of the polymer membrane,  $dc/dx$  is the concentration gradient ( $c$  - concentration,  $x$  - distance/thickness). However, the permeation of gases in a polymer is given by the function as in eqn. (5),

$$Q = P.A\Delta\phi/L \quad (5)$$

Where,  $P$  is the permeability,  $A$  is the area of the polymer,  $\Delta\phi$  is the potential difference of the polymer from one side to another,  $L$  is the thickness of the polymer. With this equation, the unit of permeability can be given as Barrer written as in eqn. (6),

$$1 \text{ barrer} = 10^{-10} \frac{\text{cm}^3\text{STP.cm}}{\text{cm}^2 \text{ s cmHg}} \quad (6)$$

Where STP is standard temperature and pressure. The higher the barrer value, more gas permeability properties of the polymer.

## 4.2 Selection of materials for packaging flexible gas sensor

The thermoplastic materials for the packaging of a gas sensor are required to be waterproof, gas permeable, flexible, and easy to apply on the circuit strips. The materials were bought however with different thicknesses as given in Table 4.1.

**Table 4.1 Materials to be used for encapsulation and bonding.**

Name	Company	Type	Materials	Thickness
PTFE glass fibre fabric	Esone	Encapsulant	Polytetrafluoroethylene PTFE	60 $\mu$ m
Zitex G - 104	Saint Gobain	Encapsulant	Microporous PTFE	104 $\mu$ m
Platilon U 4201 AU	Covestro	Encapsulant	Thermoplastic Polyurethane (TPU)	100 $\mu$ m
NLP11051	Lohmann	Adhesive	Silicone pressure sensitive	60 $\mu$ m
Acrylic adhesive	Esone	Adhesive	Acrylic adhesive	60 $\mu$ m

## 4.3 Adhesive used for bonding materials

Using flexible or semiflexible adhesive (i.e., liquid type), the thermoplastic materials can be bonded to flexible gas sensor filament. However, the binding is not uniform with these types of adhesives. It is also important to make sure the liquid adhesives do not pass through the holes in the commercial gas sensor and cause a short circuit.

### 4.3.1 Liquid Adhesives for high surface tension

Hydrophobic materials require special adhesives for bonding. Non-stick materials with high surface tension such as PTFE require special adhesives for bonding. A combination of Permabond POP Primer and cyanoacrylate adhesive can be used to bond the Zitex G - 104 to the gas sensing filament. However, the fluid state of the adhesive gave more non uniform coating and increases the stiffness of the sensor strip as shown in Fig 4.1. Instead, a uniform polymeric adhesive called the silicon pressure sensitive film can be used to bond Polytetrafluoroethylene (PTFE).

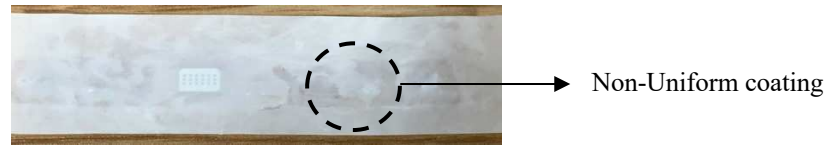


**Figure 4.1 Zitex G - 104 bonded to CO filament using Permabond POP Primer and cyanoacrylate semiflexible liquid adhesive**

#### 4.3.2 Pressure sensitive adhesive

Adhesives that bond by pressure are called pressure sensitive adhesive. There are mainly classified into three types: rubber, silicone, and acrylic. These come in uniform thicknesses. The application of silicone pressure adhesive can be achieved by applying constant pressure while rolling or surface press [100] whereas for acrylic adhesive can be directly applied to substrates. Using these adhesives can be helpful in clean and uniform packaging. However, it is important to have higher bond strength for the adhesives. The surface roughness of the substrates plays a role in bond strength. Therefore, a peel test is performed to find the average peel strength of the adhesives on the encapsulant materials, and the best solutions are used for packaging such that they withstand the mechanical stresses caused while bending or washing.

#### 4.4 Contact angle experiment for hydrophobicity of materials

The encapsulating material used for protecting the gas sensor circuits require to be low permeable to water such that the e-textile circuitry is protected and does not undergo short circuiting when washed or in presence of water. For this, the first step is to test the wettability properties of the materials, which can be determined by contact angle measurements as explained in detail below.

##### 4.4.1 Theory

Materials can be divided into groups of hydrophobic and hydrophilic properties. Hydrophobic materials have a low affinity to absorb the water molecules whereas hydrophilic materials have more affinity and cause wetting of the material.

This can be found by identifying the angle formed at the interface of liquid, gas and solid as shown in Fig 4.2. The greater the angle, more hydrophobic the material is. For super hydrophilic materials, the liquid spreads out over the material causing complete wetting and giving  $0^\circ$  contact angle (high surface energy). When the angle is between  $0^\circ$  to  $90^\circ$  the materials are considered to be hydrophilic. If the angle is between  $90^\circ$  and  $180^\circ$ , the material is hydrophobic and for angles greater than  $180^\circ$  the material is ultra- hydrophobic (low and very low surface energy respectively).

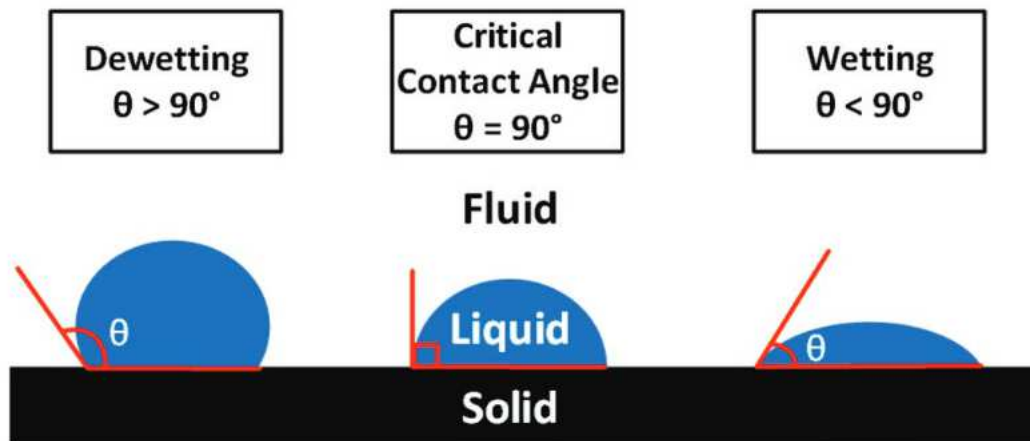


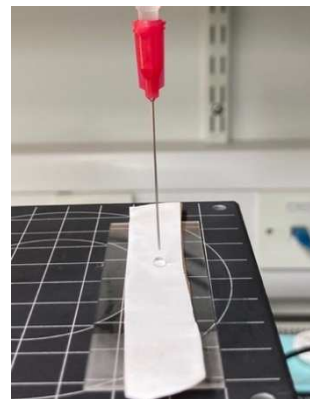
Figure 4.2 Contact angle measurement [101]

#### 4.4.2 Experiments and results

The samples – PTFE Fibre glass fabric, Zitex G - 104, Platilon U 4201 AU, Silicone pressure sensitive adhesive (NLP10051) and acrylic adhesive from Esone were cut in to 15mm width based on the standard ASTM D5946 and was placed in DSA30 Krüss Contact Angle Machine shown in Fig 4.3 (a).



(a)



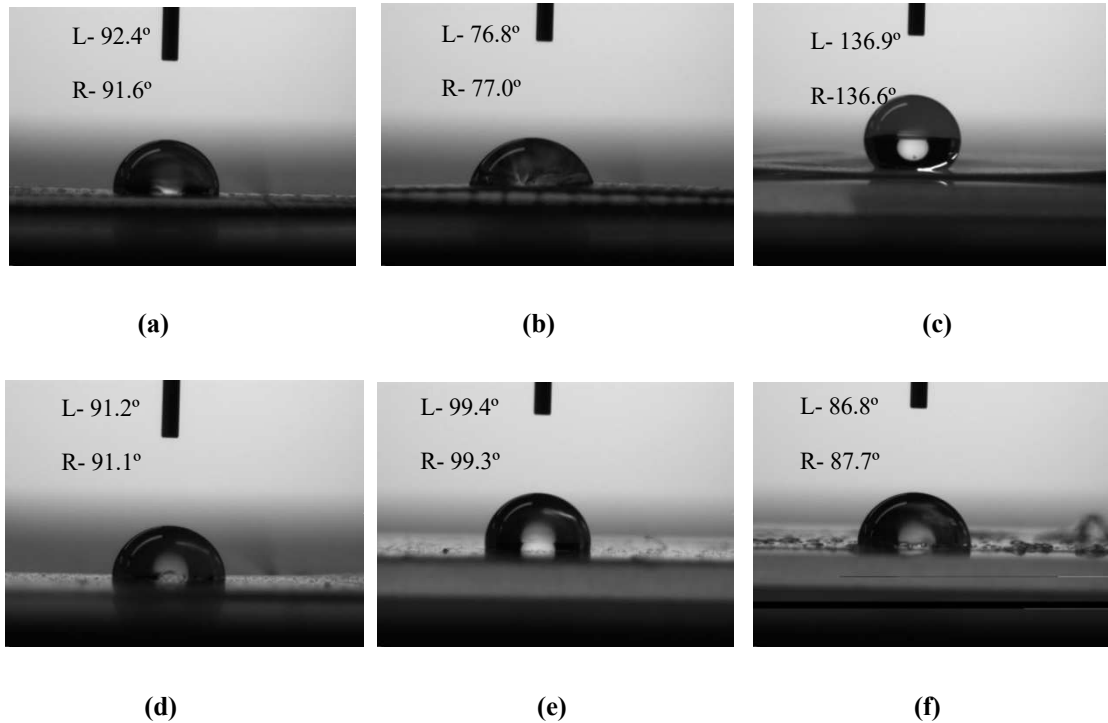
(b)

Figure 4.3 (a) DSA30 Krüss tensiometer for contact angle measurement (b) Zitex G - 104 sample with a droplet

The materials were placed on the glass slab and a syringe was filled with DI water to dispense 10 $\mu$ l droplets on the materials as shown in Fig 4.3 (b). The PSAs were placed with the carrier film on one side and the other removed and made sure that they were placed flat on the slab. The contact angle was measured 5 times for each sample to get an average. DSA4 contact angle software was used for capturing and measuring the contact angle.



Both the angles on left and right were measured. The results showed that all these materials measured contact angle was above  $90^\circ$  which meant that they were all hydrophobic. The most hydrophobic was observed to be the Zitex G - 104 as shown in Fig 4.4.



**Figure 4.4** Contact angle measurement for (a) PTFE Fibre glass fabric, (b) PTFE etched side (c) Zitex G - 104 (d) Platilon U 4201 AU (e) Silicon Pressure adhesive (SPA) (f) Acrylic adhesive

The measurements were taken 5 times for each material and the average contact angle for both the sides were noted as shown in Fig 4.5 and it is clear, that Zitex G - 104 was the most hydrophobic material. It was also observed that the etched PTFE Fibre glass fabric was hydrophilic due to surface roughness caused by etching. This aided in achieving adhesion with the silicone pressure adhesive with the substrate.

It is also important that the adhesives used for bonding must be hydrophobic as they may lose the binding strength in presence of water during washing e-textile circuits. It was observed that both the adhesives are hydrophobic, but the silicone pressure sensitive NLP11051 is more hydrophobic than acrylic adhesive.

For the adhesives, NLP11051 was hydrophobic whereas the acrylic was slight less hydrophobic ( $2^\circ$  less than  $90^\circ$ ) as shown in Fig 4.6. This might lead to early failure of packaging under wash environment however, the PTFE etched fabric would provide good adhesion using acrylic which might result in enduring the packaging under wash cycles.

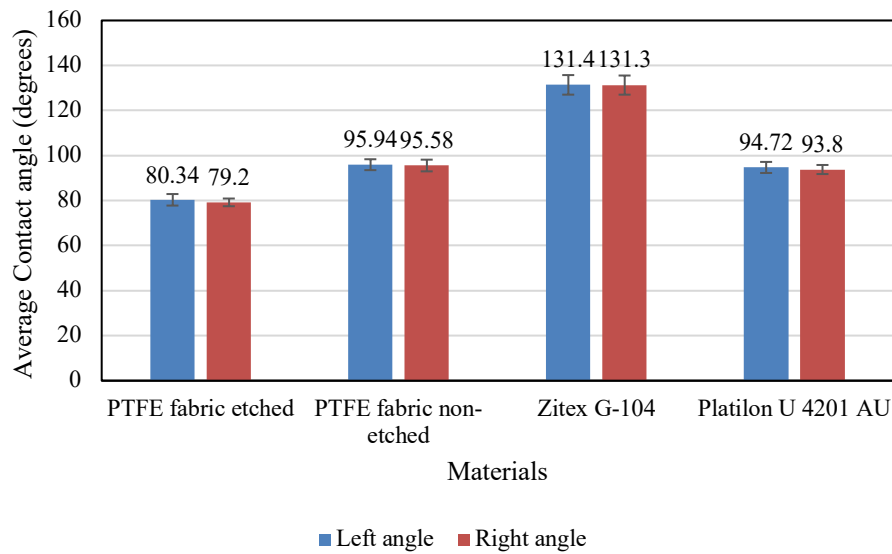


**Figure 4.5** Contact angles for one side etched PTFE Fibre glass fabric (etched side), non-etched part of PTFE Fibre glass fabric, Zitex G - 104 and Platilon U 4201 AU 4201

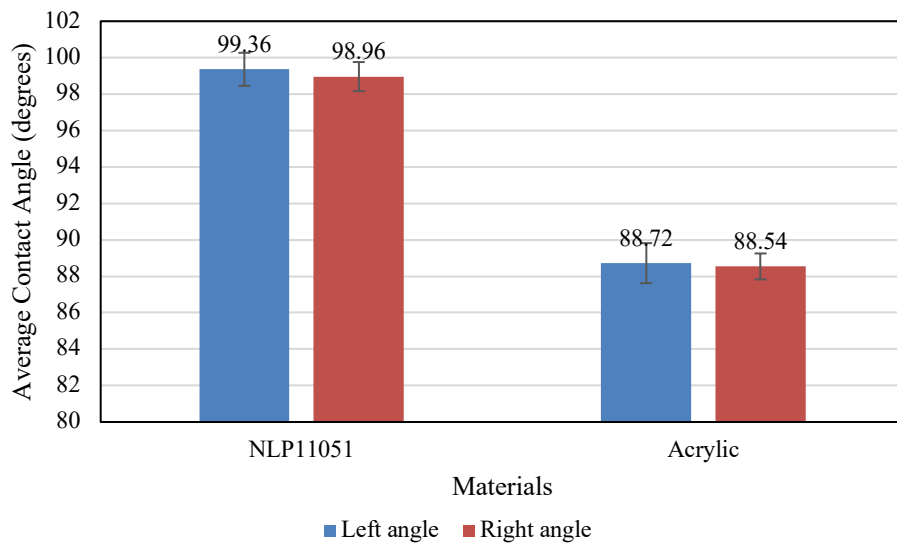


**Figure 4.6** Contact angles for Pressure sensitive adhesives, NLP11051 and acrylic

## 4.5 Peel test

A Peel test is typically performed to measure the bond strength of the hot melt adhesive and the pressure sensitive adhesive from Lohmann between encapsulants and substrate (Kapton in this case).

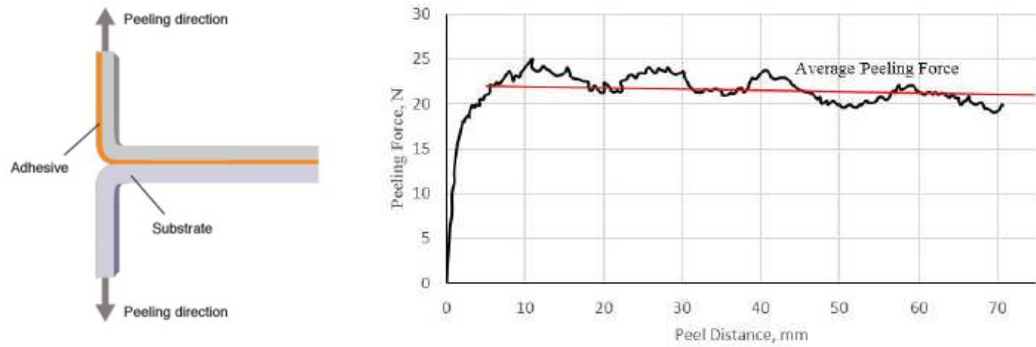


**Figure 4.7 (a) T-Peel method for demonstrating bond strength of adhesive between flexible materials [102] (b) the average peel force obtained during the test defines the bond strength of the adhesive [103]**

The main types of peel test are 90°, 180° and T peel test. T- peel test was used for finding the peel strength for flexible materials by pulling two flexible materials bonded together axially apart from each other as shown in Fig 4.7 (a), and the peel plot was drawn with applied load against displacement Fig 4.7 (b).

The TPU material was heated until it reached a molten/soft state that was enough to wet out the substrate and bond with it after cooled down. However, for non-stick materials with high surface tension such as PTFE could not be bonded using hot melt adhesives. Hence it was difficult to bond Zitex G - 104 and PTFE glass fibre fabric materials using adhesives. However, PTFE Fibre glass fabric was etched on one side to improve the surface roughness for better bonding by the company itself. The Peel strength plot looked similar to Fig 4.7. The peak load was the maximum load required to start peeling and the middle section of the plot gave the average peel force along the bonded part in the sample.

#### 4.5.1 Sample preparation

The Kapton film and encapsulating materials (Zitex G - 104 and PTFE Fibre glass fabric) were cleaned with acetone and IPA before bonding with pressure sensitive adhesive (from Lohmann).

The adhesive of 15 mm was stuck on the Kapton N (normal Kapton) and Kapton E (with epoxy adhesive) and the encapsulating materials strip (as per ASTM F88 standard). The bonding was performed using roller (~500 g) with weights of 500 g tied to it as shown in Fig 4.8 to achieve approx. 10-15 N/cm<sup>2</sup> as given in the datasheet. For hot melt, the vacuum forming machine was used for the bonding.

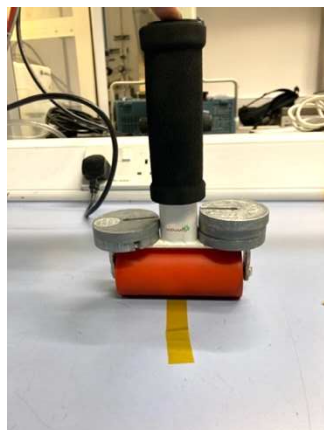


**Figure 4.8 Application of NLP11051 on Kapton N for peel test using 500g weight on the roller (standard ASTM F88)**

#### 4.5.2 Peel test experiment

The bond strength was experimentally validated using a Tinius Oslen model H25KS tensile tester with a 25 kN loadcell. Blank (i.e., no tracks or components) Kapton and samples were cut into 15 mm wide strips, 100 mm in length and were bonded as described above in the section 4.5.1. Each sample was bonded partway along its length leaving both films accessible at one end of the strip. The Kapton was mounted on the bottom fixed position clamp and the TPU was attached to the top clamp as shown in Fig 4.9 (a) and Fig 4.9 (b). The tensile test was run following the ASTM F88 standard with a pull speed of 250 mm/min. The peel test experiment was conducted using tensiometer Tinius Olsen 25N. The experiment was run with the help of a software horizon to plot the curve for the peel test with the ASTM F88 standard. Five samples were used for the evaluation of the peel strength for each peel strength test described below.

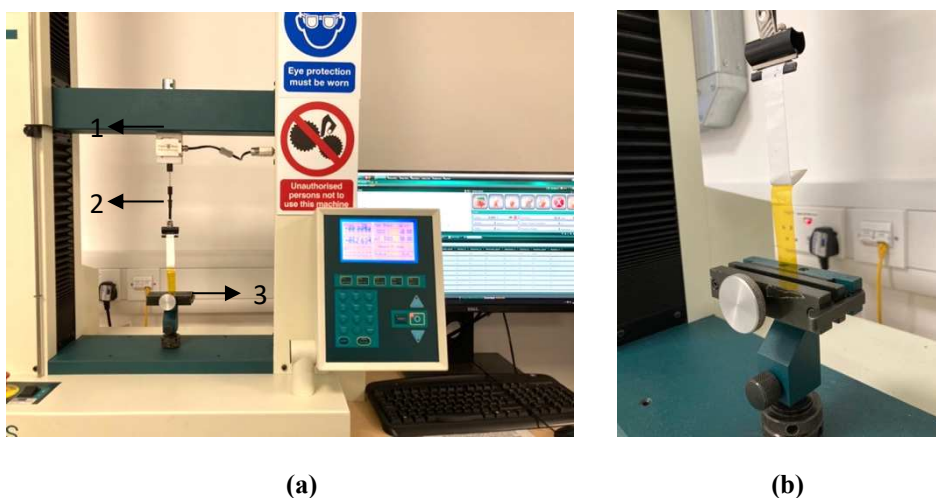


**Figure 4.9 (a) tensiometer tensile tester with 1) load cell, 2) movable grip and 3) fixed grip b) closer look of the sample (Zitex G - 104 attached to Kapton with NLP11051) fixed to the grip and forms T shape.**

## 4.6 Peel test results

The peel strength results were obtained on Horizon software that gave the force and length of the pull performed during the peel test and a graph was plotted. The plots were classified based on adhesive types used on different encapsulants.

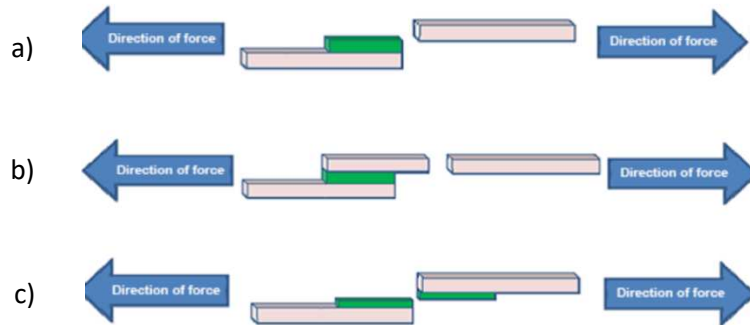


**Figure 4.10 Showing three primary adhesive failure modes (a) adhesive failure (b) cohesive failure and (c) substrate failure [103]**

The bond failure occurring between two flexible materials (adherends) during peel test could be classified into three types as shown in Fig 4.10,

- Adhesive failure – Adhesive strongly bonded to one substrate
- Cohesive failure – Adhesive splits and bonds unevenly to both adherends
- Substrate failure – Breakage in the substrate due to high bonding strength of the adhesives between adherends

The main reasons for bond failures were surface energy of the adherends, surface cleanliness, viscosity of the adhesive, thickness of the adhesive, bonding conditions such as pressure, humidity, temperature, and cure time [104]. The results of the peel strength with different bond failure for NLP 11051 and acrylic adhesive of thickness 50  $\mu\text{m}$  with adherends – Kapton (N), Kapton (E), Zitex G 104, PTFE Fibre glass fabric, Platilon U 4201 AU have been discussed below.

### 4.6.1.1 Peel strength for adhesives bonded between PTFE glass fibre fabric (etched) and Kapton

The bond failure between PTFE Fibre glass fabric and Kapton (N) using NLP 11051 and acrylic adhesive was adhesive failure from Fig 4.11 and Fig 4.12. The adhesive was attached to Kapton (N) while peeling. This showed that the adhesives had high bond strength with Kapton (N) than PTFE Fibre glass fabric itself. It was also observed that the acrylic adhesive had higher peel force with PTFE Fibre glass fabric than NLP11051. The acrylic adhesive was tested on Kapton (E) and the results remained the same with very small change as shown in Fig 4.13.

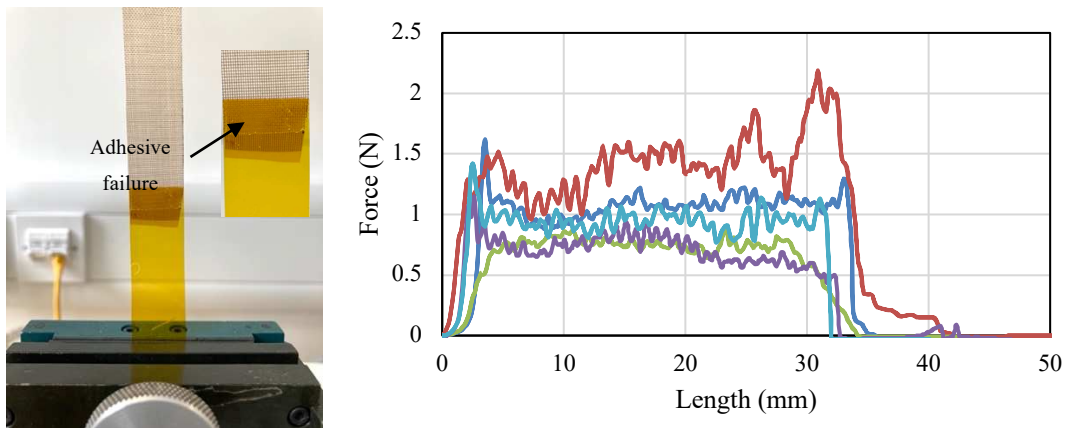


Figure 4.11 Peel strength for PTFE Fibre glass fabric on Kapton N using NLP 11051 for bonding

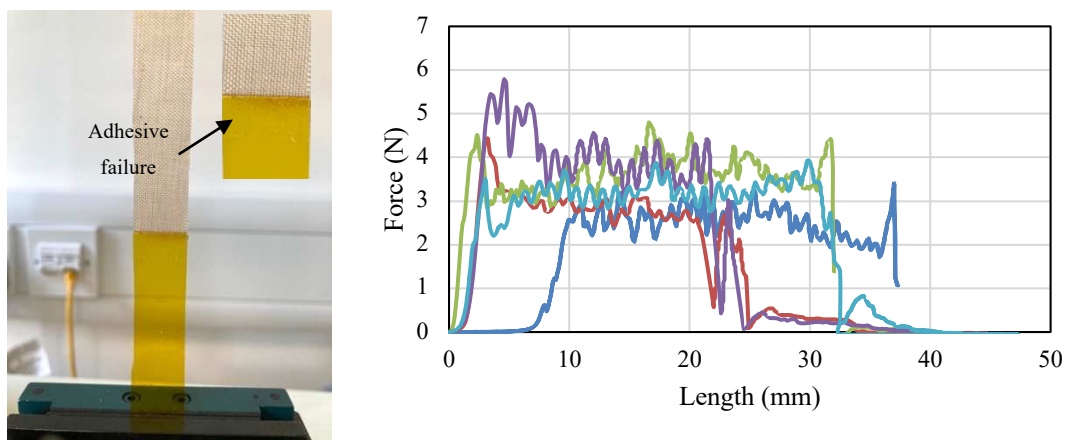


Figure 4.12 Peel Strength for PTFE Fibre glass fabric on Kapton N using acrylic adhesive for bonding

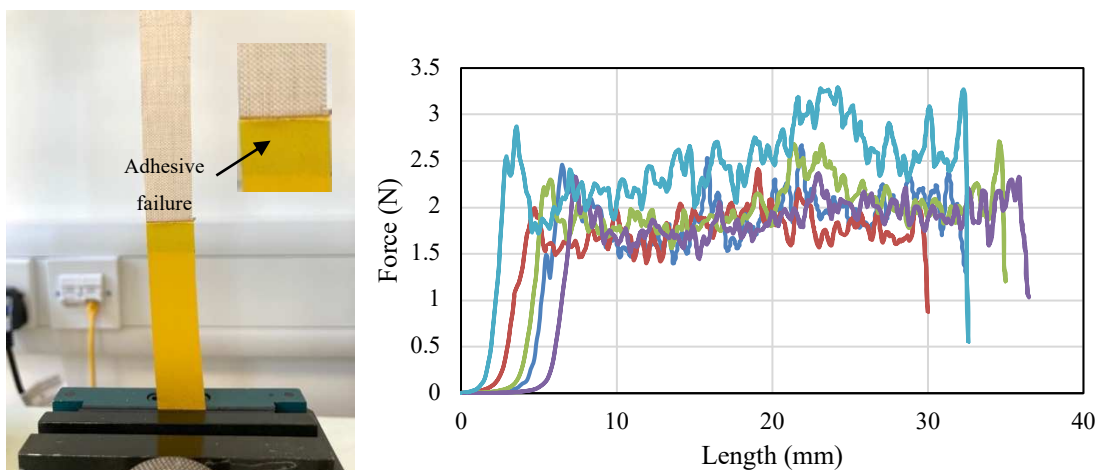


Figure 4.13 Peel Strength for PTFE Fibre glass fabric on Kapton E using acrylic adhesive for bonding

#### 4.7 Peel strength for adhesives bonded between Zitex G - 104 and Kapton N, and on Kapton E

The bond failure between Zitex G - 104 and Kapton (N) using NLP 11051 and acrylic adhesive was adhesive failure from Fig 4.14 and Fig 4.15. This showed that the adhesives had high bond

strength with Kapton (N) than PTFE Fibre glass fabric itself. It was also observed that the NLP11051 had higher peel force with Zitex G - 104 than acrylic. Hence NLP11051 adhesive was tested on Kapton (E) and the results remained the same with very small change as shown in Fig 4.16. The bond strength might also improve if the surface of the Zitex G - 104 was etched for more surface energy.

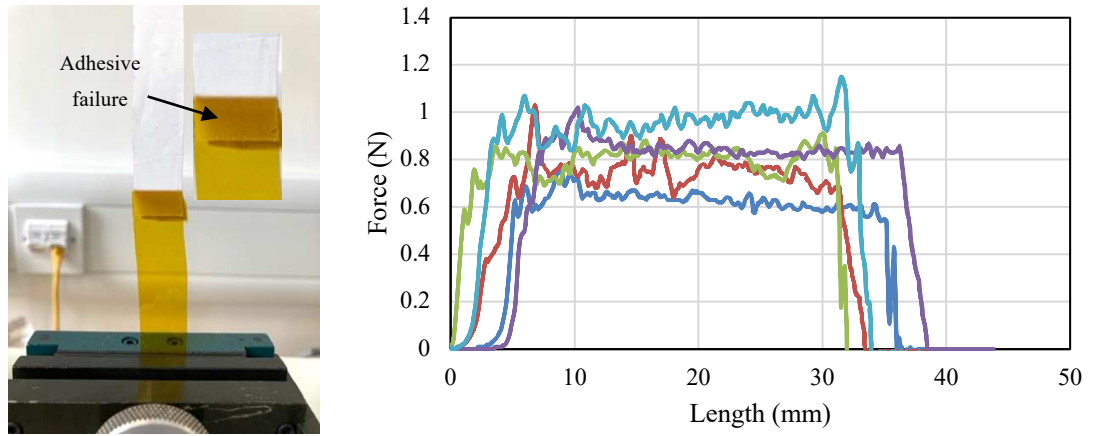


Figure 4.14 Peel Strength for Zitex G - 104 on Kapton N using NLP 11051 for bonding

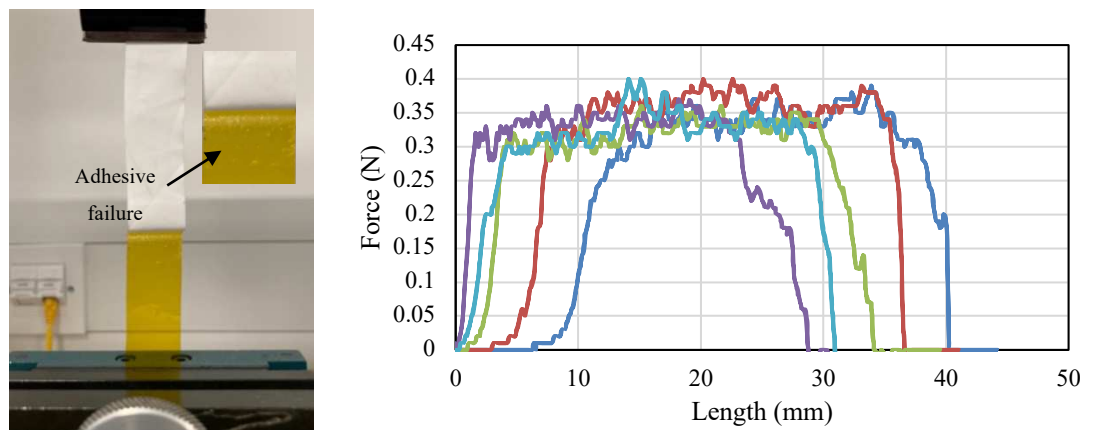


Figure 4.15 Peel Strength for Zitex G - 104 on Kapton N using acrylic adhesive for bonding

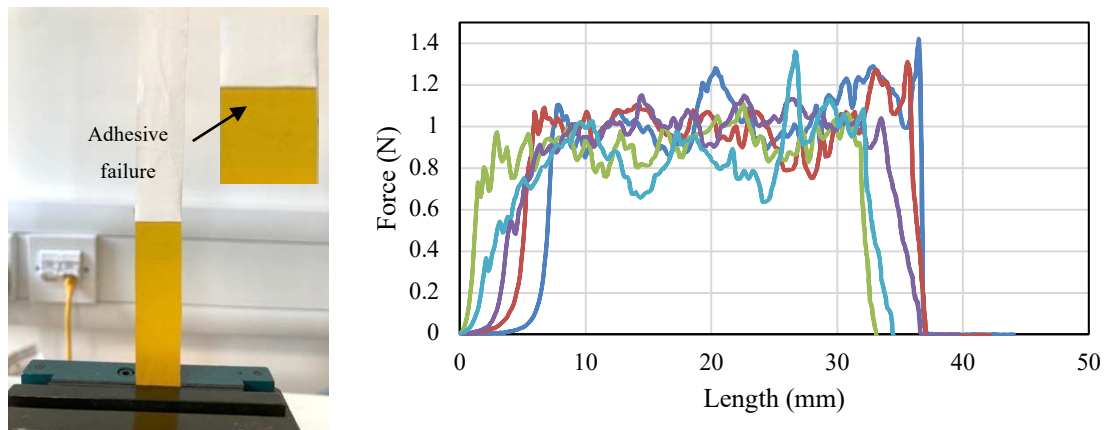
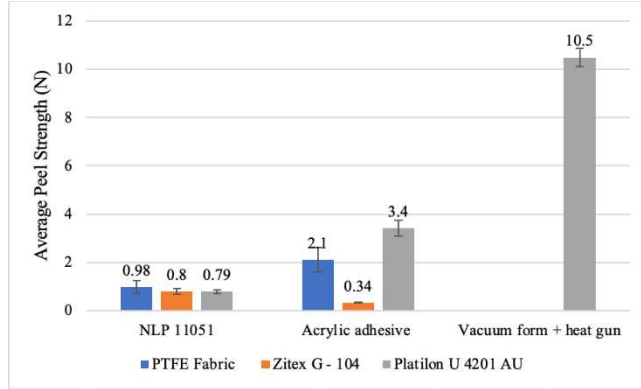
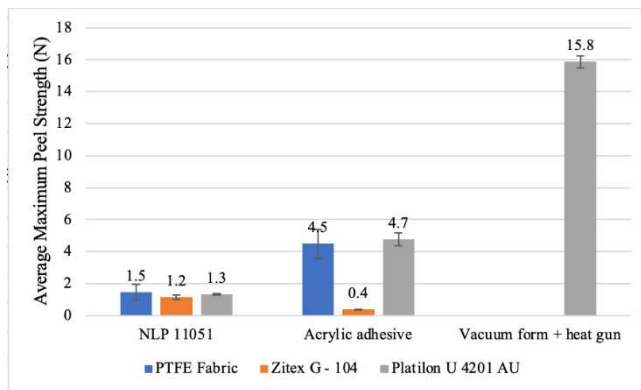


Figure 4.16 Peel Strength for Zitex G - 104 on Kapton E using NLP11051 for bonding

The Average and Maximum Peel Strength for PTFE Fibre glass fabric, Zitex G - 104, Platilon U 4201 AU and Kapton E are shown in Fig 4.17, and Fig 4.18.



**Figure 4.17 Average Peel Strength for PTFE Fibre glass fabric, Zitex G - 104, Platilon U 4201 AU and Kapton E**



**Figure 4.18 Maximum Peel Strength for PTFE Fibre glass fabric, Zitex G - 104, Platilon U 4201 AU and Kapton E**

**4.7.1.1 Peel strength of Platilon U 4201 AU 4201 with Kapton (N) and Kapton (E)**

The flexible circuits were fabricated from copper coated Kapton substrates (GTS7800, supplied by GTS Flexible Materials Ltd) that were then patterned using standard photolithography followed by a copper etching step [7]. The copper was bonded to the Kapton using a thin (17 μm) epoxy adhesive layer. The copper etching process removed the copper where it was exposed to the etchant but did not attack the adhesive which remained on the surface of the Kapton film. This remaining epoxy film was used to bond the TPU film with the Kapton substrate and meant no additional adhesives, such as hot melt films or pressure sensitive adhesives, were required. To achieve the maximum bond strength, the encapsulated circuit needed to be subsequently heated to 230-240 °C using a hot air gun positioned around 2 cm above the circuit. The quality of the bond could be visually confirmed by the transparent appearance of the TPU film and the absence of voids



across the substrate. The surface of the Kapton after etching i.e., with the epoxy (denoted Kapton E) has been compared with standard non coated Kapton (Kapton N) in Fig 4.19 (a) showed the smooth surface of the Kapton N whereas the epoxy adhesive was clearly visible in Fig 4.19 (b). The appearance of the Kapton was also different as shown in the inserts in Fig 4.19 with the Kapton N being shiny and the Kapton E being dull. It should also be noted that the epoxy was not always distributed uniformly across the Kapton with variations in thickness as shown in Fig 4.19 (c). This can impact in the bond quality between the TPU and Kapton films. The peel strength was higher for Kapton with epoxy adhesive.

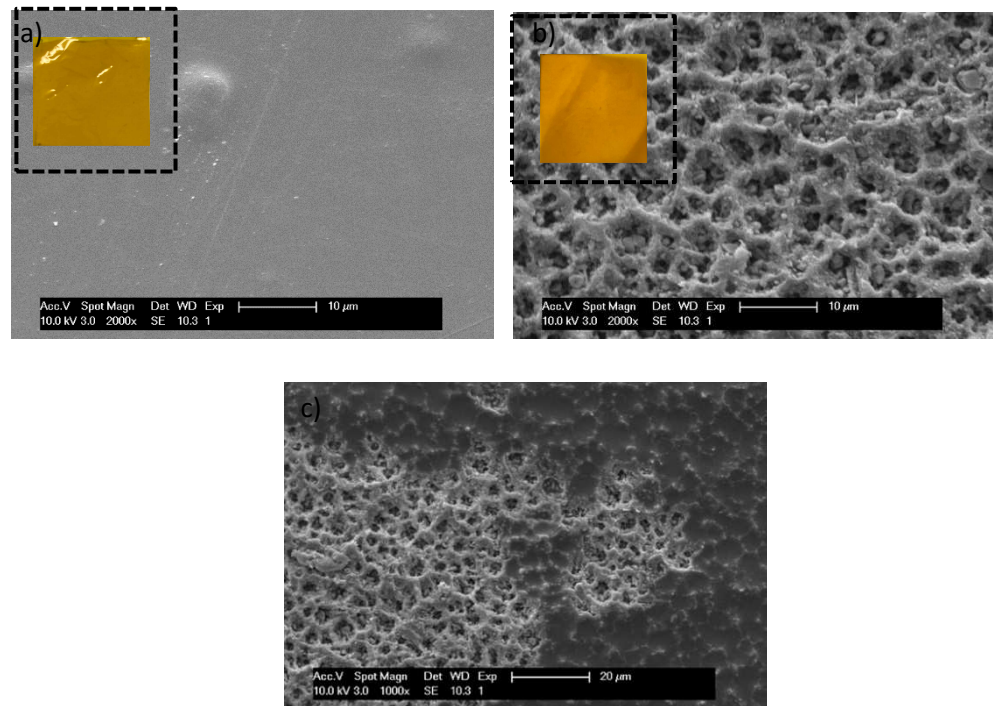


Figure 4.19 SEM image of (a) Kapton N (b) Kapton E (c) Kapton E with uneven epoxy layer

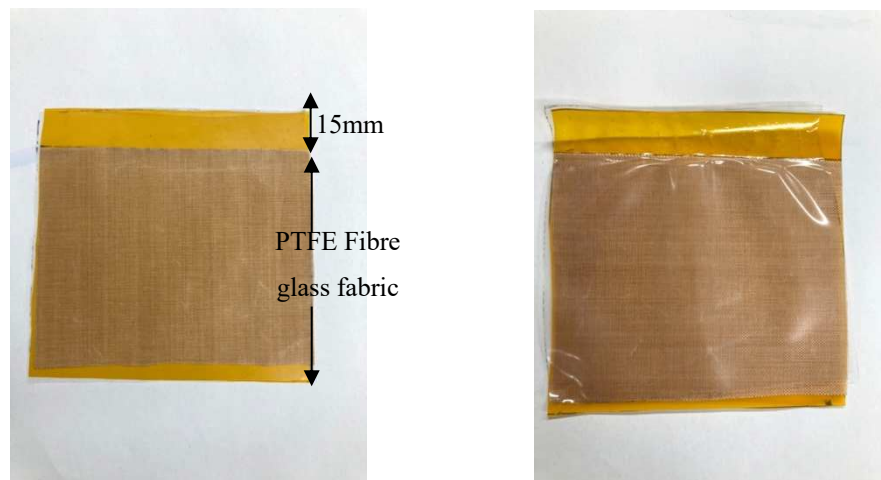


Figure 4.20 (a) Platilon U 4201 AU placed on top of Kapton with epoxy (b) After using heat gun (240°C) until Platilon U 4201 AU

The use of the remaining epoxy meant that the circuit should be designed in such a manner that sufficient copper is etched away from the substrate to maximize the area of the exposed epoxy.

There should also be a sufficient gap between the edge of the die and the edge of the strip, the size of this gap depended upon the thickness of the die. The MICS 5524 CO sensor was 1.55 mm thick and required a gap of 2 mm around it to effectively bond the TPU film.

For peel test, the Platilon U 4201 AU film was placed on top of 10x10cm Kapton N and Kapton E as shown in Fig 4.20 (a).

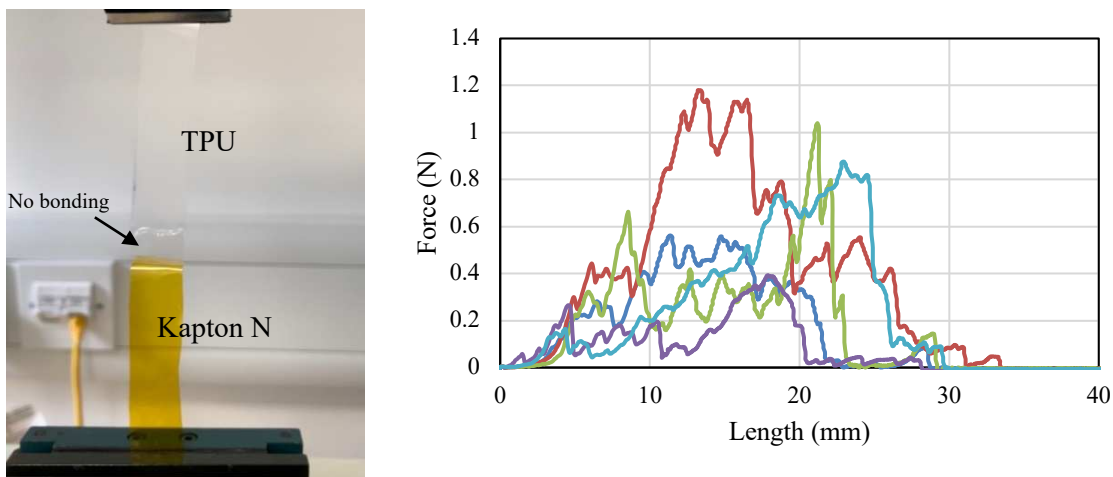


Figure 4.21 Peel strength for Platilon U 4201 AU on Kapton N using heat gun for bonding – weak bonding

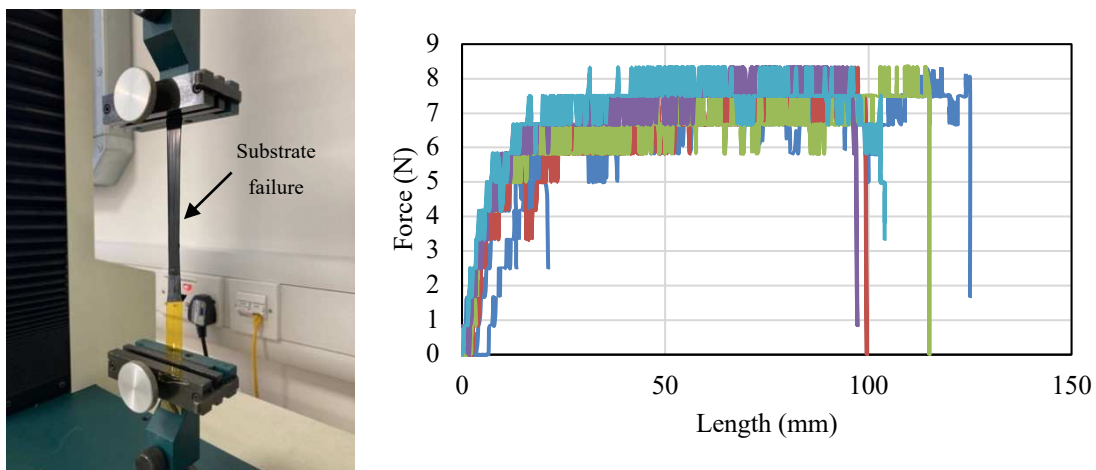
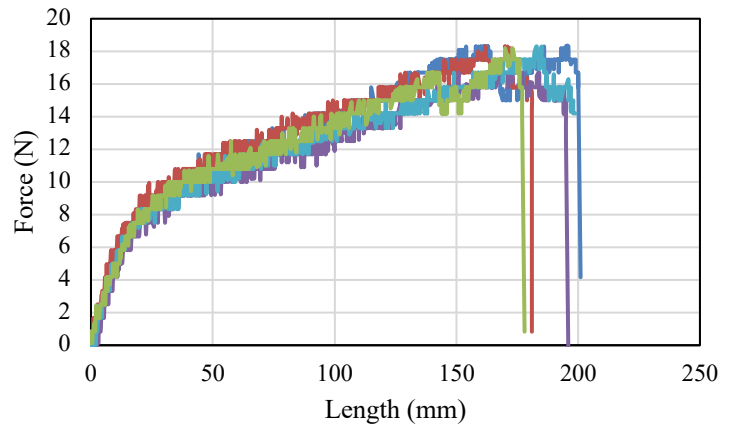
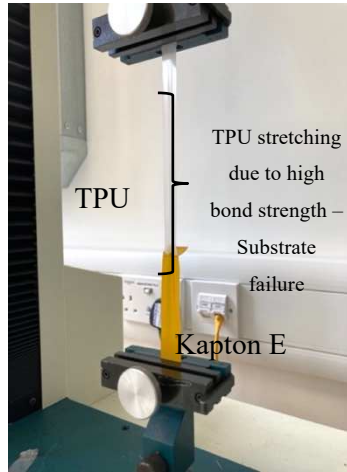
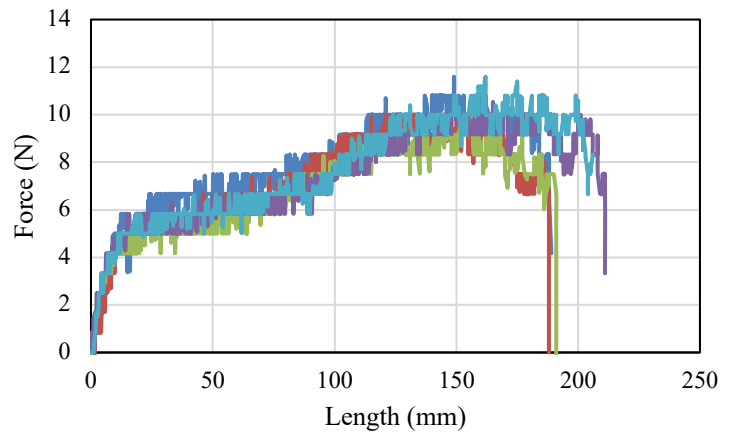
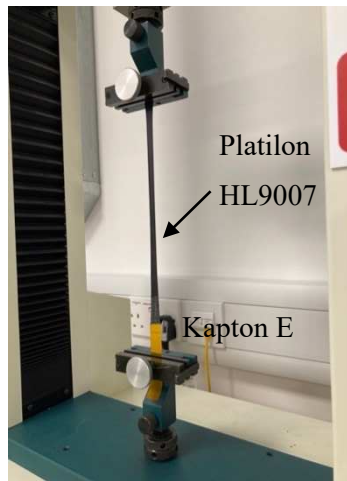


Figure 4.22 Peel strength for Platilon HL9007 on Kapton N using heat gun for bonding – substrate failure



**Figure 4.23 Peeling test of Plaiton U 4201 AU on Kapton with epoxy adhesive using heat gun – substrate failure**



**Figure 4.24 Peel strength for Plaiton HL9007 on Kapton E using heat gun for bonding**

To follow ASTM F88 standard, PTFE Fibre glass fabric (non-stick on both sides) was placed to get a width of 15mm bonding width. The film was heated using hot air gun until at different temperatures starting from 185 °C (softening point of Plaiton U 4201 AU) to 250 °C (reflow over temperature) until the film changes transparent as shown in Fig 4.20 (b). It was also observed that the film shrunk when heated in order to have strong bonding.

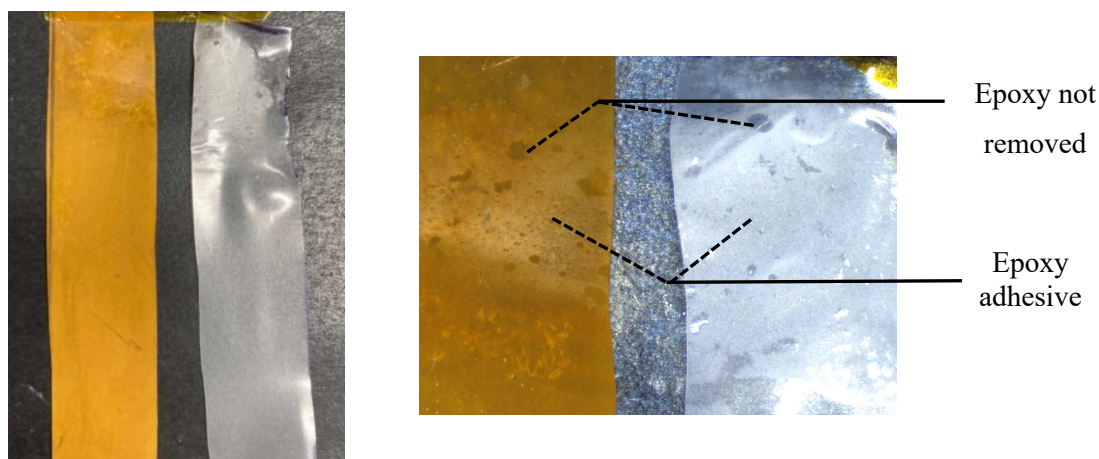


**Figure 4.25** After peel test – the epoxy layer from the Kapton is removed

Five samples of each of the standard Kapton (Kapton N) and Kapton with epoxy (Kapton E) were evaluated and shown in Fig 4.22 - Fig 4.26. The results for the Kapton N shown in Fig 4.2 indicated a weak and variable peel strength with the films separating at a force typically less than 1 N. The bond strength of the Kapton E with the TPU was significantly higher with an average maximum peel force of 15.86 N and average peel strength of 10.5 N along the bonded length of each sample. The length scale in the x axis was longer for the Kapton E substrate compared with the Kapton N substrate due to the high force required to peel the bond which caused the TPU film to stretch as shown in Fig 4.24. For a comparison to show the bonding of a thermoplastic film with hot melt adhesive, Platilon HL9007 bonding to Kapton N and E and showed a peel strength of an average 8 N and 10 N, respectively.

#### **4.8 Process for packaging gas permeable and waterproof materials on flexible gas sensing system**

Based on material properties, the technique used for the encapsulation process varies. For materials that are melt processible (the material flows as liquid above its melting point), vacuum forming can be used for moulding purpose. However, for non-melt processible such thermoplastic as PTFE, they cannot be moulded using vacuum forming. Hence, they require special techniques such as injection. Two different techniques for two thermoplastic materials are discussed below.

##### **4.8.1 Vacuum forming**

Vacuum forming is a process that transforms thermoplastic polymer sheets or films into three dimensional geometries, normally using a specifically fabricated mould. Vacuum forming method is used for making 3D plastic moulds and is also used helpful in the packaging of MEMS devices [105].

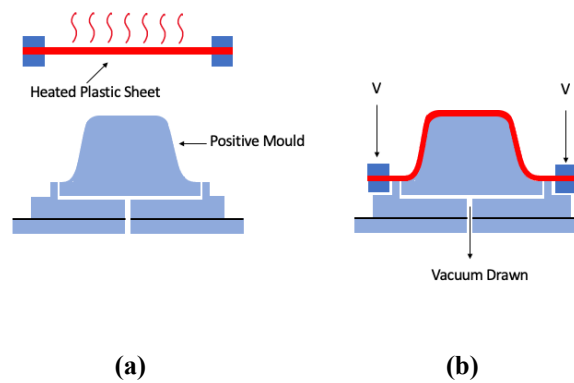


**Figure 4.26** The thermoplastic film is initially heated until it softens (b) the vacuum is applied and atmospheric pressure forces the softened material on top of the target mould. Image adapted from [15]

The working principle involves heating the thermoplastic film to reach a softened malleable state that is placed on top of the mould as shown in Fig 4.26 (a). The vacuum is formed by extracting the air from underneath the softened film causing atmospheric pressure to force the polymer against the mould as shown in Fig 4.26 (b). In this case, the mould is replaced by the circuit to be coated and the thermoplastic film conformally coats the substrate and components directly.

Formech 450DT vacuum forming machine [106] can be used to experiment encapsulating thermoplastic material on the flexible circuit. This equipment includes a Quartz infrared heater and has a maximum operating window of 450 x 300 mm. In this case the initial operating window was reduced to 150 x 150 mm using a machined aluminium top plate as shown in Fig 4.27 to avoid material waste.

The mould was placed on the mesh table below the window. The lever was pulled down to move the table near the window to position the device right below the material. The material to be moulded or encapsulated with, was placed on of the window and clamped tightly such that the material is held firmly. The heater was pulled front to heat the material and the temperature settings could be given based on heat %. After heating, the lever was pulled down to lift the table with the device and the softened material was stretched over the mould as shown in Fig 4.27. The vacuum was applied from the settings and the pressure could be viewed in the gauge. The vacuum removed the air between the material and the device to get a conformal coating. When the material had cooled, the encapsulated device could be removed.

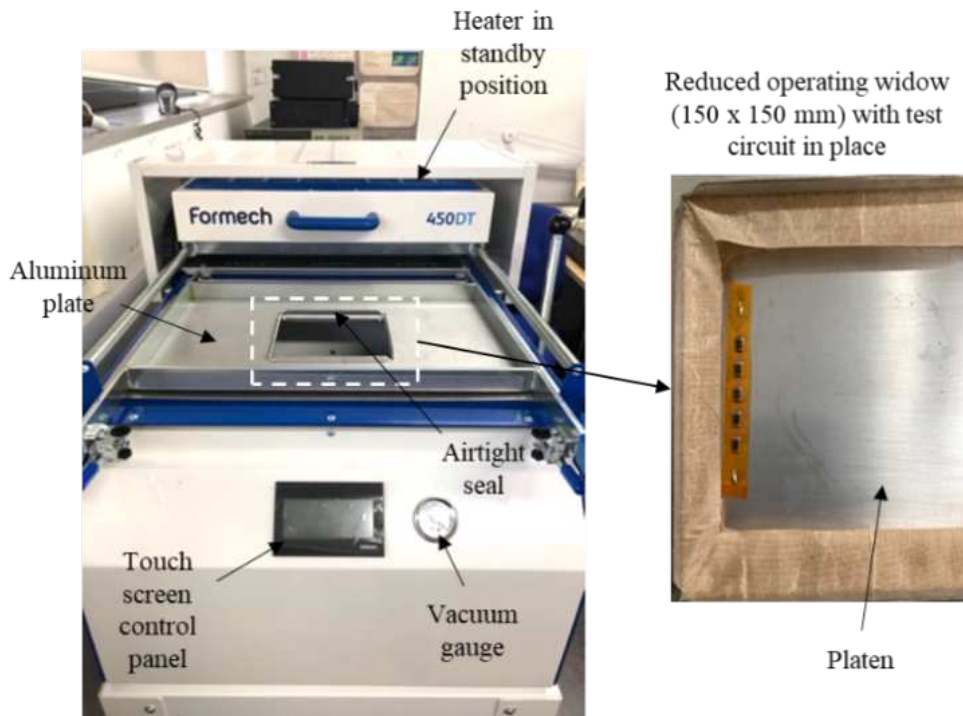


**Figure 4.27 Front view of Formech 450DT and reduced processing window is shown with flexible electronic test circuit with series resistors**

Each encapsulating material has a specific glass transition temperature ( $T_g$ ) at which it softens and becomes malleable and ready to mould. The Formech 450 DT vacuum former defines the heating power in terms of percentage and therefore the equipment was characterised to find the approximate temperature for different heating power percentages from 5 to 100%.

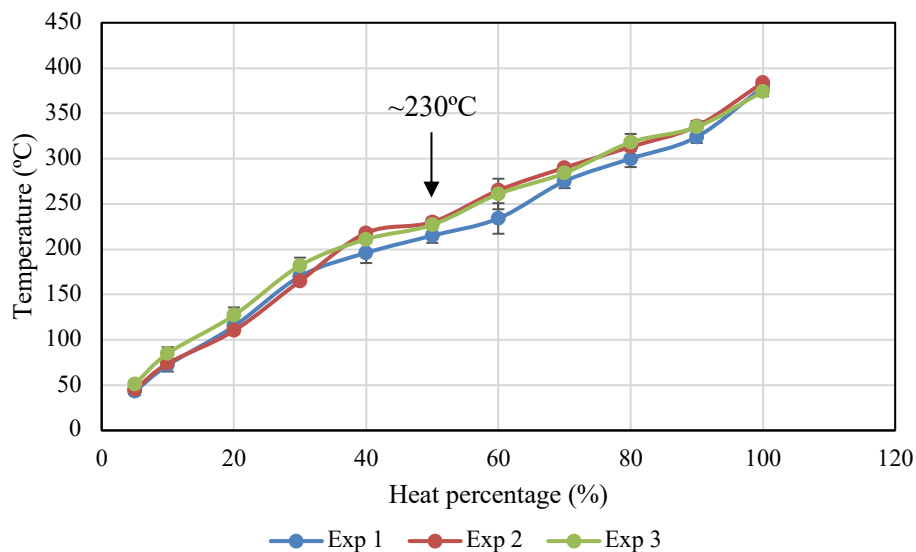


**Figure 4.28 Showing temperature rise with increase in percentage of heating percentage**

An infrared thermometer (Etekcity Lasergrip 1080, range  $-50^{\circ}\text{C} \sim 550^{\circ}\text{C}$ ) with a response time of less than 0.5 seconds was used to measure the temperature at the centre of the area under the heater at the standby position. The correlation between temperature and the heating percentage was shown in Fig 4.28 and it showed an increase in temperature for an increase in heating percentage with good repeatability up to 35%.

#### 4.8.2 Platilon U 4201 AU processing for moulding using the vacuum former – heat power setting and window size reduction

For packaging the CO flexible sensor using vacuum forming process, the Formech 450DT was first preheated at 50% heating power for 15 mins for the heater to reach the targeted temperature (around  $227^{\circ}\text{C}$ ). This was required as the softening range of Platilon U 4201 AU is  $155 - 185^{\circ}\text{C}$ . This range was for thermoforming however, for the material to have good bonding with the substrate, it should reach the viscous temperature hence it was heated a bit above the softening range. An iterative approach was used to identify the optimum heater power for the TPU film. The TPU changed appearance after heating transforming from being translucent at room temperature Fig 4.29 (a) to transparent when heated Fig 4.29 (b). This visible change in appearance indicated that the film has achieved the required soft and malleable phase and was ready to be vacuum formed. Since the heater could not be used at the same time as the vacuum was being applied, the TPU film would cool, and it was desirable to apply the vacuum as soon as possible.

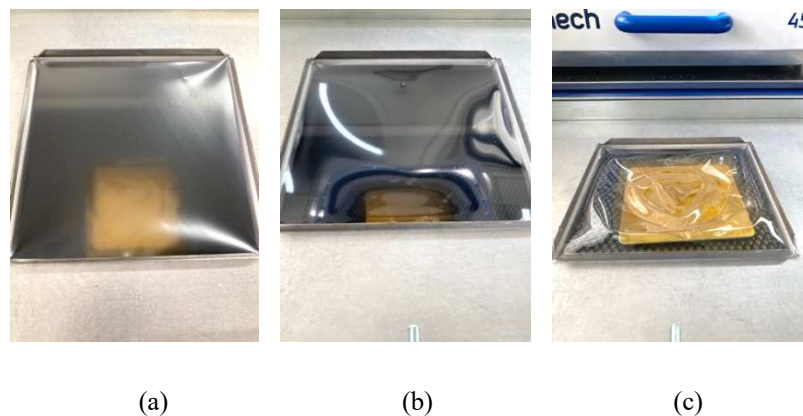


**Figure 4.29 (a) the material appears translucent and when heated up to desired heat setting and temperature turns to (b) soften, pliable and more transparent state (c) due to the weight of the material and heating it sags and forms rings on the substrate to be vacuum formed**

Another important issue was the sample wastage as the window given was quite large and needed a large piece of the sample to be clamped for the vacuum forming as shown in Fig 4.29 (c). The reduced window given by Formech was used.

As the heater was moved to the clamped material, the heater timer started. As seen, the material changed from translucent to transparent before heating and after heating respectively. This showed that the material was as soft and molten and was ready to be vacuum formed. It was observed that due to the large window size, the material was sagging downwards and formed rings on the substrate when the lever was pulled upwards for vacuum forming.

This could have been avoided by reducing the size of the window. For this purpose, two 75 $\mu$ m thickness Kapton were used with a small window at the centre about 10cmx10cm. The Platilon U 4201 AU material was sandwiched between the Kapton for the process as shown in Fig 4.30.

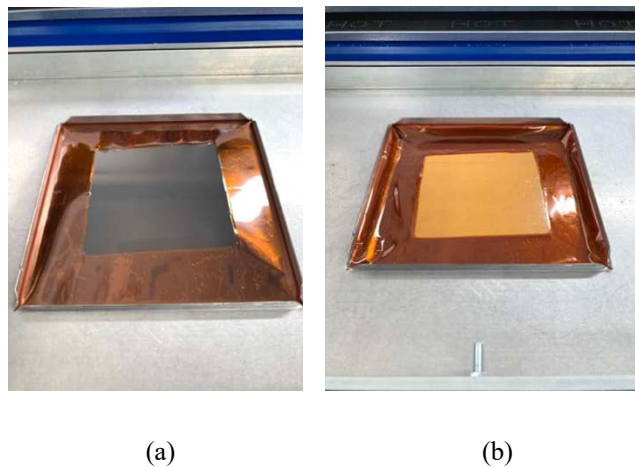


**Figure 4.30 (a) TPU clamped under reduced Kapton N 75  $\mu$ m window gives (b) even vacuum forming over the substrate without forming rings**

As seen in the Fig 4.30, due to the reduction of the window size, there was no sagging of the material after heating, and this helped in neat vacuum forming process. Though, the wrinkles vanished, now the flat material might be under stress and may damage easily. However, with this design, once the vacuum was applied, it was observed that the negative pressure was less than 0.8bar. Due to the molten polyurethane between the Kapton, it also bonded the two Kapton together making it difficult to peel as shown in Fig 4.31 which could lead to need of new Kapton windows for each test.



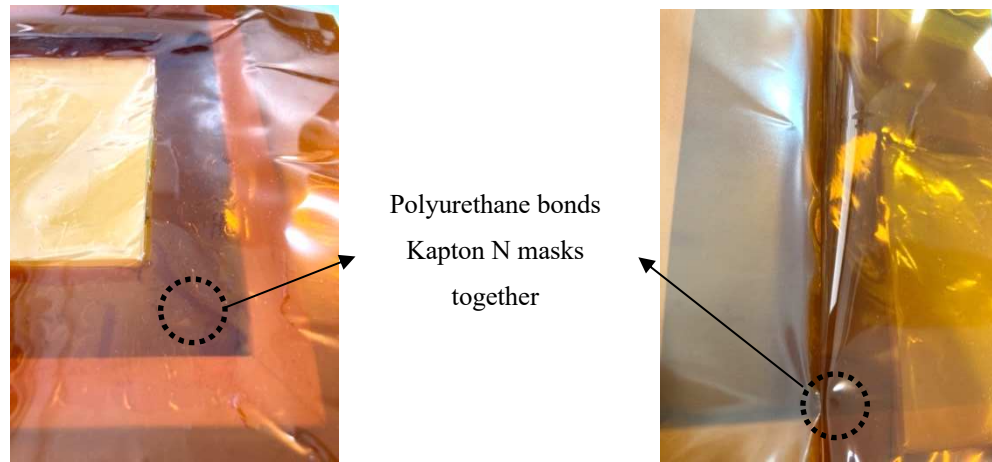


**Figure 4.31 Showing polyurethane bonds to 75 $\mu$ m thickness Kapton N window on heating in Formech 450DT**

This was solved by using two PTFE fibre glass fabric (non-etched on both sides) to avoid sticking of materials together and wastage of window material. Fig 4.32 shows the reduced window size non-etched (both sides) PTFE Fibre glass fabric for vacuum forming.

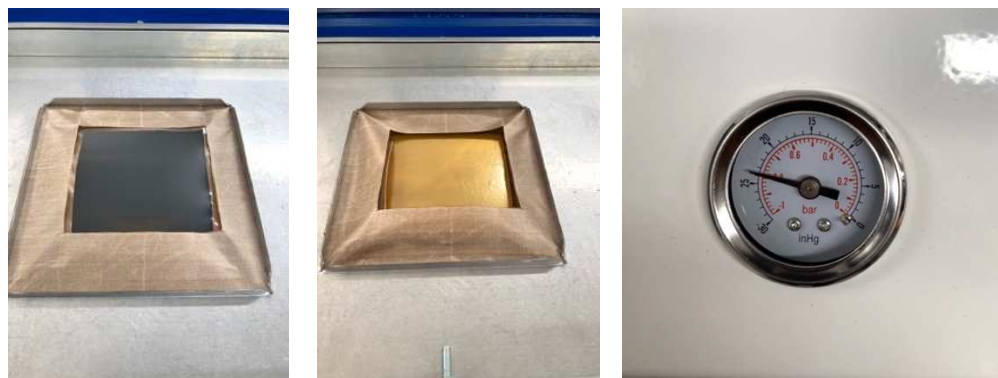


**Figure 4.32 Reduced window size with non-etched (both sides) PTFE Fibre glass fabric for vacuum forming**

The time evaluation at 50% was also experimented heating the material for different time in seconds. It was observed that the material when heated for 70s and over 100s makes the material over heated and cause holes. The time was experimented for 60s as shown in Fig 4.33. There were no holes created in the centre of the material in the window shown however, the sides of the materials were over heated. Due to these holes, the vacuum pressure was not enough to achieve -0.8bar.

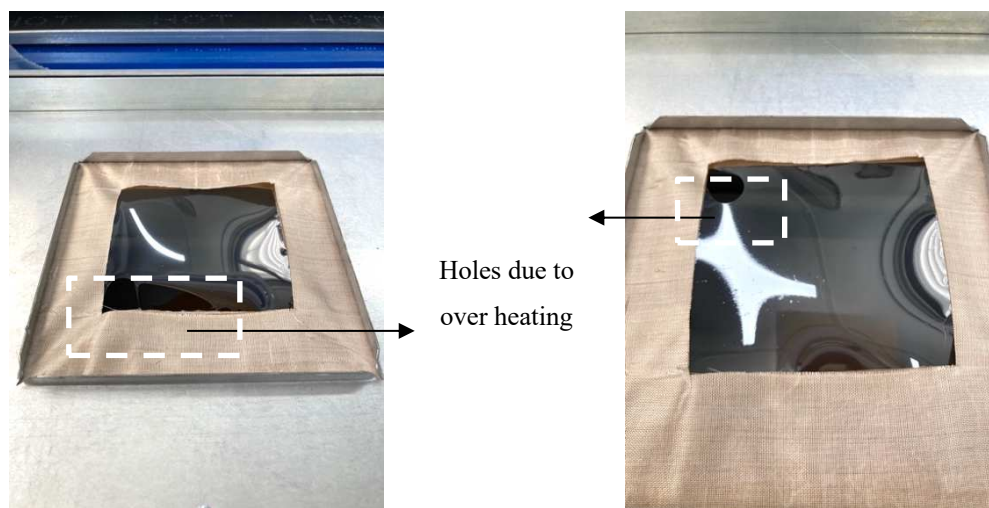


**Figure 4.33 Showing holes created due to overheating at 50% for 70s and above**

The issue with the time required for getting the material softened enough to get to the molten/viscous state to bond to the Kapton varied due to a) continuously using the machine heater, rising the temperature not only in PU, but on the metal and PTFE window near the material. The material should look transparent but should not be over heated causing holes that affected the vacuum pressure. Hence 50 - 55s was chosen to be the range to operate Platilon U 4201 AU for the vacuum forming process. The spread the heat evenly throughout the front panel of the machine, the heater is moved to the front panel and preheated the window for 2 mins. This increases the efficiency and repeatability of vacuum forming process.

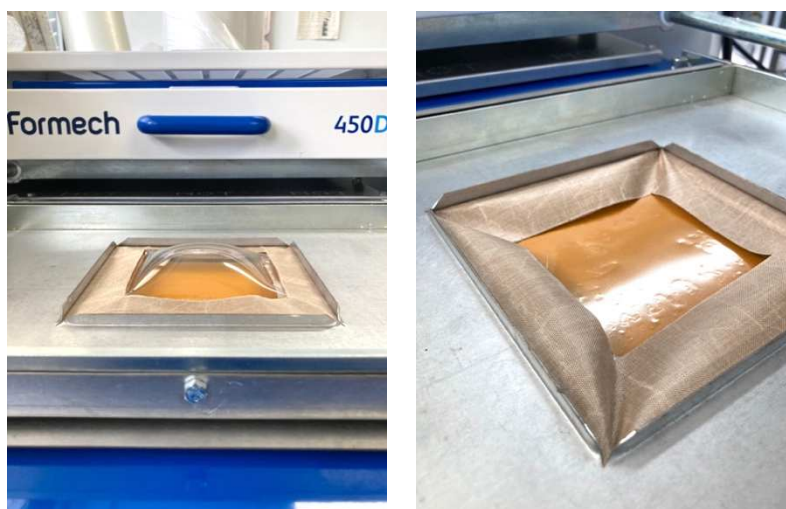


**Figure 4.34 Showing the material forming a dome when the stage is moved upward using the lever (left) and leaving uneven bonding on to the Kapton substrate (right)**

However, when the mesh and platen were raised and the seal formed with the bottom plate, the trapped air was heated by the raised temperature of the plates and the pressure rose causing the TPU film to bulge as shown in Fig 4.34. This could introduce undesirable bubbles in the final vacuum formed encapsulating films. This was minimised by gradually raising the mesh and platen but there

was a trade-off with the cooling of the TPU film. Optimising the vacuum forming process was desirable to minimise the formation of bubbles and avoid tenting of the encapsulating film around components. Where components had right angled edges, tenting could occur resulting in bubbles around each component. The position of the circuit on the platen was also found to be a factor in the quality of the encapsulation. The circuit placed at the edge of the platen had reduced tenting around the components compared with circuits located at the centre. Additional heating and vacuum steps can be repeated to further reduce this effect.

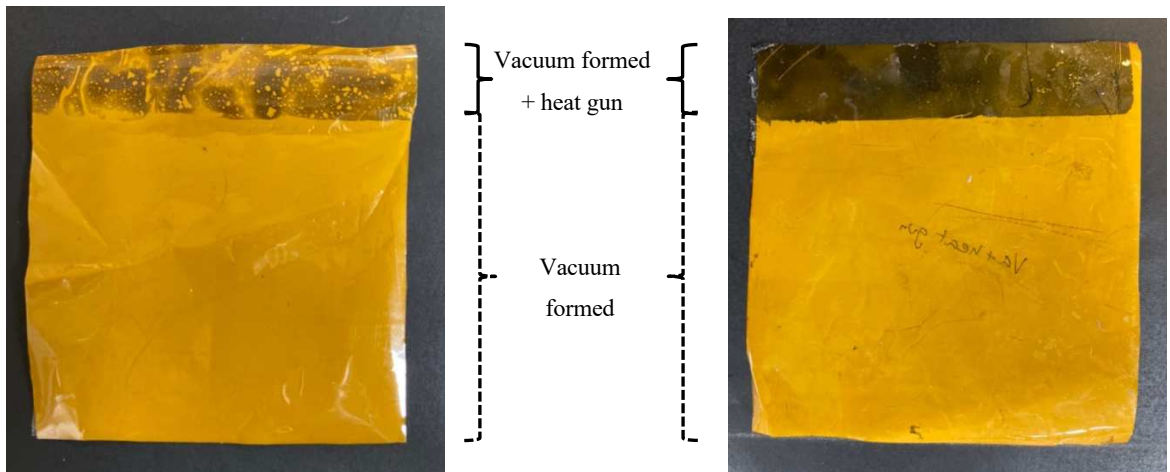


**Figure 4.35** Platilon U 4201 AU (left side) and Platilon HL9007 (right side) vacuum formed on Kapton E – Backside view (Kapton E on top and Platilon U 4201 AU and Platilon HL9007 on bottom). Top part was bonded using heat gun

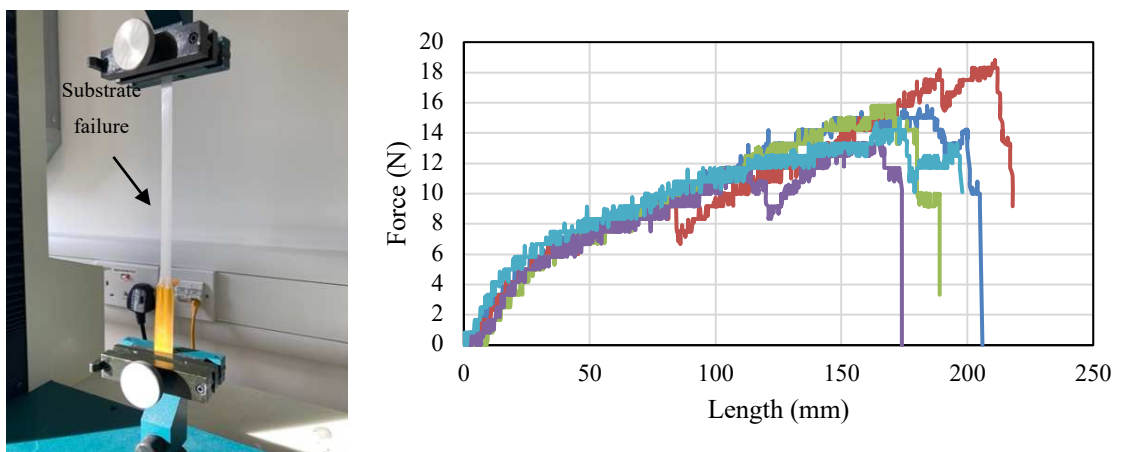


**Figure 4.36** Peel strength for Platilon U 4201 AU on Kapton E after vacuum forming and using heat gun for bonding

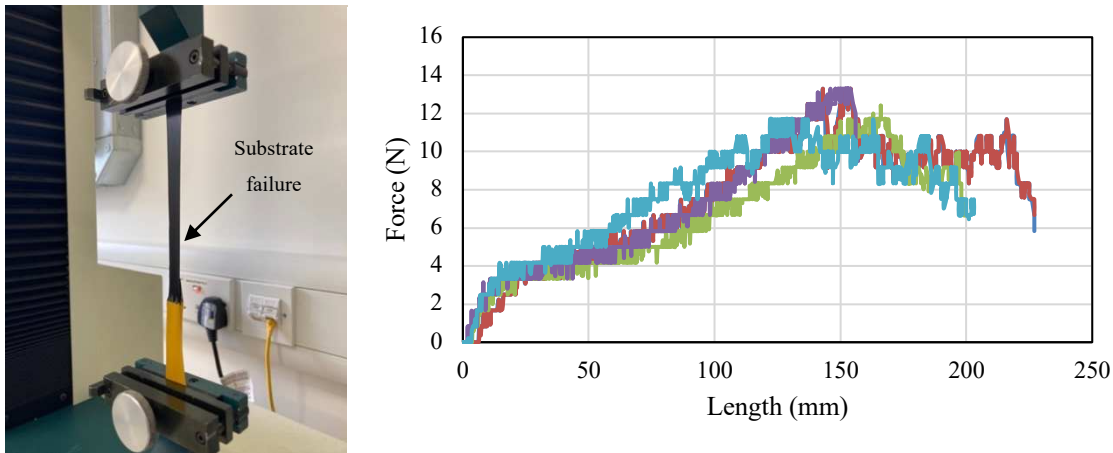


**Figure 4.37 Peel strength for Platilon HL9007 (with hot melt adhesive) on Kapton E after vacuum forming and using heat gun for bonding**

Another problem was the temperature of the material as the heater cannot be used at the same time as vacuum was being applied due to the machine setup. Hence to get the material softened to the right temperature while vacuum was being applied, heat gun was used. Both Platilon U 4201 AU and Platilon HL9007 had not bonded well i.e., easily peelable by bare hands as shown in Fig 4.35. However, these materials could have bonded using external heat source such as heat gun as which gives better bond between these materials as shown in Fig 4.36.

It was observed that the peel strength of Platilon U 4201 AU was higher than Platilon HL9007 when heat bonded to Kapton E resulting in a substrate failure as shown in Fig 4.37. This might also be due to the tensile strength of Platilon U 4201 AU (65 MPa) was higher than the Tensile strength of Platilon HL9007 L 9007 (45 MPa).

### 4.8.3 Platilon U 4201 AU Vacuum forming – optimization of substrate size optimization

The Kapton E placement with the acrylic adhesive and SMD components were placed on top of it is shown in Fig 4.38. The circuit strip width needed to be as small as possible for seamless integration in e-textile. However, it was also important to note the size of the sensor chip and the young's modulus of the encapsulant material and adhesive strength to completely seal the circuit strip without leaving any holes or unsealed gaps after packaging.

To find the optimum substrate width, the Kapton E was cut into 3 different widths with a constant 90mm width as shown in Fig 4.39 (simple way to experiment instead of using actual test circuit strips). The chip MICs 5524 was centered and attached to the Kapton E substrate using pressure sensitive adhesive to remove the chip when needed and caused no adhesive residues on the chip that occurred using glue for adhesion.

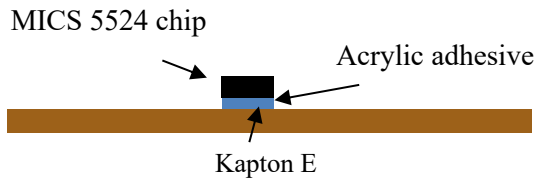


Figure 4.38 Cross section view of simple CO filament on Kapton E

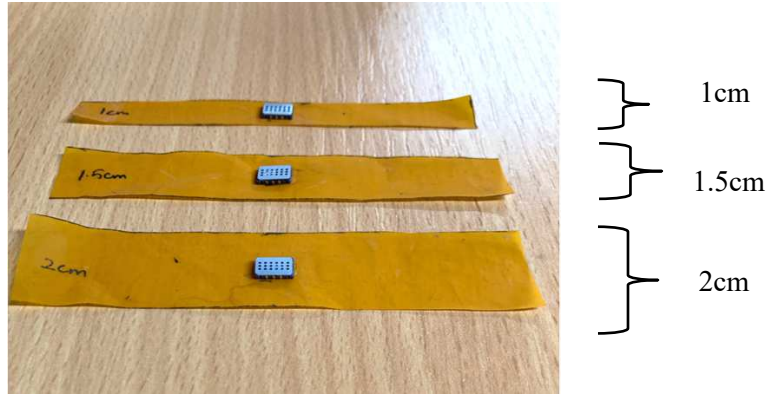


Figure 4.39 Showing 3 different substrate (Kapton) width Image shows sensor chips places on bare Kapton

A Platilon U 4201 AU vacuum produced on the 1cm wide sample is shown in Fig 4.40 (a), while Fig 4.40 (b) demonstrates that the chip's size prevents a good seal on the chip's sides.

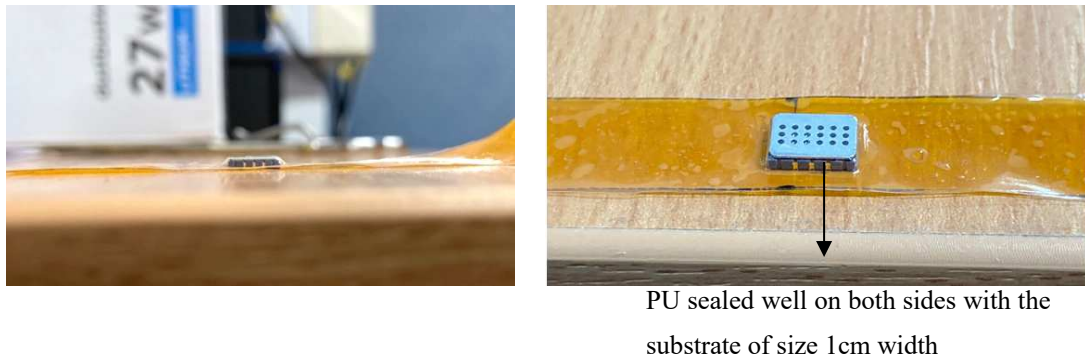
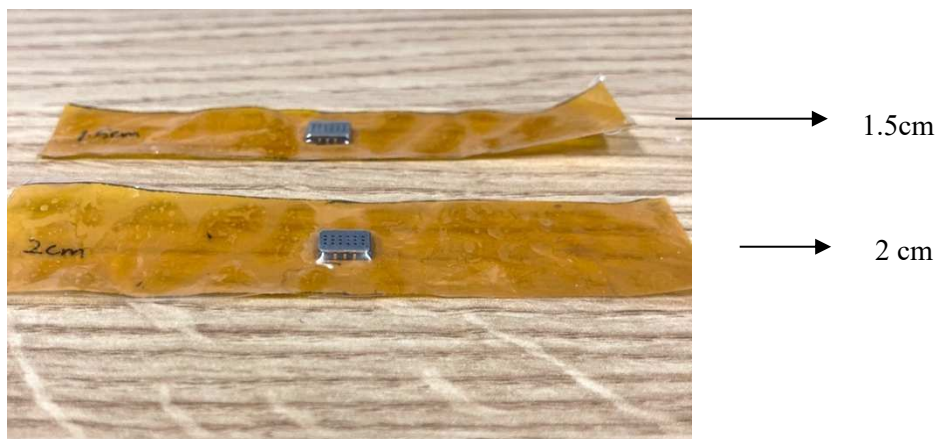


Figure 4.40 (a) Platilon U 4201 AU vacuum formed on the sample with 1cm width (b) and not sealed well at the sides due to the size of the chip

Fig 4.41 (a) shows that a bubble forms around the chip when vacuum is produced using PU because the sides are straight (not angled), and Fig 4.41 (b) shows that the bubble size can be minimized by using a heat gun and then applying vacuum again.



**Figure 4.41 (a) vacuum formed using PU forms bubble around the chip due to straight sides (not angled) (b) reduced bubble size due to usage of heat gun and applying vacuum again**

#### **4.8.4 Platilon U 4201 AU Vacuum forming – optimization of positioning the samples for the moulding process**

3 samples on Kapton E substrate of 1cm width and 9cm length were placed in different sides, 2 on the extreme left and right and one at the centre as shown in Fig 4.42 to find the positioning of samples on the stage for better moulding performance.

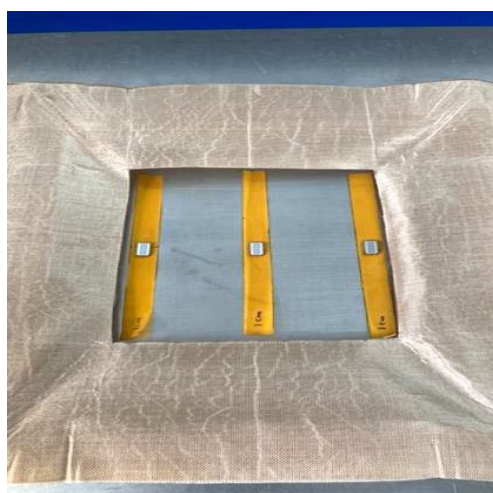


**Figure 4.42 Samples positioned at extreme right, centre, and extreme left under the window for vacuum forming**

The test samples were subject to vacuum forming with the TPU film heated at 230°C for 50 seconds. As shown in Fig 4.43 (a) and (b) the degree of tenting around the sensor die was less for the samples located on the sides of the platen compared to the sample positioned at the center.

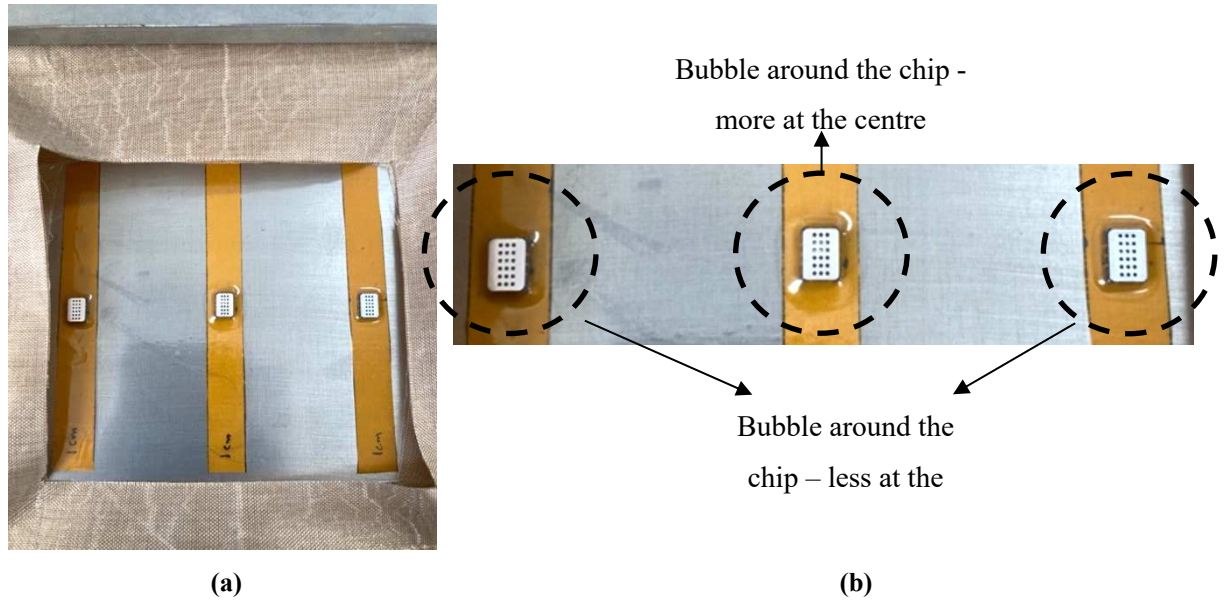


**Figure 4.43 (a) vacuum formed with Platilon U 4201 AU (b) bubble around the chip due to the dome formed after pulling the lever forward to bring the samples near the softened material**

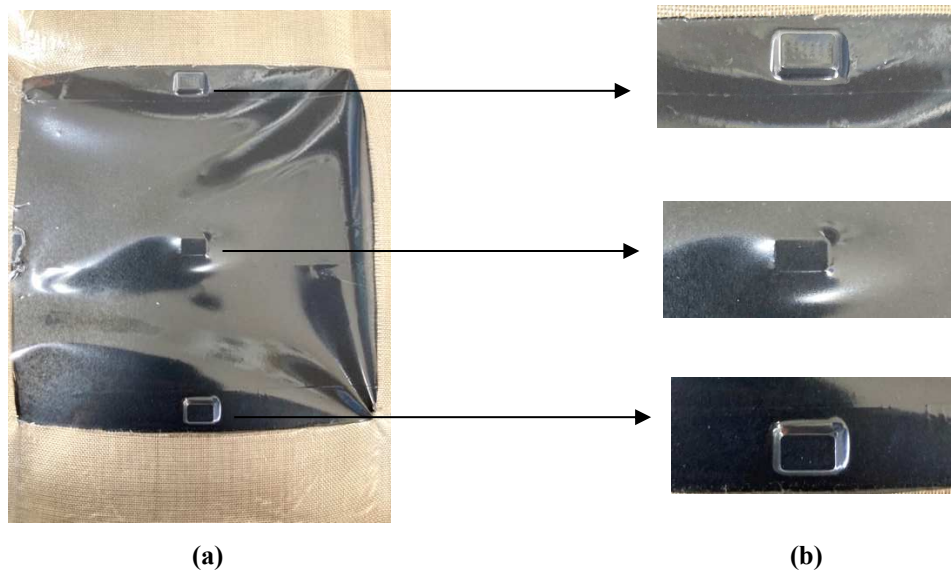


**Figure 4.44 The vacuum formed Platilon U 4201 AU on the samples. The top and bottom are well moulded (vacuum formed well whereas the sample at the centre is not) than the centre**

Platilon U 4201 AU, which was created in a vacuum, was displayed on the samples in Fig 4.44. In contrast to the centre sample, which was not vacuum formed, both top and bottom had been moulded. The tenting around the sensor could be reduced by the additional heating step using the heat gun and a second application of the vacuum. This was shown in Fig 4.45 (a) where the tenting around the die was clear and the considerable reduction in tenting was shown in Fig 4.45 (b).



**Figure 4.45 (a) vacuum formed using PU forms bubble around the chip due to straight sides (not angled) (b) reduced bubble size due to usage of heat gun and applying vacuum again**

The heat gun can be applied with the circuits in place on the platen to enable the rapid application of the second vacuum step. The additional heating and vacuum step can be repeated if required.

#### 4.8.5 Platilon U 4201 AU processing for moulding on flexible CO sensor strip packaging

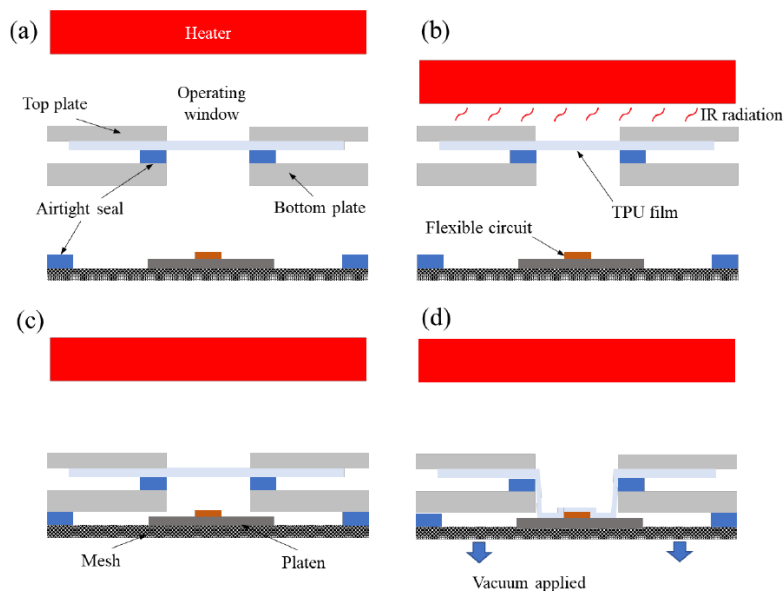


**Figure 4.46 Schematic diagram of vacuum forming process using Formech 450DT for moulding with Platilon U 4201 AU. (a) The heater is at the standby position and the sample is placed on the table below the clamped TPU film under the window; (b) the heater is moved forward to the front end from standby position to heat the TPU material; (c) the heater is moved back to the standby position and mesh and platen are raised towards the softened TPU forming a seal around the mesh; (d) vacuum is applied to force the softened material over the circuit**



The flexible sensor was first attached to a piece of Kapton with epoxy using acrylic adhesive shown in Fig 4.46 (a) since the bond between Kapton and Kapton using acrylic was higher than NLP 11051. The size of the Kapton with epoxy as the base should be greater than 1cm width and 9cm length as the desired flexible sensor strip dimension was 9x1cm. This substrate was used because the actual flexible sensor strip was narrow and might not be fully sealed with the packaging material. The fabric coated wires were soldered to the contact pads on the sides of the circuit as shown in Fig 4.46 (b)

**Step 1:** The circuit is placed onto a platen mounted on a mesh located under the operating window. The mesh allows the application of the vacuum and is initially in the lower position ~ 10 cm below the bottom plate. The TPU film is sandwiched between the top and bottom plates with an airtight seal around the operating window to form the vacuum in step 4. The heater is in the standby position as shown in Fig 4.46 (a) with the heat power set at 50% power corresponding to ~230 °C which is above the  $T_g$  for the TPU film and results in a soft pliable film.

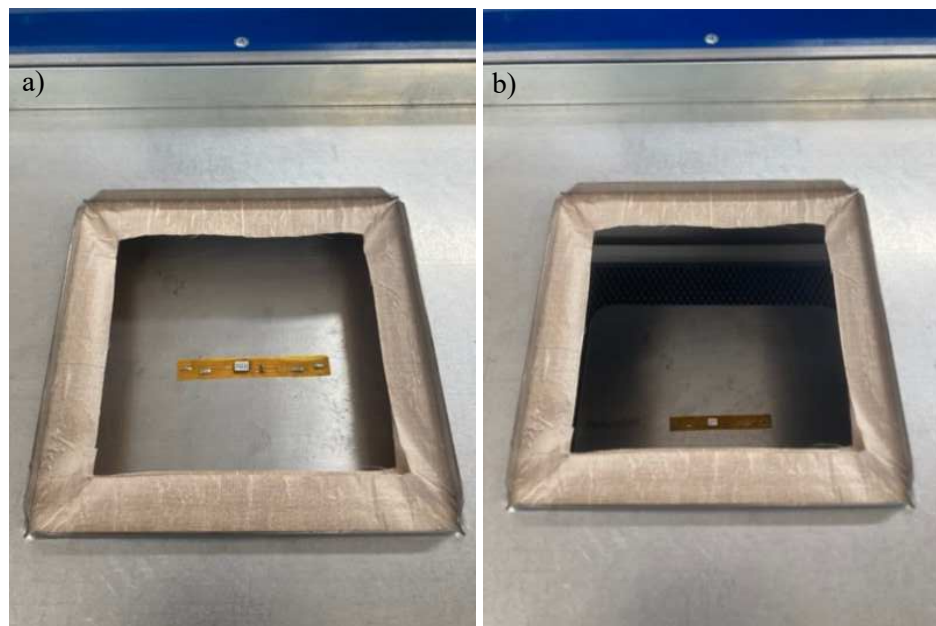


**Figure 4.47 (a) flexible CO sensor strip attached the Kapton with epoxy (b) attaching the wires by soldering to the contact pads**

**Step 2:** The heater is brought forward to be located and lowered over the TPU film which is heated for 50s as shown in Fig 4.47 (b). The coating appears to be conformal without creating any bubbles on the circuit strip.

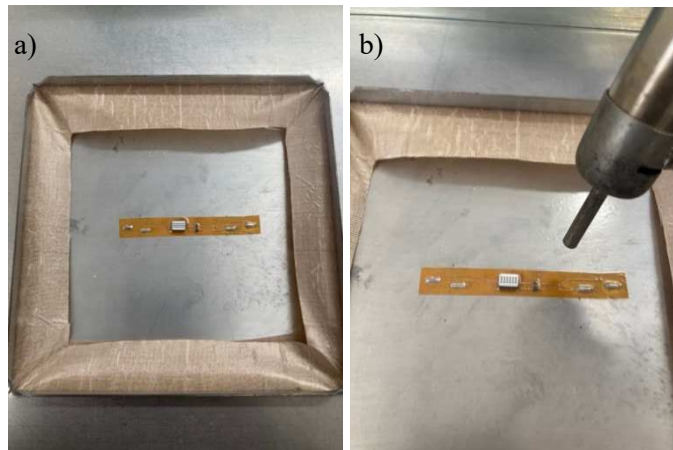


**Figure 4.48 (a) Sample placed in vacuum former table/stage (b) Platilon U 4201 AU vacuum formed on flexible sensor strip**

**Step 3:** The machine has an interlock system that does not allow heating and vacuum forming simultaneously. Hence the heater returned to the standby position and the mesh and platen containing the circuit is raised. This forms a seal between the edge of the mesh and the bottom plate. A vacuum of -0.8 bar is applied and atmospheric pressure forces the TPU film down over the circuit, Fig 4.48 (a). Once the vacuum is applied, the heat gun cannot be used as the Platilon U 4201 AU 4201 is stretched and does not have contact with the sensor strip. Hence the vacuum is turned off and the heat gun is used to bond Platilon U 4201 AU with sensor strip as shown in Fig 4.48 (b). The heat gun pushes the material while heating and bonding therefore a non-uniform coating of the packaging material is observed. This creates a bubble over the Sensor chip MICS 5524.

**Step 4:** After the process, the clamps could be released to remove the encapsulated circuit from the platen. Excess material around the circuit was removed.

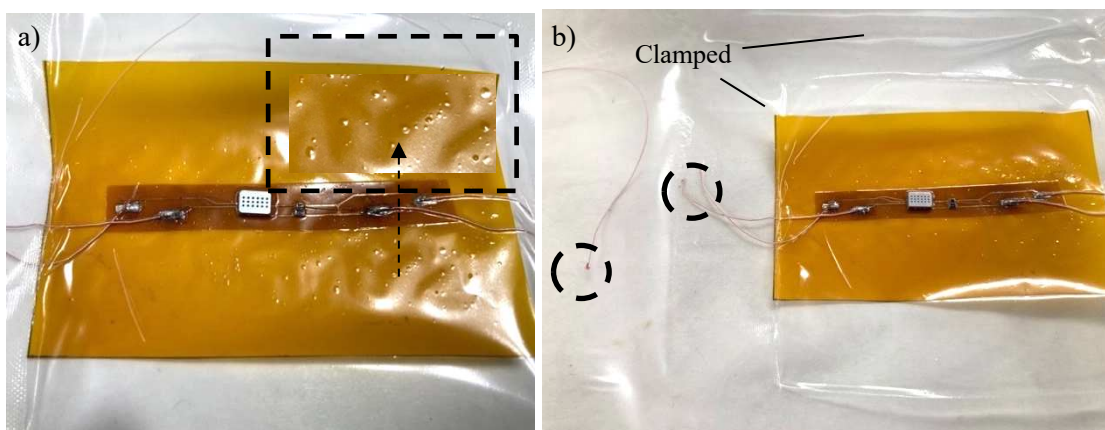


**Figure 4.49 (a) blisters or tiny bubbles on Platilon U 4201 AU after heating with heat gun at 240°C (b) wire is cut due to the pressure created between the table and the window**

There were a few drawbacks of vacuum formed Platilon U 4201 AU on flexible sensor strip for packaging. Due to the heating of PU material using heat gun being non-uniform, the blisters were

formed. Another issue was that the wires had snapped off during the vacuum forming process when the table/stage was moved upwards for vacuum forming as shown in Fig 4.49.

#### 4.8.6 Moulds for non-melt processible thermoplastic material

Vacuum forming is only for melt processible materials. For non-melt processible materials like Zitex G - 104 and PTFE glass fibre fabric, moulds can be used.

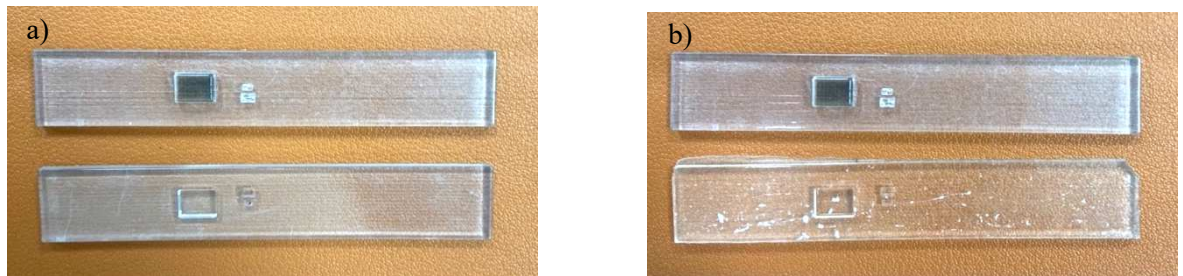


**Figure 4.50 (a) 3D printed male (top) and female (bottom) moulds with material Verclear (b) 3D printed male mould (top) and PDMS female mould (bottom)**

These moulds were made of Verclear material and were 3D printed as shown in Appendix B, two types of moulding were done – a) Male and female 3D printed Mould shown in Fig 4.50 (a) and (b) male 3D printed mould and Female PDMS mould shown in Fig 4.50 (b).

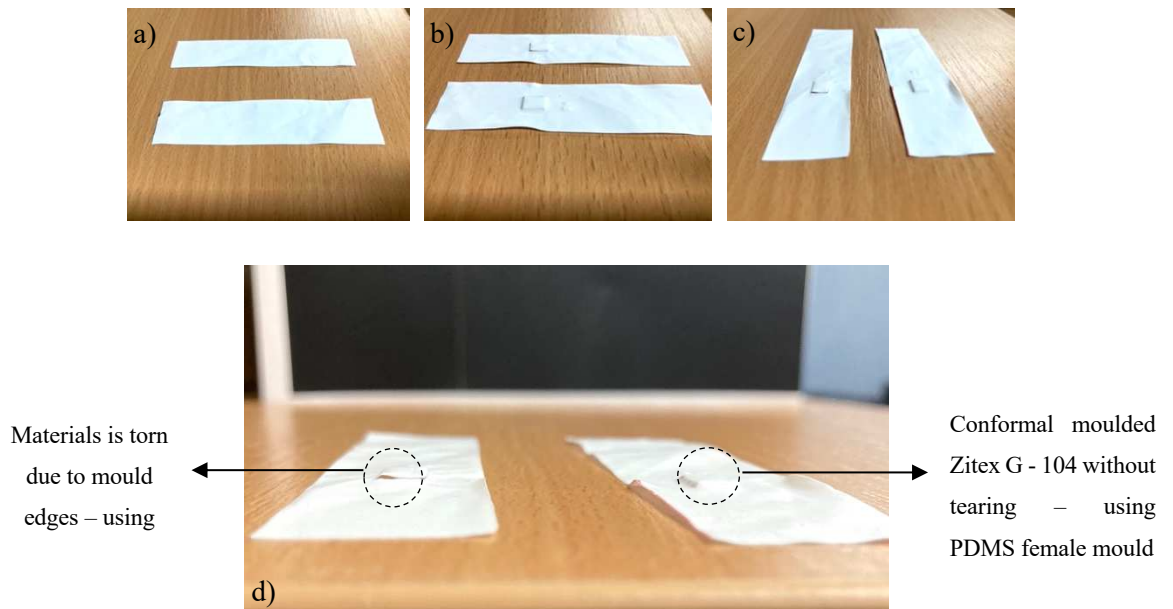


**Figure 4.51 (a) Zitex G - 104 is cut into dimensions of actual circuit strip (b) after moulding using both 3D printed, and 3D printed with PDMS moulds (horizontal view) (c) PDMS + 3D printed moulding gives more conformality than both 3D printed moulds (vertical view) (d) tearing of material when 3D moulds are used and is solved by using PDMS mould**

The 3D printed moulds on Zitex G – 104 leads to damaging the material due to sharp corners as shown in Fig 4.51. However, the flexible PDMS mould solved the issue by moulding the material to the desired shape without damaging it.

**4.8.7 Process of applying Pressure Sensitive Adhesive for bonding**

The adhesive films require flat surface for bonding to avoid peeling of the adhesive caused by bumps due to components in the substrate. Due to the presence of SMD components in the circuit strip, it is not advisable to use the adhesives directly on top of the circuit strips. This can be resolved by cutting the adhesive films into desired shape shown in fig 4.52 and placed on top of the circuit such that the adhesive does not cover the components.

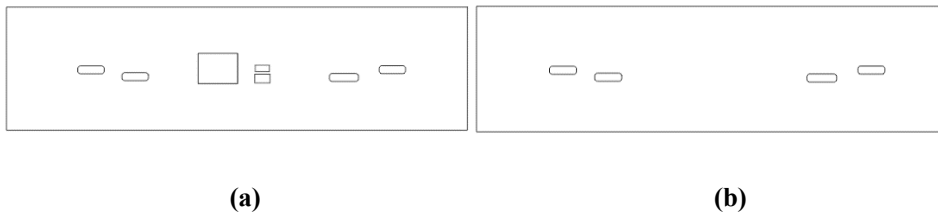


**Figure 4.52 CorelDraw design for adhesive film and solid mould for bonding (a) for the PSA and (b) for the Zitex G - 104 and PTFE Fibre glass fabric encapsulants**

The encapsulating material can also be cut to avoid packaging the soldering joints as shown in Fig 4.52. This is to provide easy soldering of wires if snapped due to mechanical stress. This was mainly for Zitex G - 104 and PTFE Fibre glass fabric as Platilon U 4201 AU 4021 AU can be easily melted around the soldering joints to attach and detach wires. Similarly, the PSA used for bonding Zitex G - 104 and PTFE Fibre glass fabric needed flat surface to bond with the substrates as shown in Fig 4.53.

The lumps formed due to the SMD components caused peeling and improper adhesion of the PSA materials to the circuit strip. The Graphtec Cutting Plotter CE600-40 shown in fig 4.53 (a) was used to get the adhesives and encapsulant cut to desired shape. The CorelDRAW app is linked to Master cut which sent the image to the cutter plotter for processing. The adhesives were placed in the sticky pad shown in Fig 4.53 (a).

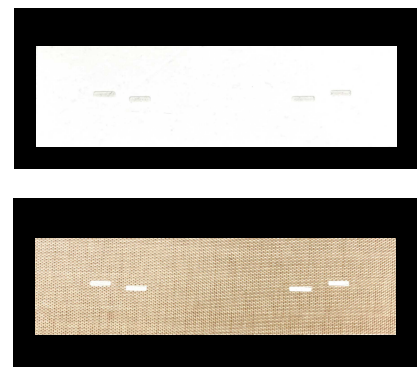
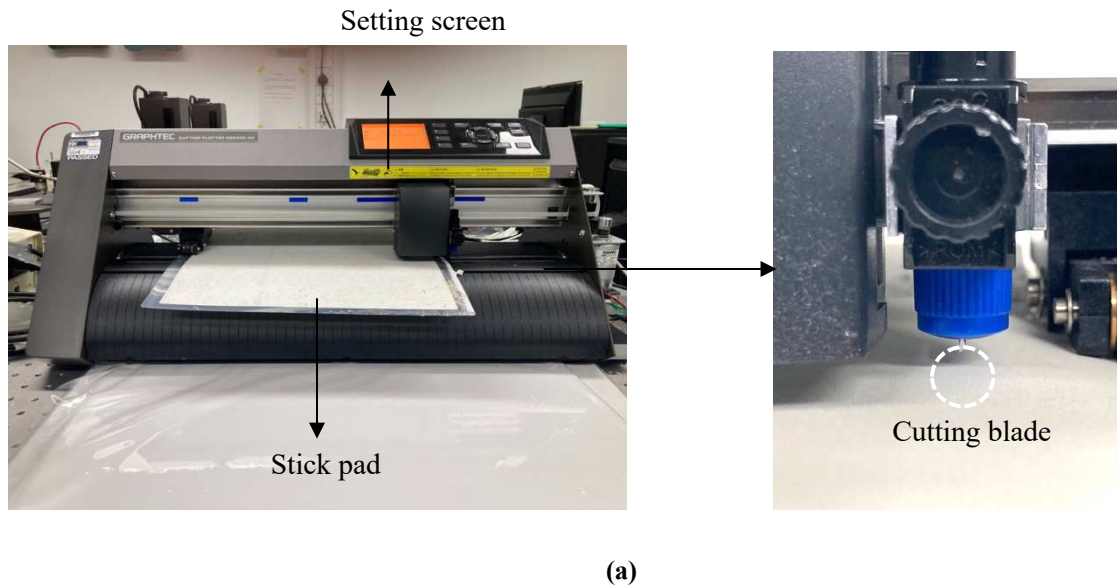


**Figure 4.53 (a) Graphtec Cutting Plotter CE600-40 (b) cut samples of adhesives – NLP 11051 (top) and acrylic adhesive (bottom) (c) cut samples of Zitex G - 104 (top) and PTFE Fibre glass fabric (bottom)**

Once the adhesive and encapsulant were cut to a desired shape shown in 4.53(b), the moulding process was achieved using the moulds. The pressure sensitive silicone adhesive NLP11051 requires a pressure of 10-15N/cm<sup>2</sup>. To achieve this for making the packaging, heat press at room temperature was used. The Max load of the heat press is 725.5kg. The heat press has Bar graph settings which allows to manually change the pressure required and varies from a scale 0 – 9. The required force for a bonding a 9cmx1.5cm circuit strip (which later was cut into desired dimension), is about 27kg. With this information, at the lowest pressure setting i.e., at 0, the approximate force would be 72.5kg.



**Figure 4.54 Heat press used for bonding NLP 11051 and Zitex G - 104**

Using this setting, the NLP 11051 can be bonded to the flexible circuit strips. So, for different area the load required to attain the desired pressure varies. A metal plate is placed as the bottom side of the heat press has a cushion and the pressure acting on an object placed over it may be affected. A solid mould shown in Fig 4.54 is used to add more contact pressure to the PSA.

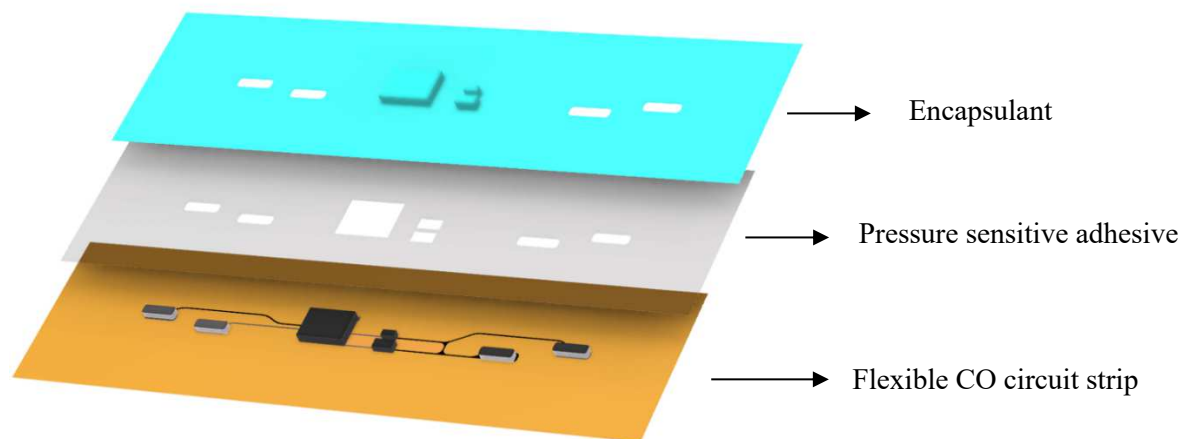


**Figure 4.55 Packaging assembly for Zitex G - 104 and PTFE Fibre glass fabric on flexible CO circuit strip**

The flexible CO circuit was removed from the alumina tile and placed flat to stick the PSA after being cut into the desired shape. The encapsulant Zitex G - 104 and PTFE Fibre glass fabric were then moulded using the PDMS and 3D print mould and attached on top on the adhesive as shown in Fig 4.55. The PDMS mould was placed on top of the encapsulant once again to get the desired shape of the circuit strip. However, since the circuit strip was very narrow and the chip being

lumpy, the encapsulant has not sealed properly. Hence the width of the circuit was optimized. Fig 4.56 (a) and (b) shows the Zitex G - 104 after packaging not sealed at the side A and side B.

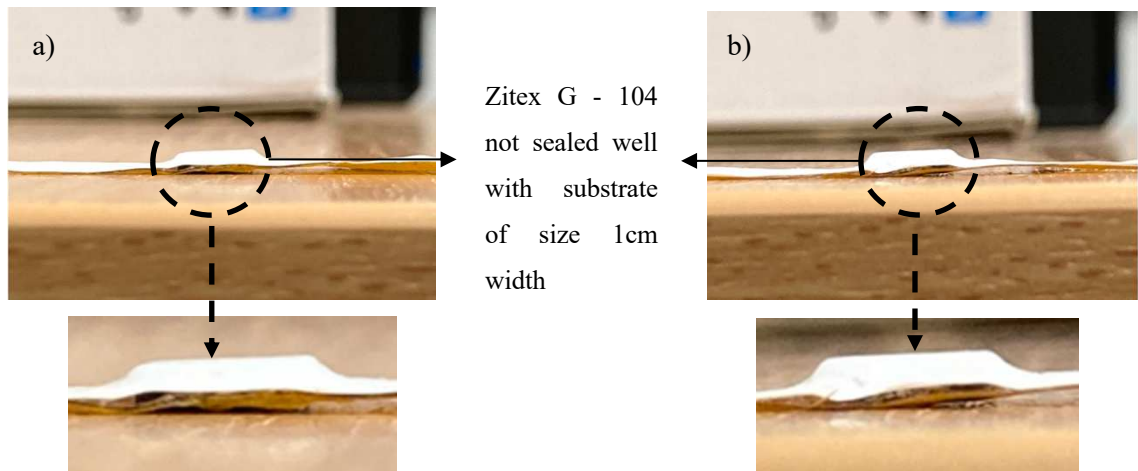


**Figure 4.56 Showing Zitex G - 104 after packaging not sealed at the (a) side A and (b) side B**

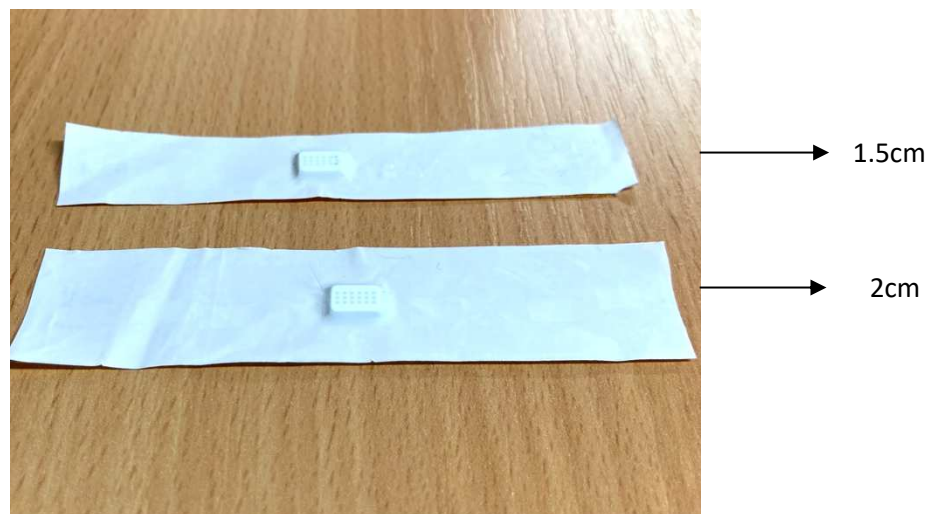


**Figure 4.57 Zitex G - 104 on substrate width of 1.5 and 2cm**

Fig 4.57 shows the Zitex G - 104 on substrate width of 1.5 and 2cm. The actual width size of the circuit strip is ~1cm hence the circuit should be attached to Kapton of higher width. For this, the bond strength between the circuit strip and Kapton using NLP11051 and acrylic adhesive.

#### **4.8.8 Packaging assembly with additional substrate of optimized width**

An additional player of Kapton of 25 $\mu$ m was used to increase the width of the flexible circuit strips. The adhesive used for attaching the flexible CO circuit strip (with Kapton E) on 25 $\mu$ m Kapton (Kapton N) was selected based on high bond strength. For this, Kapton E and Kapton N were bonded with NLP11051, acrylic adhesive, NLP 11051, and acrylic adhesive together and two acrylic adhesives together.

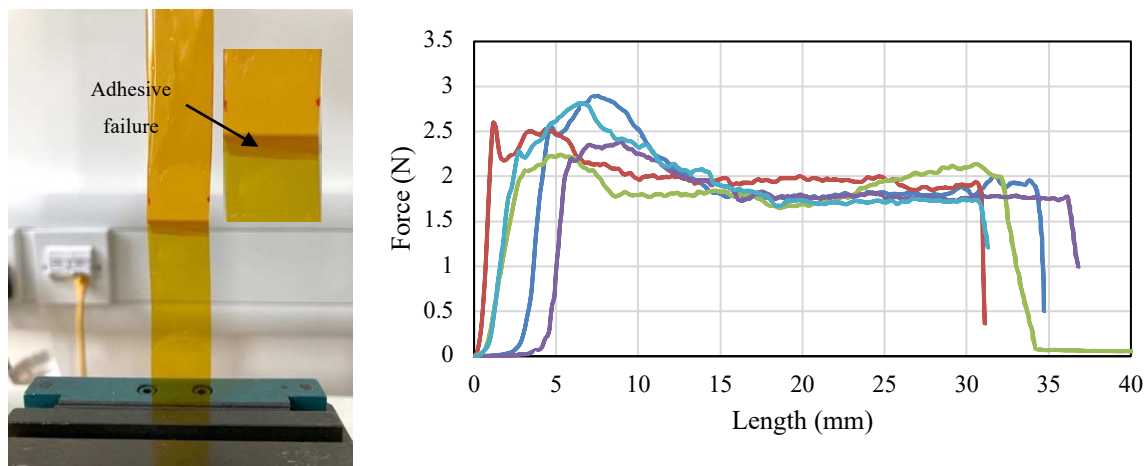


Figure 4.58 Peel Strength for Kapton E and Kapton N bonded using NLP11051 – adhesive failure

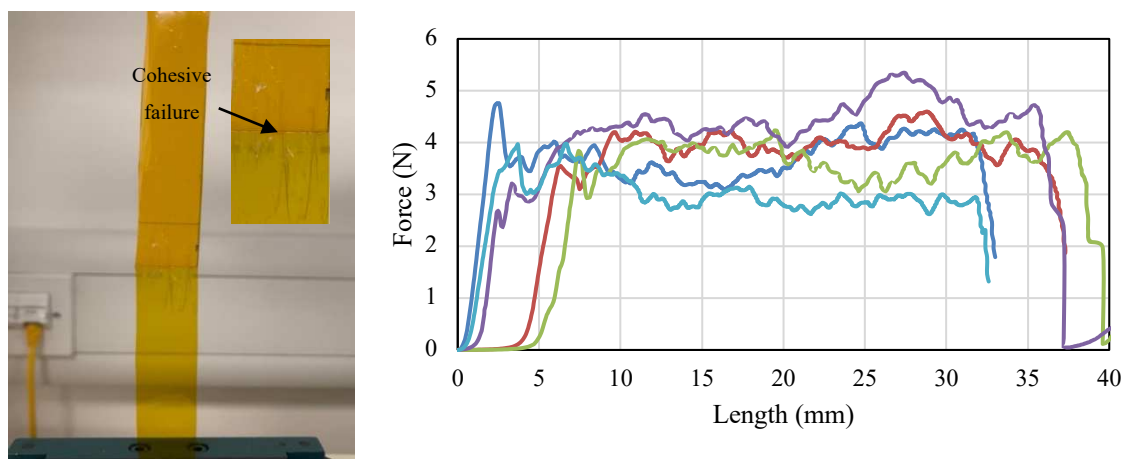


Figure 4.59 Peel Strength for Kapton E on Kapton N bonded using acrylic adhesive – cohesive failure

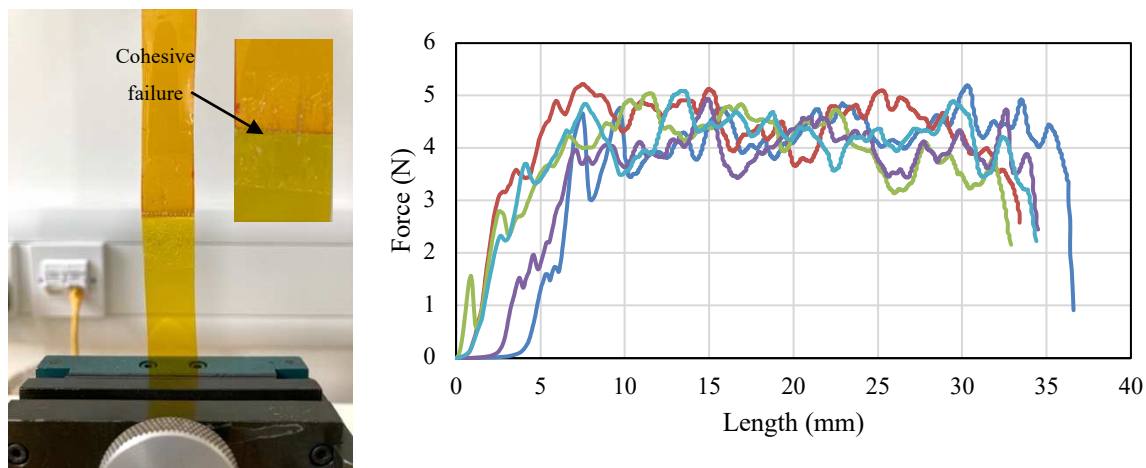
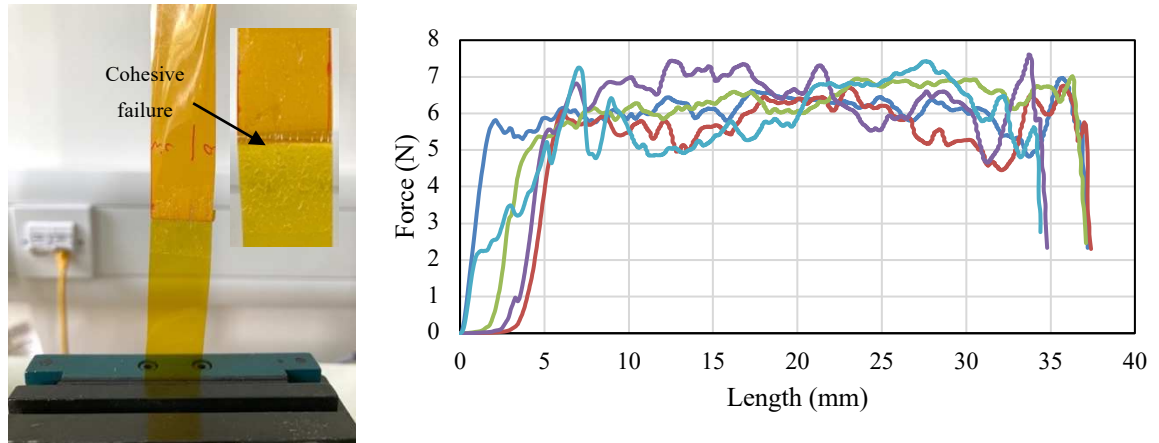


Figure 4.60 Peel Strength for Kapton E on Kapton N using NLP11051 and acrylic adhesive



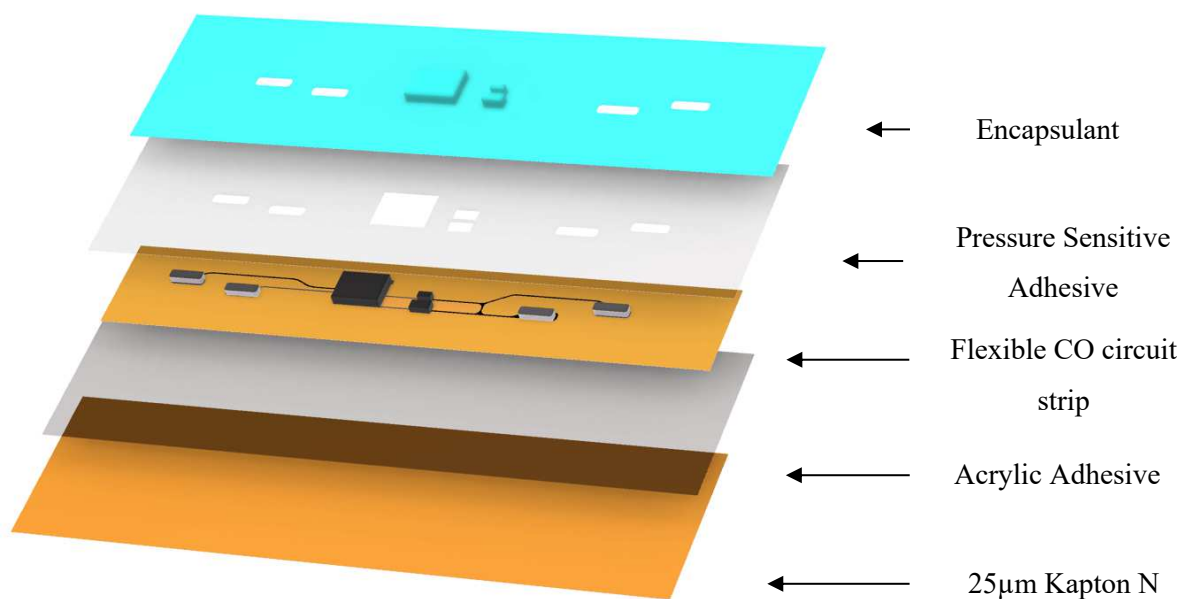


**Figure 4.61 Peel Strength for Kapton E on Kapton N using two acrylic adhesives**

It was noticed that the bond strength of acrylic adhesive for Kapton E and Kapton N was higher than NLP11051 as shown in Fig 4.58. Also, the bond strength of combination of two acrylic adhesive together was higher than the combination of NLP11051 and acrylic adhesive. Hence with the analyzed data, acrylic adhesive was used to bond the flexible CO circuit strip to Kapton N.

The packaging assembly with additional Kapton N for having optimized width of the circuit strip is as follows,

- 1) The Kapton N of thickness  $25\mu$  was cleaned and bonded with acrylic adhesive.
- 2) The flexible CO strip base was cleaned with acetone using cotton buds and attached to the top side of the acrylic adhesive bonded to Kapton N.



**(a)**

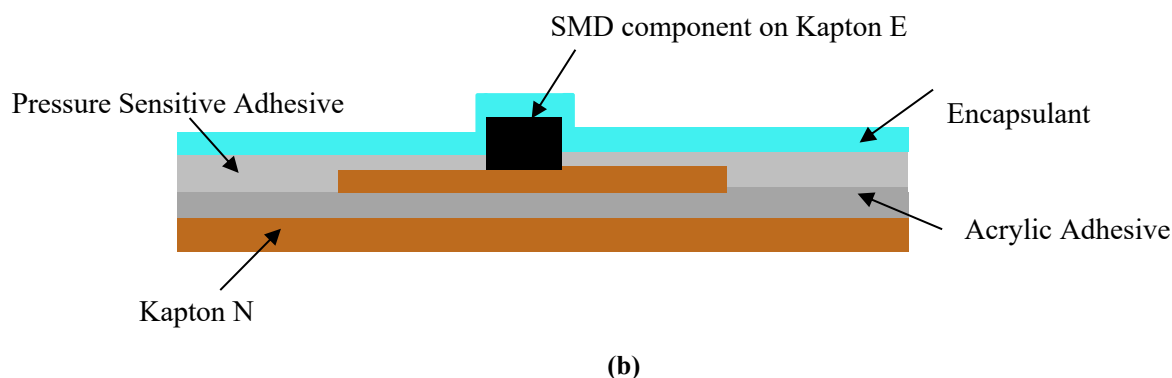


**Figure 4.62 (a) Packaging assembly for flexible CO circuit strip with additional Kapton (b) simple cross section of the packaged flexible sensor**

- 3) On top of the Flexible CO circuit strip, the patterned cut NLP11051 PSA was attached. The flexible PDMS mould was placed on top of this and placed in the digital Knight DK20 heat press at its lowest pressure setting and at room temperature. A metal plate was used to support the circuit assembly to add rigidity as the foam in the heat pressure may lead to displacement of the packaging assembly. For PTFE Fibre glass fabric, acrylic adhesive was used which did not require a certain pressure hence the adhesive was placed on the circuit and moved on to the next step.
- 4) Finally, the moulded encapsulant was placed on top of the PSA (NLP11051 for Zitex G - 104 and acrylic for PTFE Fibre glass fabric). The PDMS mould was placed on top of the assembly and bonded well using the heat press (digital Knight DK20s) once again. The process flow is shown in Fig 4.62 (a) and the cross-sectional view of the packaged filament is shown in Fig 4.62 (b).

The PTFE Fibre glass fabric and Zitex G - 104 packaged filaments are shown in Fig 4.63. To avoid packaging unseal due to the height of the sensor chip, the packaging was carefully cut to a width 1.5cm total i.e., 0.5 mm measured from top and bottom of the chip. This was performed after the materials were bonded together following the packaging assembly process.

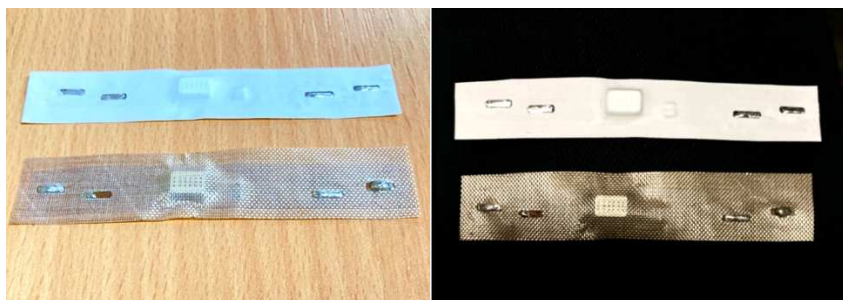


**Figure 4.63 Zitex G - 104 (top) and PTFE Fibre glass fabric (bottom) encapsulated flexible CO sensor**

The moulding of the thermoplastic material may change the dimensions of the material. To check the degree of change in dimensions after moulding, the PTFE Fibre glass fabric and Zitex G - 104 were cut exactly to 2x9 cm using the cutter plotter. The moulding of PTFE Fibre glass fabric and Zitex G - 104 had less or negligible effect on the change in dimensions of the sample width as shown in Fig 4.64. This result was also useful in cutting the holes using the cutter plotter for the soldering joints areas. An overview of the various encapsulants and adhesives that can be used to bond the elastic CO gas sensing circuit strip is provided in Table 4.2.



**Figure 4.64** Width of the sample strip of (a) PTFE Fibre glass fabric before moulding (b) PTFE Fibre glass fabric after moulding (c) Zitex G - 104 before moulding and (d) Zitex G - 104 after moulding

**Table 4.2** Summary of encapsulation method for different encapsulants with best adhesives for bonding the flexible CO gas sensor circuit strip

Materials	Method of encapsulation	Bonding material
PTFE glass fibre fabric	Vacuum forming	Acrylic adhesive
Zitex G - 104	Mould – 3D printed Verclear and PDMS	NLP 11051 Silicone pressure sensitive
Platilon U 4201 AU	Mould – 3D printed Verclear and PDMS	Epoxy adhesive in etched Kapton (Kapton E) by heating using heat gun

## 4.9 Conclusion

- This chapter discusses the different materials investigated for encapsulating the flexible CO sensor. The encapsulant materials and the adhesives used for bonding them to the flexible circuits were observed to be water resistant by the contact angle measurement method.
- Zitex G - 104 most hydrophobic among all the encapsulants and NLP11051 adhesive is more hydrophobic than acrylic adhesive.
- The bond strength for the adhesives with different materials were investigated and found that acrylic has high bond strength for PTFE Fibre glass fabric and Kapton whereas NLP11051 is better for Zitex G - 104. Different modes of failure due to peel test were observed as given in Table 4.3.

**Table 4.3 Peel Test – Modes of Failure**

Mode of Failure – Peel test								
Material	NLP11051		Acrylic		Epoxy – heat activated		NLP + Acrylic	Acrylic + acrylic
Substrate	Kapton N	Kapton E	Kapton N	Kapton E	Kapton N	Kapton E	Kapton N	Kapton N
PTFE Fibre glass fabric	A	-	A	A	-	-	-	-
Zitex G - 104	A	A	A	-	-	-	-	-
Platilon U 4201 AU	-	-	-	-	S	S	-	--
Kapton E	A	-	C	-	-	-	C	C

A - Adhesive failure mode, C – Cohesive failure mode, S – Substrate

## Chapter 5 Gas Sensing of Textile Integrated Flexible CO Sensor

The fabricated flexible gas sensors must be able to detect the targeted gas molecule after being integrated in textile. For these, the choice of the textile material plays an important role in pass the gas molecule through the material. The air/gas permeability can also be enhanced for textile based on the type of technique used to fabricate a piece of fabric. Weaving, knitting, braiding using yarns of materials are a few types of making a piece of fabric. The air permeability is enhanced by making gaps in the weaving process bigger giving it a less density woven fabric. For this project, a cotton woven fabric with 2/32s Organic cotton undyed from Esquel made with less density was fabricated and used for integration of flexible gas sensors in textile and as a carrier for washing test. Two types of fabric were made 1) opening on both the sides to pull out wires once the sensor is inserted in the pocket and opening on one side for washing test as shown in Fig 5.1.

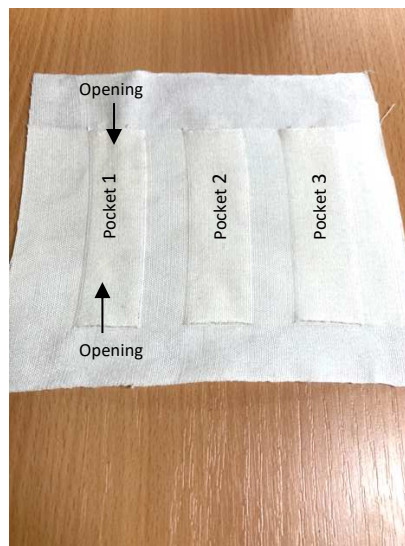
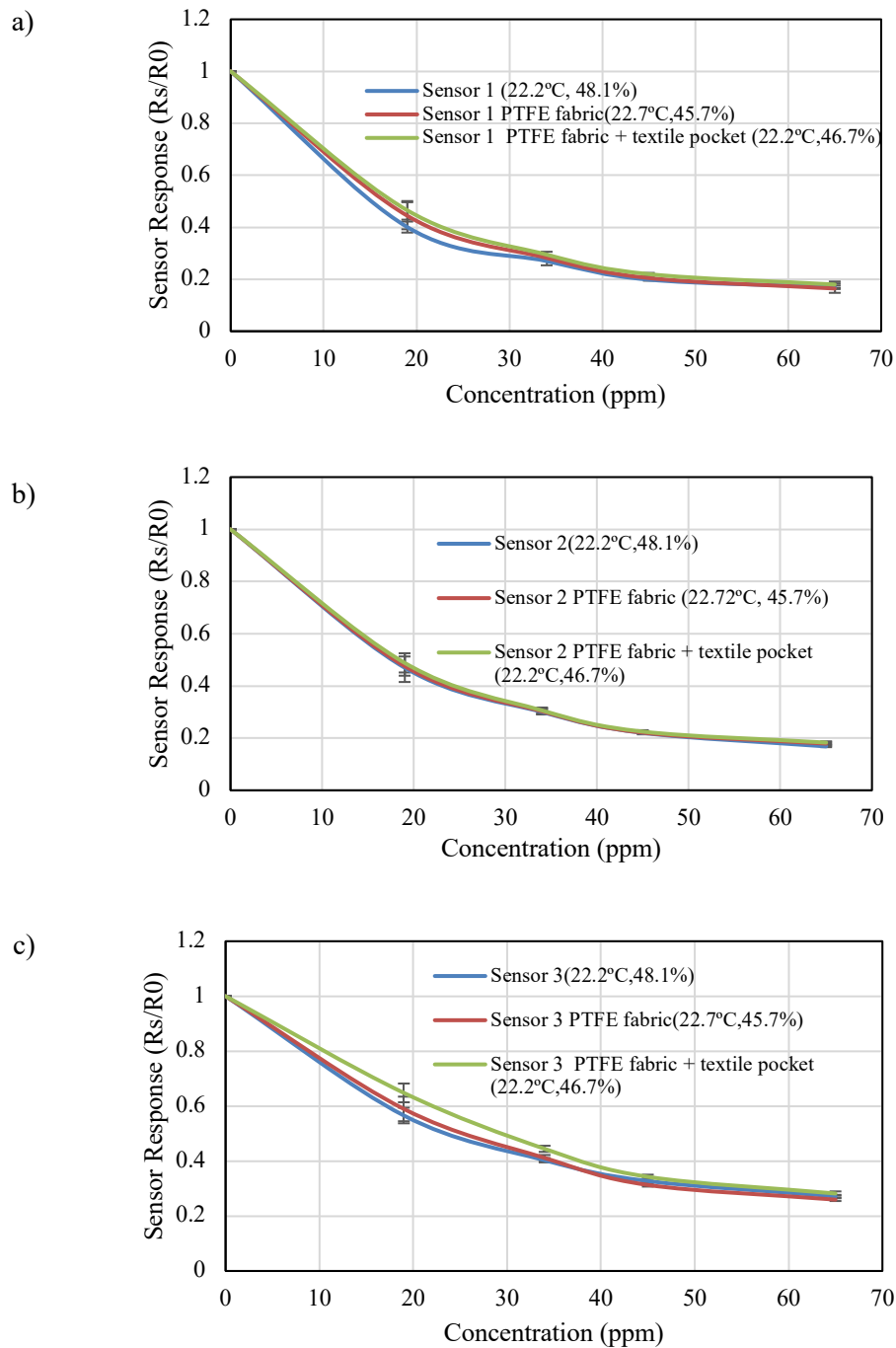


**Figure 5.1 Cotton woven fabric with pockets open at both ends**

Each fabric had three pockets to have 3 flexible sensors and test them at the same time. Each pocket is of the dimension 9cmx2.5cm.

### 5.1 Gas sensing experiments - Response of, and PTFE Fibre glass fabric, Zitex G - 104 and Platilon U 4201 AU coated filaments

The gas sensor sensors were tested with four different concentrations of CO (each concentration repeated thrice) to get the response of unencapsulated and encapsulated gas sensor integrated in a piece of cotton woven fabric. The first three sensors were encapsulated with PTFE Fibre glass fabric and the results are shown in Fig 5.2 (a), (b) and (c).

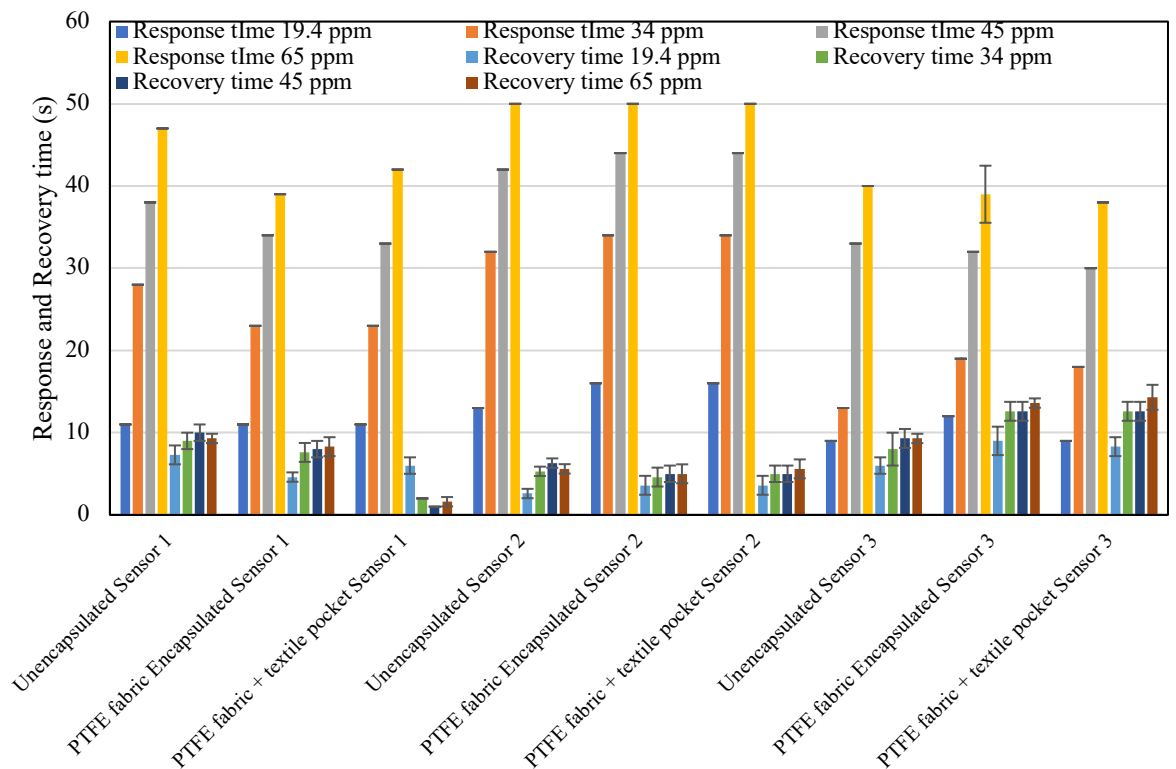


**Figure 5.2 Gas sensing response before and after encapsulating with PTFE Fibre glass fabric a) Sensor 1, b) Sensor 2 and c) Sensor 3**

It was noticed the PTFE Fibre glass fabric encapsulated of Sensor 2 has negligible effect on the sensor response and Sensor 1 and Sensor 3 has a slight effect on the response before encapsulation and after integrating into fabric respectively. The slight difference existed due to the temperature.

**Table 5.1 Time Taken for PTFE Fibre glass fabric encapsulated filaments**

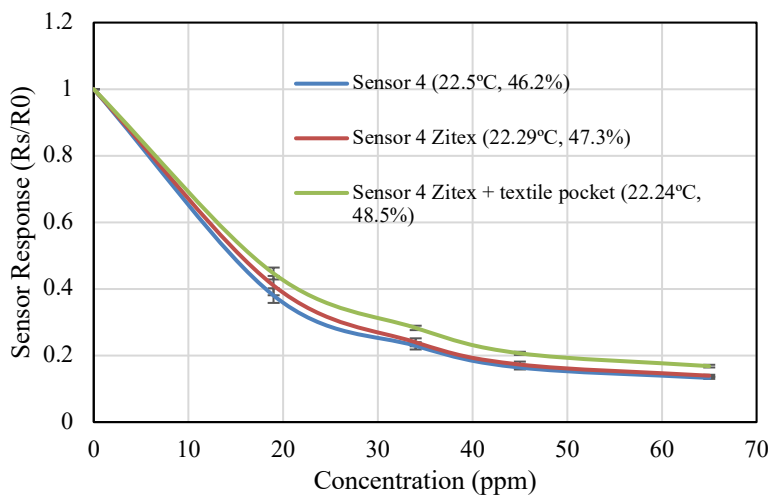
Time	Response time (s)				Recovery time (s)			
	19.4 ppm	34 ppm	45 ppm	65 ppm	19.4 ppm	34 ppm	45 ppm	65 ppm
Unencapsulated Sensor 1	11	28	38	47	7.3	9	10	9.3
PTFE Fibre glass fabric Encapsulated Sensor 1	11	23	34	39	4.6	7.6	8	8.3
PTFE Fibre glass fabric + textile pocket Sensor 1	11	23	33	42	6	2	1	1.6
Unencapsulated Sensor 2	13	32	42	50	2.6	5.3	6.3	5.6
PTFE Fibre glass fabric Encapsulated Sensor 2	16	34	44	50	3.6	4.6	5	5
PTFE Fibre glass fabric + textile pocket Sensor 2	16	34	44	50	3.6	5	5	5.6
Unencapsulated Sensor 3	9	13	33	40	6	8	9.3	9.3
PTFE Fibre glass fabric Encapsulated Sensor 3	12	19	32	39	9	12.6	12.6	13.6
PTFE Fibre glass fabric + textile pocket Sensor 3	9	18	30	38	8.3	12.6	12.6	14.3

**Figure 5.3 Gas Sensing response before and after encapsulating with Platilon U 4201 AU for sensor 7**

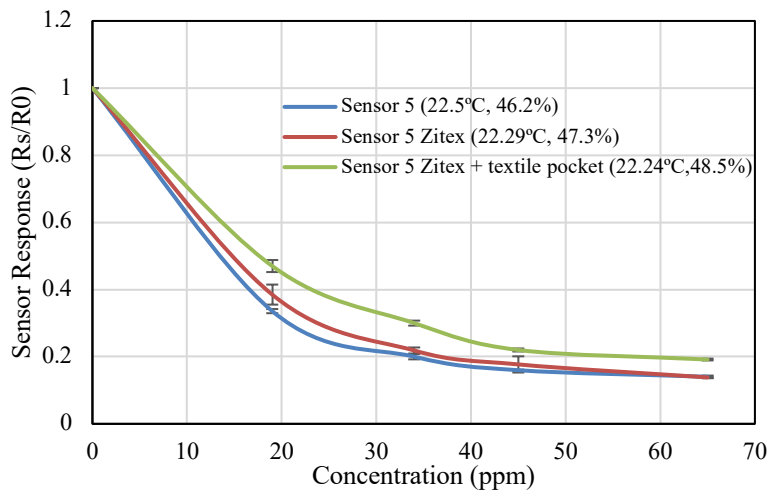
The time taken for the sensor to detect a change in the voltage (or resistance) from the  $R_0$  is considered to see the response of the sensor to carbon monoxide. It was observed that the time taken for the sensor without TPU layer to detect a change in resistance after the gas was let inside the chamber was about 10s while for the TPU encapsulated circuit it took about 30s to read a change in resistance as shown in Table 5.1.

The Zitex G - 104 encapsulated filaments also had negligible effects on the gas sensor sensitivity as shown in Fig 5.4 (a), (b) and (c).

a)



b)





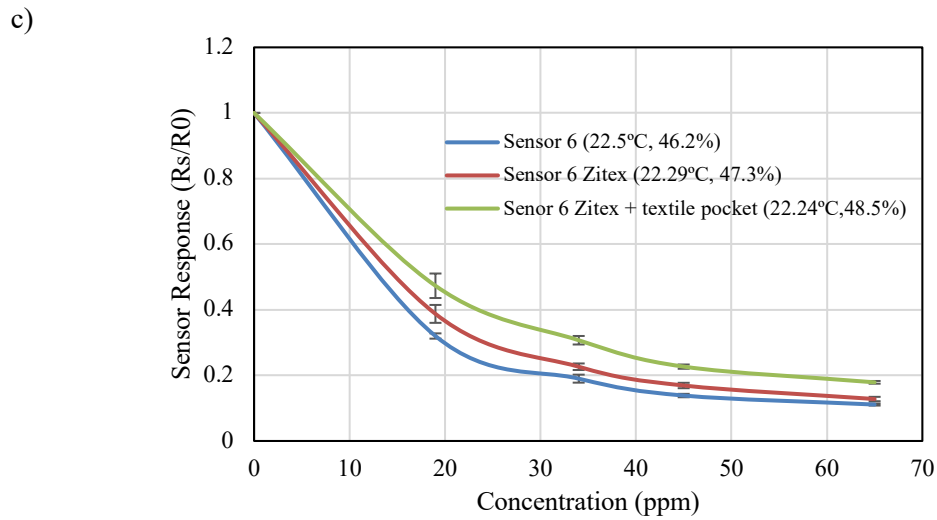


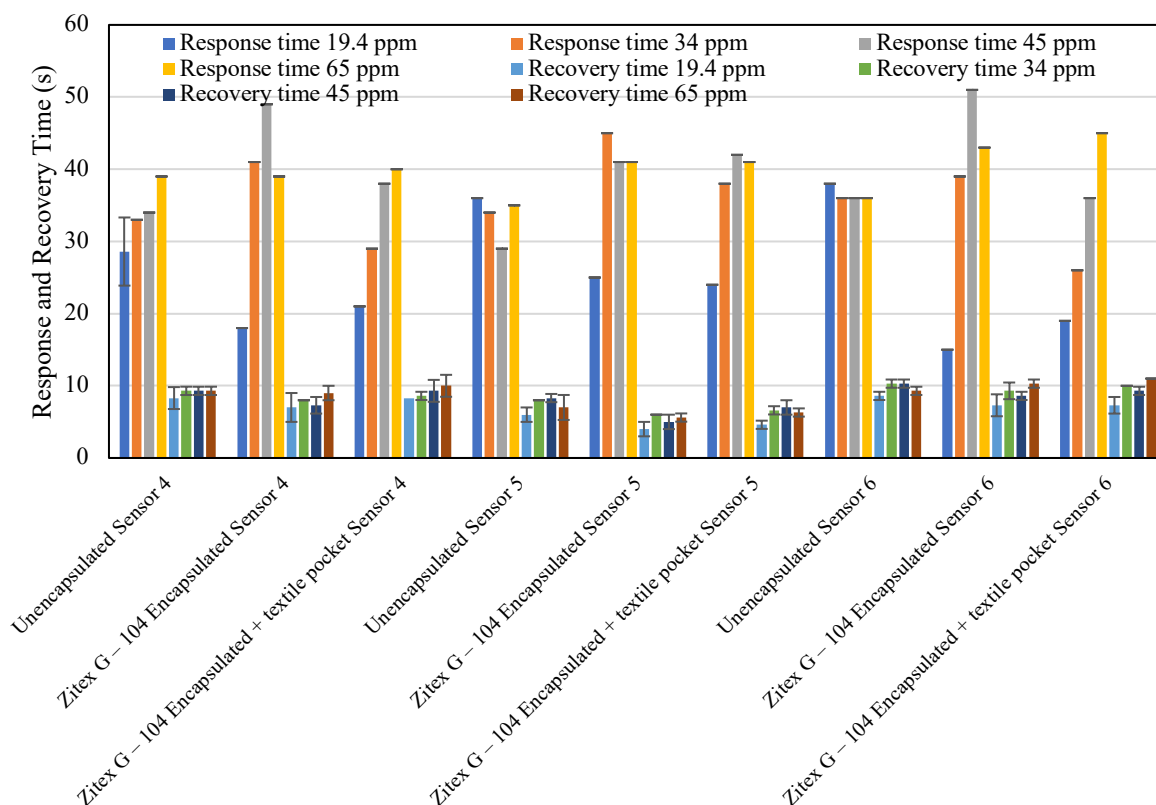
Figure 5.4 Gas sensing response before and after encapsulating with Zitex G - 104 a) Sensor 4, b) Sensor 5 and c) Sensor 6

Table 5.2 Time Taken for Zitex G - 104 Encapsulated filaments

Time	Response time (s)				Recovery time (s)			
	19.4 ppm	34 ppm	45 ppm	65 ppm	19.4 ppm	34 ppm	45 ppm	65 ppm
Unencapsulated Sensor 4	28.6	33	34	39	8.3	9.3	9.3	9.3
Zitex G - 104 Encapsulated Sensor 4	18	41	49	39	7	8	7.3	9
Zitex G - 104 Encapsulated + textile pocket Sensor 4	21	29	38	40	8.3	8.6	9.3	10
Unencapsulated Sensor 5	36	34	29	35	6	8	8.3	7
Zitex G - 104 Encapsulated Sensor 5	25	45	41	41	4	6	5	5.6
Zitex G - 104 Encapsulated + textile pocket Sensor 5	24	38	42	41	4.6	6.6	7	6.3
Unencapsulated Sensor 6	38	36	36	36	8.6	10.3	10.3	9.3
Zitex G - 104 Encapsulated Sensor 6	15	39	51	43	7.3	9.3	8.6	10.3
Zitex G - 104 Encapsulated + textile pocket Sensor 6	19	26	36	45	7.3	10	9.3	11

However, the gas sensitivity appeared to have been slightly affected after the filament is placed inside the fabric and was higher for sensors 5 and 6 as shown in Fig 5.4 (b) and (c). This might have been due to the variation in chamber temperature and relative humidity.

The time taken for the sensor to detect a change in the voltage (or resistance) for both PTFE and Zitex G – 104 were fairly similar to the response time of unencapsulated flexible filament. The porous nature of these two materials has negligible impacts on the sensor response and recovery time.



**Figure 5.5 Gas Sensing response before and after encapsulating with Zitex G – 104 for sensor 4 5 and 6**

The response of both the sensors with and without TPU decreased with increase in the concentration of CO. However, the response of the TPU encapsulated sensor was less sensitive than the sensor response without encapsulation. The Platilon U 4201 AU 4201AU encapsulated filaments acted as a gas barrier film which gave a gas response of 1 (showing 0 ppb of CO) as shown in Fig 5.6 (a), (b) and (c). The gas response of sensor 7 shown in Fig 5.6 (a) shows detection of gas which may be due to TPU not sealed or high baseline variation.

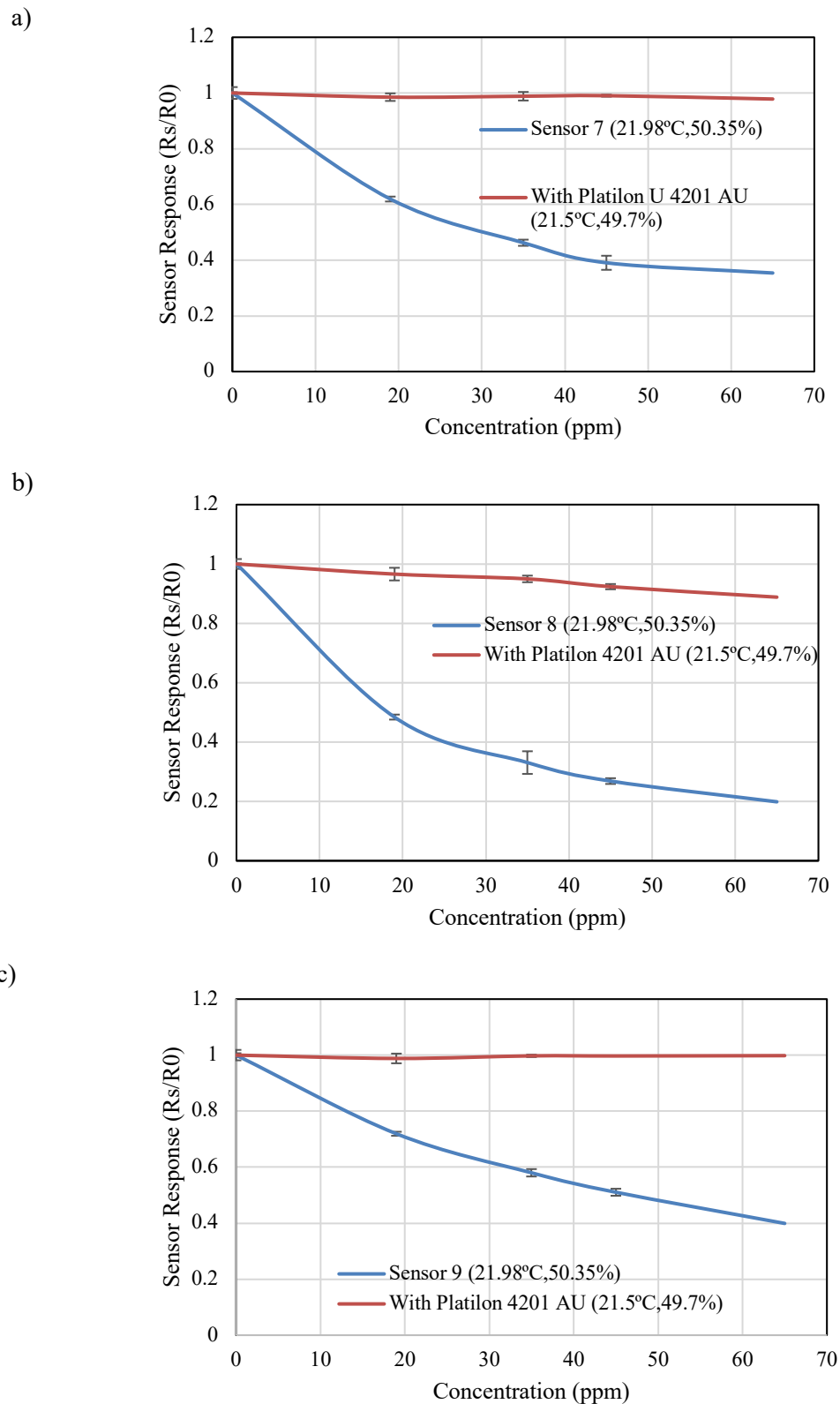


Figure 5.6 Gas Sensing response before and after encapsulating with Platilon U 4201 AU) Sensor 7, b) Sensor 8 and c) Sensor 9

## Conclusion

- Finally for the CO sensing, it was shown that Zitex G - 104 and PTFE Fibre glass fabric had negligible effects on the sensor response when compared with the unencapsulated circuits.
- The recovery times for encapsulated sensors were lower than the response times similar to the unencapsulated filaments
- Platilon U 4201 AU was a breathable material but acted as a gas barrier film for carbon monoxide

## Chapter 6 Evaluation of E-textile Gas Sensor Under Mechanical Stresses - Bending and Washing Environments

To make sure that the encapsulated circuits can provide higher durability without affecting the performance of the sensor, the three encapsulated circuits have been tested under bending and washing cycles.

### 6.1 Stress analysis

The stress caused in e-textile fabrics due to folding, bending or mechanical stresses had caused during washing, and this could lead to disfunction of the electronic circuits. This mainly brought forward the need of packaging of flexible electronic circuits. The circuit can mainly fail due to failure in the sensor chip, or any contact issue in the copper track. In a beam or a planar circuit, the neutral axis (NA) was the axis in the cross section of the beam where the stress and strain were zero as shown in Fig 6.1. Packaging this sensor so that the copper track is close to the neutral axis where the stresses are minimum can higher the durability of the circuit filament under mechanical stresses.

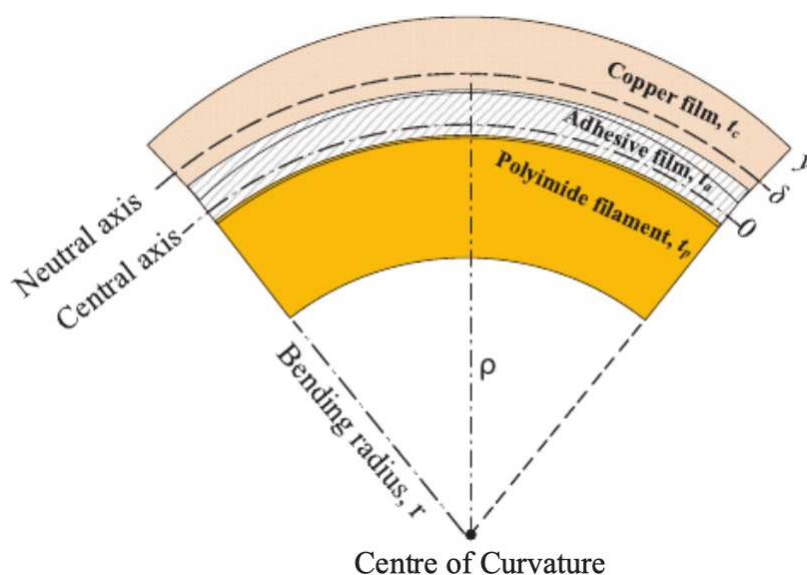


Figure 6.1 Neutral axis when flexible materials are subjected to bending [14]

Since each material in the packaged circuit has different properties mainly thicknesses and stiffnesses affects the location of the neutral axis and this can affect the durability of the circuit due to stresses acting on the copper track. The location of neutral axis can be calculated by,

The maximum stress caused in at a location in the circuit can be found by eqn. (7),

$$NA = \frac{\sum_{i=1}^n E_i t_i (2 \sum_{j=1}^i t_j - t_i)}{2 \sum_{i=1}^n E_i t_i} \quad (7)$$

Where E is the Young's modulus and t is the thickness of the material. The location of the neutral axis depends on E and t of the material. The NA being close to the copper track helps in improving the durability of the circuit as the stress induced whilst bending will be minimal. With the material properties of the materials used in packaging given in Table 6.1, the NA for unencapsulated filament, PTFE Fibre glass fabric, Zitex G - 104 and Platilon U 4201 AU encapsulated filaments were calculated using MATLAB coding and is given in Table 6.2.

**Table 6.1 Material properties**

Material	Thickness (um)	Young's modulus (GPa)
Kapton	25	3
Epoxy adhesive	17	1.8
Copper	18	70
Platilon U 4201 AU	100	0.0076
Zitex G - 104	104	0.131
PTFE Fibre glass fabric	60	0.6
Acrylic adhesive	25	2.5
Silicone adhesive	25	0.001

**Table 6.2 Neutral axis calculated**

Materials	Without encapsulation	With encapsulation
Platilon U 4201 AU	48.49um	48.5um
PTFE Fibre glass fabric		49.3um
Zitex G - 104		54.5um

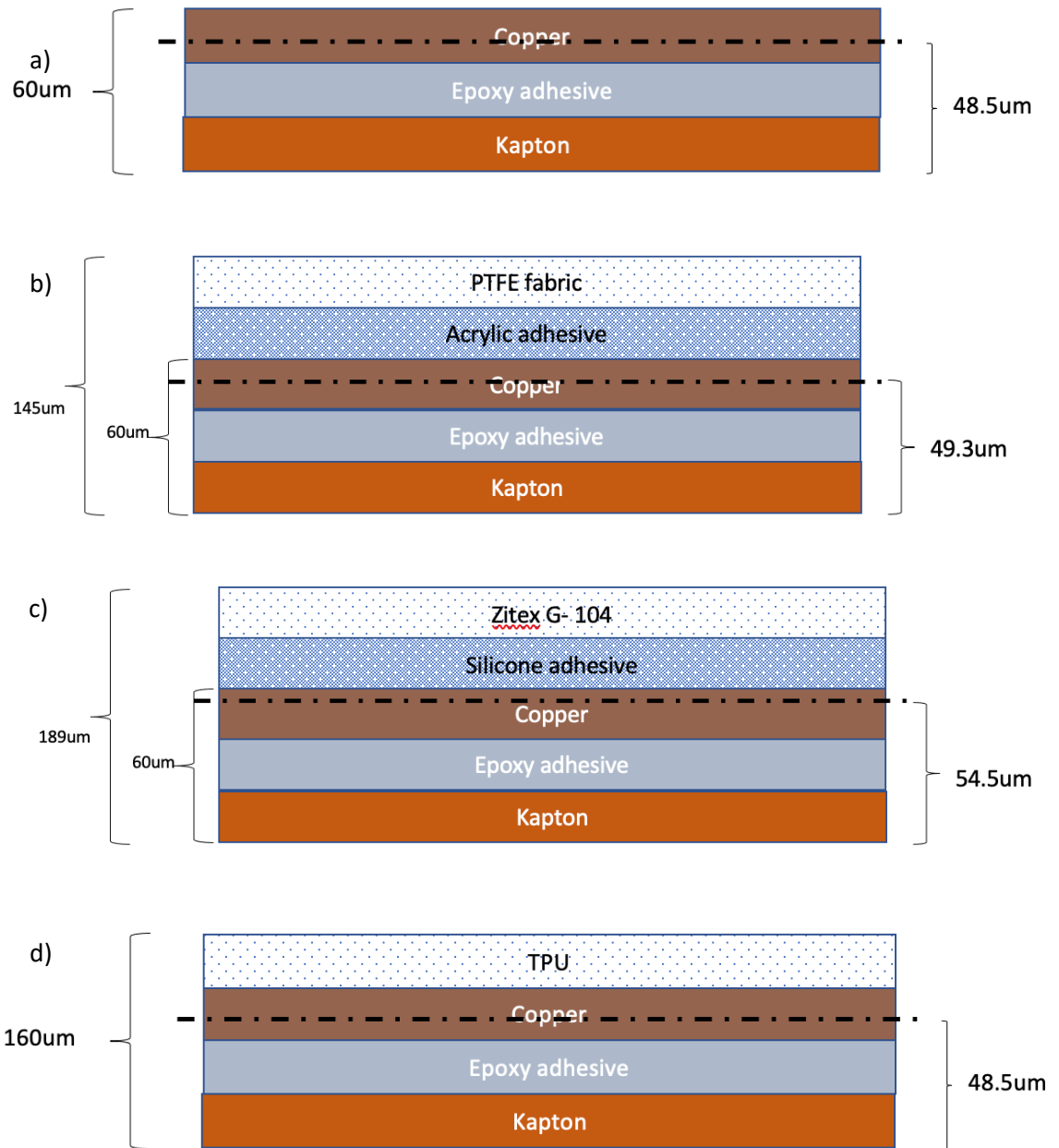


**Figure 6.2 Neutral axis analysis for a) unencapsulated filament, b) PTFE Fibre glass fabric, c) Zitex G - 104 and d) Platilon U 4201 AU encapsulated filament**

The NA for all the packaging method is on the copper track however, the bonding strength, tear strength of the packaging material, chemical resistivity of the encapsulant play an important role in achieving high durability over mechanical stresses caused by bending and washing. Fig 6.2 shows the analysis of neutral axis for unencapsulated filament, PTFE Fibre glass fabric, Zitex G - 104, and Platilon U 4201 AU encapsulated filament.

## 6.2 Bending test

To assess the mechanical robustness of the flexible filament, the filament was moved to and froth over a roller such that its bent over could cause stress on the circuit leading to failure of the circuitry such as failure in electrical connections, failure in bonding of the adhesives to the encapsulant and circuit strip or failure in encapsulant.

### 6.2.1 Experimental setup

The experimental setup has two movable clamps; top horizontal clamp that moves back and forth horizontally via motorised conveyor belt and the vertical clamp to move back and forth vertically as shown in Fig 6.3. The setup has a roller over which one end of the sample clamped to the horizontal clamp bends over and the other end of the sample clamped to the vertical clamp with a counterweight. 100 g counterweight (cylindrical metallic weight) is used to add tension and keep the sample flat over the roller. Since the sensor chip MICS 5524 is quite lumpy, the flexible circuit was inserted in a textile pocket and the 5mm diameter bending roller was used. The textile pocket ends were attached to the movable clamps in the bending rig. The cotton fabric was cut into 15mm width and sewed to the sides of the circuit strips as shown. A weight of 200 g was added to the one end of the grip (bottom). The resistance was measured across the contact pad for the power supply and the contact pads connecting to the load resistance for output measurement.

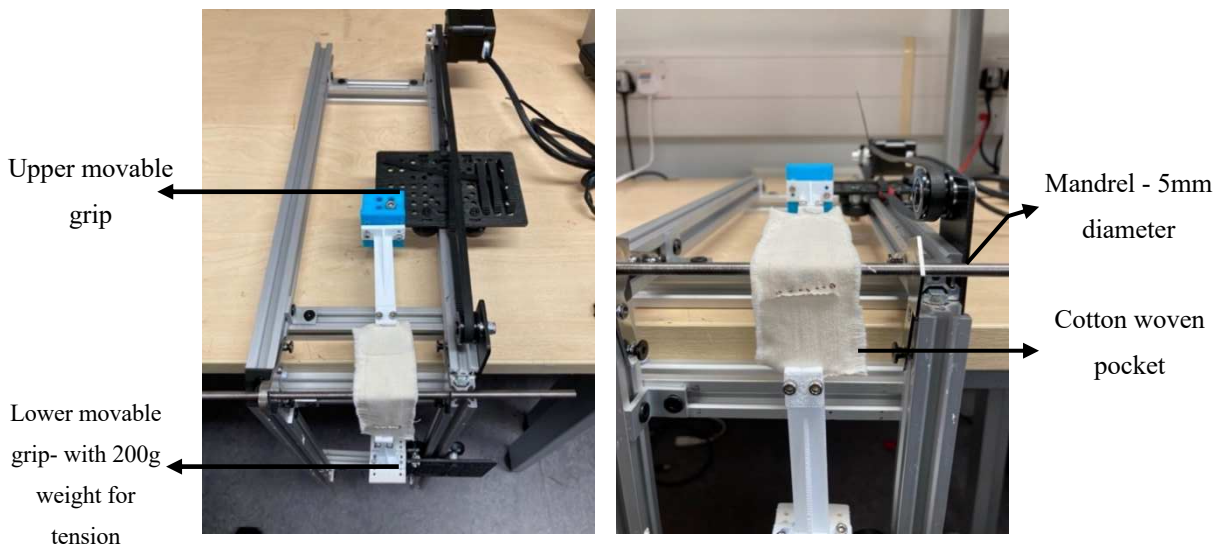


Figure 6.3 Bending rig for cyclic bending connected to microcontroller for setting number of cycles, position, and speed

### 6.2.2 Result

Any failure in the circuit could be found by measuring the resistance of the circuit. Any damage leading to failure of circuit led to an open circuit giving infinite resistance. This meant that



the circuit was disconnected which was due to the failure in connection of the SMD components or copper track in the circuit. The bending test for unencapsulated CO flexible circuit for different samples are shown in Table 6.3. In the Table 6.3,6.4,6.5 and 6.6, P = Resistance across contact pads for power, L= Resistance across the load resistor (820Ω), F(en) = Failure of encapsulant, F(ec) = Failure of electrical connections and F(b) = Failure of bonding.

**Table 6.3 Bending test for unencapsulated CO flexible circuits**

Sample	Resistance		Cycle 10		Cycle 100		Cycle 1000		Cycle 5000		Cycle 10000	
	P	L	P	L	P	L	P	L	P	L	P	L
1	141.3	818	141.3	818	141.3	818	141.3	818	143.5	819	144 (failed at 7000 <sup>th</sup> cycle) <b>F(ec)</b>	
2	144.2	818	144.2	818	144.2	818	144.2	820	150.8	825	152.2 (failed at 7500 <sup>th</sup> cycle) <b>F(ec)</b>	856
3	142.7	819	142.7	819	142.7	819	142.7	818	147.9	821	164.6 (failed at 11500 <sup>th</sup> cycle) <b>F(ec)</b>	831

The failure mode can be categorised into failure due to encapsulation layer F(en), failure due to electrical connectivity caused mostly by SMD detachment or cracks in the copper track F(ec), or failure due to bonding F(b) i.e., adhesive failure. The unencapsulated circuit filaments failed due to detachment of the gas sensor chip leading to very high resistance across the power pads of the circuit.

It was observed that the change in resistance over bending cycles is not linear. The resistance kept toggling between high and low resistance before reaching infinite resistance where complete failure of the circuit occurred. This might have been due to the strain caused in the copper track whilst bending gave rise to high resistance and then low resistance when the circuit was relaxed. This also depends on how the circuit was placed whilst measuring the resistance. When the circuit was bent, there were chances of re-joining the copper tracks or SMD to the soldering joints to give closed circuit. The unencapsulated filaments mostly failed due to soldering joints failure due to bending

stress. As shown in Fig 6.4, the change in resistance was not linear. Sample 3 had an increase of 16% before completely failing and had survived the highest number of bending cycles (up to 12,000).

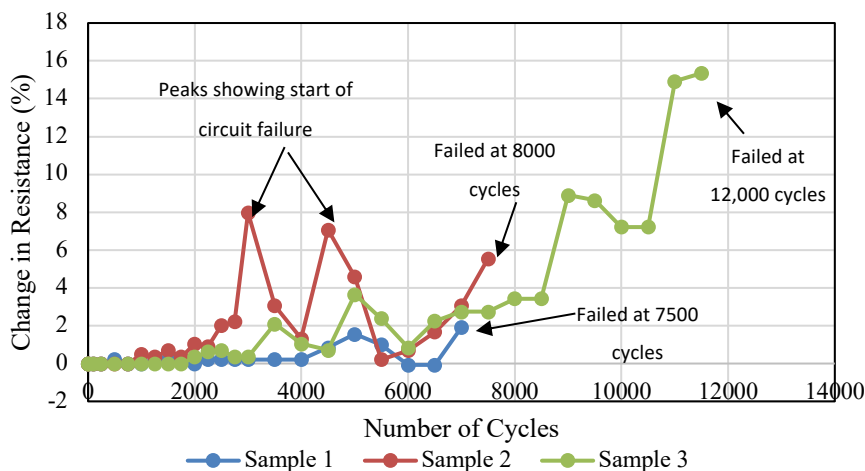


**Figure 6.4 Change in resistance due to bending and number of bending cycles survived by unencapsulated filament**

**Table 6.4 Bending test for PTFE Fibre glass fabric with acrylic adhesive**

Sample	Cycle 0		Cycle 100		Cycle 1000		Cycle 5000		Cycle 10000		Cycle 50000	
	P(mV)	L(Ω)	P(mV)	L(Ω)	P(mV)	L(Ω)	P(mV)	L(Ω)	P(mV)	L(Ω)	P(mV)	L(Ω)
1	144.2	821	143.7	821	143.5	821	145	822	182	850		
									(failed at 30,000 <sup>th</sup> cycle)			
									<b>f(ec)</b>			
2	141.7	820	141.7	820	143.2	821	146.6	839	155.4	834	197.6	882
											(failed at 50,000 <sup>th</sup> cycle)	
											<b>f(ec)</b>	
3	140.1	821	139.8	821	140.3	820	141.7	821	145.2	Soldering failure – No cracks in copper track		
									(failed at 25,000 <sup>th</sup> cycle)			
									<b>f(ec)</b>			

Table 6.4 shows the bending test for PTFE Fibre glass fabric with acrylic adhesive. And the bending test for Zitex G - 104 with NLP 11051 is shown in Table 6.5.

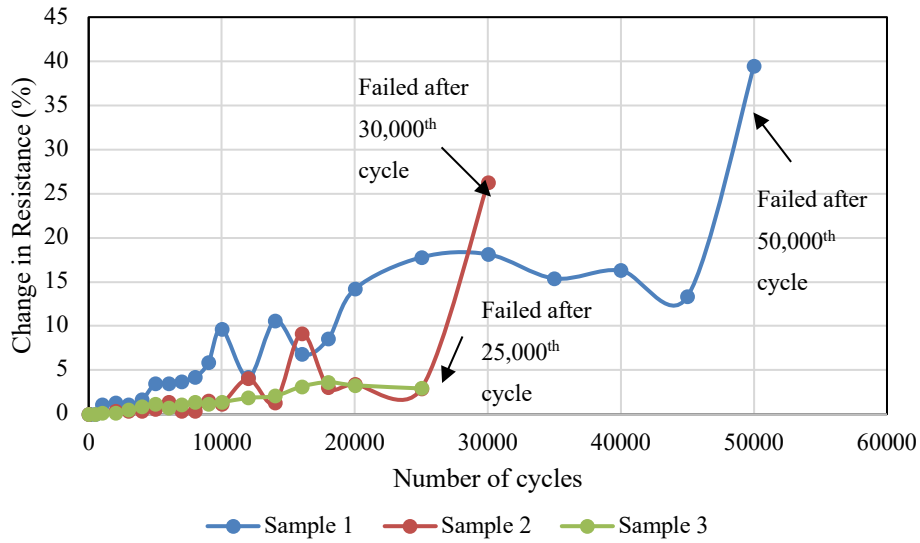


**Figure 6.5 Change in resistance due to bending and number of bending cycles survived by PTFE Fibre glass fabric encapsulated filament**

**Table 6.5 Bending test for Zitex G - 104 with NLP 11051**

Sample	Cycle 0		Cycle 100		Cycle 1000		Cycle 5000		Cycle 10000		Cycle 50000	
	P(mV)	L( $\Omega$ )	P(mV)	L( $\Omega$ )	P(mV)	L( $\Omega$ )	P(mV)	L( $\Omega$ )	P(mV)	L( $\Omega$ )	P(mV)	L( $\Omega$ )
1	144.5	819	144	819	147.9	819	156.9	819	208	832		
									(failed at 40,000 <sup>th</sup> cycle)			
									<b>F(b)</b>			
2	140.6	818	140.8	818	140.6	818	141.1	820	141.6	821	166.5	851
											(failed at 60,000 <sup>th</sup> cycle)	
											<b>F(ec)</b>	
3	143	817	142.7	817	142.5	817	144	820	150.5	835		
									(failed at 45,000 <sup>th</sup> cycle)			
									<b>F(ec)</b>			

The change in resistance due to bending and number of bending cycles survived by PTFE Fibre glass fabric encapsulated and Zitex G - 104 filament is shown in Fig 6.5 and Fig 6.6.

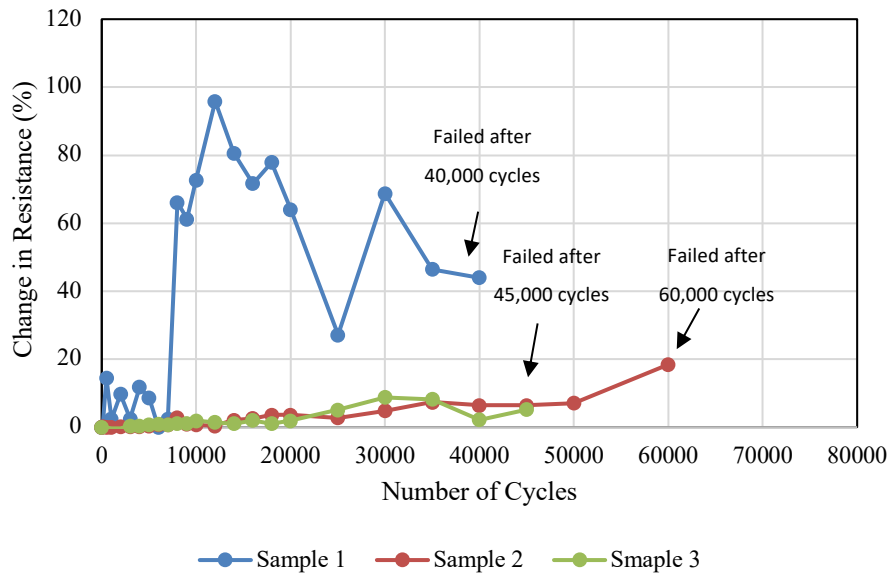
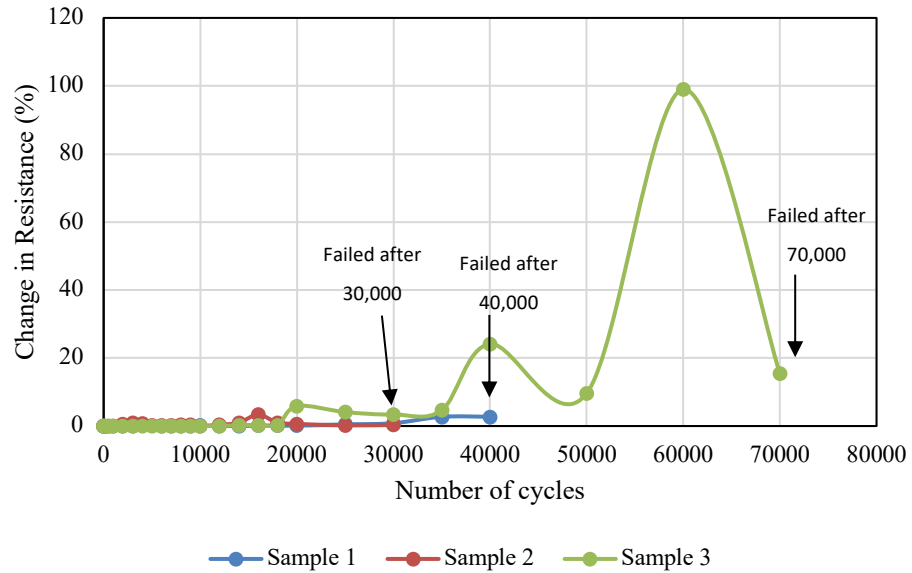


Figure 6.6 Change in resistance due to bending and number of bending cycles survived by Zitex G - 104 filament

Table 6.6 Bending test for Platilon U 4201 AU with heat bonding

Sample	Cycle 0		Cycle 100		Cycle 1000		Cycle 5000		Cycle 10000		Cycle 50000	
	P(mV)	L( $\Omega$ )	P(mV)	L( $\Omega$ )	P(mV)	L( $\Omega$ )	P(mV)	L( $\Omega$ )	P(mV)	L( $\Omega$ )	P(mV)	L( $\Omega$ )
1	143.5	819	143.5	819	143.2	818	143.2	818	147.4			
									(failed at 40,000 <sup>th</sup> cycle)			
									<b>F(ec)</b>			
2	140.8	818	140.8	819	140.8	819	141.1	819	141.3	823		
									(failed at 30,000 <sup>th</sup> cycle)			
									<b>F(ec)</b>			
3	141.3	822	141.3	822	141.3	823	141.3	830	141.3	889	163.1	
											(failed at 70,000 <sup>th</sup> cycle)	
											<b>F(ec)</b>	

The sample 1 filament had a bonding failure at the end of 40<sup>th</sup> cycle i.e., the Zitex G - 104 was unsealed due to adhesive failure. Sample 2 and 3 had failed due to development of cracks in the copper track. Sample 3 survived the highest number of bending cycles (up to 60,000 cycles) and shows about 20% increase in the resistance as shown in Fig 6.7. For different samples the bending test for Platilon U 4201 AU with heat bonding is shown in Table 6.6.



**Figure 6.7 Change in resistance due to bending and number of bending cycles survived by Platilon U 4201 AU filament**

The average number of cycles survived by unencapsulated filament, PTFE Fibre glass fabric, Zitex G - 104 and Platilon U 4201 AU encapsulated filament is shown in Fig 6.8.

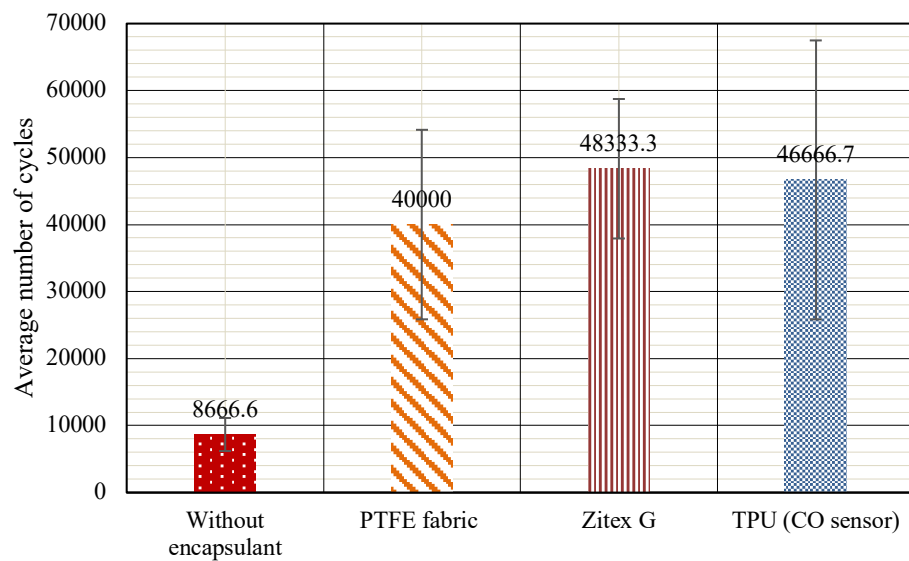


**Figure 6.8 Average number of cycles survived by all the unencapsulated filament, PTFE Fibre glass fabric, Zitex G - 104 and Platilon U 4201 AU encapsulated filaments**

### 6.2.3 Analysis

The failure points in the filament were observed using GXCAM-U3-18 microscope. The unencapsulated circuits failed typically due to breakage in the solder joints and detachment of the chip from the solder pads in the flexible PCB. One of the unencapsulated filament failed due to crack formed in the copper track as shown in Fig 6.9 (a). Both PTFE and Zitex G - 104 encapsulated filaments were viewed from the bottom side (Kapton side) to assess failure points. All the encapsulated filaments were observed to have failure points by appearance of cracks in the copper track near the resistors as shown in Fig 6.9 (b) and (c).

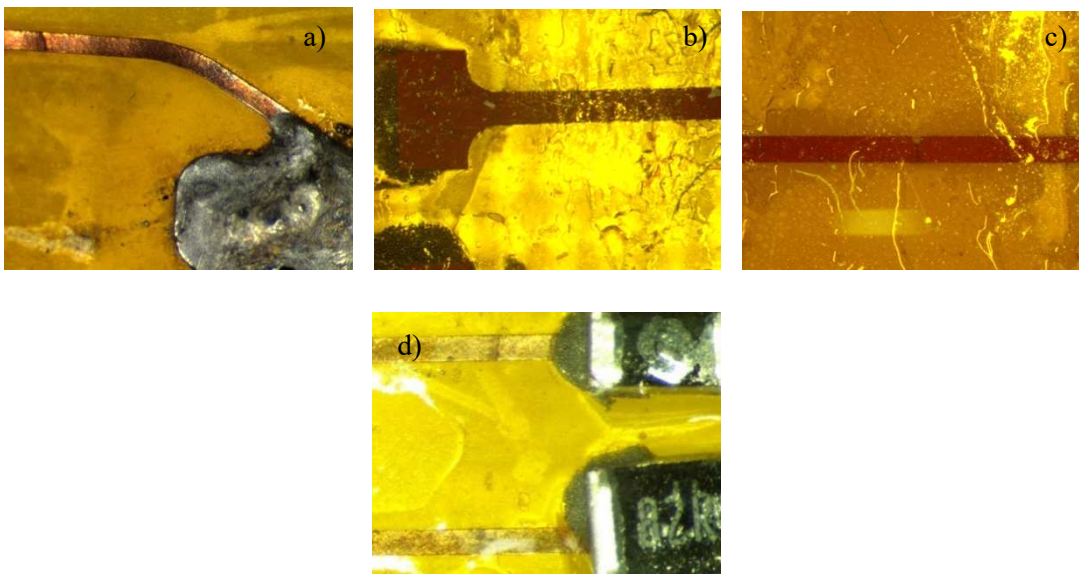
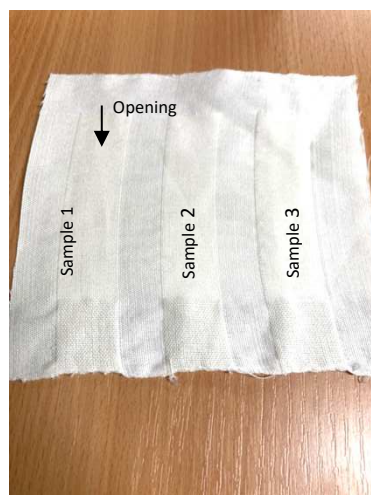


Figure 6.9 a) Without encapsulant b) with PTFE Fibre glass fabric c) With Zitex G - 104 d) with TPU

### 6.3 Washing test

For an e-textile, it is vital that the filament should be able to withstand washing cycles in washing machine with detergents. This section discusses the experimental setup and the mechanical robustness of unencapsulated and all encapsulated CO filaments under washing. The flexible filaments were inserted inside the cotton fabric with three pockets as shown in Fig 6.10. Each fabric has three pockets to have 3 flexible sensors and test them at the same time.



**Figure 6.10 Cotton woven fabric with pockets open at one end and other end sewed**

The resistance across the power and output were measured before and after each wash cycle. The open end was sewed with cotton thread for each wash cycle to secure the filament in the pockets and remove the thread after each wash cycle for measuring the resistances.

### 6.3.1 Experimental setup

The WME7247 Beko washing machine was used for washing all the unencapsulated and encapsulated for 58min at 40°C and 1000rpm spin for 15mins as shown in Fig 6.11. All the samples were washed with 2 kg of clothing mostly including lab coats and cotton t-shirts. This cycle represents the normal washing method as stated in the ISO 6330:2000 6A standard for domestic washing and drying procedures for textile testing. Three samples for all the types of packaging were inserted into the pockets on the woven textile and sewed at the ends. The fairy non biological laundry detergent was used for washing.



**Figure 6.11 Washing machine WME7247 Beko with 58min wash cycle at 40°C, 1000 rpm and 15min spin for all the filaments**

### 6.3.2 Results

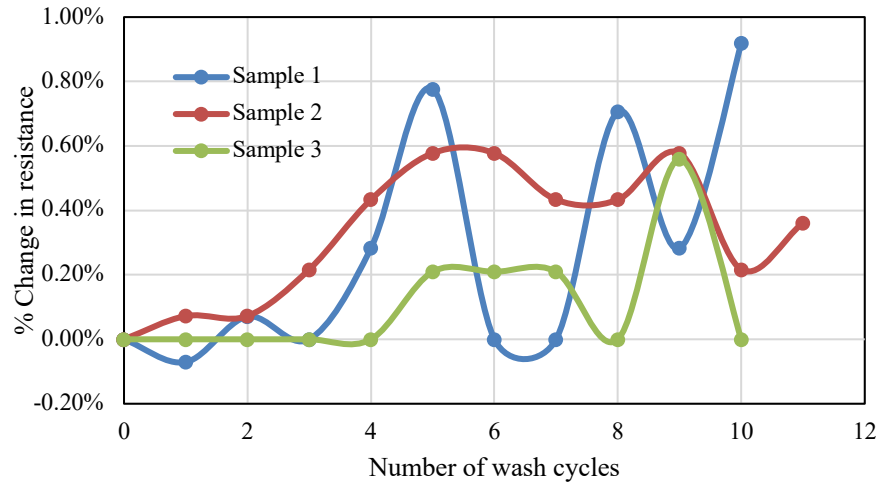
The electrical connections were measured by checking the voltage across the power pads and the output pads. The gas sensitivity was also measured for every 3 cycles with a concentration of 45ppm. In the Table 6.7,6.8,6.9 and 6.10, P = Resistance across contact pads for power, L= Resistance across the load resistor (820 $\Omega$ ), F(en) = Failure of encapsulant, F(ec) = Failure of electrical connections and F(b) = Failure of bonding.

**Table 6.7 Washing test for unencapsulated flexible circuit**

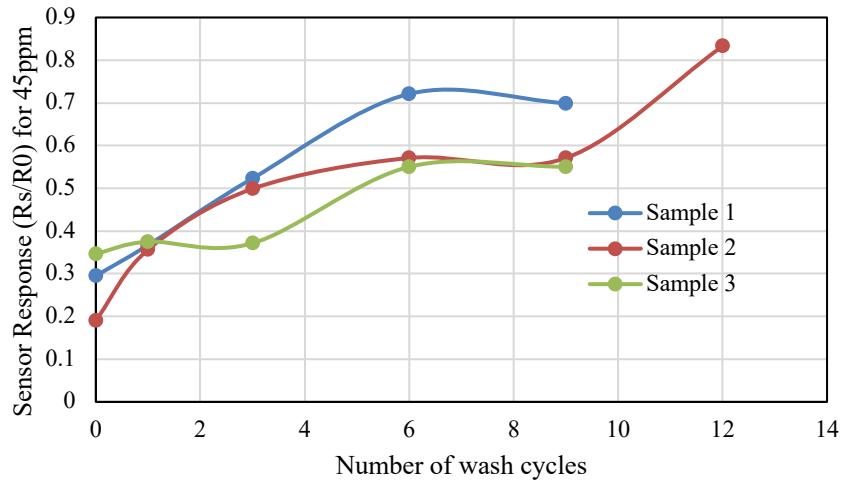
Sample	Cycle 0		Cycle 1		Cycle 5		Cycle 10		Cycle 15	
	P(mV)	L( $\Omega$ )	P(mV)	L( $\Omega$ )	P(mV)	L( $\Omega$ )	P(mV)	L( $\Omega$ )	P(mV)	L( $\Omega$ )
1	141.6	817	141.5	818	142.7	817	142.9	818		
							Failed after 10 <sup>th</sup> cycle <b>F(ec)</b>			
2	138.5	818	138.6	819	139.3	819	138.9	819	139	819
									Failed after 12 <sup>th</sup> cycle <b>F(ec)</b>	
3	143.2	819	143.2	819	143.5	816	143.2	819		
							Failed after 10 <sup>th</sup> cycle <b>F(ec)</b>			

Table 6.7 shows the washing test for unencapsulated flexible circuit. The Percentage change in resistance across the filament of Unencapsulated filaments with wash cycles are shown in Fig 6.12 and Fig 6.13 shows the Gas sensing response of Unencapsulated filaments with wash cycles.





**Figure 6.12 Percentage change in resistance across the filament of Unencapsulated filaments with wash cycles**



**Figure 6.13 Gas sensing response of Unencapsulated CO filaments after every 3<sup>rd</sup> wash cycles for 45ppm**

Washing test for PTFE Fibre glass fabric with acrylic adhesive is given in Table 6.8. Fig 6.14 shows the percentage change in resistance across the filament of PTFE glass fibre fabric encapsulated filaments with wash cycles, and Fig 6.15 shows the Gas sensing response of PTFE glass fibre fabric encapsulated filaments with wash cycles.

**Table 6.8 Washing test for PTFE Fibre glass fabric with acrylic adhesive**

Sample	Cycle 0		Cycle 1		Cycle 5		Cycle 10		Cycle 15		Cycle 20	
	P(mV)	L( $\Omega$ )	P(mV)	L( $\Omega$ )	P(mV)	L( $\Omega$ )	P(mV)	L( $\Omega$ )	P(mV)	L( $\Omega$ )	P(mV)	L( $\Omega$ )
1	143	821	143	819	143	820	143	820	143	821	142.6	9.8M $\Omega$ Failed after 15 <sup>th</sup> cycle F(ec)
2	138.8	819	138.6	819	140.1	819	138.9	818	138.8	40M $\Omega$ Failed after 12 <sup>th</sup> cycle F(ec)		
3	143.5	817	143.5	817	143.5	817						817 Failed after 8 <sup>th</sup> cycle F(ec)

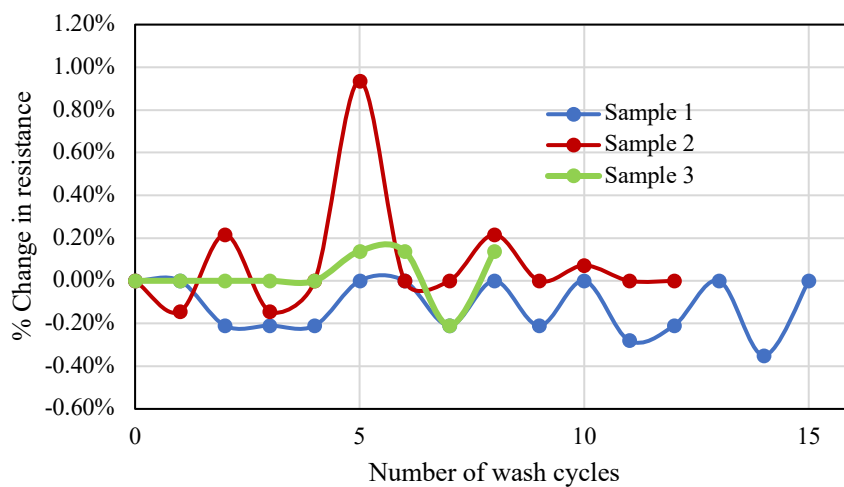


**Figure 6.14 Percentage change in resistance across the filament of PTFE glass fibre fabric encapsulated filaments with wash cycles**

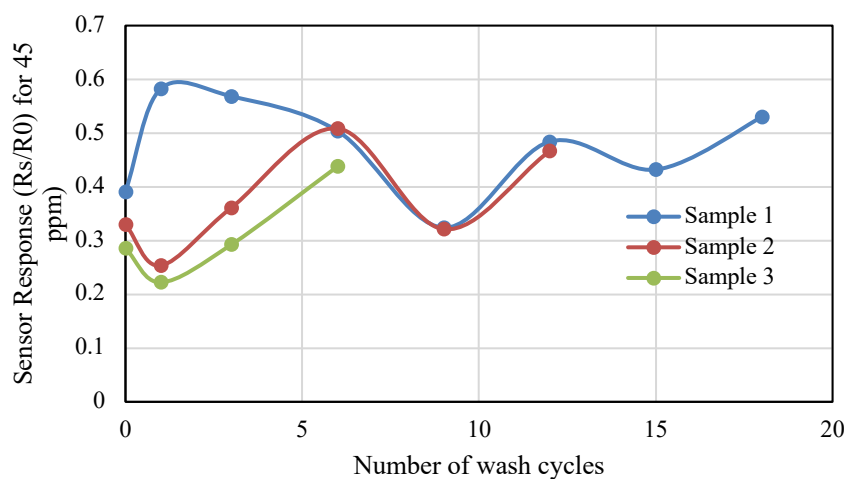


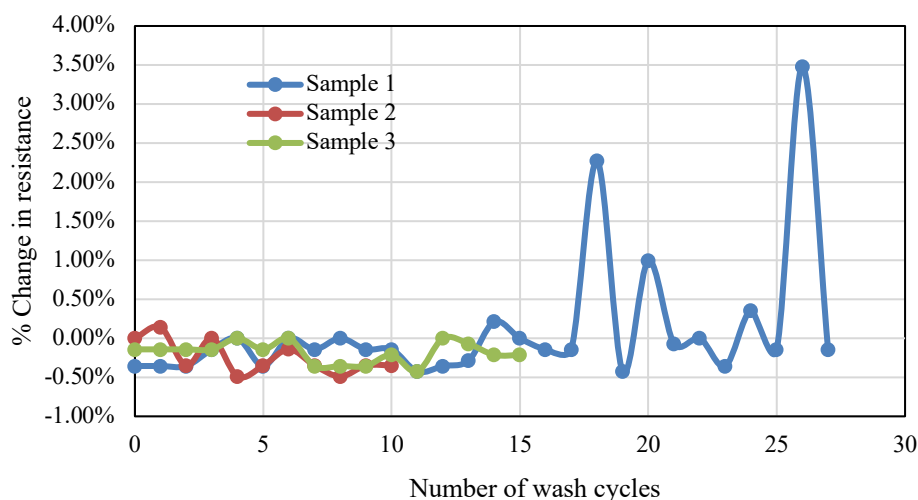
Figure 6.15 Gas sensing response of PTFE glass fibre fabric encapsulated CO filaments after every 3<sup>rd</sup> wash cycles for 45ppm

Table 6.9 Washing test for Zitex G - 104 with NLP 11051

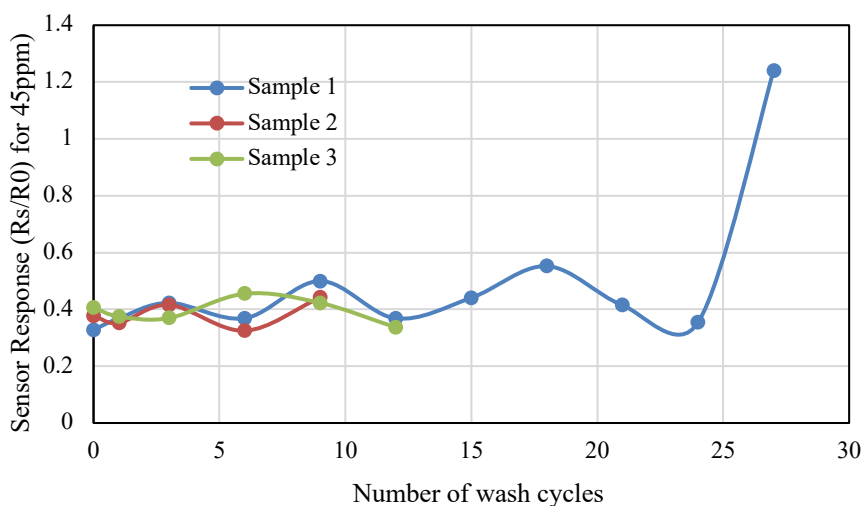
Sample	Cycle 0		Cycle 1		Cycle 5		Cycle 15		Cycle 25		Cycle 30	
	P(mV)	L( $\Omega$ )	P(mV)	L( $\Omega$ )	P(mV)	L( $\Omega$ )	P(mV)	L( $\Omega$ )	P(mV)	L( $\Omega$ )	P(mV)	L( $\Omega$ )
1	140.8	818	140.3	817	140.3	817	140.8	821	140.6	817	140.6	817 Failed after 27 <sup>th</sup> cycle) <b>F(ec)</b>
2	143.4	817	142.7	817	142.7	817	142.7	818 Failed after 11 <sup>th</sup> cycle <b>F(ec)</b>				
3	140.6	822	140.6	823	140.6	822	140.5	822	140.5	11.26 Failed after 15 <sup>th</sup> cycle <b>F(ec)</b>		

Table 6.9 gives the washing test results of different samples for Zitex G - 104 with NLP 11051. The Zitex G - 104 encapsulated filament 2 and 3 showed less impact on the gas sensitivity after

washing until completely failed at 11<sup>th</sup> and 15<sup>th</sup> cycle respectively shown in Fig 6.16 and 6.17. Sample 1 appears to have survived 27 cycles in terms of electrical connectivity in the circuit (**Sample 1 failed at 27<sup>th</sup> cycle with the CO sensor performance testing**). From the datasheet of MICS 5524, the sensor response for a CO concentration for a range of 0 to 1000ppm is 1 to 0.01. It is seen that the sample 1 gas sensing response exceeds beyond 1 as shown in Fig 6.17. This is a sign that the sensor has failed its functionality even though the electrical connectivity of the circuit has not failed.



**Figure 6.16 Percentage change in resistance across the filament of Zitex G - 104 fibre fabric encapsulated filaments with wash cycles**



**Figure 6.17 Gas sensing response of Zitex G - 104 encapsulated CO filaments after every 3<sup>rd</sup> wash cycles for 45ppm**

Platilon U 4201 AU 4201 was shown to act a gas barrier film to CO. Hence the electrical connection of the circuit was tested after each wash cycle shown in Fig 6.18. Sample 1 and 2 survived around 22 cycles however, sample 1 survived only 5 cycles which is less than the unencapsulated circuit as shown in Table 6.10.

Table 6.10 Washing test for Platilon U 4201 AU

Sample	Cycle 0		Cycle 1		Cycle 5		Cycle 10		Cycle 15		Cycle 20	
	P(mV)	L( $\Omega$ )	P(mV)	L( $\Omega$ )	P(mV)	L( $\Omega$ )	P(mV)	L( $\Omega$ )	P(mV)	L( $\Omega$ )	P(mV)	L( $\Omega$ )
1	141.7	819	141.7	818	141.7	818	142	817	143	817	142.4	817 failed after 22 <sup>nd</sup> cycle <b>F(ec)</b> <b>and</b> <b>F(en)</b>
2	139.8	817	140.1	817	140.1	814	139.8	816	140.1	816	138.9	814 Failed after 21 <sup>st</sup> cycle <b>F(ec)</b> <b>and</b> <b>F(en)</b>
3	141.6	820	141.6	820	145.8	12.62M $\Omega$ Failed after 5 <sup>th</sup> cycle <b>F(ec)</b> <b>and</b> <b>F(en)</b>						

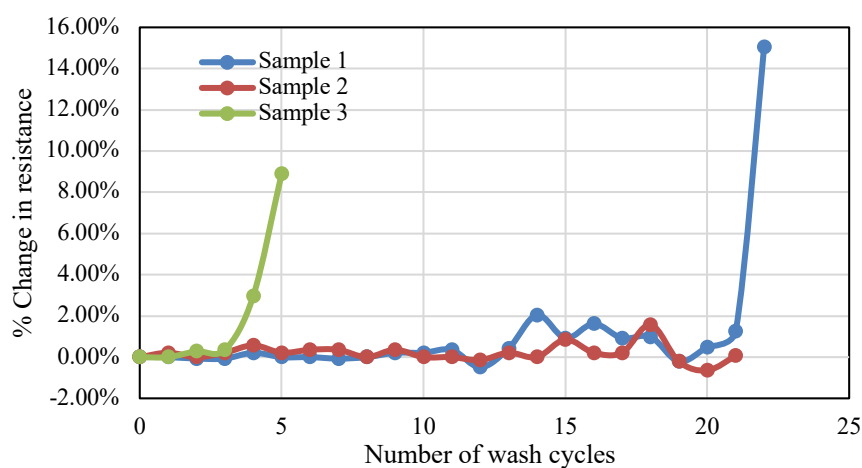
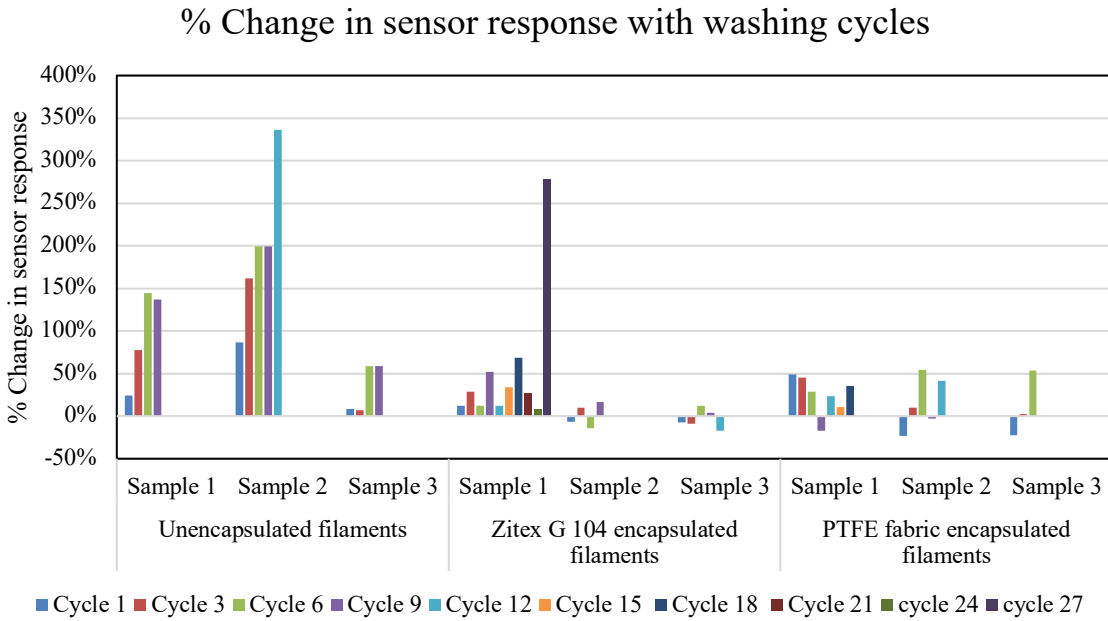
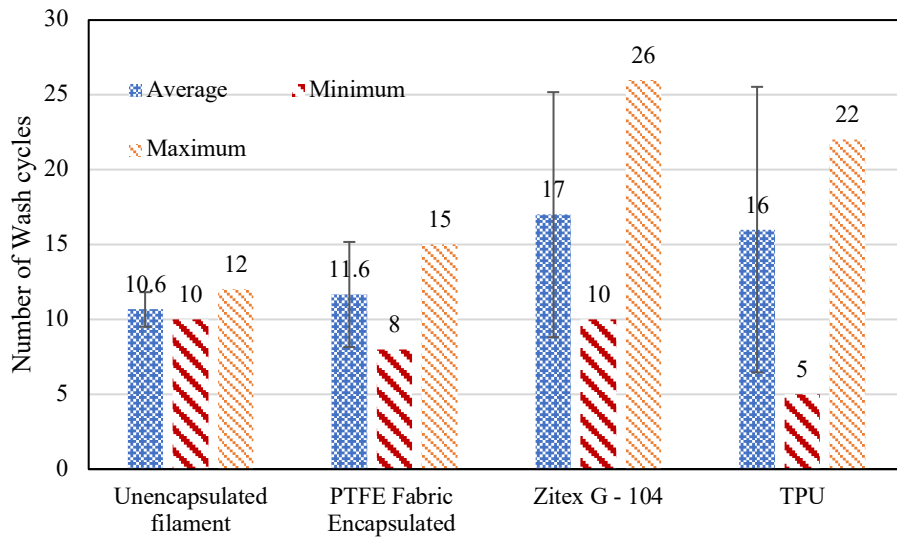


Figure 6.18 Percentage change in resistance across the filament of Platilon U 4201 AU encapsulated filaments with wash cycles



**Figure 6.19 Percentage change in gas sensor response for unencapsulated and Zitex G - 104 and PTFE glass fibre fabric encapsulated filaments**

The sample 1 of Zitex G – 104 packaged CO filament at 27<sup>th</sup> cycle has the highest change in response as seen in Fig 6.19. The average and maximum cycles survived by unencapsulated filament, and all the encapsulated filaments are given in Fig 6.20.



**Figure 6.20 Average and Maximum number of wash cycles survived by unencapsulated filaments, PTFE Fibre glass fabric, Zitex G - 104 and Platilon U 4201 AU encapsulated filament**

### 6.3.3 Analysis

All the images were captured using GXCAM U3-18 microscope for analysis. The unencapsulated filaments did not show any appearance of cracks in the copper tracks hence the failure of the filament could be directly linked to water pass through the holes of the gas sensor chip causing short circuiting after 10 cycles.

The unencapsulated CO filament failed due to the fracturing of the soldering joints causing detachment of the chip from the filament. The appearance of cracks was typically positioned near the resistors on the filament as shown in Fig 6.21 (a) and (b) for PTFE Fibre glass fabric and Zitex G – 104 encapsulated CO filaments respectively.

It was also noticed that in the TPU encapsulated CO filament, the film appearance was altered by repeated exposure to the detergent which changes the color of the film from transparent to almost white as shown in Fig 6.21 (c).

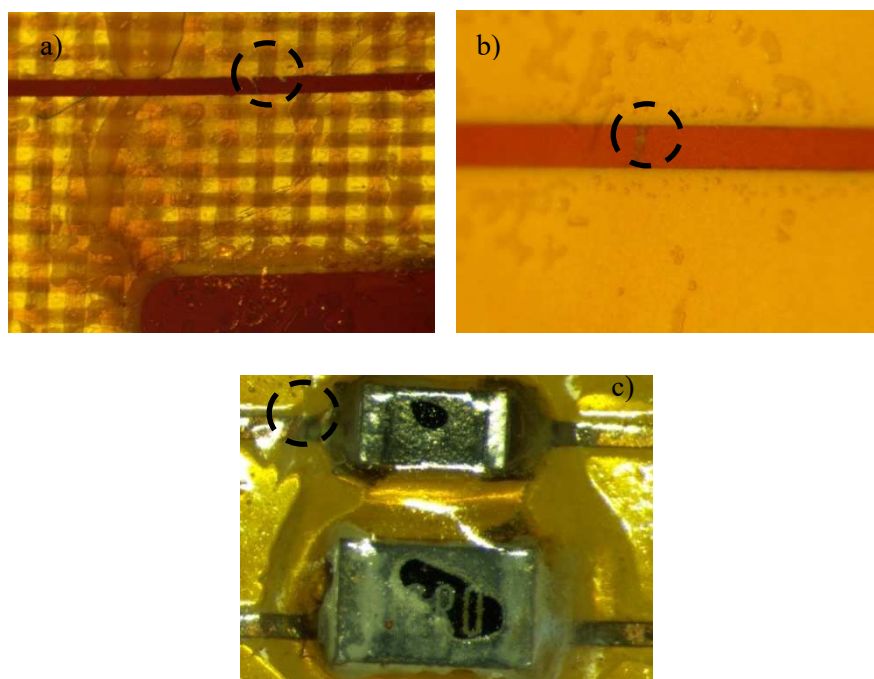


**Figure 6.21 Filament functionality failure due to cracks in the copper tracks after washing (a) PTFE (b) Zitex G - 104 and (c) Platilon U 4201 AU encapsulated filament**

The reason behind high durability for Zitex G – 104 is mainly due to its higher Young's Modulus and thickness compared to other encapsulants. These two factors make the flexible filament stiffer hence having minimal stresses on the copper track.

## Conclusion

- The bending results showed that the Zitex G - 104 encapsulated filaments have the highest robustness to bending cycles with a durability of 5.5 times better than the unencapsulated filament. The durability of TPU was 5.3 times and PTFE Fibre glass fabric was 4 times better than the unencapsulated filament.
- The washing results showed that the Zitex G - 104 encapsulated filaments have the highest durability of 1.8 times better than unencapsulated filaments with the maximum number of washes cycles the sample can withstand. The PTFE Fibre glass fabric with 1.25 and TPU with 1.8
- The failure of the filaments was typically due to cracks in the copper tracks causing open circuitry for bending cycles and washing cycles and change of appearance of TPU film over repeated washing cycles



## Chapter 7 Flexible Nitrogen Dioxide Gas Sensor

Nitrogen dioxide is one of the main pollutants in the UK, especially in Southampton. This pollutant is mainly caused by traffic and has negative effects at a very low concentration of 100 ppb. The NO<sub>2</sub> molecule is heavier than CO molecule. This may have an effect in NO<sub>2</sub> permeation through the encapsulants discussed in the previous chapters. Packaging flexible NO<sub>2</sub> sensor can be useful in detection of outdoor NO<sub>2</sub> detection in Southampton. In this chapter, a flexible nitrogen dioxide is fabricated. Photolithography technique was used to build flexible PCB on which the chip VOC Sens NO<sub>2</sub> sensor is mounted. This sensor has a detection range of 0 to 20ppm with a LOD of 10ppb. Lower detection limit (LOD) is important for NO<sub>2</sub> as the ambient levels of this gas molecule typically are very low in concentration (< 10ppb). The chamber was characterised using a reference NO<sub>2</sub> sensor Drager XSS. It can measure a range of 0 - 50ppm with lower detection limit (LDL) of 40ppb and a resolution of 20ppb.

### 7.1 Interface circuit for VOCsens NO<sub>2</sub> microsensor

The microsensor had a baseline resistance ranging from 0.8 to 10k $\Omega$  and to obtain better performance the output voltage is kept under 1V. For designing an interface circuit for receiving the output resistance, the sensor must be tuned to meet the specifications of output voltage being less than 1V. For this purpose, Multisim 14.1 is used to simulate Wheatstones bridge circuit to find the unknown resistance with the given sensor baseline resistance range.

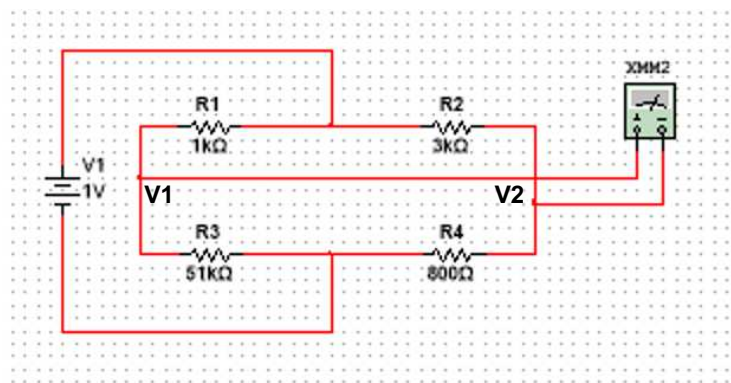


Figure 7.1 Wheatstone's bridge circuit design and simulation on Multisim

The output is the difference between the voltage dividers; the difference between the output of the first voltage divider consisting of R1 and R3 (V1) and output of the second voltage divider consisting of R2 and R<sub>sensor</sub> (V2). For making the design easy, the resistor values for the first voltage divider were selected to get an output voltage of 1V. The R2 value is changed to tune the circuit for the R<sub>sensor</sub> ranging from 0.8k $\Omega$  to 10k $\Omega$  to achieve the desired output and the values are shown in Table 7.1. From the Table 7.1, the R2 value was selected to be 3k $\Omega$  due to high change in

the output and not close to 1V. This may be useful in making the output voltage in presence of NO<sub>2</sub> exceed 1V.

**Table 7.1 Selection of resistors for achieving high sensitivity by output voltage less than 1V**

Output	Resistance (R2)						
	100	500	1k	2k	3k	4k	5k
Input	1V						
V1- V20.8kΩ to 10kΩ	91.88mV -9.3mV	365.3 to 28.3mV	536.3mV to 71.6mV	695.0mV To 147.4mV	770.2mV to 211.5mV	814.1mV to 266.4	842.8mV to 314.1

## 7.2 Flexible Circuit Design and fabrication

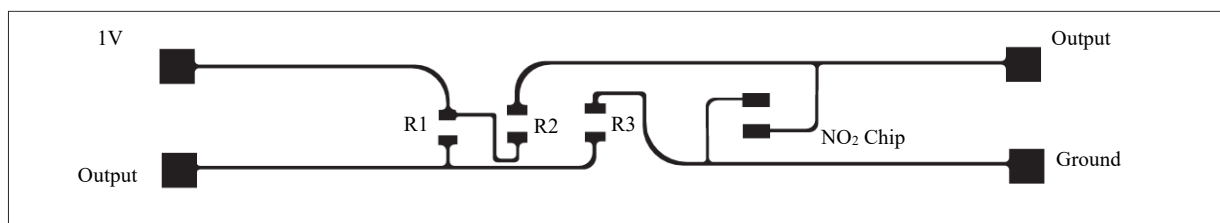


**Figure 7.2 Schematic design of NO<sub>2</sub> sensor flexible filament representing Wheatstone's bridge**

The NO<sub>2</sub> flexible PCB was fabricated using the standard lithographic technique. The flexible PCB was fabricated using the schematics shown in Fig 7.2. The pin details for measuring voltage/resistance across the sensitive material is shown in Fig 7.3 (a).

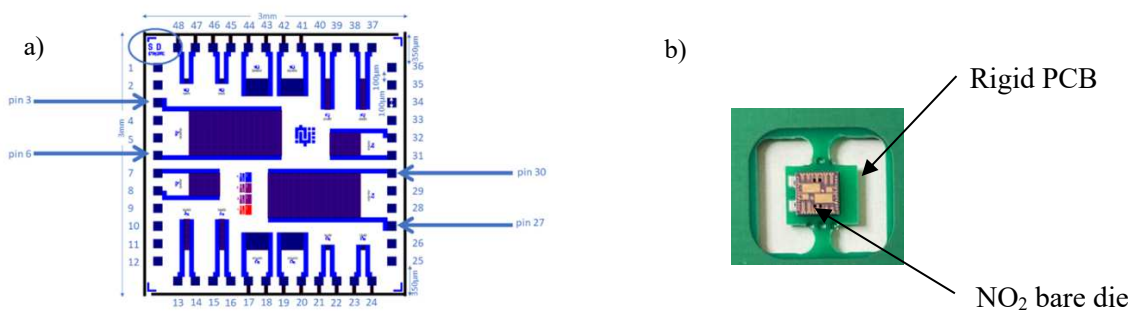


**Figure 7.3 (a) Pin details of VOC sens NO<sub>2</sub> bare die and (b) the bare die attached to the rigid PCB before wire bonding**

The NO<sub>2</sub> bare die was attached to a rigid PCB shown in Fig 7.3 (b) using adhesive making it a SMD to mount on to the flexible PCB. The rigid PCB was designed on Eagle and fabricated by Newbury electronics. The NO<sub>2</sub> bare die was placed on top of the rigid PCB using EP37 3FLF adhesive.

For the contact between the bare die and rigid PCB, wire bonding was required. The wire bonding was performed by Accelonix, UK with 25µm Au wire Wedge bonding, at 50°C to increase the bonding strength. The wire bonding involved gentle cleaning of the bare die surface with IPA which might have affected the sensitive layer (shown in Appendix C). However, the contact pads of the rigid PCBs as shown in Fig 7.4 (a) and (b) was wire bonded to the contact pads of the bare die as shown in Fig 7.4 (c).

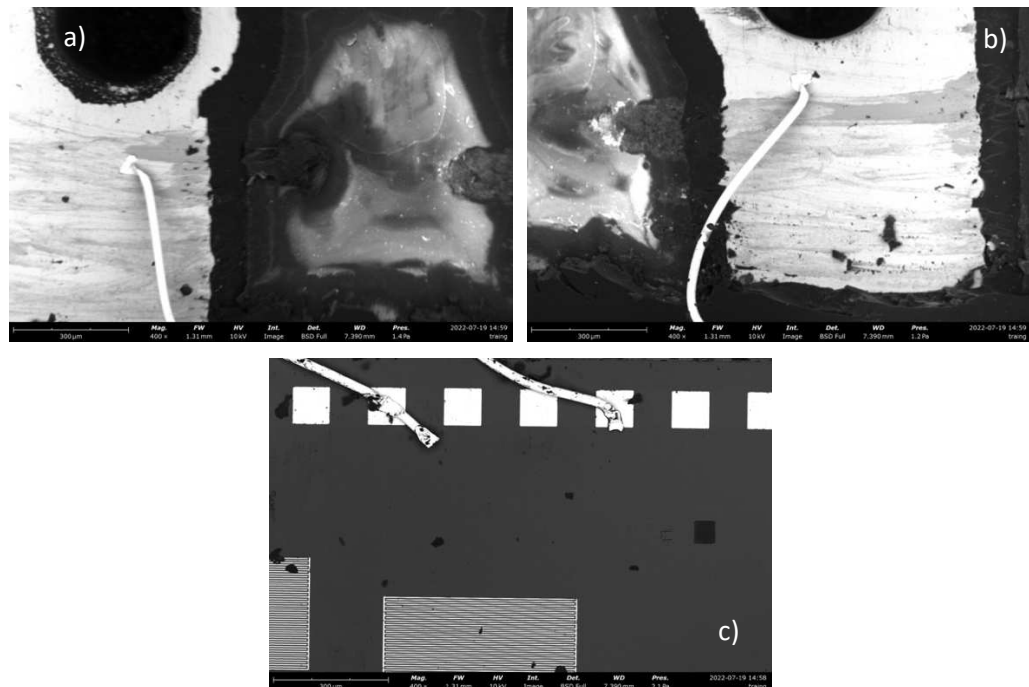


**Figure 7.4** Showing (a) and (b) wires bonded to rigid PCBs from (c) pin 3 and pin 6 of the NO<sub>2</sub> bare die

The SMD components along with the wire bonded bare to the rigid PCB was mounted to the flexible PCB using silver conductive epoxy as shown in Fig 7.5.

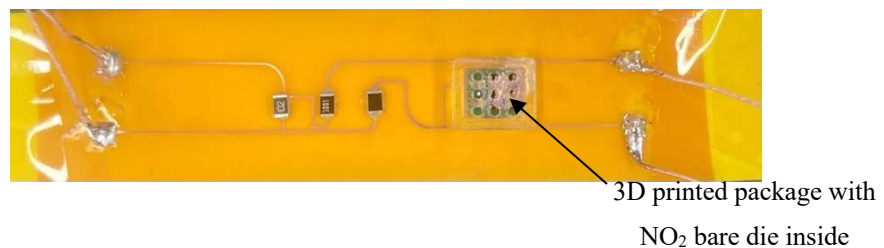


**Figure 7.5** Flexible NO<sub>2</sub> sensor design representing Wheatstone's bridge

To protect the wire bonding and the sensitive material on the bare die, a 3D printed packaging was made using VerClear plastic of size 7x6 mm with holes for the gas to pass through and attached using EP 37 – 3FLF adhesive. The wires for power and output were soldered.

### 7.3 Characterisation of NO<sub>2</sub> reference sensor

All the experiments involving NO<sub>2</sub> were taken place in the chamber used for carbon dioxide characterisation (described in Chapter 3). A NO<sub>2</sub> gas cylinder of 58L and 25ppm was used, and the valve was opened for different time duration; 1,2,3,4 and 5 seconds to achieve concentrations less than 1ppm.

**Table 7.2 Calculated and experimental gas concentration inside the chamber for NO<sub>2</sub>**

Gas valve open time (s)	Concentration of the gas in the cylinder (ppm)	Volume of gas coming from the cylinder (ml)	Volume of chamber with air and concentration (ml)*	Concentration of the gas in the chamber – theoretical (ppb)	Average Concentration of the gas in the chamber – practical (ppb)
1	25	8.3	3608.3	57.7	46.6
2		16.6	3616.6	115.2	80
3		25.0	3625	172.4	120
4		33.3	3633.3	229.35	140
5		41	3641	281	180

1 cm<sup>3</sup>= 1 ml, 1 l=1000 ml, 1 ppm-1000 ppb

The theoretical and practical concentrations inside the chamber for different time duration of the flow regulator valve is given in Table 7.2. The difference between the theoretical and experimental gas concentration increases with increase in gas dosage inside the chamber. However, the reference sensor gives 5 different concentrations for 5 different time duration of NO<sub>2</sub> dosage as shown in Fig 7.6. The response time typically appears to be 50s for all the 5 concentrations.

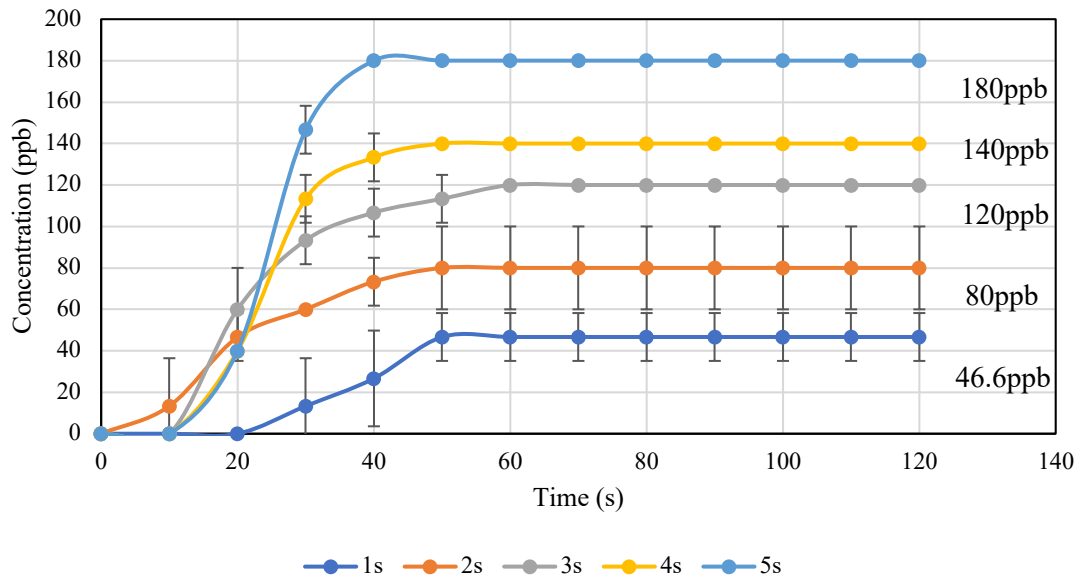


**Figure 7.6** Sensor response for Daeger NO<sub>2</sub> sensor for different duration of flow regulator valve opening

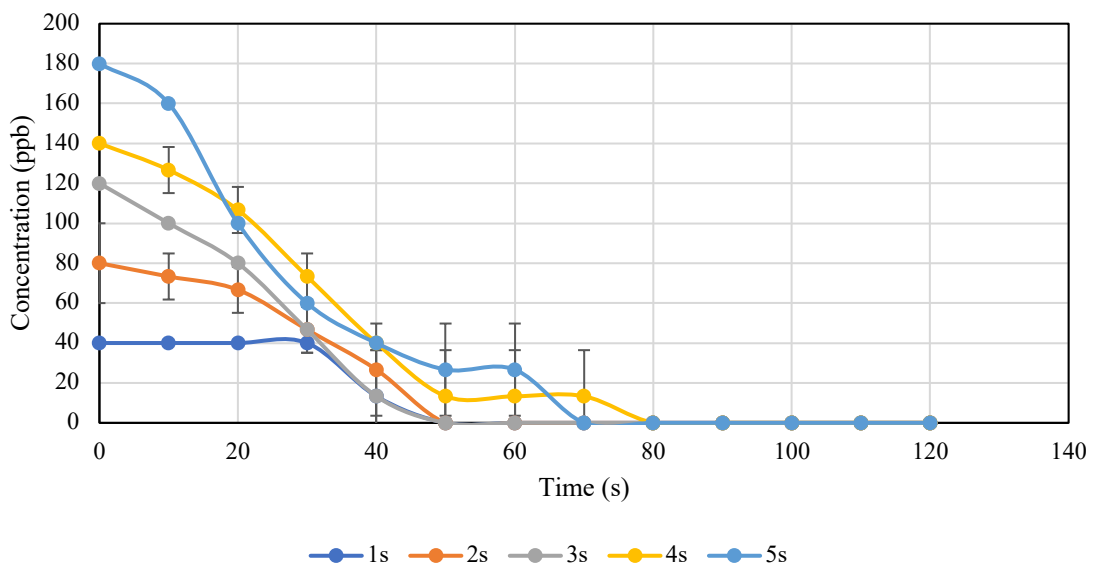


**Figure 7.7** Sensor recovery for Daeger NO<sub>2</sub> sensor when the top is lid open

The recovery time was observed by opening the top lid of the chamber to vent out the gas and observed that the reference sensor takes more than a min to read 0 as shown in Fig 7.7. The NO<sub>2</sub> reference sensor was also used to observe any leakage in the chamber by leaving the gas dosed in the chamber and noted down the time taken for the reference sensor to read 0.

For concentrations of NO<sub>2</sub> inside the chamber, a drop in concentration from the steady state was observed around 200 seconds as shown in Fig 7.8. The time taken to read 0ppm of NO<sub>2</sub> in the reference sensor was longer for higher concentrations and shorter for lower concentrations.

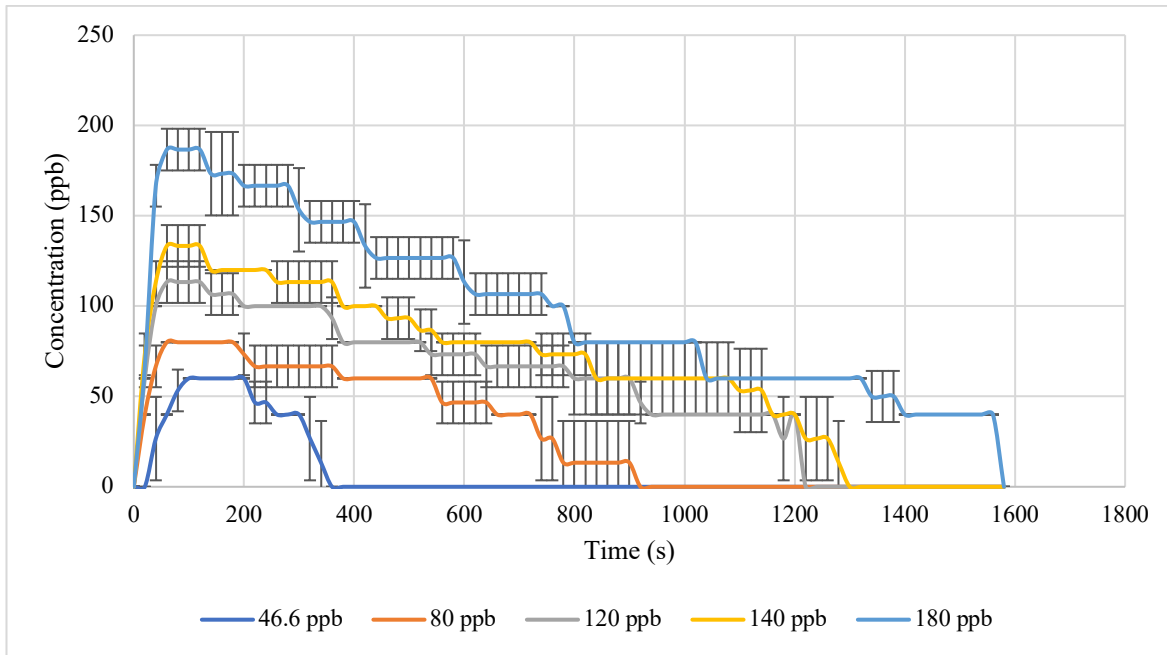


Figure 7.8 Leak test with NO<sub>2</sub> reference sensor – average 50s for 46.6ppb, 80ppb and 120ppb, 70s for 140ppb and 80s for 180ppb

### 7.4 Characterisation of flexible NO<sub>2</sub> Filament

The resistance of the flexible NO<sub>2</sub> filament was measured using multimeter to check the circuit connection across the output and power terminals of the flexible PCB. Most of the NO<sub>2</sub> bare die connected to the flexible PCB did not read resistance. The SEM was used to observe the faults in the bare die. Dust particles were found on the sensitive material area on top of the IDE as shown in Fig 7.9.

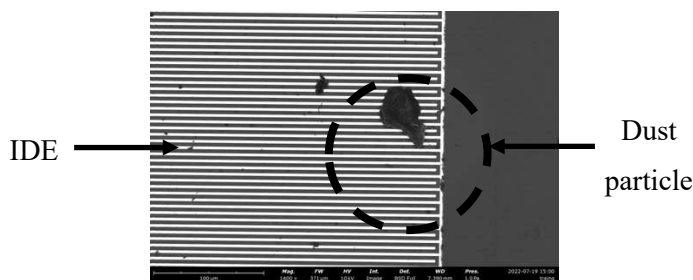
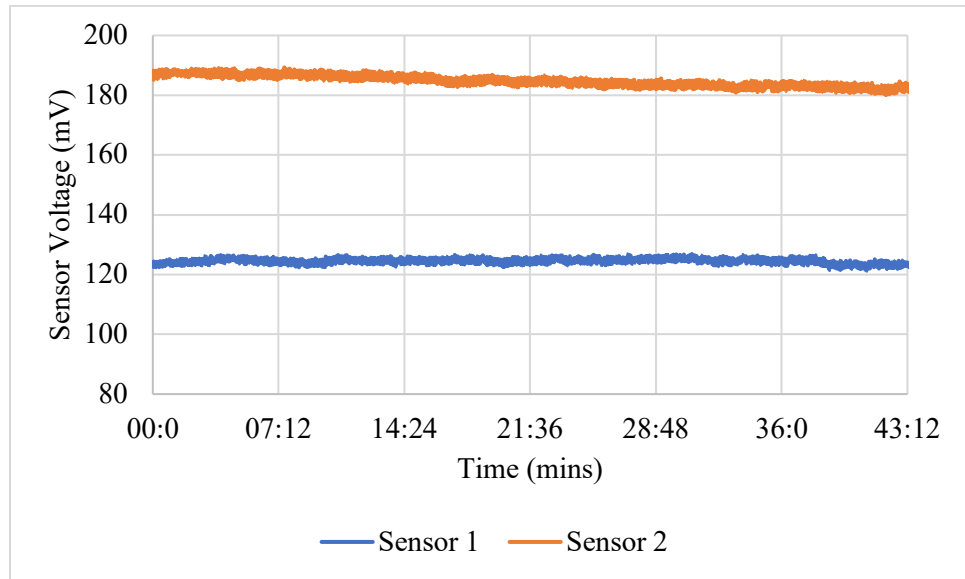


Figure 7.9 Showing SEM image of small remains of the sensitive material on the IDE of the NO<sub>2</sub> bare die

Two filaments with closed circuitry giving resistance across power and output ends were used for gas sensing experiments. To check the baseline stability of the bare die under room temperature, the sensors were switched on for one hour as shown in Fig 7.10. The voltage/resistance appears to be stable over an hour however sensor 2 appears to have noise.



**Figure 7.10 Baseline voltage measurement for the flexible NO<sub>2</sub> filament**

Two working flexible filaments were used for characterising their gas sensing performance. The NO<sub>2</sub> was dosed for 5 seconds and left for one hour to see the response of the gas sensors and the lid was opened to vent the gas out of the chamber and left for another 60 mins to see the recovery of the sensor. These time durations were chosen as the bare die has a response time of less than 20 mins and recovery time of less than or equal to 120 mins at 1ppm of NO<sub>2</sub>. This is challenging to observe variations in the output voltage of the flexible filaments as NO<sub>2</sub> levels drop and reaches 0ppb within 26 mins as shown in Fig 7.8 for 5 seconds of NO<sub>2</sub> dose. The gas experiment was however performed twice as shown in Fig 7.11 and 7.12.

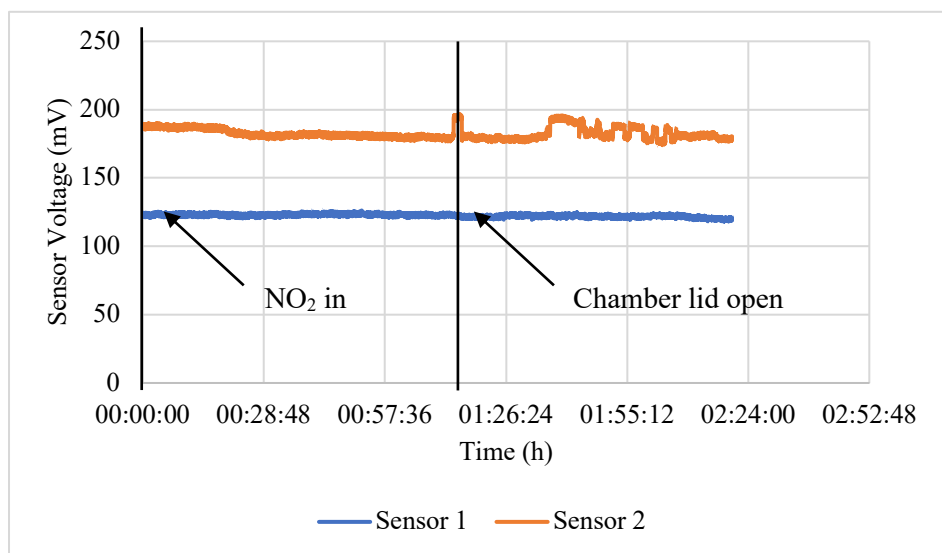


**Figure 7.11 Output Voltage measurement for the flexible NO<sub>2</sub> filament for 180ppb of NO<sub>2</sub> experiment**

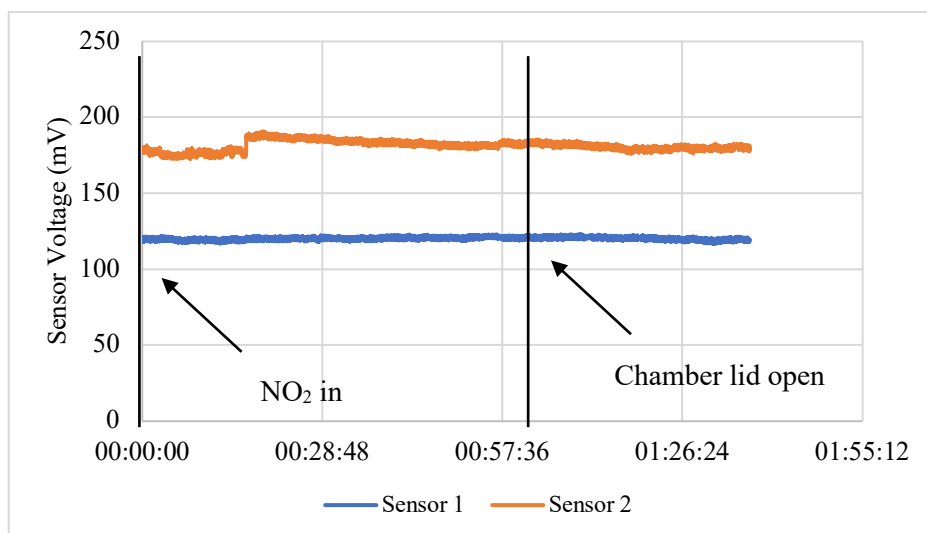


**Figure 7.12 Output Voltage measurement for the flexible NO<sub>2</sub> filament for 180ppb of NO<sub>2</sub> experiment**

2

### Conclusion

- The flexible NO<sub>2</sub> filament was fabricated and tested for electrical connectivity of the Wheatstone's bridge circuitry
- Plastic chamber absorbs NO<sub>2</sub> hence a steel chamber with minimal plastic objects should be placed inside the chamber for maintaining NO<sub>2</sub> level for a long time
- The VOC Sens bare die was still under development which was one of the main reasons for unreliable functionality. A packaged and commercially available NO<sub>2</sub> sensor will be more reliable in making flexible filaments in the future
- Off the shelf NO<sub>2</sub> sensor chip that has quicker response and recovery time typically less than 200 seconds can also be useful to observe gas sensing performance using the plastic chamber designed in this resea



## Chapter 8 Conclusion and Future Recommendations

This chapter summarizes investigation and its success in the research along with future recommendations that can help in expanding this research.

### 8.1 Conclusions

E-textiles are a viable way of making wearable air pollution monitoring systems. This can be achieved efficiently using off the shelf gas sensor chip integrated on flexible PCBs. These flexible filaments can be fitted in to bespoke pockets attached to textile or made into yarns depending on size of the off the shelf components. The problem with e-textile gas sensor filaments is to create an effective e-textile system that leverages the seamlessness, flexible, and washable qualities of conventional clothing textile. This should also retain the functionality of a gas sensor for air pollution detecting.

This research involves overcoming challenges faced in developing an e-textile gas sensor filament which are reliable and durable. To achieve a flexible gas sensing filament, the smallest commercially available MEMS CO sensor of dimensions 7 x 5 x 1.55 mm is used such that a thin flexible PCB filament of 10 mm width and 90 mm length could be fabricated using standard lithography technique and fitted into textile pocket. This gas sensor filament was able to four different concentration of carbon monoxide gas in ambient condition.

The primary goal of the research was to come up with a hydrophobic and gas permeable circuit filament that could endure the process of washing the electronic textile in a washing machine while still enabling the gas sensor to detect the concentration of the desired CO gas. This research addressed the investigation of three different thermoplastic hydrophobic films i.e., PTFE glass fibre fabric, Zitex G-104 and Platilon U 4201 AU for packaging CO sensor filament. The bonding material and process were experimented to achieve best bond strength for each thermoplastic film to CO filament. This includes acrylic adhesive for bonding PTFE fabric, silicone pressure sensitive adhesive for bonding Zitex G – 104 and heat stimulated bonding for Platilon U 4201 AU with aid of epoxy adhesive present in etched Kapton surface of flexile PCB. The use of vacuum forming to package flexible CO filaments with Platilon U 4201 AU for simple packaging without the requirement for conventional moulds used to mould PTFE fabric and Zitex G-104 was one of the novel concepts demonstrated in this research. The investigation has proven that PTFE fabric and Zitex G -104 are both hydrophobic and gas permeable and Platilon U 4201 AU is hydrophobic but gas barrier film for CO. The study also demonstrates that encapsulated filaments can be inserted into cotton textile pockets with minimal effects on gas sensitivity performance.

**Table 8.1 Comparison of packaged e-textile based gas sensor**

Gas sensor type	Target gas	Encapsulation material	Durability over bending cycle	Durability over washing cycle	Ref
Colorimetric	NH <sub>3</sub> and HCL	PDMS	-	10	[73]
MEMS MOX sensor	Carbon monoxide	Zitex G -104	Average of 48,333	Average of 17 (maximum of 26)	This research

Table 8.1 provides a comparison of the available electronic textile (e-textile) gas sensor packaging methods. The packaged e-textile gas sensor filament was tested for its mechanical robustness through bending and washing tests. Zitex G – 104 demonstrates the best performance in terms of mechanical robustness giving durability of 2.1 times more than unencapsulated filament with very slight impact on gas sensitivity when fitted into textile pocket.

This research extends to more real time application by focusing on nitrogen dioxide sensing which is one of the main air pollutants in Southampton. A small NO<sub>2</sub> bare die produced by VOCSens under research was used for fabricating flexible NO<sub>2</sub> sensor with intentions of increased sensitivity by using Wheatstone’s bridge circuit. The cleaning process during wire bonding caused damage to the graphene layer on the bare die leading to almost no sensitivity to NO<sub>2</sub>. To understand the behaviour of the bare die, the chamber design also needs to be altered in order to hold the gas concentration for a longer period of time.

## 8.2 Research Limitations

- The flexible CO sensor is highly influenced by variations in temperature and relative humidity. This will be a problem in applications that change the relative humidity and temperature in real time, especially when moving from indoor to outdoor environments. Events like such gives rise to false positives of CO detection when the actual CO concentration might be low. To resolve this, algorithm development is needed to compensate the effects of relative humidity and temperature variation of gas sensor response. CO sensor is also cross sensitive to other gases such as VOC involving events (acetone and hand sanitiser). Selection of gas sensor with less cross sensitive to other gases can be investigated and used for avoiding such cross sensitivity.

- With the process of packaging PTFE fabric and Zitex G-104, the alignment of layers in packaging should be considered to have uniform positioning of layers with high repeatability. This can help in achieving similar durability of circuits on an average. With the vacuum forming process, thickness of TPU material after vacuum forming might have reduced changing the bending stress caused on circuit. The thickness of TPU before and after vacuum forming should be analysed.
- For the bending test, flexible strips (both unencapsulated and encapsulated) with a higher number of bending cycles require more time for the resistance to return to a stable value. This difference could arise because of hysteresis effect over the sensing filament. With higher number of bending cycles, there would be mechanical stress accumulated in sensor unit. This in turn causes longer time to reach stable value in resistance measurement. To determine how long it takes for the circuit strips to reach a steady resistance, the measurement of resistance across the circuits should be timed.

### **8.3 Future Recommendations**

The durability of filaments can be improved with thickness used such that NA is fitted on to the copper tracks and this reduce stress level caused whilst bending and washing. This mostly entails reducing the encapsulant's thickness, packaging adhesives, and size of gas sensor chip utilized in the flexible circuit. The chamber design can also be changed by expanding to accommodate 5 samples for testing simultaneously. A Thermocouple can be placed inside chamber for measuring temperature together using Pico logger ADC 20/24 along with resistances measured from samples. Instead of Plastic, Steel chamber can be used to avoid NO<sub>2</sub> absorption and decay also to maintain the concentration for running test.

To create a functional e-textile air quality monitoring system, future research can concentrate on real-time monitoring of NO<sub>2</sub> levels integrated in e-textile in cities with high concentrations of motor ways. The flexible filament can also incorporate a wireless module, such as Bluetooth, to enable the phone to receive valuable data.



## Bibliography

- [1] WHO, “7 million premature deaths annually linked to air pollution,” 2014. <http://www.who.int/mediacentre/news/releases/2014/air-%0A0apollution/en/>
- [2] I. Sitaras and P. Siskos, *The role of primary and secondary air pollutants in atmospheric pollution: Athens urban area as a case study*, vol. 6. 2008.
- [3] S. M. Al-Salem and A R. Khan, “COMPARATIVE ASSESSMENT OF AMBIENT AIR QUALITY IN TWO URBAN AREAS ADJACENT TO PETROLEUM DOWNSTREAM/UPSTREAM FACILITIES IN KUWAIT,” *Brazilian J. Chem. Eng.*, vol. Vol. 25, N, 2008.
- [4] M. Rieu *et al.*, “Inkjet printed SnO<sub>2</sub> gas sensor on plastic substrate,” *Procedia Eng.*, vol. 120, pp. 75–78, 2015, doi: 10.1016/j.proeng.2015.08.569.
- [5] A. Therrien, “Low levels of air pollution linked to changes in the heart,” 2018.
- [6] X. Liu, S. Cheng, H. Liu, S. Hu, D. Zhang, and H. Ning, “A survey on gas sensing technology,” *Sensors (Switzerland)*, vol. 12, no. 7, pp. 9635–9665, 2012, doi: 10.3390/s120709635.
- [7] L. M. Castano and A. B. Flatau, “Smart fabric sensors and e-textile technologies: A review,” *Smart Mater. Struct.*, vol. 23, no. 5, 2014, doi: 10.1088/0964-1726/23/5/053001.
- [8] G. Mattana *et al.*, “Woven temperature and humidity sensors on flexible plastic substrates for e-textile applications,” *IEEE Sens. J.*, vol. 13, no. 10, pp. 3901–3909, 2013, doi: 10.1109/JSEN.2013.2257167.
- [9] X. Juan, L. Hairu, and M. Menghe, “High sensitivity knitted fabric strain sensors,” *Smart Mater. Struct.*, vol. 25, no. 10, p. 105008, 2016, [Online]. Available: <http://stacks.iop.org/0964-1726/25/i=10/a=105008>
- [10] R. Cao *et al.*, “Screen-Printed Washable Electronic Textiles as Self-Powered Touch/Gesture Tribo-Sensors for Intelligent Human-Machine Interaction,” *ACS Nano*, vol. 12, no. 6, pp. 5190–5196, 2018, doi: 10.1021/acsnano.8b02477.
- [11] C. T. Wang, K. Y. Huang, D. T. W. Lin, W. C. Liao, H. W. Lin, and Y. C. Hu, “A flexible proximity sensor fully fabricated by inkjet printing,” *Sensors*, vol. 10, no. 5, pp. 5054–5062, 2010, doi: 10.3390/s100505054.
- [12] A. Abellán-Llobregat *et al.*, “A stretchable and screen-printed electrochemical sensor for

- glucose determination in human perspiration,” *Biosens. Bioelectron.*, vol. 91, no. January, pp. 885–891, 2017, doi: 10.1016/j.bios.2017.01.058.
- [13] R. Matheson, “Wireless, wearable toxic gas sensor detector,” *Massachusetts Institute of Technology*, Jun. 2016. <http://news.mit.edu/2016/wireless-wearable-toxic-gas-detector-0630>
- [14] A. Komolafe *et al.*, “Integrating Flexible Filament Circuits for E-Textile Applications,” *Adv. Mater. Technol.*, vol. 4, no. 7, 2019, doi: 10.1002/admt.201900176.
- [15] M. Li, S. Beeby, R. Torah, J. Tudor, J. Liu, and A. Komolafe, “Novel electronic packaging method for functional electronic textiles,” *IEEE Trans. Components, Packag. Manuf. Technol.*, vol. 9, no. 2, pp. 1–1, 2019, doi: 10.1109/tcpmt.2019.2892404.
- [16] “Pellistor sensors – how they work.” <https://www.crowcon.com/blog/pellistor-sensors-how-they-work/>
- [17] Z. Yunusa, M. N. Hamidon, A. Kaiser, and Z. Awang, “Gas sensor: A Review,” *Sensors and transducers*, 2014.
- [18] SGX SensorTech, “Pellistor Application Note 5 Thermal Conductivity Sensors.” <https://www.sgxsensortech.com/content/uploads/2014/08/AN5---Thermal-Conductivity-Sensors.pdf>
- [19] D. D. Radu T., Fay C., Lau K. T., Waite R., “Wearable Sensing Application- Carbon Dioxide Monitoring for Emergency Personnel Using Wearable Sensors,” vol. 3, no. 10, pp. 1–4, 2009, [Online]. Available: <http://doras.dcu.ie/14986/>
- [20] P. Kuberský, T. Syrový, A. Hamáček, S. Nešpůrek, and L. Syrová, “Towards a fully printed electrochemical NO<sub>2</sub> sensor on a flexible substrate using ionic liquid based polymer electrolyte,” *Sensors Actuators, B Chem.*, vol. 209, no. 2, pp. 1084–1090, 2015, doi: 10.1016/j.snb.2014.12.116.
- [21] Figaro, “Operating Principle - MOS type.” <http://www.figarosensor.com/technicalinfo/principle/mos-type.html>
- [22] G. F. Fine, L. M. Cavanagh, A. Afonja, and R. Binions, “Metal oxide semi-conductor gas sensors in environmental monitoring,” *Sensors*, vol. 10, no. 6, pp. 5469–5502, 2010, doi: 10.3390/s100605469.
- [23] S. Benedict, P. K. Basu, and N. Bhat, “Low power gas sensor array on flexible acetate substrate,” *J. Micromechanics Microengineering*, vol. 27, no. 7, pp. 0–8, 2017, doi: 10.1088/1361-6439/aa71de.

- [24] Z. Zheng, J. Yao, B. Wang, and G. Yang, "A flexible, transparent and high-performance gas sensor based on layer-materials for wearable technology," *Nanotechnology*, vol. 28, no. 41, 2017, doi: 10.1088/1361-6528/aa8317.
- [25] Z. Q. Zheng, J. D. Yao, B. Wang, and G. W. Yang, "Light-controlling, flexible and transparent ethanol gas sensor based on ZnO nanoparticles for wearable devices," *Sci. Rep.*, vol. 5, no. June, pp. 1–8, 2015, doi: 10.1038/srep11070.
- [26] S. J. Park, C. S. Park, and H. Yoon, "Chemo-electrical gas sensors based on conducting polymer hybrids," *Polymers (Basel)*, vol. 9, no. 5, 2017, doi: 10.3390/polym9050155.
- [27] J. S. Lee *et al.*, "Fabrication of ultrafine metal-oxide-decorated carbon nanofibers for DMMP sensor application," *ACS Nano*, vol. 5, no. 10, pp. 7992–8001, 2011, doi: 10.1021/nn202471f.
- [28] B. Ding, J. Kim, Y. Miyazaki, and S. Shiratori, "Electrospun nanofibrous membranes coated quartz crystal microbalance as gas sensor for NH<sub>3</sub> detection," *Sensors Actuators, B Chem.*, vol. 101, no. 3, pp. 373–380, 2004, doi: 10.1016/j.snb.2004.04.008.
- [29] H. Bai and G. Shi, "Gas sensors based on conducting polymers," *Sensors*, vol. 7, no. 3, pp. 267–307, 2007, doi: 10.3390/s7030267.
- [30] T. Le, Y. Kim, and H. Yoon, "Electrical and Electrochemical Properties of Conducting Polymers," *Polymers (Basel)*, vol. 9, no. 4, p. 150, 2017, doi: 10.3390/polym9040150.
- [31] Z. Stempien *et al.*, "Ammonia gas sensors ink-jet printed on textile substrates," *Proc. IEEE Sensors*, pp. 2–4, 2017, doi: 10.1109/ICSENS.2016.7808457.
- [32] G. E. Collins and L. J. Buckley, "Conductive polymer-coated fabrics for chemical sensing," *Synth. Met.*, vol. 78, no. 2, pp. 93–101, 1996, doi: 10.1016/0379-6779(96)80108-1.
- [33] D. Kincal, A. Kumar, A. D. Child, and J. R. Reynolds, "Conductivity switching in polypyrrole-coated textile fabrics as gas sensors," *Synth. Met.*, vol. 92, no. 1, pp. 53–56, 1998, doi: 10.1016/S0379-6779(98)80022-2.
- [34] T. Kinkeldei, C. Zysset, N. Münzenrieder, and G. Tröster, "An electronic nose on flexible substrates integrated into a smart textile," *Sensors Actuators, B Chem.*, vol. 174, pp. 81–86, 2012, doi: 10.1016/j.snb.2012.08.023.
- [35] M. L. Homer *et al.*, "Polymer-based carbon monoxide sensors," *Proc. IEEE Sensors*, pp. 1504–1508, 2010, doi: 10.1109/ICSENS.2010.5690345.
- [36] W. Zhang, Y. Y. Tan, C. Wu, and S. R. P. Silva, "Self-assembly of single walled carbon nanotubes onto cotton to make conductive yarn," *Particuology*, vol. 10, no. 4, pp. 517–521,

- 2012, doi: 10.1016/j.partic.2011.06.011.
- [37] T. Kinkeldei, C. Zysset, K. Cherenack, and G. Tröster, “A flexible gas sensor for the integration into smart textiles,” *AIP Conf. Proc.*, vol. 1362, no. 2011, pp. 245–246, 2011, doi: 10.1063/1.3626376.
- [38] N. Indarit, Y. Kim, N. Petchsang, and R. Jaisutti, “Highly sensitive polyaniline-coated fiber gas sensors for real-time monitoring of ammonia gas,” *RSC Adv.*, vol. 9, no. 46, pp. 26773–26779, 2019, doi: 10.1039/c9ra04005f.
- [39] E. Llobet, “Gas sensors using carbon nanomaterials: A review,” *Sensors Actuators, B Chem.*, vol. 179, pp. 32–45, 2013, doi: 10.1016/j.snb.2012.11.014.
- [40] J. T. W. Yeow and Y. Wang, “A review of carbon nanotubes-based gas sensors,” *J. Sensors*, vol. 2009, 2009, doi: 10.1155/2009/493904.
- [41] S. Shahidi and B. Moazzenchi, “Carbon nanotube and its applications in textile industry – A review,” *J. Text. Inst.*, vol. 5000, pp. 1–14, 2018, doi: 10.1080/00405000.2018.1437114
- [42] T. Seesaard, P. Lorwongtragool, and T. Kerdcharoen, “Development of fabric-based chemical gas sensors for use as wearable electronic noses,” *Sensors (Switzerland)*, vol. 15, no. 1, pp. 1885–1902, 2015, doi: 10.3390/s150101885.
- [43] J. W. Han, B. Kim, J. Li, and M. Meyyappan, “A carbon nanotube based ammonia sensor on cotton textile,” *Appl. Phys. Lett.*, vol. 102, no. 19, pp. 2–6, 2013, doi: 10.1063/1.4805025.
- [44] D. Maity, K. Rajavel, and R. T. R. Kumar, “Polyvinyl alcohol wrapped multiwall carbon nanotube (MWCNTs) network on fabrics for wearable room temperature ethanol sensor,” *Sensors Actuators, B Chem.*, vol. 261, pp. 297–306, 2018, doi: 10.1016/j.snb.2018.01.152.
- [45] B. Lee, W. Kim, D. Kim, H. Kim, S. Hong, and W. Yu, “Fabrication of SnO<sub>2</sub> nanotube microyarn and its gas sensing behavior,” *Smart Mater. Struct.*, vol. 20, no. 10, p. 105019, 2011, doi: 10.1088/0964-1726/20/10/105019.
- [46] O. Monereo, “Gas sensors based on carbon nanofibres a low power consumption approach,” University of Barcelona, 2016.
- [47] Z. H. Lim, Z. X. Chia, M. Kevin, A. S. W. Wong, and G. W. Ho, “A facile approach towards ZnO nanorods conductive textile for room temperature multifunctional sensors,” *Sensors Actuators, B Chem.*, vol. 151, no. 1, pp. 121–126, 2010, doi: 10.1016/j.snb.2010.09.037.
- [48] H. Park, H. Ahn, D.-J. Kim, and H. Koo, “Nanostructured Gas Sensors Integrated into Fabric for Wearable Breath Monitoring System,” *Proc. IEEE Int. Symp. Wearable Comput.*, pp.



- 129–130, 2013, doi: 10.1145/2493988.2494337.
- [49] S. Zhang, J. Lim, J. Huh, and W. Lee, “Selective Growth of ZnO Nanorods and Its Gas Sensor Application,” *IEEE Sens. J.*, vol. 12, no. 11, pp. 3143–3148, 2012, doi: 10.1109/JSEN.2012.2211005.
- [50] T. Wang *et al.*, “A Review on Graphene-Based Gas/Vapor Sensors with Unique Properties and Potential Applications,” *Nano-Micro Lett.*, vol. 8, no. 2, pp. 95–119, 2016, doi: 10.1007/s40820-015-0073-1.
- [51] H. J. Yoon, D. H. Jun, J. H. Yang, Z. Zhou, S. S. Yang, and M. M. C. Cheng, “Carbon dioxide gas sensor using a graphene sheet,” *Sensors Actuators, B Chem.*, vol. 157, no. 1, pp. 310–313, 2011, doi: 10.1016/j.snb.2011.03.035.
- [52] F. Schedin *et al.*, “Detection of individual gas molecules adsorbed on graphene,” *Nat. Mater.*, vol. 6, no. 9, pp. 652–655, 2007, doi: 10.1038/nmat1967.
- [53] S. Gupta Chatterjee, S. Chatterjee, A. K. Ray, and A. K. Chakraborty, “Graphene-metal oxide nanohybrids for toxic gas sensor: A review,” *Sensors Actuators, B Chem.*, vol. 221, no. 2, pp. 1170–1181, 2015, doi: 10.1016/j.snb.2015.07.070.
- [54] Y. J. Yun, W. G. Hong, N. J. Choi, B. H. Kim, Y. Jun, and H. K. Lee, “Ultrasensitive and highly selective graphene-based single yarn for use in wearable gas sensor,” *Sci. Rep.*, vol. 5, no. June, 2015, doi: 10.1038/srep10904.
- [55] Y. J. Yun, D. Y. Kim, W. G. Hong, D. H. Ha, Y. Jun, and H.-K. Lee, “Highly stretchable, mechanically stable, and weavable reduced graphene oxide yarn with high NO<sub>2</sub> sensitivity for wearable gas sensors,” *RSC Adv.*, vol. 8, no. 14, pp. 7615–7621, 2018, doi: 10.1039/C7RA12760J.
- [56] H. J. Park *et al.*, “Highly flexible, mechanically stable, and sensitive NO<sub>2</sub> gas sensors based on reduced graphene oxide nanofibrous mesh fabric for flexible electronics,” *Sensors Actuators, B Chem.*, vol. 257, pp. 846–852, 2018, doi: 10.1016/j.snb.2017.11.032.
- [57] B. Cho *et al.*, “Graphene-based gas sensor: Metal decoration effect and application to a flexible device,” *J. Mater. Chem. C*, vol. 2, no. 27, pp. 5280–5285, 2014, doi: 10.1039/c4tc00510d.
- [58] M. K. Smith and K. A. Mirica, “Self-Organized Frameworks on Textiles (SOFT): Conductive Fabrics for Simultaneous Sensing, Capture, and Filtration of Gases,” *J. Am. Chem. Soc.*, vol. 139, no. 46, pp. 16759–16767, 2017, doi: 10.1021/jacs.7b08840.

- [59] J. Devkota, P. R. Ohodnicki, and D. W. Greve, "SAW sensors for chemical vapors and gases," *Sensors (Switzerland)*, vol. 17, no. 4, pp. 13–15, 2017, doi: 10.3390/s17040801.
- [60] C. Y. Cheng, S. S. Huang, C. M. Yang, K. T. Tang, and D. J. Yao, "Detection of third-hand smoke on clothing fibers with a surface acoustic wave gas sensor," *Biomicrofluidics*, vol. 10, no. 1, pp. 1–9, 2016, doi: 10.1063/1.4939941.
- [61] K. Hashimoto and T. Nakamoto, "Tiny Olfactory Display Using Surface Acoustic Wave Device and Micropumps for Wearable Applications," *IEEE Sens. J.*, vol. 16, no. 12, pp. 4974–4980, 2016, doi: 10.1109/JSEN.2016.2550486.
- [62] P. Kulha, J. Kroutil, A. Laposa, V. Procházka, and M. Husák, "Quartz Crystal Micro-Balance Gas Sensor with Ink-Jet Printed Nano-Diamond Sensitive Layer," *J. Electr. Eng.*, vol. 67, no. 1, pp. 61–64, 2016, doi: 10.1515/jee-2016-0009.
- [63] C. E. Limited, "FBAR Sensor," vol. 44, no. 0.
- [64] R. Hoffmann, M. Schreiter, and J. Heitmann, "The concept of thin film bulk acoustic resonators as selective CO<sub>2</sub> gas sensors," *J. Sensors Sens. Syst.*, vol. 6, no. 1, pp. 87–96, 2017, doi: 10.5194/jsss-6-87-2017.
- [65] M. Zhang, L. Du, Z. Fang, and Z. Zhao, "A sensitivity-enhanced film bulk acoustic resonator gas sensor with an oscillator circuit and its detection application," *Micromachines*, vol. 8, no. 1, 2017, doi: 10.3390/mi8010025.
- [66] A. Kooser, R. L. Gunter, W. D. Delinger, T. L. Porter, and M. P. Eastman, "Gas sensing using embedded piezoresistive microcantilever sensors," *Sensors Actuators, B Chem.*, vol. 99, no. 2–3, pp. 474–479, 2004, doi: 10.1016/j.snb.2003.12.057.
- [67] Y. Cui, "A Feasibility Study of Micromachined Ultrasonic Transducers Functionalized for Ethanol Detection," University of Waterloo, 2017.
- [68] P. Bahoumina *et al.*, "Chemical Gas Sensor Based on a Flexible Capacitive Microwave Transducer Associated with a Sensitive Carbon Composite Polymer Film," *Proceedings*, vol. 1, pp. 3–7, 2017, doi: 10.3390/proceedings1040439.
- [69] T. V. Dinh, I. Y. Choi, Y. S. Son, and J. C. Kim, "A review on non-dispersive infrared gas sensors:Improvement of sensor detection limit and interference correction," *Sensors Actuators, B Chem.*, 2016.
- [70] D. Gibson and C. MacGregor, "A novel solid state non-dispersive infrared CO<sub>2</sub> gas sensor compatible with wireless and portable deployment," *Sensors (Switzerland)*, vol. 13, no. 6, pp.

- 7079–7103, 2013, doi: 10.3390/s130607079.
- [71] Adeo, “Innovative sensor technology assists NASA with vital wearable CO<sub>2</sub> monitoring equipment,” vol. 44, no. 0, 2018.
- [72] C. Lin *et al.*, “High Performance Colorimetric Carbon Monoxide Sensor for Continuous Personal Exposure Monitoring,” *ACS Sensors*, vol. 3, no. 2, pp. 327–333, 2018, doi: 10.1021/acssensors.7b00722.
- [73] R. E. Oweyung, M. J. Panzer, and S. R. Sonkusale, “Colorimetric Gas Sensing Washable Threads for Smart Textiles,” *Sci. Rep.*, vol. 9, no. 1, pp. 1–8, 2019, doi: 10.1038/s41598-019-42054-8.
- [74] T. Chen, Y. Yang, H. Liu, C. Yang, M. Meyyappan, and C. Lai, “The Effect of Monolayer Graphene on the UV Assisted NO<sub>2</sub> Sensing and Recovery at Room Temperature,” *Proceedings*, vol. 1, no. 5, p. 461, 2017, doi: 10.3390/proceedings1040461.
- [75] T. Sgp, “Multi-Pixel Gas Sensor SGP Overview of Sensirion ’ s Gas Sensors Test Our Environmental Sensors with Sensirion ’ s Evaluation Kits Long-Term Stability of Metal-Oxide Gas Sensors”.
- [76] K. H. Hong, K. W. Oh, and T. J. Kang, “Polyaniline – Nylon 6 Composite Fabric for Ammonia Gas Sensor,” *J. Appl. Polym. Sci.*, vol. 92, pp. 37–42, 2003, doi: Doi 10.1002/App.13633.
- [77] J. Burgués, J. M. Jiménez-Soto, and S. Marco, “Estimation of the limit of detection in semiconductor gas sensors through linearized calibration models,” *Anal. Chim. Acta*, vol. 1013, pp. 13–25, 2018, doi: 10.1016/j.aca.2018.01.062.
- [78] Q. Nie *et al.*, “Facile fabrication of flexible SiO<sub>2</sub>/PANI nanofibers for ammonia gas sensing at room temperature,” *Colloids Surfaces A Physicochem. Eng. Asp.*, vol. 537, no. October 2017, pp. 532–539, 2018, doi: 10.1016/j.colsurfa.2017.10.065.
- [79] S. Wu, P. Liu, Y. Zhang, H. Zhang, and X. Qin, “Flexible and conductive nanofiber-structured single yarn sensor for smart wearable devices,” *Sensors Actuators, B Chem.*, vol. 252, pp. 697–705, 2017, doi: 10.1016/j.snb.2017.06.062.
- [80] H. Di Zhang *et al.*, “Electrospun PEDOT:PSS/PVP Nanofibers for CO Gas Sensing with Quartz Crystal Microbalance Technique,” *Int. J. Polym. Sci.*, vol. 2016, 2016, doi: 10.1155/2016/3021353.
- [81] O. S. Kwon *et al.*, “Carboxylic acid-functionalized conducting-polymer nanotubes as highly

- sensitive nerve-agent chemiresistors,” *Sci. Rep.*, vol. 6, no. May, pp. 1–7, 2016, doi: 10.1038/srep33724.
- [82] Won Taek JungJun Woo JeonHyun-Seok JangDo Yeob KimHyung-Kun LeeByung Hoon, “Commercial silk-based electronic textiles for NO<sub>2</sub> sensing”.
- [83] W. Li *et al.*, “Reduced Graphene Oxide/Mesoporous ZnO NSs Hybrid Fibers for Flexible, Stretchable, Twisted, and Wearable NO<sub>2</sub> E-Textile Gas Sensor,” *ACS Sensors*, vol. 4, no. 10, pp. 2809–2818, 2019, doi: 10.1021/acssensors.9b01509.
- [84] Y. K. Park *et al.*, “Fabrication of colorimetric textile sensor based on rhodamine dye for acidic gas detection,” *Polymers (Basel)*., vol. 12, no. 2, 2020, doi: 10.3390/polym12020431.
- [85] O. Ojuroye, “Improving the integration of e-textile microsystems encapsulation by modifying PDMS formulation .,” *2018 Symp. Des. Test, Integr. Packag. MEMS MOEMS*, pp. 1–6, 2018, doi: 10.1109/DTIP.2018.8394200.
- [86] M.L.White, “Encapsulation of integrated circuits,” *Proc. IEEE Sensors*, vol. 57, 1969.
- [87] X. Li, H. Hu, T. Hua, B. Xu, and S. Jiang, “Wearable strain sensing textile based on one-dimensional stretchable and weavable yarn sensors,” *Nano Res.*, vol. 11, no. 11, pp. 5799–5811, 2018, doi: 10.1007/s12274-018-2043-7.
- [88] Y. Yang *et al.*, “Waterproof, Ultrahigh Areal-Capacitance, Wearable Supercapacitor Fabrics,” *Adv. Mater.*, vol. 29, no. 19, 2017, doi: 10.1002/adma.201606679.
- [89] X. Tao, V. Koncar, T. H. Huang, C. L. Shen, Y. C. Ko, and G. T. Jou, “How to make reliable, washable, and wearable textronic devices,” *Sensors (Switzerland)*, vol. 17, no. 4, 2017, doi: 10.3390/s17040673.
- [90] S. B. Dunkerton, “Glob top materials to chip on board components,” *The 1998 International Conference on Advances in Welding Technology*, 1998.
- [91] S. J.Adamson and C. Q.Ness, “Dam and Fill Encapsulation for Microelectronic Packages,” 1999, [Online]. Available: [www.asymtek.com](http://www.asymtek.com)
- [92] “The essential guide to conformal coating.” <https://www.techspray.com/the-essential-guide-to-conformal-coating>
- [93] T. Linz *et al.*, “Embroidered Interconnections and Encapsulation for Electronics in Textiles for Wearable Electronics Applications,” vol. 60, pp. 85–94, 2008, doi: 10.4028/www.scientific.net/AST.60.85.

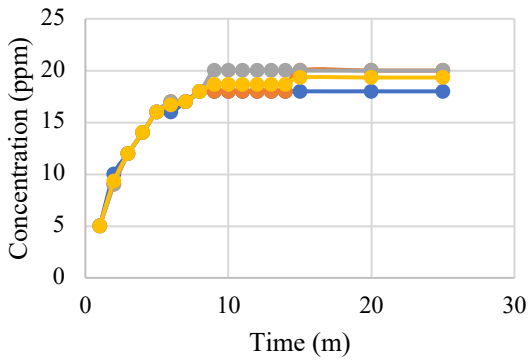
- [94] Figaro, "FIGARO GAS SENSORS 1-Series 8-Series," pp. 1–8, 2003, [Online]. Available: [www.figarosensor.com](http://www.figarosensor.com)
- [95] T. Tille, "Automotive suitability of air quality gas sensors," *Sensors Actuators, B Chem.*, vol. 170, no. 2, pp. 40–44, 2012, doi: 10.1016/j.snb.2010.11.060.
- [96] "MICS 4514 Datasheet (0278 Revision 15)." [https://www.sgxsensortech.com/content/%0Duploads/2014/08/0278\\_Datasheet-MiCS-4514.pdf](https://www.sgxsensortech.com/content/%0Duploads/2014/08/0278_Datasheet-MiCS-4514.pdf)
- [97] "SGX Metal Oxide Gas Sensors (How to Use Them and How They Perform)." <https://www.sgxsensortech.com/content/uploads/2014/08/AN-0172-SGX-Metal-Oxide-Gas-Sensors-V1.pdf>
- [98] G. Akovali, "Thermoplastic Polymers Used in Textile Coatings," *Adv. Polym. Coat. Text. Smithers Rapra Technol.*, pp. 1–24, 2012.
- [99] C. Woodford, "GORE-TEX," 2018. <https://www.explainthatstuff.com/goretex.html>
- [100] "Instructions for use of double-sided pressure-sensitive adhesive tape."
- [101] C. H. Kung, P. K. Sow, B. Zahiri, and W. Mérida, "Assessment and Interpretation of Surface Wettability Based on Sessile Droplet Contact Angle Measurement: Challenges and Opportunities," *Adv. Mater. Interfaces*, vol. 6, no. 18, pp. 1–27, 2019, doi: 10.1002/admi.201900839.
- [102] "T- type Peeling Strength Test." <https://www.dexterials.jp/en/products/eMethod/>
- [103] M. Eizadjou, H. Danesh Manesh, and K. Janghorban, "Investigation of roll bonding between aluminum alloy strips," *Mater. Des.*, vol. 29, no. 4, pp. 909–913, 2008, doi: 10.1016/j.matdes.2007.03.020.
- [104] "5 Common Reasons for Adhesive Failure." <https://www.jbc-tech.com/blog/posts/5-common-reasons-for-adhesive-failure/>
- [105] D. Zhang *et al.*, "A novel wafer level hermetic packaging for MEMS devices using micro glass cavities fabricated by a hot forming process," *Proc. - 2010 11th Int. Conf. Electron. Packag. Technol. High Density Packag. ICEPT-HDP 2010*, pp. 921–924, 2010, doi: 10.1109/ICEPT.2010.5582657.
- [106] Formech International Limited, "Manual 450DT Vacuum forming." [http://formech.com/wp-content/uploads/Manual-450DT\\_UK\\_V1.0\\_241017.pdf](http://formech.com/wp-content/uploads/Manual-450DT_UK_V1.0_241017.pdf)

# APPENDIX A

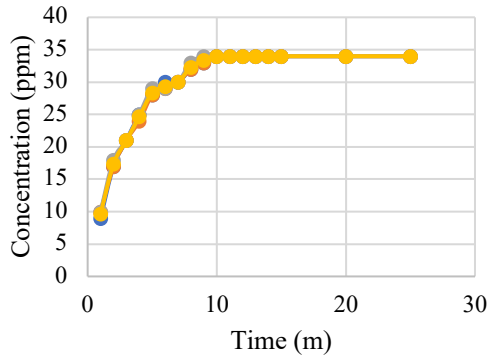
## Characterization of reference sensor - response time

Reference sensor response time repeated 3 times for the gas in time duration for 10s, 20, 30s and 40s

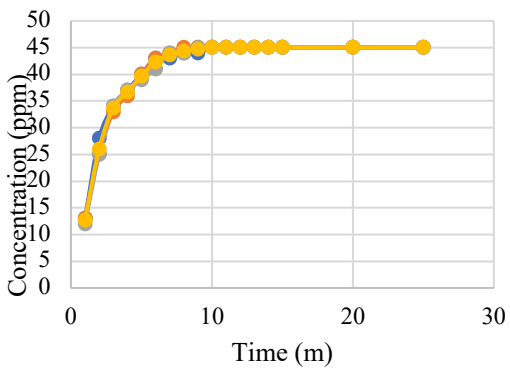
Valve open for 10s - experimented repeated 3 times



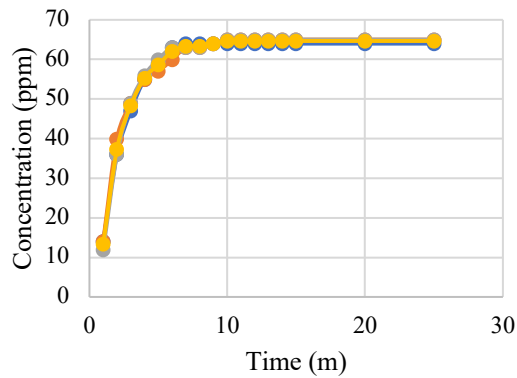
Valve open for 20s experimented repeated 3 times



Valve open for 30s- experimented repeated 3 times

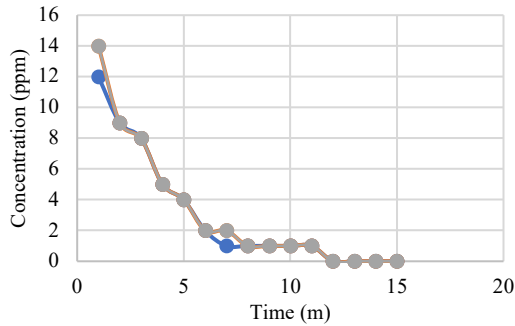


Valve open for 40s -experimented repeated 3 times

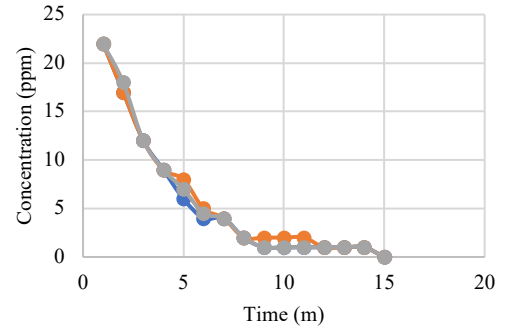


### Characterization of reference sensor - recovery time

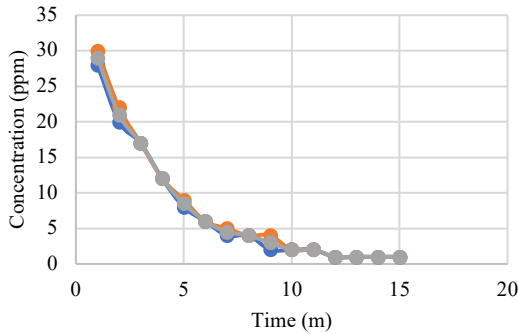
Reference Sensor recovery for 19 ppm - experimented repeated 3 times



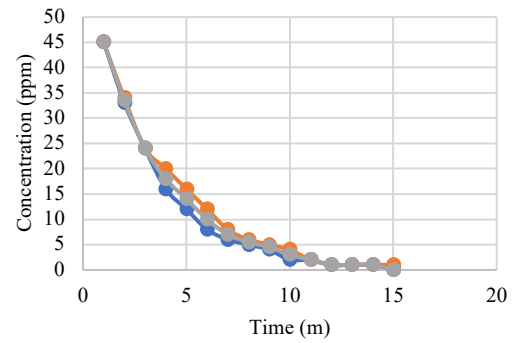
Reference sensor recovery for 34 ppm - experimented repeated 3 times



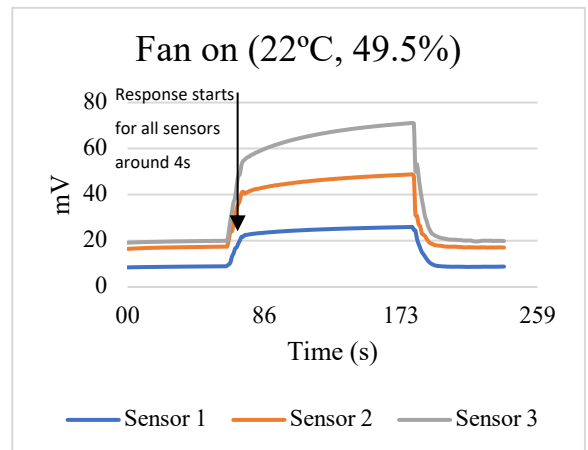
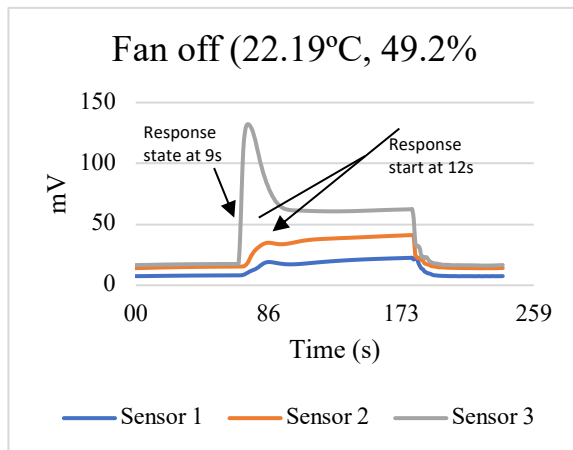
Reference sensor recovery for 45 ppm - experimented repeated 3 times

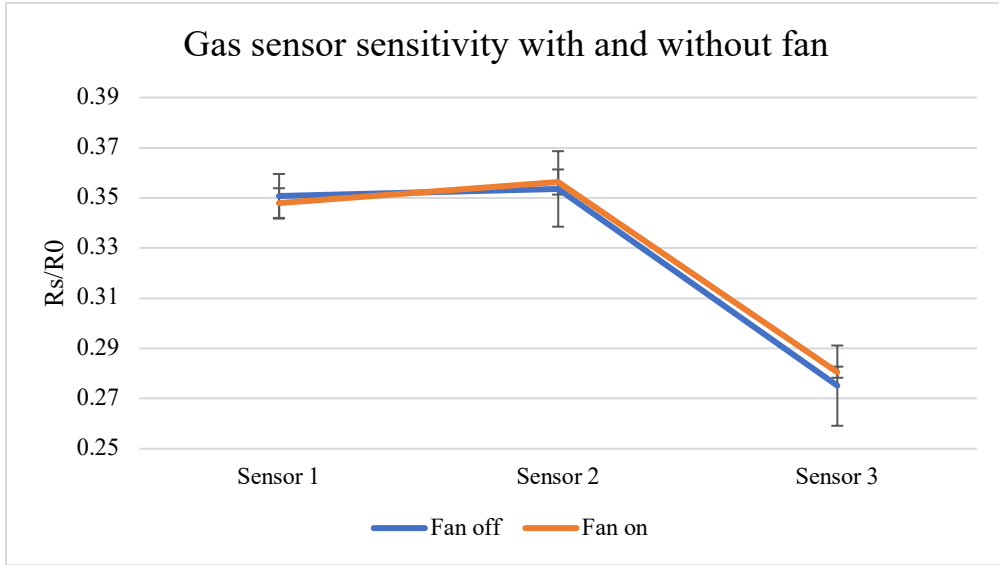


Reference sensor recovery for 65 ppm - experimented repeated 3 times



### Gas Sensor response with and Without fan

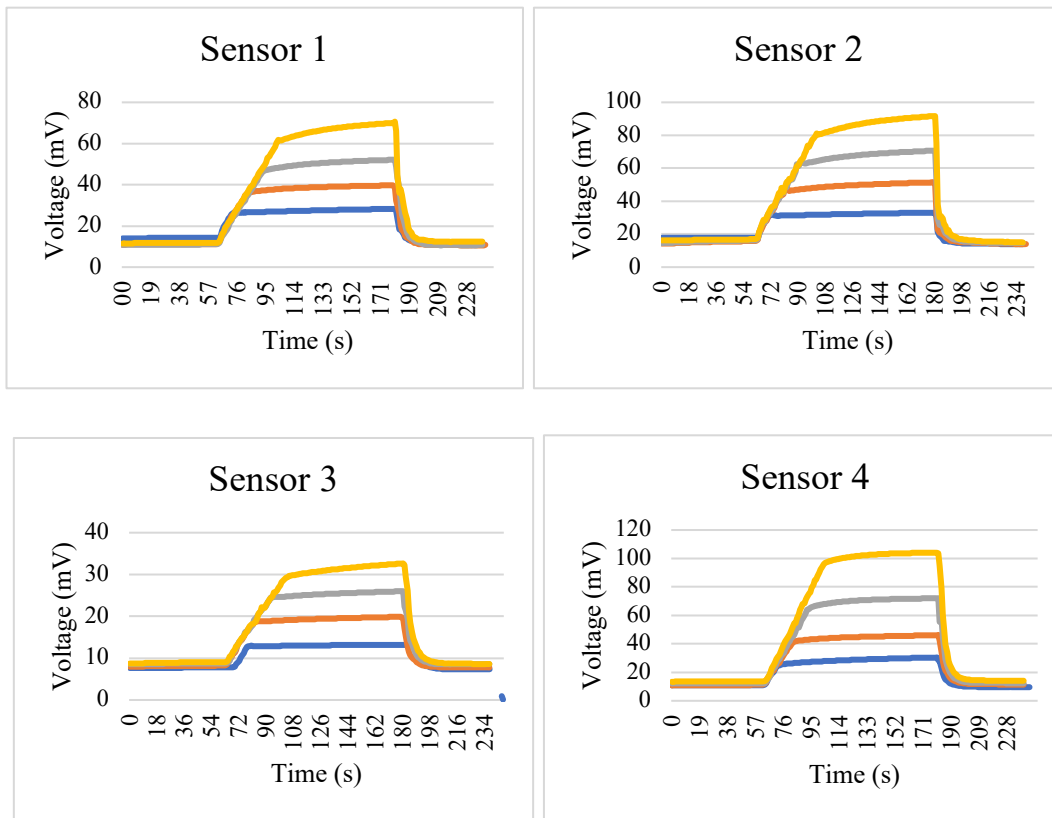




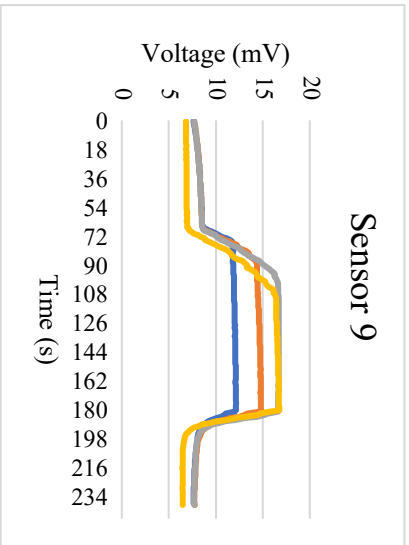
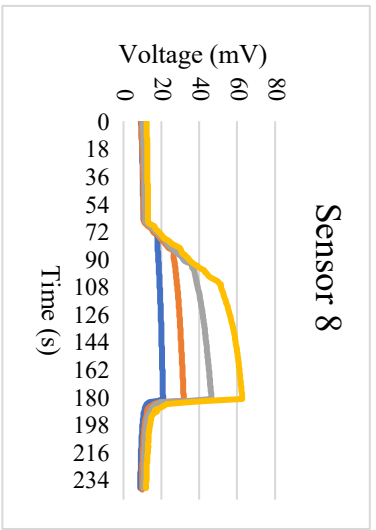
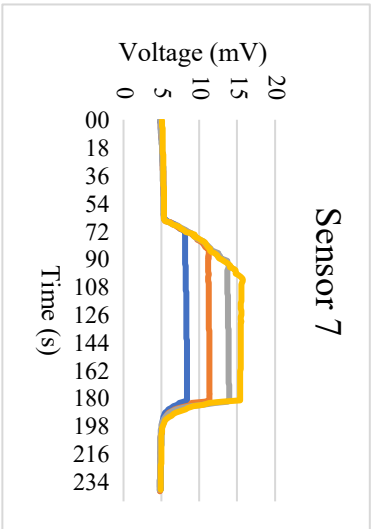
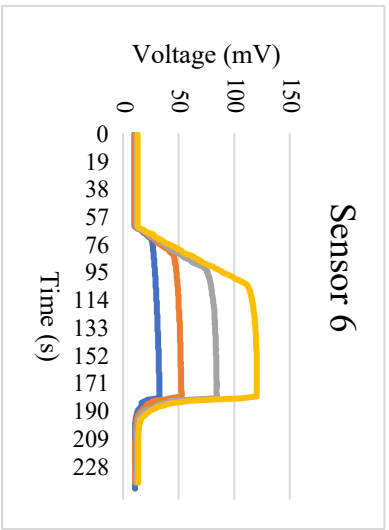
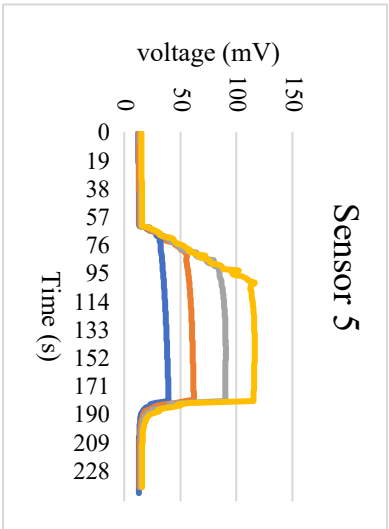
**Characterization of flexible CO sensor**

The sensor response obtained for all the 9 sensors without encapsulant, with encapsulant (Zitex G - 104, PTFE Fibre glass fabric and Platilon U 4201 AU) are shown below for experiment 1.

**1. Sensor response for different concentrations of unencapsulated CO filament – experiment 1**

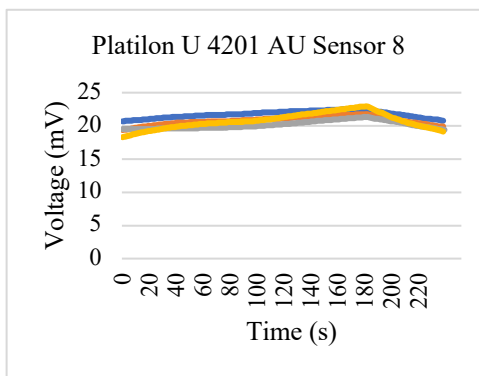
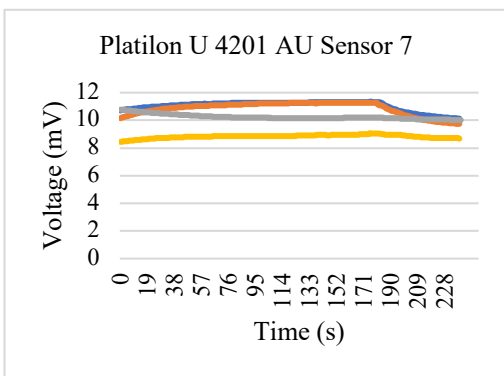
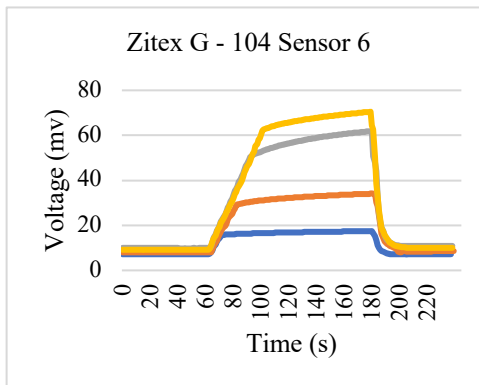
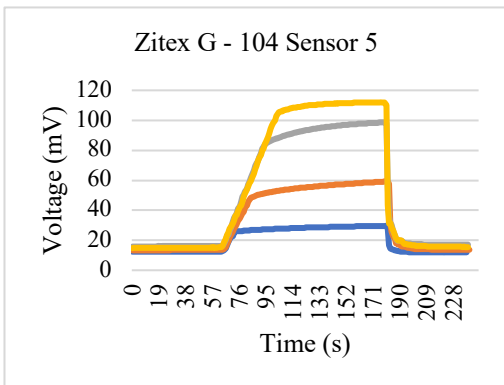
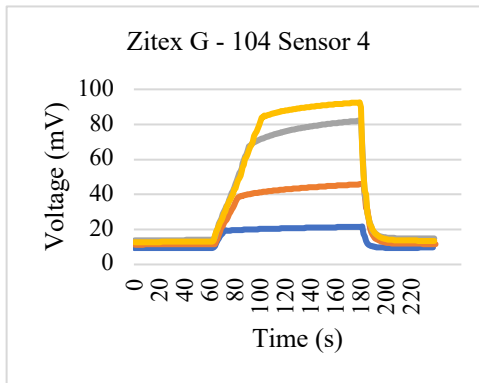
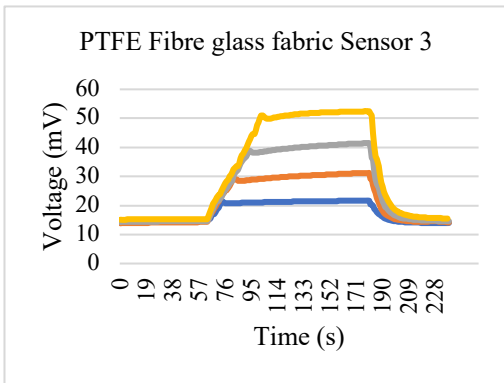
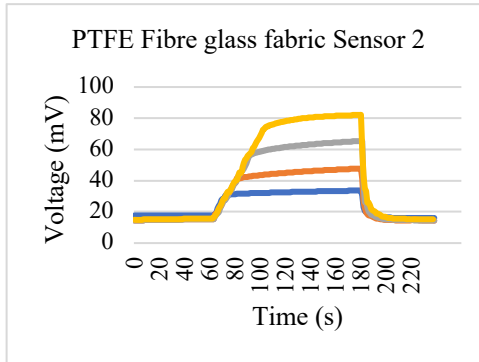
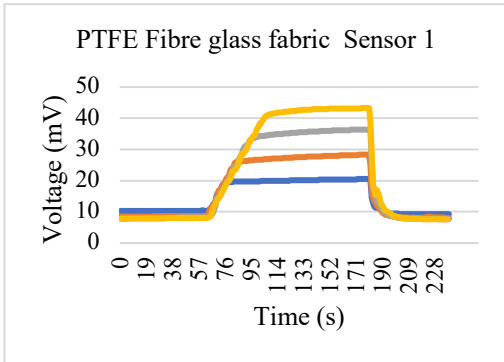


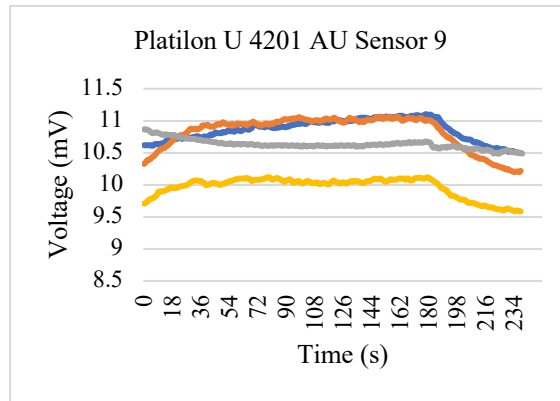




— 19ppm — 35ppm — 45ppm — 65ppm

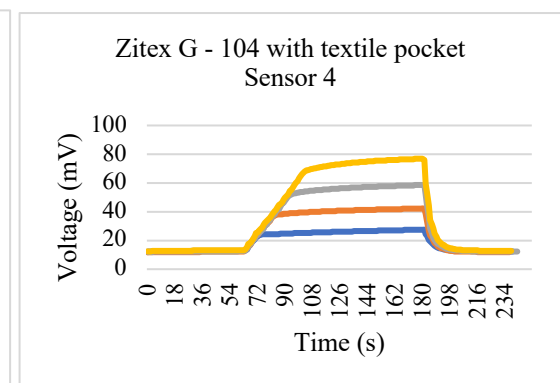
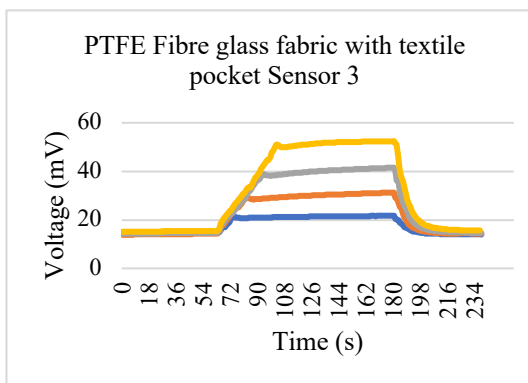
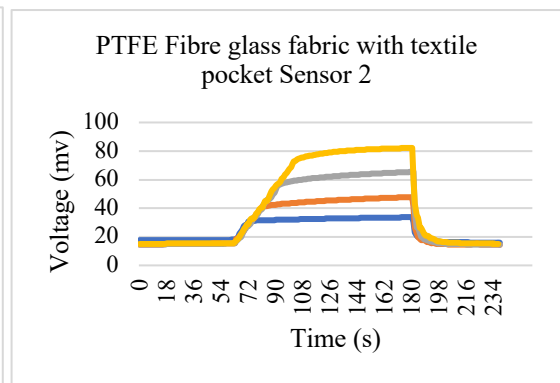
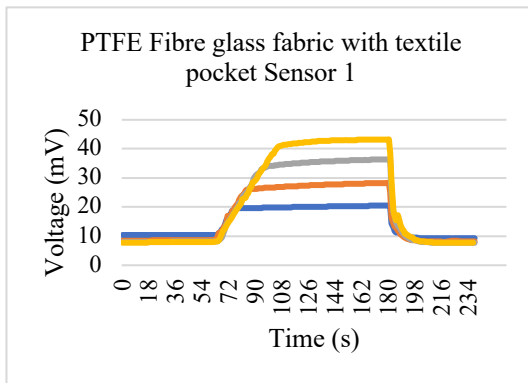
2. Sensor response for different concentrations of encapsulated CO filament – experiment 1

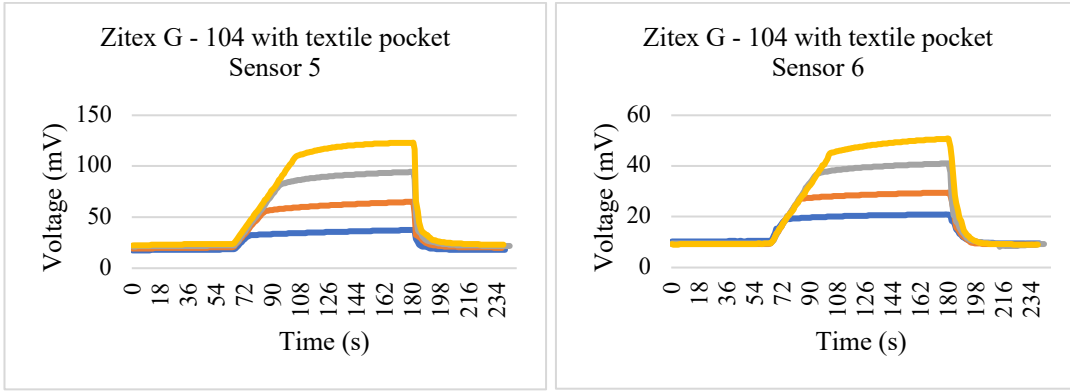




— 19ppm    — 35ppm    — 45ppm    — 65ppm

**3) Sensor response for encapsulated sensors integrated in textile pocket**



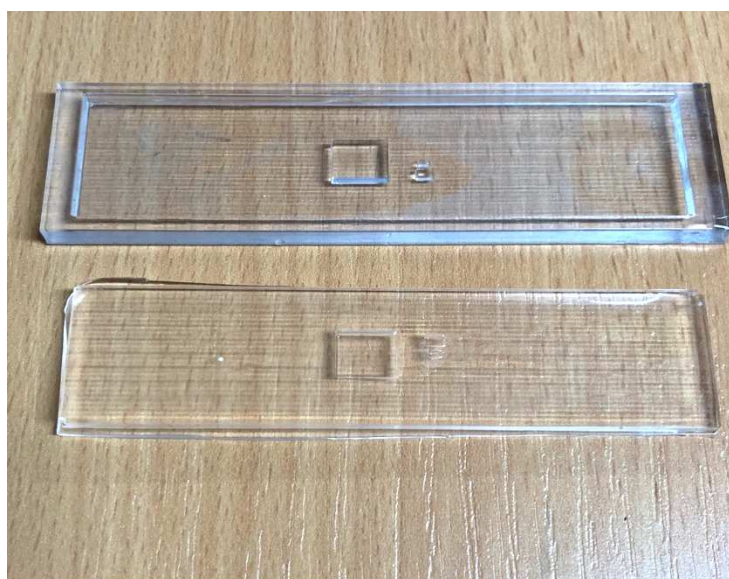


— 19 ppm    — 35 ppm    — 45 ppm    — 65 ppm

## APPENDIX B

### MAKING OF PDMS

The flexible mould made of PDMS was made using resin and hardener at the ratio of 1:10 and mixed well until mixture is bubble free. This can be achieved using the vacuum chamber to remove the bubbles until a clear mixture of PDMS is observed. The male moulds were 3D printed as shown in below and are cleaned and baked in the oven at 80°C for 24 hours. The 3D printed mould is then placed on deaerator using Trichloro (1H,1H,2H,2H-perfluorooctyl) silane to form a thin film coating on the solid moulds which helps in making them non-stick to PDMS and helps in removing after PDMS is cured. The bubble free mixture of PDMS is then poured to the cleaned 3D printed moulds and cured in an oven at 80°C for 2 hours and then removed from the solid mould shown in figure below.



**3D printed VerClear male mould (top) and flexible PDMS mould (bottom)**

## PACKAGING ASSEMBLY

Step 1: Flexible CO is removed from the alumina tile for packaging



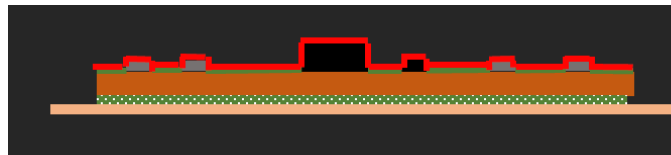
Step 4: Adhesive patterned cut is attached to the top side of the flexible strip. The opening in the adhesive is placed exactly on the SMD and



Step 2: Acrylic adhesive is attached on the bottom side of the flexible circuit strip










Step 5: The moulded thermoplastic materials Zitex G - 104 / PTFE Fibre glass fabric is attached to the circuit



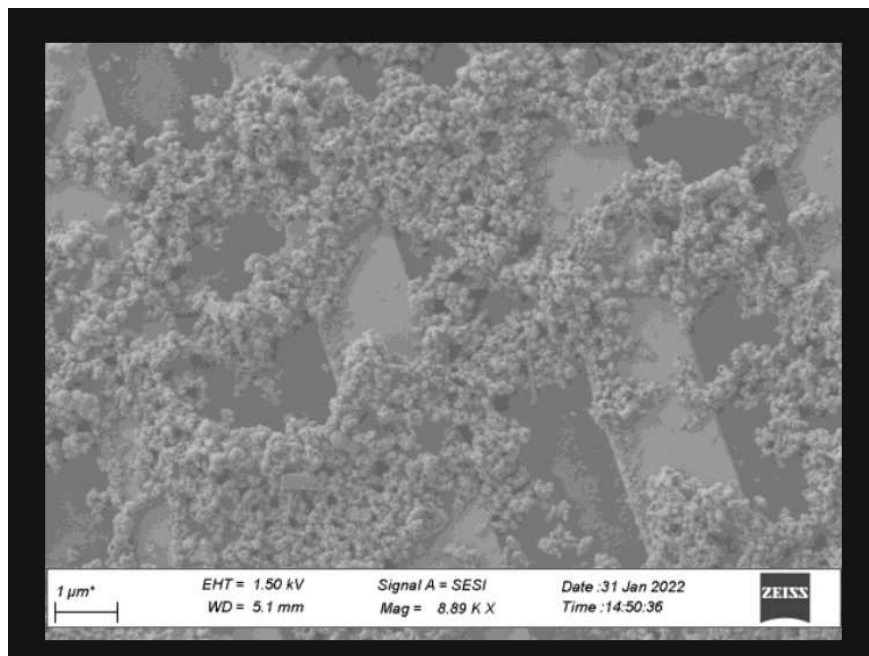
Step 3: 25µm Kapton is attached to the adhesive on the bottom side of the flexible strip



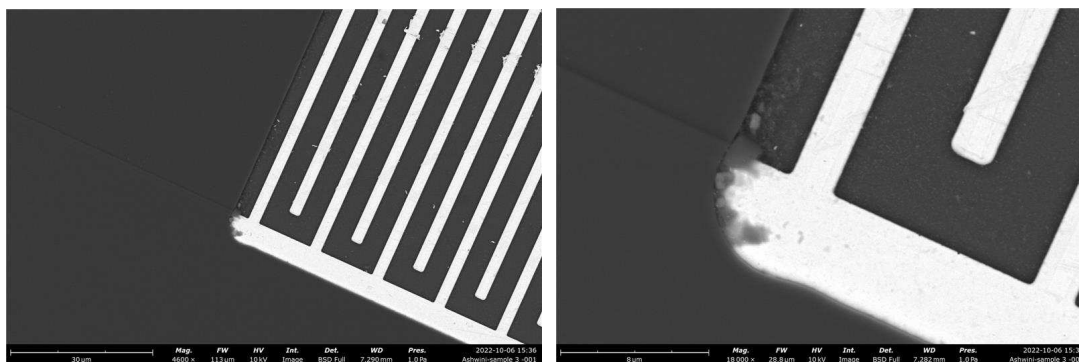
- |  |   |   |   |
|--|---|---|---|
|  | Kapton with epoxy and copper tracks   |  | Acrylic adhesive  |
|  | Adhesive (NLP 11051 for Zitex G - 104 and acrylic adhesive for PTFE glass fibre fabric) |  | Thermoplastic encapsulant (Zitex G - 104 or PTFE glass fibre) |
|  | Soldering joints for connecting wires   |  | SMD components – Sensor chip and resistors                    |
|  | 25µm Kapton   |   |   |

# APPENDIX C

## SENSITIVE MATERIAL IN NO<sub>2</sub> BARE DIE



(a)



(b)

Scanning Electron Microscopy (SEM) picture (a) from VOC Sens showing sensitive material deposited on top of IDE and (b) bare die after wire bonding taken at University of Southampton